Gel-based sensors involving supramolecular interactions with pillar[5]arene for the detection of environmental pollutants and biomarkers

D I S S E R T A T I O N

zur Erlangung des akademischen Grades

Doctor rerum naturalium (Dr. rer. nat.)

vorgelegt

der Fakultät der Naturwissenschaften

der Universität Paderborn

eingereicht von

Maksim Rodin

geboren am 30. Mai 1995 in Moskau, Russland

2025

Gutachter: Prof. Dr. Dirk Kuckling
Prof. Dr. Jan Paradies

Eingereicht am: 05.02.2025
Datum der Verteidigung: 26.03.2025

Diese Arbeit wurde in einem Zeitraum vom 02.09.2019 bis zum 31.12.2023 im Fachbereich Organische und Makromolekulare Chemie der Universität Paderborn unter der Leitung von Prof. Dr. Dirk Kuckling angefertigt.

An all diejenigen, die mich über die Jahre unterstützt, inspiriert und motiviert haben.

Table of Contents

Abstract

Dually crosslinked gels constructed by polymer strands interconnected using covalent and supramolecular linkages are versatile materials exhibiting outstanding mechanical properties as well as reversibility, which renders them materials of choice for numerous applications including sensor devices for monitoring the levels of environmentally and physiologically relevant substances. If a host–guest complex is used as a supramolecular crosslink, the analyte can act as a competitive guest and disrupt the original complex leading to a macroscopic change—a change in gel volume, which can be quantitatively used for selective analyte detection. Within the scope of the current work, pillar[5]arene-based host–guest chemistry was applied for the construction of a polymeric sensing platforms for adiponitrile detection in an organic solvent as well as spermine in aqueous solutions.

Firstly, a pillar[5]arene-based dually crosslinked gel sensor for industrial pollutant adiponitrile was designed. The amino-functionalized host moiety was synthesized, and a suitable guest moiety was selected based on NMR titration data. RAFT-polymerization and subsequent modification of the polymer with host, guest and photo-crosslinker moieties yielded host and guest polymers, which were characterized with NMR and GPC. The polymers were mixed and spin-coated onto a gold-coated quartz wafer to obtain an SPR sensor chip. Due to the gel expansion upon presence of adiponitrile, the system demonstrated high sensitivity with LOD = 25 μM, as determined by SPR spectroscopy.

Secondly, a hydrogel with embedded water-soluble pillar[5]arene was manufactured as a sensing platform for cancer biomarker spermine. A 10-fold carboxylate-substituted pillar[5]arene was synthesized. The complexes of the host with the analyte as well as with the guest moieties and guest-modified polymers were investigated using various methods including NMR, MS and ITC. SPR sensor chips were fabricated from the guest polymers and the host molecules were non-covalently embedded in the gel. The responsiveness of the chips was probed by various spermine concentrations in the course of SPR investigations.

Kurzzusammenfassung

Die doppelt vernetzten Gele, die von den durch kovalente und supramolekulare Vernetzungen gebundenen Polymerketten gebildet sind, stellen vielseitige Materialien dar, die über hervorragende mechanische Eigenschaften sowie Reversibilität verfügen, was sie zu perfekten Stoffen für zahlreiche Anwendungen macht, u. a. als Sensoren für die Überwachung von umwelt- und physiologisch relevanten Verbindungen. Wenn ein Wirt–Gast-Komplex als solche supramolekulare Vernetzung verwendet wird, kann der Analyt als Konkurrenzgast agieren und den ursprünglichen Komplex spalten. Dies führt zu einer makroskopischen Änderung des Gelvolumens, die eine quantitative und selektive Analytendetektion ermöglicht. Im Rahmen dieser Arbeit wurde die Wirt–Gast-Chemie auf Pillar[5]aren-Basis für die Herstellung von polymeren Sensorplattformen für die Detektion von Adiponitril in einem organischen Lösungsmittel sowie von Spermin in wässrigen Lösungen angewendet.

Zuerst wurde ein Pillar[5]aren-basiertes doppelt vernetztes Gel als Sensor für den industriellen Schadstoff Adiponitril entwickelt. Die aminofunktionalisierte Wirt-Spezies wurde synthetisiert und eine passende Gast-Spezies anhand der NMR-Titrationsdaten ausgewählt. Die RAFT-Polymerisation und darauffolgende Modifikation des Polymers mit den Wirt-, Gast- und Photovernetzer-Spezies ergab die Wirt- und Gastpolymere, die mittels NMR und GPC charakterisiert wurden. Die Polymere wurden zusammengeführt und mittels Rotationsbeschichtung auf ein goldbenetztes Quarz-Substrat aufgetragen, wodurch ein SPR-Sensorchip erhalten wurde. Aufgrund des in Anwesenheit des Adiponitril steigenden Gelvolumens konnte eine hohe Sensitivität des Systems demonstriert werden. Der mittels SPR-Spektroskopie bestimmte LOD-Wert betrug 25 µM.

Des Weiteren wurde ein Hydrogel mit eingebettetem wasserlöslichem Pillar[5]aren als Sensorplatform für den Krebsbiomarker Spermin hergestellt. Das 10-fach Carboxylat-substituiertes Pillar[5]aren wurde synthetisiert. Die Komplexe des Wirtes mit dem Analyten sowie mit den Gast-Spezies und Gast-modifizierten Polymeren wurden mit verschiedenen Methoden einschließlich NMR, MS und ITC untersucht. Die SPR-Sensorchips wurden aus Gastpolymeren und in das Gel nicht-kovalent eingebetteten Wirtmolekülen hergestellt. Die Responsivität der Chips wurde mit verschiedenen Spermin-Konzentrationen im Rahmen der SPR-Experimente untersucht.

Eidesstattliche Erklärung

Hiermit versichere ich, Maksim Rodin, die vorliegende Arbeit selbstständig, ohne Hilfe Dritter und nur mit den angegebenen Quellen und Hilfsmitteln angefertigt zu haben. Alle Stellen, die aus anderen Quellen entnommen wurden, sind als solche kenntlich gemacht worden. Ich habe an keiner anderen Stelle eine Eröffnung des Promotionsverfahrens beantragt und die vorliegende Dissertation wurde von keinem anderen Fachbereich bzw. keiner anderen Fakultät zurückgewiesen.

_____ _____

Maksim Rodin Ort, Datum

Anerkennung der Promotionsordnung

Hiermit erkenne ich, Maksim Rodin, die Promotionsordnung der Fakultät für Naturwissenschaften der Universität Paderborn, welche am 31. März 2021 von der Universität erlassen wurde, an. Bisher wurde weder an der Universität Paderborn noch an einer anderen Hochschule im In- oder Ausland ein Promotionsversuch unternommen.

_____ _____

Maksim Rodin Ort, Datum

Scientific contributions

Publications

1. Pillar[5]arene-based dually crosslinked supramolecular gel as a sensor for the detection of adiponitrile
   M. Rodin, D. Helle, D. Kuckling, *Polym. Chem*. **2024**, *15*(7), 661–679.
   DOI: 10.1039/D3PY01354E
2. Dually cross-linked single networks: structures and applications
   M. Rodin, J. Li, D. Kuckling, *Chem. Soc. Rev.* **2021**, *50*(14), 8147–8177.
   DOI: 10.1039/D0CS01585G

Participation in conferences

1. Nitrile detection with a dually crosslinked supramolecular gel sensor based on pillar[5]arene (Poster)
   M. Rodin, D. Kuckling, *The International Symposium on Macrocyclic and Supramolecular Chemistry (ISMSC 2023)*, **2023**, Reykjavik, Iceland.
2. Pillar[5]arene-based supramolecular gel sensor for the detection of nitriles (Poster)
   M. Rodin, D. Kuckling, *EUPOC 2023 – Dynamic Polymer Networks*, **2023**, Bertinoro, Italy.
3. Cancer biomarker sensor based on a hydrogel containing water soluble pillar[5]arene (Oral presentation)
   M. Rodin, R. Probst, D. Kuckling, *EPF 2022*, **2022**, Prague, Czech Republic
4. Pillar[5]arene-based dually cross-linked hydrogels for cancer biomarker sensing (Oral presentation)
   M. Rodin, D. Kuckling, *Polymer Networks Group – PNG 2022*, **2022**, Rome, Italy.

Acknowledgements / Danksagung

When I compare myself at the moment of writing these lines with the version of me from 2019, I truly understand what a life-changing journey it has been. The current thesis is so far the biggest project I have ever dared to undertake in my life and by far the most challenging one. The progress and the success of this project would be impossible without the huge support that I received from many people, from many different parts of the world, whom I would like to thank from the bottom of my heart.

First and foremost, I would like to express my gratitude to my supervisor, Prof. Dr. Dirk Kuckling, who offered me the opportunity of pursuing the PhD in Paderborn and whose guidance and valuable contribution of ideas helped me enormously in my academic progress and growth as a professional. Also, I would like to appreciate Dirk's optimistic attitude towards life and his openness towards new ideas and initiatives. I would like to extend my thanks to the Kuckling family who was welcoming and supportive during tough times and whose annual summer parties are always a highlight of the year.

Second, I would like to express my appreciation to Prof. Dr. Jan Paradies for the introduction into the intriguing world of computational chemistry and support in modelling the supramolecular complexation.

Further, a word of gratitude goes to PD Dr. Hans Egold for his inexhaustible support and expertise in all the NMR-related questions, which had a profound impact on the quality of the obtained data. I would also like to thank Karin Stolte for numerous measured samples and her willingness to help even when the schedule of an NMR titration was very tight.

My appreciation goes to the MS team, Dr. Adam Neuba und Christiane Gloger for always prompt measurements and help with especially complicated samples.

Big thanks go to Dr. Christoph Ebbert, Gisella Jünnemann-Held and Sandra Gołębiowska for their effort with all the PVD gold coatings for the quartz wafers.

I would like to offer my heartfelt thanks to the past and current members of the Kuckling group: Dr. Artjom Herberg for his expertise in GPC and valuable scientific input during the work reports; Daniela Kästing, Annette Lefarth, Mariola Zukowski, and Claudia Berkemeier who were a huge support for me professionally and morally.

I would like to express special appreciation to all (current and former) PhD students in the organic chemistry at the University of Paderborn, with whom I was lucky to share these years in the lab

and many of whom I feel happy to call friends. Dimitri Jung and Tarik Rust introduced me to the instruments and techniques in the lab as well as to the important aspects of German culture, cuisine and humor and were my big inspiration in the first phase of my PhD. Rafael Methling shared with me the passion for SPR and RAFT polymerization. Matthias van der Linde showed me the German fraternity life and introduced me to Discofox and Boogie. I wish to express my gratitude to Katharina Völlmecke whose contribution cannot be underappreciated: with her I shared the lab, the toughness of pursuing a PhD and with time even the taste in music; thanks to her, I started bouldering, polished my German and learnt not to confuse minuses with dashes. Sascha Bierbach was my first Bachelor student and impacted the progress of the PhD project. From then on, his unstoppable energy and curiosity have been a source of inspiration for me. René Probst and David Helle contributed within the scope of their Bachelor theses substantially to the research topics. Oliver Dückmann's positive attitude, kindness and inexhaustible creativity have always been a good support, as well as Robert Salewski's humor and home quizzes. I would like to express my gratitude to Viktorija Medvarić who has always had a superpower of finding right words of support and appreciation during tough times and who introduced me to my dearest person. Thanks to Rundong Zhou there has always been a possibility to escape the everyday problems with a hot pot. Heartly discussions with Benedikt Sieland have been very helpful morally and professionally. The optimism of Sebastian Peschtrich and seriousness of Axel Hoppe have also been always very enriching. Nicole Dickmann's creativity in house parties provided a very good distraction from a stressful routine. Naresh Killi, Sabith SKP and Pariksha Rana introduced me to Indian hospitality, showed how to have fun on parties and have been very supportive all along. A big thank you goes to the international community who made every Friday's lunchtime special. And of course, I would like to appreciate all the members of Chemistry Department for everyone's unique contribution to the professional and simultaneously friendly atmosphere.

Further, I am thankful to people from other universities and institutions for their time, expertise and skills. Firstly, to Prof. Dr. Monika Schönhoff in WWU Münster for providing the support with ITC, which generated invaluable data for the supramolecular complexes. In this relation I would like to extend my thanks to Leonard Wyszynski and Katja Hoffmann for conducting the measurements.

Secondly, I would like to express my gratitude to PD Dr.-Ing. habil. Margarita Günther in TU Dresden for demonstrating the applicability of the hydrogel systems in real devices.

Thirdly, special thanks go to Prof. Dominique Hourdet for supervision within the walls of ESPCI Paris and Dr. Guylaine Ducouret for her expertise in the field of rheology. Furthermore, I cannot

help expressing my appreciation of the former PhD students of SIMM, with whom I shared a lot of nice moments in Paris and in Rome, especially Lucile Barbier and Anusree Ausgustine.

Throughout the years, I have been receiving enormous moral support and encouragement from my friends from Russia, and even in today's reality they continue to be one of the main sources of my energy and motivation from afar. Therefore, I would like to send words of appreciation to Japan to Anna Bulygina, and to Moscow to Ivan Kasyanov, who not only supported me at a distance but managed to visit me in Germany, Ivan Demiachenko, Igor Kovalenko, Nikita Orlov and Artem Petrov. Also, I am thankful for the mutual support of the university comrades who share the challenges of pursuing a PhD in Germany: Valeriia Muraveva, Yulia Perevedentseva, Roman Barmin, Konstantin Korenkov, and Nikolai Kochetov.

I would like to acknowledge my dearest person, Silvia, for her constant support, wise advice and willingness to help in difficult situations, for giving me strength, care and love, even from the other end of Germany. Without her, I would never be able to finish this mammoth task.

Finally, I am extremely grateful to my family: my mom, my dad, and my grandmas. Thank you for supporting me all these years and believing in me from the very beginning. Мама, папа и бабушки, спасибо вам, что поддерживали все эти годы и верили в меня с самого начала.

List of abbreviations

Abbreviation	Meaning
1,2-DCE	1,2-Dichloroethane
A	Absorbance
A	Slope of the calibration curve
Å	Angstrom
AAc	Acrylic acid
ADMI	1-allyl-3,4-dimethyl-1*H*-pyrrole-2,5-dione
ag	Attogram
AIBN	Azobis(isobutyronitile)
AN	Adiponitrile
ATRP	Atom-transfer radical polymerization
BAPA	*tert*-butyl (3-azidopropyl)carbamate
BBHA	*tert*-butyl (6-bromohexyl)carbamate
BBPA	*tert*-butyl (3-bromopropyl)carbamate
BHA	6-bromohexan-1-amine hydrobromide
BHT	3,5-Di-*tert*-butyl-4-hydroxytoluene
BPA	Bisphenol A
C	Concentration
c	Wiseman parameter for ITC experimental setup
c	Speed of light in vacuum
cal	Calory
CBn	Cucurbit[n]uril
CC/CN/NN DCSG	Covalent-covalent/covalent-non-covalent/non-covalent-non-covalent DCSG
CD	Cyclodextrin
CGTase	Cyclodextrin glycosyl transferase
CnA	Calix[n]arene
Conv	Conversion
COSY	Correlation spectroscopy
COVID-19	Coronavirus disease 2019
CTA	Chain-transfer agent
D	Diffusion coefficient
d	Layer thickness
Đ	Polydispersity
DBU	1,8-Diazabicyclo[5.4.0]undec-7-ene
DCM	Dichloromethane
DCMP5A	Deca(carboxylatomethoxy)-P5A
DCSG	Dually crosslinked supramolecular gels
DDT	Dichlorodiphenyltrichloroethane

Abbreviation	Meaning
DECMP5A	Deca(ethoxycarbonylmethoxy)-P5A
DHP5A	Decahydroxy-P5A
DMAAm	Dimethyl acrylamide
DMAc	Dimethyl acetamide
DMB	1,4-Dimethoxybenzene
DMF	Dimethyl formamide
DMIEA	*N*-(2-aminoethyl)-3,4-dimethyl maleimide
DMIEA-Boc	*tert*-butyl (2-(3,4-dimethyl-2,5-dioxo-2,5-dihydro-1*H*-pyrrol-1-yl)ethyl)carbamate
DMP	2-(Dodecylthiocarbonothioylthio)-2-methylpropionic acid
DMP5A	Decamethoxy-P5A
DMSO	Dimethyl sulfoxide
DNA	Desoxyribonucleic acid
DOSY	Diffusion-ordered spectroscopy
E	Energy
EDA-Boc	*tert*-butyl (2-aminoethyl)carbamate
ESI	Electrospray ionization
Eq.	Equivalent
f	Fraction of binding sites
Fc	Ferrocene
Fc+	Ferrocenium
G	Guest
[G]	Equilibrium concentration of the guest
G	Gradient strength
G_0	Total guest concentration
GPC	Gel permeation chromatography
h	Hour
H	Host
[H]	Equilibrium concentration of the host
$\boldsymbol{H}$	Magnetic vector
H_0	Total host concentration
HFIP	1,1,1,3,3,3-Hexafluoro-2-propanol
[HG]	Equilibrium concentration of the complex
HT	P5A with a single triazole-containing amine-terminated side chain
HT-Boc	P5A with a single triazole-containing *tert*-butyl carbamate-terminated side chain
Hz	Hertz
I	Integral/Signal intensity
IHA-Boc	1-(6-((*tert*-butyloxycarbonyl)amino)hexyl)-1*H*-imidazole
^{i}J	Coupling constant
ITC	Isothermal titration calorimetry
J	Joule

Abbreviation	Meaning
k	Reaction rate constant
K_a	Equilibrium/binding/complexation constant
k_{app}	Apparent rate constant
k_B	Boltzmann constant
k_x	x-component of a wave vector
L	Liter
l	Beam path length
LC	Lethal concentration
LCST	Low critical solubility temperature
ln	Natural logarithm
LOD	Limit of detection
log	Logarithm to the base 10
LPA	Lysophosphatidic acid
L_{pd}	Penetration depth of an evanescent wave
M	mol/L
[M]	Monomer concentration
MBA	Methylene bis(acryl amide)
MIHA	1-(6-ammoniohexyl)-3-methyl-1*H*-imidazol-3-ium (chloride/bromide)
MIHA-Boc	3-(6-((*tert*-butyloxycarbonyl)amino)hexyl)-1-methyl-1*H*-imidazol-3-ium bromide
min	Minute
M_n	Number-average molecular weight
mol	Mole
MOPS	3-(*N*-morpholino)-propanesulfonic acid
MS	Mass-spectrometry
M_w	Weight-average molecular weight
n	Stoichiometry
NB	Nile blue
n_d	Refractive index
NIPAAm	*N*-isopropylacrylamide
nm	Nanometer
NMR	Nuclear magnetic resonance
NOE	Nuclear Overhauser enhancement
NOESY	Nuclear Overhauser enhancement spectroscopy
ODC	Ornithine decarboxylase
P10	poly($DMAAm_{0.9}$-co-$VDMA_{0.1}$)
P10TAHA	TAHA-modified P10
P10TAHAP	TAHA- and DMIEA-modified P10
P10THA	THA-modified P10
P10THAP	THA- and DMIEA-modified P10
P20	poly($DMAAm_{0.8}$-co-$VDMA_{0.2}$)

Abbreviation	Meaning
P20HTP	HT- and DMIEA-modified P20
P20MIHAP	MIHA- and DMIEA-modified P20
P20P5AHA	P5AHA-modified P20
P20PC	DMIEA-modified P20
P5AHA	(6-aminohexyloxy)-P5A
P5AOH	Mono-demethylated DMP5A
P5APR	P5A with a single propargyl rim-group
PBS	Phosphate-buffered saline
PDI	Polydispersity
PEG	Poly(ethylene glycol)
PHA-Boc	1-(6-((*tert*-butyloxycarbonyl)amino)hexyl)-pyridin-1-ium bromide
PMMA	Poly(methyl methacrylate)
P_n	Degree of polymerization
PnA	Pillar[n]arene
ppm	parts per million
PS	Polystyrene
PUT	Putrescine
PVD	Physical vapor deposition
Q	Heat
Q	Swelling ratio
Q_r	Swelling ratio calculated by the calibration curve
r	Particle size
RAFT	Reversible addition−fragmentation chain-transfer polymerization
R_{eq}	Equilibrium intensity of a reflected light
RI	Refractive index
R_{max}	Maximum intensity of a reflected light
RNA	Ribonucleic acid
rpm	Revolutions per minute
RT	Room temperature
SAV	Streptavidin
s	Second
S	Entropy
SD	Spermidine
SEC	Size-exclusion chromatography
SP	Spermine
SP4HCl	Spermine tetrahydrochloride
SPR	Surface plasmon resonance
T	Temperature
t	Time
TAHA	N^1,N^1,N^1-trimethylhexane-1,6-diaminium (chloride/bromide)

Abbreviation	Meaning
TAHA-Boc	6-((*tert*-butoxycarbonyl)amino)-*N*,*N*,*N*-trimethylhexan-1-aminium bromide
TFA	Trifluoroacetic acid
THA	6-(1*H*-1,2,4-triazol-1-yl)hexan-1-amine hydrochloride
THA-Boc	*tert*-butyl (6-(1*H*-1,2,4-triazol-1-yl)hexyl)carbamate
THF	Tetrahydrofuran
TLC	Thin-layer chromatography
TM	Transversal magnetic
UPy	Ureidopyrimidinone
UV/Vis	Ultraviolet, visible light
VDMA	4,4-dimethyl-2-vinylazlactone
W	Watt
WSPnA	Water-soluble pillar[n]arene
X_i	Mole fraction of the i-th component
Y	Arbitrary physical property
γ	Gyromagnetic ratio
δ	Chemical shift
Δ	Before physical units: indicates the change of the value
ΔG	Change in Gibbs free energy
δ^{grad}	Duration of the gradient
Δ^{grad}	Diffusion time
ΔH	Process enthalpy
ΔS	Process entropy
ε	Molar absorptivity
ε	Dielectric constant
ε_d	Dielectric constant of a dielectric
ε_{imag}	Imaginary part of the dielectric constant
ε_m	Dielectric constant of a metal
ε_{real}	Real part of the dielectric constant
η	Viscosity
θ	Angle of incidence of light
θ_{SPR}	Angle of surface plasmon resonance
θ_{TR}	Angle of total internal reflection
λ	Wavelength
ν	Frequency
τ	Characteristic time/state lifetimes
ω	Angular frequency of a light wave
ω	Rotation speed

"La créativité demande du courage."

— attributed to Henri Matisse

1 Introduction

1.1 Motivation

Polymeric gels incorporating supramolecular interactions such as hydrogen bonds, metal–ligand complexes, hydrophobic and host–guest interactions have been attracting considerable attention of researchers in the past years and are currently emerging into a highly important field of studies.[1] Due to the inherent reversibility of the supramolecular interaction, such materials possess responsiveness towards various stimuli including light, temperature, pH of the medium, or certain molecules.[2,3] Therefore, such systems are termed stimuli-responsive gels and are considered materials of tomorrow because of the environmental drawbacks, mechanical flaws, and lack of adaptivity of the covalently crosslinked systems. The marriage of the two types of crosslinks in one material endows it with the advantages of both types, and as a result, a system is obtained which is mechanically robust and tough and simultaneously adaptive and responsive.[4] Such dually crosslinked single gels (DCSG) are irreplaceable for the applications as self-healing, shape-memory materials, or especially as sensors, since DCSGs possess the two elements required for a sensor, namely, a responsive element (the supramolecular bond) as well as a transducer element (a macroscopic parameter), *e.g.*, swelling ratio.[5] Hereby, the covalent crosslink serves the purpose of maintaining the integrity of the gel.

Surface plasmon resonance (SPR) spectroscopy is an optical technique which allows one to investigate the behavior of thin layers with high precision.[6] When applied to study gold-coated substrates with sub-micrometer thick gel layers, SPR provides a real-time monitoring of the gel thickness and its refractive index. If such a gel contains a chemo responsive site as a crosslink, it will disrupt upon presence of a certain analyte, leading to a change in the thickness of a swollen gel *via* drop in crosslink density, which can be detected by the SPR method.[7]

One of the most promising chemo responsive supramolecular interactions is clearly host–guest interactions.[8] The design of macrocycles plays a crucial role for the fabrication of such systems since it is possible to create a cavity, which would precisely accommodate a desired molecule (analogous to the enzymatic systems), thus, endowing the sensor with selectivity. Pillar[n]arenes (PnAs),[9,10] a young family of macrocycles, are characterized by a straight cylindrical shape of the electron-rich cavity and a high flexibility in terms of chemical modification, which opens broad possibilities for host–guest interactions with neutral and positively charged molecules as well as

for the design of the macrocycles as a responsive element in a sensor. Stable complexes of PnAs are formed, for instance, with dinitriles,[11] which are toxic pollutants but vastly used in industrial processes,[12] and (poly)alkylamines such as biologically relevant spermine and spermidine,[13] which act as important regulators and biomarkers *in vivo*, whose content in bodily fluids (at a μmol/L level) can indicate development of severe diseases including cancer.[14] Therefore, PnAs are the macrocycles of choice for the fabrication of a gel-based sensor chip for the detection of dinitriles and alkylamines using SPR technique.

1.2 The aim and the objectives of the current work

The aim of the current work is to devise a SPR-based sensor of determining various small molecules such as dinitriles and alkylamines in the solution in order to detect the potential exceeding of a dangerous threshold for a pollutant in the wastewater or for a biomarker in bodily fluids.

To achieve the aim, a crosslinked gel should be devised incorporating a responsive element, which is based on an inclusion complex with PnA. Firstly, the macrocycle should be synthesized, and a way should be found to embed the host species into the gel: either covalently by mono-functionalizing the macrocycle (with a perspective of introducing a second crosslink into the system) or non-covalently *via* pendant guest groups. The host–guest complex should be stable enough to either function as a second crosslink in a swollen state or to ensure the macrocycle is non-covalently attached to the polymeric chains. At the same time, the complex should be more labile than that between the PnA and the analyte to provide the responsiveness upon the presence of the latter. Therefore, a thorough screening of various guests is required including the determination of their binding affinity to the host under the operating conditions of the sensor, which can be performed by NMR titration or isothermal titration calorimetry.

After the suitable guest moiety is found, a polymer with pendant covalent crosslinker and guest groups (and, possibly, one polymer with pendant host groups) should be synthesized. Possibly, the desired responsiveness of the supramolecular system towards the analyte should be proved for an uncrosslinked polymer using, *e.g.*, NMR spectroscopy.

Further, a thin layer of the polymer or the polymer mixture should be obtained on a gold-coated quartz substrate by spin-coating and subsequent curing. Swelling behavior of the obtained gel layer should be investigated by the SPR spectroscopy in the presence of different concentrations of the analyte to be able to prove the applicability of the method as well as to determine its limit of detection.

2 Theoretical background

2.1 Supramolecular chemistry

2.1.1 Supramolecular interactions

According to Jean-Marie Lehn, who introduced this term in the 1970s in his works on cryptates, supramolecular chemistry is a field at the confluence of chemistry, physics and biology that addresses entities of a higher organizational complexity than molecules.[15] Such entities are constituted by molecular species bound together by intermolecular non-covalent forces, which are weaker than covalent bonds. Still, these forces provide the supramolecular entities with precise structural organization due to which they possess molecule-like features.[16]

The spectrum of the non-covalent interactions that can be employed for the formation of supramolecular species varying from highly energetic ionic bonds down to hydrophobic interactions[17] is shown in Figure 1 and summarized in Table 1 together with the typical bond energies E in comparison to the covalent (or chemical) bond.[4] It is important to note that non-covalent interactions are inherently dynamic, or reversible. Therefore, typical values for association constants K_a representing binding affinity of two molecules bound by a given type of interactions are also presented in the table.

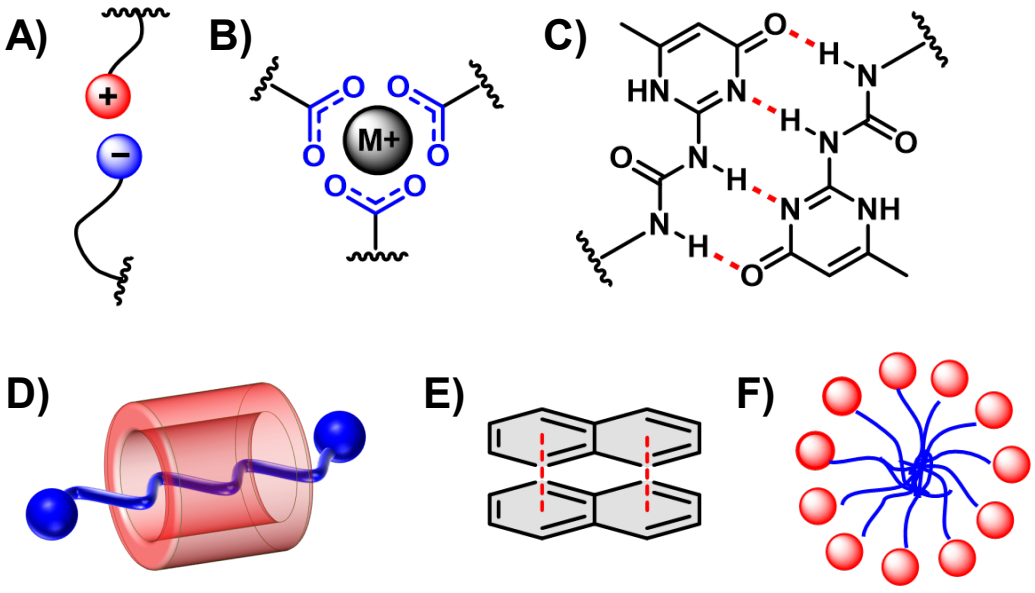

Figure 1. Various types of supramolecular interactions. A) Ionic interactions, B) Metal–ligand complexes, C) Hydrogen bonds with UPy as an example, D) Host–guest inclusion complexes, E) π–π stacking, F) Hydrophobic interactions.

Table 1. Comparative data of typical bond energy ranges and typical equilibrium constants of non-covalent interactions.[4]

Type of interactions	E, kJ mol^{-1}	K_a, M^{-1}
Covalent bonds	100 – 450	—
Ionic interactions	200 – 300	—
Metal-ligand coordination	< 400	$<10^{37} – 10^{40}$
Hydrogen bonding	4 – 120	$\leq 10^{9}$
Host-guest interactions	5 – 40	$10^{3} – 10^{15}$
π–π stacking	~ 10	$10^{1} – 10^{2}$
Hydrophobic interactions	< 10	—

One of the important properties of the covalent bonds is that their spatial parameters—such as the number of bonds, their lengths and angles—are precisely defined by the geometry of the electron orbitals. For supramolecular interactions these properties, *i.e.*, the governance over species' geometry and spatial features, will be collectively described by the term directionality.[18]

2.1.2 Ionic interactions

Clearly, covalent bonds with energies up to 450 kJ/mol (calculated per single bond) are the most stable compared to the non-covalent ones and are normally not influenced by changes in the environment such as solvent, temperature (up to certain limits), or pH. Nevertheless, relying on Coulomb forces, ionic interactions, resulting from the attraction of spatially separated charged species, exhibit a pronounced bonding energy that lies in the same order of magnitude as covalent bonds. However, what differentiates them is that since Coulomb attraction (and repulsion) are only dependent on a distance between interacting entities, ionic bonds lack directionality, which is essential for forming ordered supramolecular structures in solutions.[18]

Metal-ligand complexes as a special case of ionic interactions, on the other hand, possess directionality due to the architecture of chelating ligands and metal ion electron orbitals. The "core" in a majority of such complexes is represented by first-row transition metals or alkaline earth metals. Nonetheless, other transition and noble metals are of great use as well.[19] Because of their relatively high stability and since they offer an outstanding control over the structure, metal coordination bonds are an established tool in a supramolecular toolbox for a design of smart materials combining good mechanical properties and reversibility which provides such properties as self-healing, shape memory, *etc*.[20,21]

2.1.3 Hydrogen bonds

Perhaps, the most well-known type of a non-covalent interaction is a hydrogen bond, which can be treated as another special case of an ionic interaction where a partial positive charge (or free

electron orbital) on hydrogen atoms and moieties bearing a partial negative charge (an orbital occupied with a lone electron pair) attract forming a looser type of bond. Although somewhat lower in energy (up to 120 kJ/mol), hydrogen bonds tend to be highly directional, especially when the moieties are capable of forming multiple bonds per interacting site.[18,22] This has an utmost importance for all cellular organisms since hydrogen bonds between nucleobases are forces that provide stability to the DNA double helix.[23] This demonstrates how tailor-made species (including natural ones) are capable of endowing the system with complementarity, or broadly speaking, selectivity. So, due to the structural features, certain purine-pyrimidine pairs are formed: adenine–thymine sharing two hydrogen bonds and guanine–cytosine sharing three bonds.

A self-complementarity motif employing multiple hydrogen bonding, 2-ureido-4-pyrimidinone (UPy) moiety was introduced by the group of Prof. Meijer.[24] Due to its 4 hydrogen bonds, UPy (Figure 1, C) exhibits a highly effective dimerization with a binding constant up to $K_a = 6\times10^8\ M^{-1}$ in toluene.[25] This high stability of the dimer led to its vast utilization as a supramolecular building block in materials chemistry for endowing the systems with reversibility without impairing their mechanical properties.[26,27]

2.1.4 Hydrophobic interactions

Hydrophobic interactions and π–π stacking demonstrate the lowest binding energies of the non-covalent interactions ($E \lesssim 10$ kJ/mol), which also highly depends on the solvent. In case of the π–π complexes, it is an interplay between the dispersion forces and Pauli exchange repulsion (and not, as was assumed, quadrupole electrostatic interactions) combined with sterical conditions that determine the binding strength and geometry of the complex.[28] Despite the low binding energy, such interactions exhibit the directionality and cooperativity, and different geometries of the π–π bonds between aromatic amino acids were described in literature.[29]

The predisposition of non-polar species to aggregate in aqueous solutions is described by a general term of hydrophobic effect. This effect is thermodynamically driven and is determined by the change of state of water molecules surrounding the hydrocarbon groups. An earlier—"classical"—approach suggests an entropic benefit through the release of water molecules from the solvating shell (*via* destruction of clathrate structures) upon aggregation of multiple hydrophobic droplets and, therefore, formation of a larger cavity.[30] A more recent "non-classical" approach brings an enthalpic gain into the focus, which arises from the amount of the hydrogen bonds formed by water molecules.[31] This approach was used to describe the cases of, for instance, inclusion complex formation. Water molecules encompassed by host molecules containing no functional groups within their cavity possess higher energy because of the lack of stabilization and, hence, serve for a significant energy benefit when replaced by guest molecules.

Hydrophobic interactions were proved to be of extreme importance in biochemistry since they are the factor underlying many processes such as protein folding and conformational stability thereof.[32] Furthermore, hydrophobic bonds are often utilized in the field of materials chemistry for smart materials fabrication,[33,34] where their special design even enables directionality in such interactions.[35]

2.1.5 Host-guest complexes

Host-guest inclusion complexes, in which a guest molecule is encapsulated by a host molecule, represent a category of highly directional and selective as well as versatile supramolecular motifs, thanks to which they resemble the interaction between receptor and enzyme, one of the essential and most important recognition motifs in biological processes. What makes host-guest complexes extraordinary among non-covalent interactions is that they are not a genuinely "unique" class of supramolecular bonds but rather a combination of different interactions (such as hydrogen bonds, hydrophobic or electrostatic interactions, etc.),[36] which is characteristic for a given host-guest pair and which makes these complexes so selective. Therefore, the thermodynamic driving force of the host-guest interactions are diverse but can be reduced to two general effects: a) an energetic gain upon complexation due to a higher host–guest interaction energy than guest solvation energy; b) release of highly energetic solvent molecules from the host cavity (see Chapter 2.1.4).

Host molecules, which are represented mostly by macrocycles, are usually meticulously designed in order to achieve the best fit for a chosen guest molecule. Emerging from the creation of cyclic crown ethers in 1960s,[37,38] the family of host entities has been developing ever since and is currently enjoying a heyday due to the advances of synthetic methods paving the way for the design of highly sophisticated and highly selective moieties.[39] Among this significant variety of the host molecules emerged in the past years, there are several which, due to the facility of their synthesis, as well as tunability and versatility, were thoroughly studied in terms of their fabrication, modification, and applications (Figure 2).

2.1.5.1 Cyclodextrins

As a rare example of naturally occurring macrocycles, cyclodextrins (CDs), cyclic oligosaccharides constituted by 6, 7 or 8 α-1,4-connected D-glucopyranosyl units (for the smallest homologues, namely α-, β- and γ-cyclodextrins respectively, Figure 2, A, were discovered at the end of the 19th century by Villiers[40] and characterized in the works of Schardinger[41] some years later. Yet even now, after more than a century since their discovery, CDs stay one of the most employed macrocyclic compounds. This long-lasting popularity and interest are determined by several features of CDs. Structurally these macrocycles resemble a torus with uneven sides so that

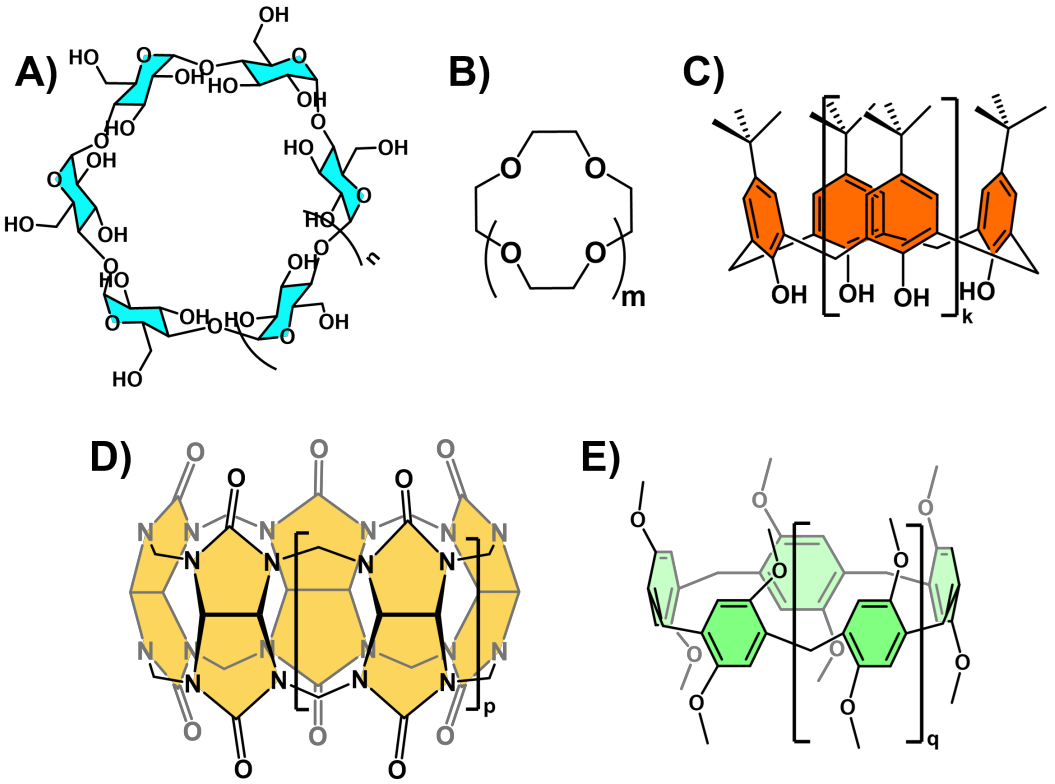

Figure 2. Various macrocycle families. A) Cyclodextrins (n = 1, 2, 3 for α-, β- and γ-CD, respectively). B) Crown ethers (m = 1, 2, 3 for [12]crown-4, [15]crown-5, [18]crown-6, respectively). C) Calix[n]arenes (k = 1, 3, 5…). D) Cucurbit[n]urils (p = 1, 2, 3…). E) Pillar[n]arenes (q = 1, 2, 3…).

the internal diameters range from 4.4–5.7 Å (corresponding to the narrow and wide side, respectively) for α-CD to 7.4–9.5 Å for γ-CD.[42] Due to the structural particularities arising from cyclooligomerization, the outer surface of the macrocycle is hydrophilic whereas the inner cavity is hydrophobic implying that CDs exhibit good solubility in water and simultaneously high binding affinity towards hydrophobic or amphiphilic small molecules in aqueous solutions. Furthermore, OH-groups on the rims of CD are beneficial for guest molecules with polar end groups due to the possibility of forming hydrogen bonds. Over decades of research on cyclodextrins, affinity to diverse guest molecules with diverse architectures was demonstrated for homologues of CDs.[43] Different cavity sizes of different CD family members also increase selectivity of such host-guest interactions. For instance, the complex of α-CD with azo-benzene, which is dimensionally the best fit for its cavity[44], exhibits the highest binding affinity compared to the other cyclodextrins.[45] The cavity of β-CD is, on the other hand, particularly suitable for larger guests such as ferrocene[46] (Fc; $K_a = 1.7\times10^4\ M^{-1}$) or adamantane[47] ($K_a = 3.5\times10^4\ M^{-1}$).

Nowadays CDs are synthesized enzymatically by the action of cyclodextrin glycosyl transferases (CGTases) on starch,[48] making CDs fully biocompatible, which defines the broad scope of applications in industry[49] as well as in biomedical research.[50] Further, the interest of synthetic

chemists is directed to the increased yield of single homologues[51] as well as to the fabrication of larger homologues such as δ-CD.[52]

2.1.5.2 Crown ethers

The first synthetically obtained macrocycles—cyclic oligoethers, which for their specific conformation in complexes were named "crown ethers" by their creator—were reported by Pedersen in 1967.[37,38] In their simplest form, they are composed of repeating ethyleneoxy units (Figure 2, B) which oligomerize in a fashion that the oxygen atoms are located on the inner surface of the cavity and the outer surface is constituted by ethylene fragments making crown ethers less polar on the outside, which endows them with solubility in organic solvents. The oxygen atoms in the interior of the molecule implies electron donating properties of the macrocycle in complexes.[53] Hence, crown ethers are well-known to bind metal ions (which makes them outstanding phase transfer catalysts[54]), especially alkali-metals, and other cations (*e.g.*, primary amines[55]). Noteworthy is the selectivity of each of the crown ether oligomers for the alkali ions: due to the suitable radii stable complexes are formed between (*n*+2)-mer and the alkali ion of the *n*-th period: [12]crown-4 with Li^+ (ionic diameter of 1.4 Å), [15]crown-5 with Na^+ (1.9 Å) and [18]crown-6 with K^+ (2.7 Å), *etc*.[56] Employing crown ethers of larger sizes ([24]crown-8), which can be threaded by dialkylammonium cations in an effective fashion due to hydrogen bond formation and electrostatic interactions, Stoddart and coworkers developed a new class of mechanically interlocked complexes: (pseudo-) rotaxanes.[57] These ideas were developed further to obtain molecular machines prototypes, *i.e.*, complexes in which external stimuli are able to induce molecular motion in a highly precise manner.[58] Nowadays crown ethers as macrocycles are utilized in various other fields including material chemistry.[59]

2.1.5.3 Calix[n]arenes

Further development of host-guest chemistry was achieved with isolation of calix[n]arenes (CnAs) first conducted by Zinke[60] during his investigations of phenol–formaldehyde reactions and was expanded in the works of Gutsche, who also coined the term for the new class of supramolecular hosts.[61] Cone-shaped CnAs are constructed by *para*-substituted phenol units bridged by methylene groups in *ortho*-positions to hydroxyl groups, typically as tetra-, hexa-, and octamers (Figure 2, C). Due to their structure, CnAs possess an electron-rich cavity which can encompass, for instance, positively charged species (*via* electrostatic interactions) or aromatics (*via* π–π stacking). The disadvantage that these macrocycles have in their original form (*tert*-butyl substituted phenols) is a poor water solubility which can be overcome by chemical modifications. This renders CnAs highly versatile host species[62] with outstanding molecular recognition

possibilities.[63] Furthermore, notable is the ability of CnAs to bind fullerenes,[64] thus, opening an important way of their purification.[65]

2.1.5.4 Cucurbit[n]urils

The next rich contribution to the macrocyclic family happened upon discovery of cucurbit[n]urils (CBns). First reported in 1905,[66] these macrocycles were not characterized until 1981 when Mock[67] described the structure of hexamer CB6 and gave the new species its name due to its similarity to a pumpkin (Figure 2, D). Indeed, CBns resemble a highly symmetrical torus comprised of glycouril repeating units connected by two methylene groups with each of the neighboring units. Hydrophilic ureidocarbonyl rim groups surround each of the two equal portals into a hydrophobic cavity. Therefore, CBn can encapsulate neutral species within the cavity *via* hydrophobic interactions as well as polar and positively charged species *via* ion–dipole interactions and hydrogen bonds with the rim groups, which defines generally higher binding affinities with guests than in case of cyclodextrins.[68,69] A rapid development of the synthetic and host-guest chemistry of CBns in the decades after their discovery led to the fabrication of various homologues[70] (from CB5 to CB10 and beyond) as well as various methods of their modification.[71] As in the case of other macrocyclic species, the host properties of the CBns are drastically dependent on the size of the homologue: the cavity diameter increases from 4.4 Å for CB5 to 8.8 Å for CB8.[68] Therefore, whereas the cavity of CB5 is small enough to form complexes with gases,[72] metal ions,[73] or aliphatic amines (including spermine)[74], CB6 (due to its larger size) is capable of binding to a vast variety of different guest molecules including alkylammonium salts, charged *N*-heterocyclic compounds, alcohols, amino acids, nitriles, *etc*.[69,75] Noteworthy is the next homologue, CB7, that due to a higher water solubility (somewhat analogous to β-CD) was shown to form exceptionally stable complexes with K_a reaching ~10^{17} M^{-1} for a complex with diamantane diammonium guests,[76] thanks to the diamantane body perfectly fitting the hydrophobic cavity of the host and two ammonium moieties forming 14 ion–dipole bonds with the rim groups. The size of the cavity of CB8, in its turn, allows two guest molecules being encompassed simultaneously, thus, forming a supramolecular termolecular complex.[77] Among all the advantages that are offered by the efficient binding affinities of the CBn family in chemical and biomedical applications,[75,78] it is worth noting the utilization of the ternary CB8 complexes as supramolecular crosslinks in the fabrication of thermally responsive hydrogels[79] and photo-switchable adhesives.[80]

2.2 Pillar[n]arenes

One of the most recent breakthroughs in the field of host-guest chemistry happened in 2008 when Ogoshi for the first time reported a synthesis of a new pillar-shaped macrocycle—pillar[5]arene (P5A)—by the reaction of 1,4-dimethoxybenzene (DMB) with paraformaldehyde (Scheme 1) in the presence of a Lewis acid in 1,2-dichloroethane (1,2-DCE).[9]

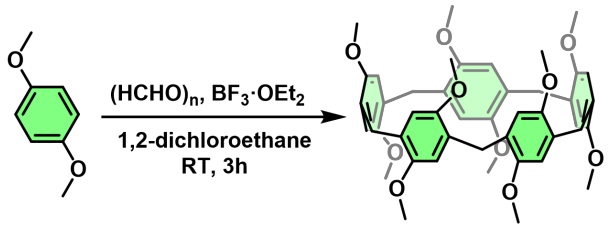

Scheme 1. Original DMP5A synthesis by Ogoshi.[9]

DMP5A as a cyclic pentamer has a highly symmetrical structure resembling a pentagonal cylinder with its 5 sides formed by DMB units connected *via* methylene bridges located in 2- and 5-positions (Figure 2, E; Figure 3, A, B). The inner cavity of the macrocycle is formed by aromatic faces being, therefore, π-electron-rich, and capable to accommodate electron-accepting moieties as guests.[81] Both rims of the DMP5A are composed of 10 (5 per rim) easily modifiable methoxy groups, which determines an outstanding versatility of the host. As pointed out by Ogoshi *et al.*,[10] each of the described features resembles previously discussed macrocycles: structural symmetry is characteristic for CBns; electron-rich cavity is a feature of CnAs; and CDs possess a high number of rim-groups.

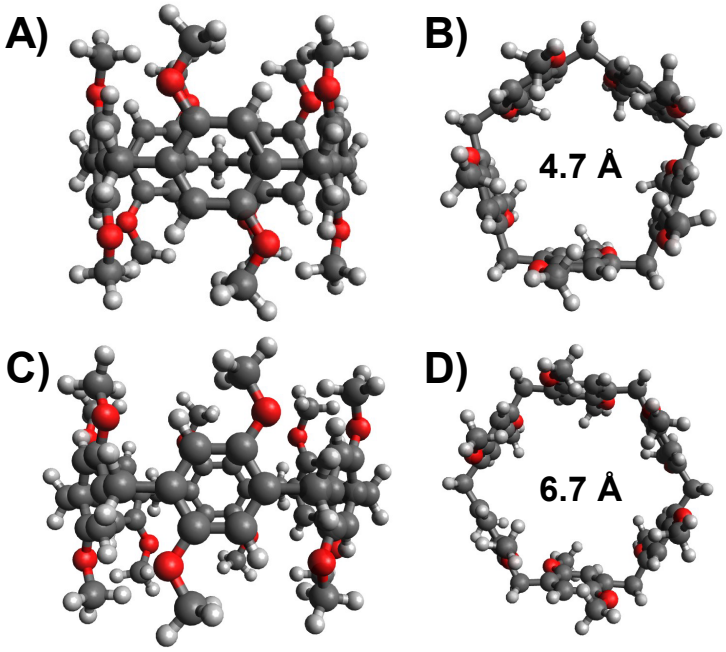

Figure 3. Side and top view of structures of the first two PnA homologues: A), B) P5A; C), D) P6A. Grey, white, and red spheres represent carbon, hydrogen and oxygen atoms, respectively. (The models are based on the data published by Zuilhof et al.[82])

A year after the pentamer, a hexamer, hexagonal pillar[6]arene (P6A, Figure 3, C, D), was synthesized and isolated.[83] Due to its larger (compared to P5A) cavity size, this homologue significantly expanded the horizons of host-guest chemistry of the new macrocycle family. In the following years, homologues with higher number of repeating units (up to 15) were reported,[84,85] however, obtaining them in high yields still remains a challenge.

2.2.1 Synthesis of pillar[n]arenes

As already mentioned, PnAs are obtained, in a general procedure, by reacting equimolar quantities of hydroquinone diether and paraformaldehyde in the presence of a catalyst—a Lewis acid (Scheme 2). Originally, dimethyl-/dialkylethers were used as a repeating unit, however, the scope of the monomers was later significantly expanded onto numerous other ether substrates that do not interfere with Friedel–Crafts alkylation conditions. The cyclooligomerization reaction proceeds as shown in Scheme 3.[86] In the first step, hydroquinone diether **1** reacts with paraformaldehyde **2a** activated by Lewis acid yielding benzyl alcohol **3**. Then, by the elimination of water a benzylic cation **4a** is formed, which reacts with another benzylic alcohol **3** giving a dimer **5**. In the following, the steps of benzyl cation formation/benzyl alcohol addition are repeated until finally the macrocycle **6** is formed.

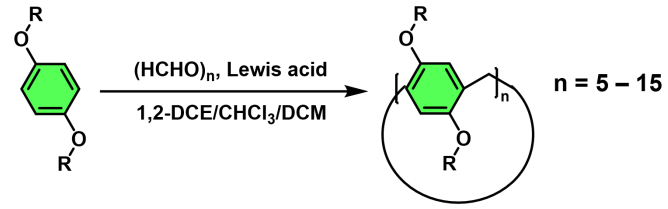

Scheme 2. General synthetic scheme of PnAs.

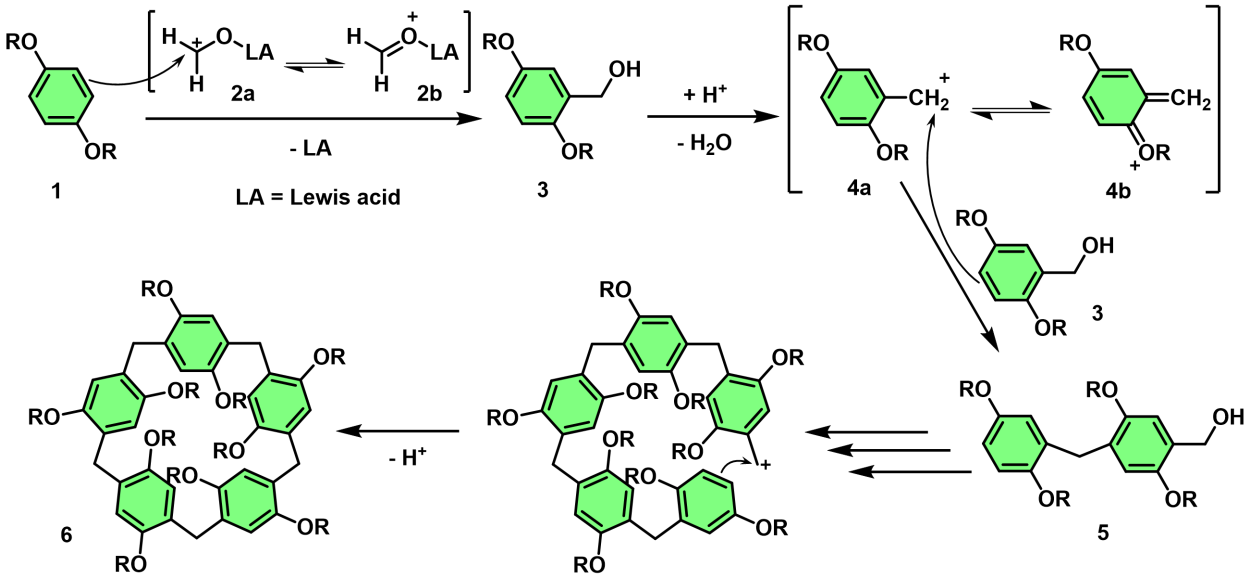

Scheme 3. Friedel-Crafts mechanism of P5A formation (based on Ref. [86])

In order to achieve a selective synthesis of each of the cyclic homologues, and to suppress formation of polymeric by-products, the reaction conditions were meticulously studied and optimized (Table 2).

Formation of the pentamer is conducted under thermodynamic control.[87] Firstly, the solvent has a great impact on the yield of the reaction. As shown by Szumna,[88] a pronounced template effect is observed if 1,2-DCE is used as a solvent for the reaction. Whereas the yields achieved in dichloromethane (DCM) and chloroform only reach 26 % and 15 %, respectively, DCE as a solvent provided 81 % yield of per-methylated P5A due to the geometry of the solvent molecules, which are a perfect fit for the cavity of the P5A and, therefore, act as a template for the macrocycle to form "around" them. Furthermore, the choice of the catalyst was also proven to be crucial for the selectivity of the reaction: under optimized conditions, trifluoromethanesulfonic acid (P5A yield: 66 %[89]) and $BF_3{\cdot}OEt_2$ (71 %[90]) were demonstrated to be among the most effective, however, still being inferior to trifluoroacetic acid (TFA), as proposed in the work of Szumna.[88] Interestingly, conducting the reaction in DCE with TFA as a catalyst not only provides P5A with a very high yield, but is also little moisture-sensitive with the yield dropping to 77 % in the presence of 0.05 M water. Although even higher yield (88 %) was reported for a system proposed by Cao and Meier[91] based on DCM with $FeCl_3$ as Lewis acid, the pathway is not as selective as previously discussed systems.

Table 2. Reported reaction conditions for the synthesis of PnA homologues.

Macrocycle	Solvent	Catalyst	Temperature	Time	Yield	Ref.
P5A	DCM	TFA, 5 vol.%	n/r	2 h	26 %	[88]
	$CHCl_3$	TFA, 5 vol.%	n/r	2 h	15 %	[88]
	1,2-DCE	TFA, 5 vol.%	Reflux	2 h	81 %	[88]
	DCM	TfOH, 5 mol.%	RT	6 h	66 %	[89]
	DCM	TsOH	Reflux	50 h	65 %	[89]
	1,2-DCE	$BF_3{\cdot}OEt_2$	30 °C	30 min	71 %	[90]
	DCM	$FeCl_3$	RT	2–3 h	88 %	[91]
P6A	$CHCl_3$	$FeCl_3$	RT	2–3 h	30–45 %	[91]
	DCM	$[ChCl][FeCl_3]_2$	RT	4 h	53 %	[92]
	MeCN	H_2SO_4, 30 mol.%	RT	5 min	71 %	[86]
	neat	H_2SO_4, 10 mol.%	RT	10 min	84 %	[93]

Selective synthesis of P6A is, however, more challenging. Because of a larger cavity size, the template method in the case of P6A requires use of special agents.[94] So, using chlorocyclohexane as a solvent the group of Ogoshi[95] obtained P6A under thermodynamic control at a high yield (87 %). Noteworthy, by switching the solvent templates the interconversion between P5A and P6A was shown, confirming the proposed reaction control (and proving the dynamicity of the covalent chemistry underlying pillar[n]arenes[96]). More commonly, the synthesis is conducted under kinetic control, with subsequent isolation of the product from the mixture of homologues (P5A is always formed as a by-product in comparable quantities) and linear oligomers.[84] $FeCl_3$ was demonstrated[91] to be the most effective catalyst for the fabrication of P6A in reasonable yields, especially if the reaction is conducted in $CHCl_3$: for various *O*-alkyl-substituted hydroquinones the yield of the hexamer ranged between 30 % and 45 % (with 22–31 % P5A formed). This ratio could be further improved by using a deep eutectic solvent choline chloride–2·$FeCl_3$ as a catalyst.[92,96] Finally, the use of polar solvents (*e.g.*, acetonitrile) as well as solid-state reaction were proven efficient for selective synthesis of P6A.[86,93]

2.2.2 Functionalization

One of the intrinsic features of PnAs that determined the extraordinary rapid development of their chemistry and possible applications is facility of their functionalization. Indeed, the alkyl rim groups can be easily removed and replaced with other functional groups or moieties allowing further modifications *via* Williamson etherification, which results in a vast range of possibilities to tailor their properties such as solubility or molecular recognition.[97–99] In order to achieve a precise control over the properties of PnAs, various protocols were devised that offer mono-, di-, multi- (*e.g.*, rim-differentiated), and per-substitution of the rim alkyl groups (Figure 4). Although solutions were reported for the substitution of phenyl protons of the hydroquinone units[100] as well as at methylene bridges[101], these modification ways will not be covered in the present work.

2.2.2.1 Mono-functionalized pillar[n]arenes

Monosubstitution of PnAs, by which only one of the 10 alkyl groups is replaced with a functional moiety is a promising way of their chemical modification without significant alteration of the host-guest affinity.[97] In 2011, two different approaches were suggested for obtaining mono-functionalized PnAs.

The first approach, co-cyclooligomerization, developed independently by the groups of Huang[102] and Stoddart,[13] implies that the functional group is introduced in the hydroquinone to form a non-symmetric diether before macrocyclization reaction, which is then reacted with an excess (4–16 eq.[103]) of DMB and paraformaldehyde (Scheme 4, route A). This way, groups can be

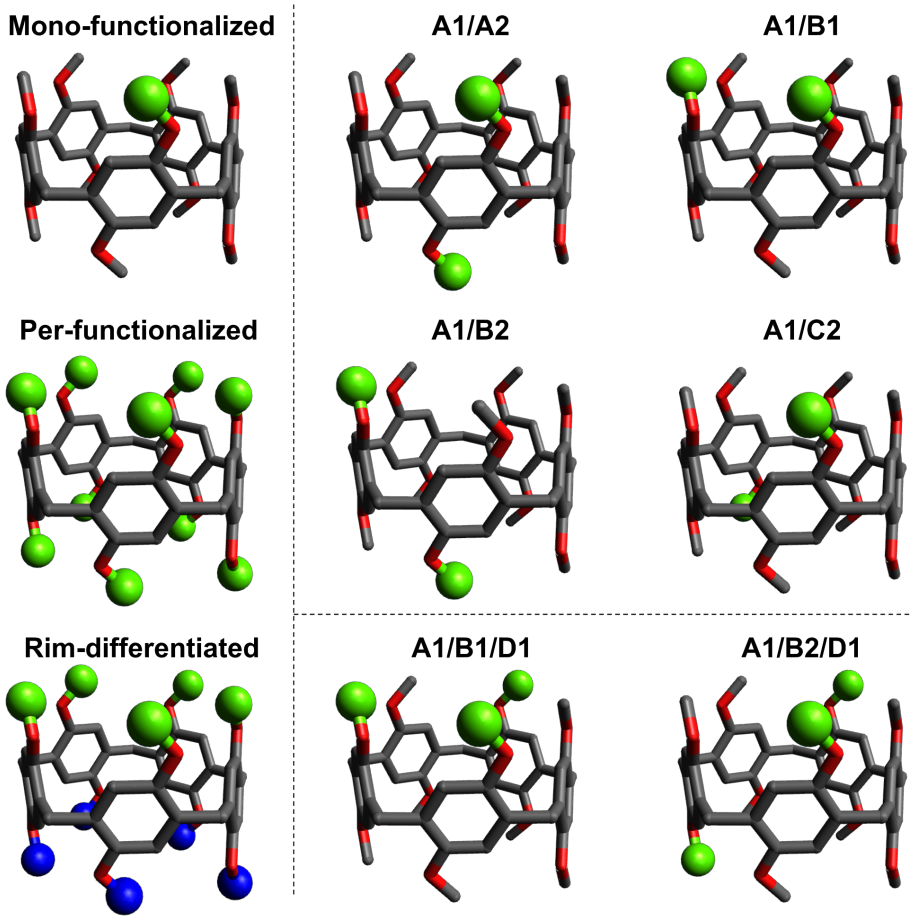

Figure 4. P5A functionalization patterns discussed in the chapter.

incorporated as "side chains" such as bromide or alkyne that can serve as reactive platforms to obtain more complex architectures.[104] For instance, introduction of a UPy group led to a formation of a supramolecular polymer based on orthogonal interactions (charge-transfer host-

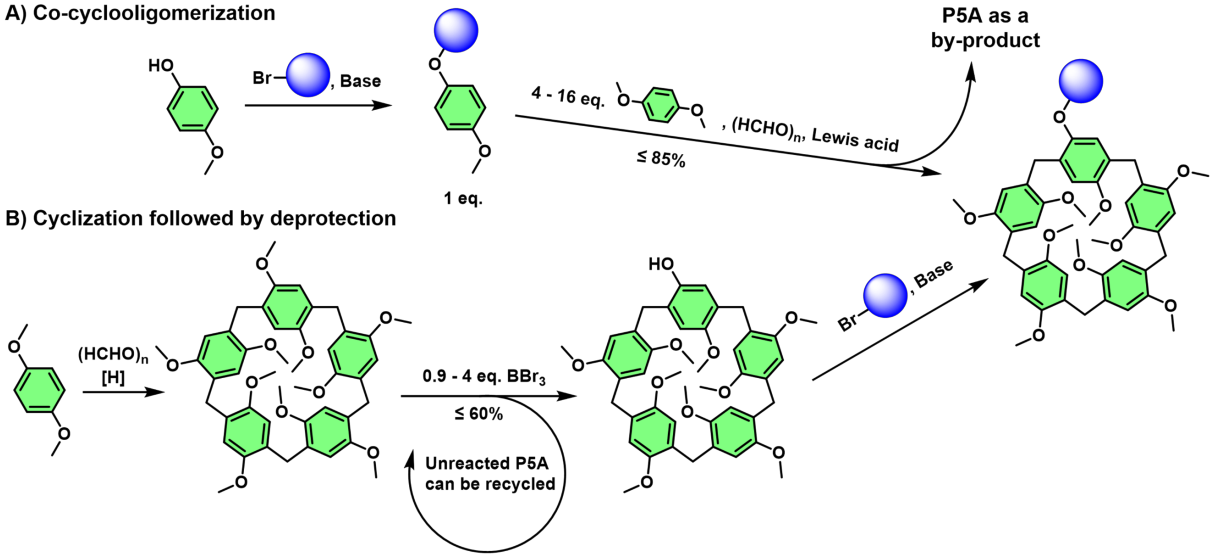

Scheme 4. Synthetic pathways towards monofunctionalized P5A: A) co-cyclooligomerization[13] and B) deprotection of non-functionalized P5A.[107] The shaded sphere represents a functional group.

guest interaction and hydrogen bonding).[105] A P5A-based chain transfer agent for controlled radical polymerization was synthesized by bromide with amine and further reaction with a thiocarbonothioylthio-moiety.[106] Despite relative simplicity, co-cyclooligomerization has a drawback, namely, statistical distribution of products, which indicates that a tedious separation of the product mixture is a defining step. This, in its turn, limits this approach to P5A, since it is the only homologue that can be obtained selectively.

The second approach, mono-de-*O*-methylation, devised by the group of Ogoshi[107] suggests that per-alkyl-PnA without "unique" functional groups is formed in the first step followed by removal of one alkyl group using deficient amount (0.9 eq.) of BBr_3 to form a hydroxyl group, which can be etherified in presence of a suitable base (*e.g.*, K_2CO_3 or NaH) to introduce a functionality onto the macrocycle (Scheme 4, route B). Clearly, the demethylation proceeds in a statistical manner and the desired product must be isolated from the mixture containing unreacted PnA and multi-OH-products. Interestingly, the reaction was later found to proceed under kinetic control and optimized conditions were found affording mono-OH-P5A in a 60 % yield after 1.5 h by using an excess (4 eq.) of BBr_3 at cooling (–8 to –5 °C).[108] Since the substrate for this reaction is a pure PnA, the approach is not limited to one homologue.[109] Moreover, the unreacted substrate can be isolated and re-used for the de-methylation reaction once again, which further increases the conversion, and which is impossible in case of co-cyclooligomerization. Using this approach, Wang's group[110] obtained an acrylate-functionalized P6A, which was co-polymerized with methyl acrylate. By mixing this host-polymer with a ferrocene-containing guest polymer a redox-responsive supramolecular hydrogel was developed.

2.2.2.2 Di- and multisubstitution

Whereas synthesis and isolation of monofunctionalized PnAs can be considered an established procedure, obtaining macrocycles with a higher number of substituents is a challenging task, since because of the high number of possible regioisomers (5 and 10 in case of di- and tri-substituted P5A, respectively[111,112]) complications with product mixture purification arise. Usually, to differentiate between the regioisomers a special nomenclature is used, in which each of the substituents receives a code consisting of a letter A to E (for P5A) referring to a hydroquinone unit and a number 1 to 2 referring to a rim, at which the substituent is located.

A1/A2 isomer (*i.e.*, having two substituents at the same aromatic unit of the macrocycle) is by far the easiest one to fabricate, for which two strategies were developed (Scheme 5). Firstly, the above mentioned co-cyclooligomerization method yields the A1/A2 isomer of P5A if a di-substituted hydroquinone ether is used.[113] This approach proved feasible for fabrication of P5A-based supramolecular polymeric structures and networks.[114,115] In the second approach devised by

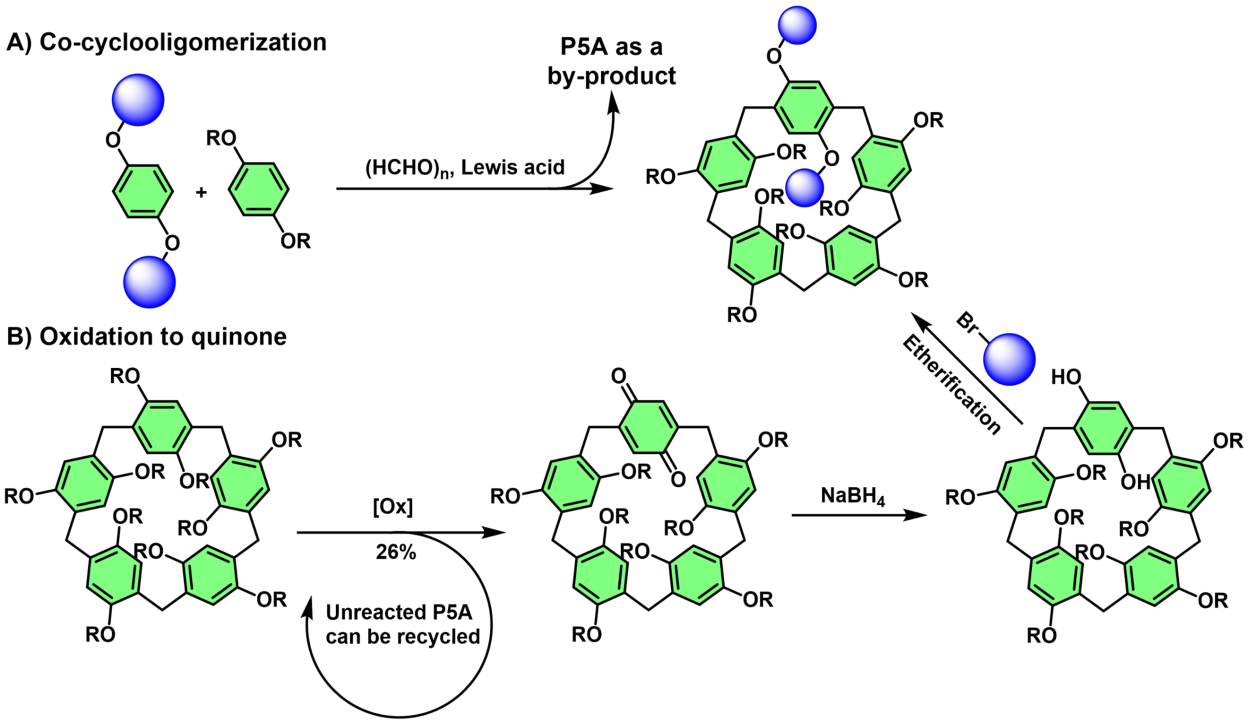

Scheme 5. Pathways towards A1/A2-di-functionalized P5A. A) Co-cyclooligomerization;[113] B) Oxidation–reduction route.[112] R = alkyl chain.

Ogoshi,[112] hydroquinone unites are oxidized to quinone providing two OH-groups at A1/A2 positions of the macrocycle.[116] Noteworthy, unlike co-oligomerization, this strategy is applicable to both P5A and P6A and offers recycling of unreacted PnA.

Despite the complex endeavor, researchers achieved progress in isolating other isomers of di- and trifunctionalized macrocycles. This far, an A1/B2-substituted P5A was selectively obtained by Ogoshi[111] using $AlBr_3$ in a simultaneous cyclization-and-deprotection approach. After a thorough investigation of the kinetics of per-methoxy-P5A deprotection with BBr_3 the Stoddart's group[117] devised a strategy involving deprotection and activation (by modification with triflate groups) steps to isolate several regioisomers from the mixture. The group was able to obtain crystals of A1/B1, A1/B2 and A1/C2 di-modified species as well as A1/B1/D1 and A1/B2/D1 tri-modified isomers (Figure 4).

A special type of multifunctionalized PnA, which is possible to fabricate due to symmetry of the unmodified macrocycle, is rim-differentiated PnA (Scheme 6).[98] Statistically, if a non-symmetric hydroquinone diethers are used for the homo-oligocyclization, only 1/16th part of the P5A macrocycles are in C_5-symmetric conformation (*i.e.*, when each rim contains only substituents of one sort).[118] Despite this fact, a pre-oriented strategy was devised by Sue, Zuilhof and coworkers[119,120] that increases fraction of rim-differentiated P5A up to 56 % with an isolated yield as high as 19 %. When this approach was combined to obtain P5As with substituents exhibiting different susceptibilities towards hydrogenation (like benzyloxy and methoxy groups), a platform

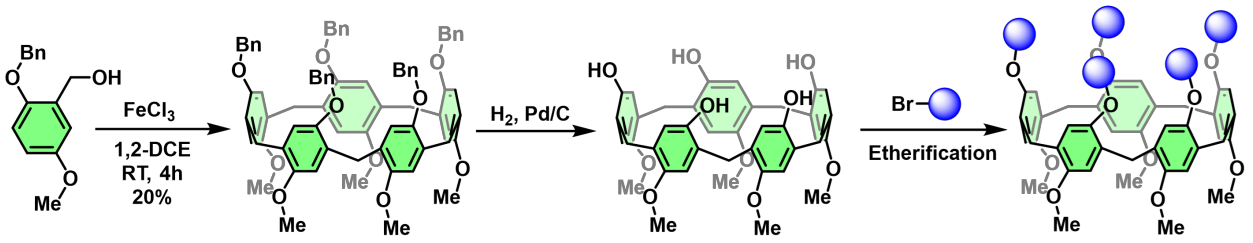

Scheme 6. Fabrication of rim-differentiated P5A by the pre-oriented approach according to Sue, Zuilhof and co-workers.[120] Blue spheres represent functional groups.

was created for fabricating P5As with numerous combinations of functional groups on opposite rims of the macrocycle.

2.2.2.3 Per-functionalized and water-soluble pillar[n]arenes

Finally, one of the most important types of functionalization is the one, by which all the rim groups are substituted with the same functional group (Figure 4). The fact that only one per-functionalized isomer can be obtained renders obtaining such species relatively simple. Similarly to the previously described protocols, two major strategies are applicable for the production of per-functionalized PnAs (Scheme 7): cyclooligomerization of modified hydroquinones, and full dealkylation of alkyl-PnAs followed by etherification.[97]

Following the first approach, a hydroquinone diether is synthesized bearing two modifiable moieties, such as bromide[121,122] (modification by nucleophilic substitution) or alkyne[123,124] (Huisgen-type [2+3]-cycloaddition). Importantly, unlike in case of lower degrees of functionalization, this approach is not restricted to P5A: formation of dodeca-bromoalkyl-P6A was reported in $CHCl_3$ with $FeCl_3$ as Lewis acid.[125] Despite the clear versatility of this method due to

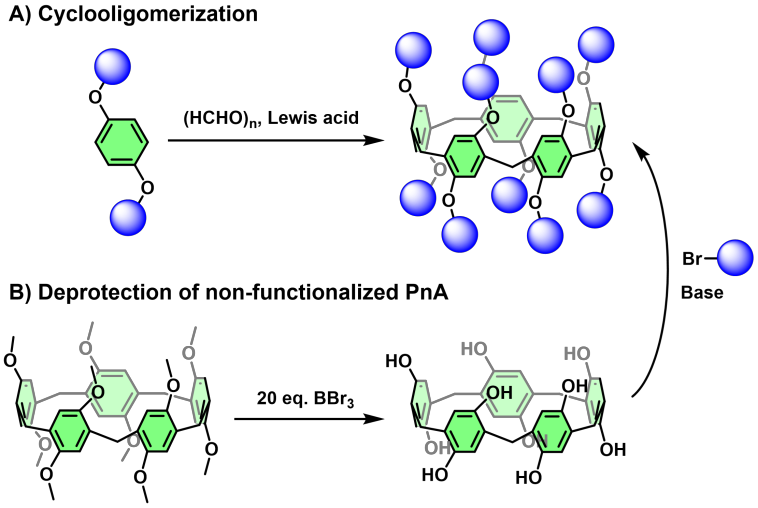

Scheme 7. Synthetic pathways towards per-functionalized PnAs. A) Cyclooligomerization of functionalized hydroquinone ethers; B) Full demethylation of non-functionalized PnA followed by etherification. Blue spheres represent functional groups.

a broad possibilities of further chemical modification, one drawback of it is that it is still limited to the substituents that do not undergo any reactions under Friedel–Crafts alkylation conditions.

The way for the second approach was paved in the seminal work by Ogoshi,[10] in which his group implemented a complete demethylation of per-methoxy-P5A using an excess (20 eq.) of BBr_3. Per-OH-PnA obtained this way serves as an important intermediate for introduction of functional groups, such as carboxylic groups or oligoethyleneglycols.[126,127] Noteworthy, functionalized homologues composed of up to 10 hydroquinone unites were reported to be obtained by this approach.[128]

Investigation of molecular recognition in host–guest complexes in water is essential since biochemical processes take place in aqueous medium, hence, making the estimation of transferability of experimental results onto biological systems more precise. Although pillar[n]arenes are, undoubtedly, highly versatile macrocycles, their poor water-solubility is a major issue for a broad range of biomedical, sensing applications, etc.[129] Therefore, work of many research groups was aimed at synthesizing water-soluble PnA (WSPnA) derivatives (Figure 6). The first ones to reach this milestone were Ogoshi's group[126] who created a deca-carboxylate P5A (Figure 5, A) by reacting per-OH-P5A with ethyl bromoacetate followed by basic hydrolysis and ammonium salt formation. Later using an analogous approach anionic P6As were obtained.[130] Wang's group developed water-soluble P5A and P6A by substituting bromide in per-bromoalkylated macrocycles obtained by cyclooligomerization method by anionic phosphate groups.[131]

Similar strategies were employed to synthesize fully substituted cationic water-soluble pillar[n]arenes (Figure 5, B) with various functional groups, such as quaternary ammonium,[121] pyridinium[132] and imidazolium[133] moieties. Furthermore, as a non-ionic water-soluble P5A

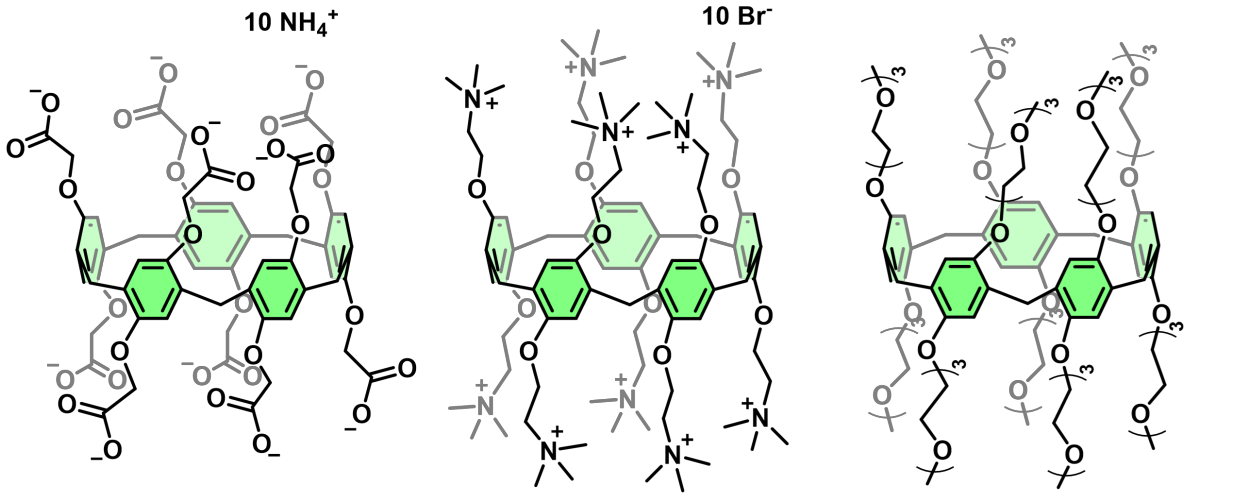

Figure 5. Different types of water-soluble PnAs (examples): A) anionic, B) cationic and C) non-ionic

derivative, per-(triethylene oxide)-P5A (Figure 5, C) was developed showing an LCST behavior that can be tuned by host–guest interactions.[127]

2.2.3 Host–guest properties

As already mentioned, it is a unique combination of different supramolecular interactions that defines the binding affinity between a host and a guest molecule. In the previous chapters it was shown how rich the chemical toolbox is, which allows the researchers to adapt PnA structures for almost any kind of purpose. The main purpose of using a macrocycle is encapsulation of guest molecules, and, therefore, the host properties of PnAs have been extensively investigated and significantly expanded over the past years due to the facility of their functionalization.[10,81,99,134]

2.2.3.1 Features defining affinity towards guest molecules

Generally, there are three features which all PnA homologues and derivatives share that dictate their molecular recognition properties: 1) hydroquinone-constructed walls, which render the cavities highly electron-rich; 2) a cavity size defined by the number of the aromatic monomers, and 3) rim-substituents.

Similarly to other host molecules, the cavity size of PnAs is an intrinsic property of the macrocycle, which not only serves as the upper limit for a guest molecule dimensions but, generally, shows which size would maximize the strength of the interactions inside of the cavity, *i.e.*, which molecule would be a perfect fit. P5A and P6A possess cavities of 4.7–5.5 Å (close to cavity sizes of α-CD and CB6, and alkyl chain thickness) and 6.7–7.5 Å (comparable with γ-CD and CB7), respectively,[135,136] which determines the range of guest moieties capable of being accommodated in the cavities of the two homologues. Whereas P5A is affine to such moieties like linear alkanes,[137] (charged) amines,[113] five-membered cyclic groups[138] and (charged) pyridine,[139] P6A can engulf bulkier entities like branched alkanes,[140] aromatics,[141] adamantane[142] and ferrocene.[109]

The increased electron density within PnA cavities implies that electron-accepting moieties can be beneficial for inclusion complexes relying on charge transfer or electrostatic interactions. This group of guest moieties include, for instance, positively charged amines and heterocycles.[9,143,144] Further, the aromatic ring enables formation of a special type of hydrogen bonds, namely, C – H···π,[145] which can also play a role due to a multiplicity of the hydroquinone units. Such hydrogen bond is considered for a current host–guest pair if the distance between a hydrogen atom and a π-plane is less than 3.05 Å.[10] This is the reason for a good affinity to alkyl-substituted guest molecules.[137,146] Importantly, binding affinity can be additionally increased by introducing

electron-withdrawing end-groups to the alkyl chain. However, complexes with aldehydes, ketones and esters were shown to be rather unstable.[147]

In addition to the above-mentioned features that lie, literally, in the core of PnA–guest interactions, rim-groups have, clearly, a pronounced effect on the molecular recognition properties by accommodating the end-groups of guest molecules. As an example of their influence on inclusion complex formation, it was shown that a rim-differentiated P5A containing 5 methoxy and 5 pentoxy group on its opposite rims forms regioselective complexes with non-symmetrical guests.[148] 1-bromo-4-cyanobutane was oriented in the cavity in the way of CN-group facing the methoxy rim and bromine facing the pentoxy one due to preferrable interactions.

The cooperativity between all three features is what determines the manifold of precise inclusion complexation patterns of PnAs emerged rapidly since their first discovery. In the following, several examples will be discussed highlighting the influence of these features.

2.2.3.2 Complexes of neutral PnAs with neutral guest molecules

Li and co-workers conducted an extensive research on PnA-based inclusion complexes having investigated a broad range of various guest molecules interacting with PnAs.[81] In the course of their studies it was found that one of the strongest binding affinities to P5A is exhibited by alkane dinitriles[11] (Table 3). The complexes of per-methoxy- and per-ethoxy-P5A with succinonitrile and adiponitrile (AN) in $CDCl_3$ demonstrated such a high stability that on NMR spectra no free host is present in the system at host:guest ratios < 1 and no free guest at ratios > 1 (according to the condition (15), Chapter 2.4.2), which suggests $K_a > 10^5$. Such a strong binding affinity was explained by a cooperative action of multiple C–H···π and C–H···O bonds, which are more polarized due to the electron-withdrawing cyano groups, as well as interactions of the CN groups with alkoxy rim groups *via* C–H···N bonds. The effect of the third type of interactions was proven by using mono-nitrile 1-cyanobutane, whose affinity appeared to be at least 3 orders of magnitude lower (K_a = 400 M^{-1}).

Table 3. Binding affinities of PnA complexes with aliphatic and aromatic (di-)nitriles obtained by NMR.

Host	Guest	Solvent	Exchange	K_a, M^{-1}	Ref.
Per-EtO-P5A	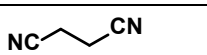	$CDCl_3$	Slow	>> 10^4	[11]
	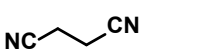	DMSO-d_6/$CDCl_3$ (1:9, v/v)	Slow	>> 10^4	[11]
	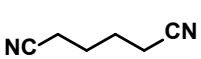	$CDCl_3$	Slow	>> 10^4	[11]
	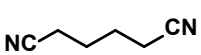	DMSO-d_6/$CDCl_3$ (1:9, v/v)	Slow	1.5×10^4	[11]

Host	Guest	Solvent	Exchange	K_a, M^{-1}	Ref.
	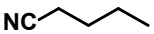	$CDCl_3$	Fast	400	[11]
	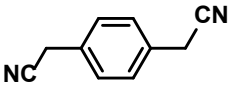	DMSO-d_6/$CDCl_3$ (1:9, v/v)	—	—	[11]
Per-MeO-P5A	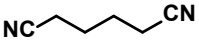	DMSO-d_6/$CDCl_3$ (1:9, v/v)	Slow	2.4×10^4	[11]
Per-EtO-P6A	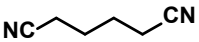	$CDCl_3$	Fast	9.5	[141]
	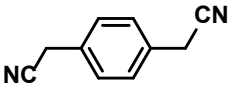	$CDCl_3$	Fast	41	[141]

As already mentioned, linear alkane chains fit perfectly into the cavity of P5A, which maximizes the interaction between the host and the guest. A benzene ring, however, is too bulky to fit inside, therefore, no interaction with P5A was observed for a 1,4-bis(cyanomethyl)benzene. In contrast to P5A-based complexes, host-guest interactions with P6A demonstrated opposing trend and generally significantly weaker affinity.[141] In $CDCl_3$, from the investigated aliphatic dinitriles only AN demonstrated somewhat quantifiable binding strength ($K_a = 9.5\ M^{-1}$). This value was around 4 times smaller than the affinity of 1,4-bis(cyanomethyl)benzene that proved to form the most stable complexes with P6A ($K_a = 41\ M^{-1}$) of all nitriles under investigation. The reason for such a dramatic difference of the interactions of alkane dinitriles with P5A is the larger cavity of P6A, which does not provide an optimal engulfing of the aliphatic chains leading to a reduction of the hydrogen bonds number. Aromatic rings, on the contrary, are a better match for the cavity dimensions; the complex is, therefore, stabilized by 4 different types of hydrogen bonds: C–H···N, C–H···O, $C–H^{guest}\cdots\pi^{host}$ and $C–H^{host}\cdots\pi^{guest}$, as shown by X-ray crystallography.

The same interactions are responsible for effective complexation between P5A and guest species containing neutral heterocyclic substituents. Li and co-workers demonstrated (Table 4) that alkane chains with heterocyclic end-groups (imidazoles and triazoles) are capable of binding to a per-alkoxy-P5A with association constants reaching $K_a > 10^4$.[138,149] The highest K_a values were achieved with 1,4-bis(1,2,3-trazol-1-yl)butane and 1,4-bis(imidazol-1-yl)butane as guest species ($1.6\times10^4\ M^{-1}$ and $2.0\times10^4\ M^{-1}$, respectively), which were by 2 order of magnitude higher than in case of corresponding guests with only one heterocyclic substituent. According to the reported results, formation of, firstly, C–H···O bonds between guests' hydrogen atoms and P5A's oxygen atoms on the rim, and, secondly, C–H···N hydrogen bonds between the nitrogen-containing end-groups and alkyl rim-groups plays a crucial role in stabilizing the complex. The former type determined the highest affinity of the bis(imidazole)-substituted guest: three such hydrogen bonds

are formed compared to one in case of the bis(triazole)-substituted species. C–H···N bonds define that the presence of an "outer" nitrogen atom endowed the complexes with higher stability through more efficient interaction with the rim groups: *e.g.*, the binding affinity of 1,4-bis(1,2,3-trazol-2-yl)butane to P5A was by 3 orders of magnitude lower, $K_a = 11\ M^{-1}$. This was additionally proved by studying complexes of 1,4-bis(1,2,4-triazol-1-yl)butane with P5A containing butoxy, ethoxy and methoxy rim-groups. Per-methoxy-P5A demonstrated up to 6.1 times lower binding affinity than the other macrocycles, thus, establishing the influence of the rim groups on the inclusion complex stability.

Table 4. Binding affinities of P5As complexes with aliphatic guests bearing neutral heterocyclic groups obtained by NMR.

Host	Guest	Solvent	Exchange	K_a, M^{-1}	Ref.
Per-EtO-P5A	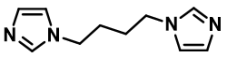	$CDCl_3$	Slow	2.0×10^4	[149]
	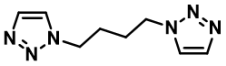	$CDCl_3$	Slow	1.6×10^4	[138]
	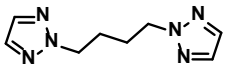	$CDCl_3$	Fast	11	[138]
		$CDCl_3$	Slow	6.6×10^3	[138]
	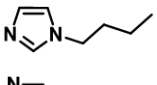	$CDCl_3$	Fast	240	[149]
	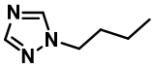	$CDCl_3$	Fast	100	[138]
Per-MeO-P5A	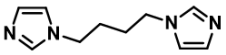	$CDCl_3$	Slow	4.7×10^3	[149]
	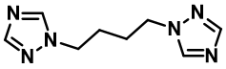	$CDCl_3$	Slow	1.2×10^3	[138]

The rim-groups effect can be highlighted further by alkane diamines complexation (Table 5). Stoddart's group[13] studied inclusion complex formation between per-methoxy-P5A and 1,8-diaminooctane. However, because the binding predominantly relied on the C–H···π interactions, the complex stability in $CDCl_3$was reported to be relatively weak: $K_a = 70\ M^{-1}$. Li and co-workers[123] modified the macrocycle by decorating it with ten 1,2,3-triazole groups around its portals. As a result, a drastic increase of the binding affinity occurred by 2 orders of magnitude ($K_a = 2.6\times10^3\ M^{-1}$ for the same guest and $9.0\times10^3\ M^{-1}$ for 1,4-diaminobutane), which is considered to be due to formation of stabilizing C–H···N and N–H···N hydrogen bonds between the guests' end groups and the triazole moieties.

Table 5. Comparison of binding affinities of 1,8-diaminooctane with P5A bearing various rim substituents.

Guest	P5A substituents	Solvent	Method	K_a, M^{-1}	Ref.
1,8-diamino-octane 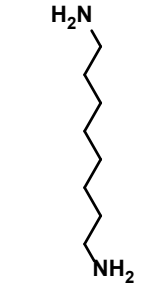	10× 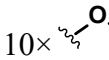	$CDCl_3$	NMR	70	[13]
	10× 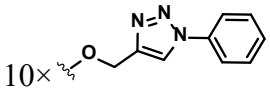	$CDCl_3$	NMR	2.6×10^3	[123]
	8× 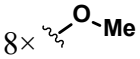 2× 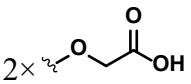	$CHCl_3$/MeOH (1:1, v/v)	ITC	2.89×10^5	[116]
	10× 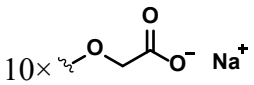	Na phosphate buffer	ITC	3.0×10^7	[150]

2.2.3.3 Complexes of neutral PnAs with charged guest molecules

The high electron density inside of the cavity of PnAs allows formation of electrostatic cation–π bonds. Since this type of supramolecular interactions is characterized by a higher energy than hydrogen bond or hydrophobic interactions (Chapters 2.1.3 and 2.1.4), it is expected that inclusion complexes with positively charged species would exhibit better stability, *i.e.*, higher association constants.

One of the prominent examples of the cationic organic molecules viologens (Table 6), or quaternary bipyridinium salts, which due to their dicationic nature can form strong electrostatic bonds. First reported in the seminal work by Ogoshi,[9] the inclusion complex formation between viologens and per-hydroxy-P5A was further developed by the group of Li.[143] It was shown that charge transfer occurred upon complexation with a characteristic absorption UV/Vis band at 450 nm. The inclusion complex in methanol was proven to be highly stable with K_a exceeding 10^4 M^{-1}. Even stronger binding was demonstrated by Huang and co-workers[151] for paraquat (or methyl viologen) with per-(ethylene oxide)-substituted P5A in acetonitrile: $K_a = 3.35\times10^4$ M^{-1} (Table 6), the key for the stability being a combined strength of multiple hydrogen bonds (in a similar fashion as discussed above) and a π–π stacking interaction inside of the P5A cavity. Noteworthy, the binding strength of the host and guest moieties was controlled by redox stimulus: reduction of paraquat dication by Zn powder led to the decrease in binding affinity to the point of complete decomplexation (as proved by NMR spectroscopy), afterwards, the system was brought to the bound state upon exposure to the air oxygen.

Table 6. Binding affinities of selected PnA–charged guest complexes.

Host	Guest	Solvent	Method	K_a, M^{-1}	Ref.
Per-OH-P5A	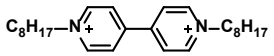	MeOH	Fluorescence	1.2×10^4	[9]
Per-(ethylene oxide)-P5A	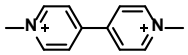	MeCN	ITC	3.35×10^4	[151]
	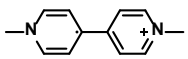	MeCN	—	—	[151]
Mono-carbazole-undecabutoxy-P6A	Ferrocenium (Fc^{+})	$CHCl_3$/MeCN (5:1, v/v)	Fluorescence	2.0×10^4	[109]
Per-butoxy-P6A	Ferrocene (Fc)	$CDCl_3$/CD_3CN (5:1, v/v)	NMR	18	[109]

Analogous stimuli responsiveness was reported by Wang's group[109] for the complex of ferrocenium cation with per-butoxy-P6A. Whereas the oxidated form (Fc^{+}) exhibited pronounced affinity towards P6A ($K_a = 2\times10^4\ M^{-1}$ for the complex with mono-carbazole-substituted P6A, Table 6), the affinity of its reduced form (Fc) was over 1000 times lower ($18\ M^{-1}$). Such redox-responsiveness of the complex Fc^{+}@P6A was further employed by the same group for the formation of a supramolecular gel capable of switching between sol and gel states on demand.[110] This behavior is, in fact, reciprocal to the system $Fc^{(+)}$–β-CD, which exists in a bound state in a solution with the reduced form of Fc.[152]

2.2.3.4 Complexes of charged and water-soluble PnAs with ionogenic and charged guest molecules

Decorating the macrocycle with ionogenic/ionic rim-groups inevitably leads to a further increase in the binding affinity, especially in the case of oppositely charged host and guest molecules. Previously it was mentioned that a P5A macrocycle containing 10 1,2,3-triazole groups on its rims was reported to form stable complexes with alkane diamines ($K_a \leq 9\times10^3\ M^{-1}$).[123] Introducing just two carboxylic moieties into the A1/A2 positions of the macrocycle enabled ionic interaction/proton transfer formation between the rim groups and the amino end-groups of the alkane diamines. As a result, all homologues from pentane diamine to decane diamine were reported to exhibit association strength in the range $K_a = (2–3.5)\times10^5\ M^{-1}$ in the system chloroform–methanol[116] (Table 5).

Further improvement of the complex stability can be achieved if more ionic groups are introduced onto the rims, therefore, implying that in the systems with per-functionalized WSPnAs and ionogenic guest moieties the equilibrium might be shifted towards the complex formation even

further. The group of Ma[150] investigated the interactions between Na salts of 5, 6 and 7-membered per-carboxylic-PnAs (Table 7) with various dyes, alkyl-, and arylamines in aqueous medium (sodium phosphate buffer). The influence of three binding modes on the stability of the complexes was evaluated in their study—electrostatic forces, hydrophobic interactions, and π–π stacking—which was found to decrease in this row. The factor that affects the stability the most was the matching encapsulated guest length to the distance between the carboxylic groups on the opposite portals (9.8 Å). It was demonstrated that linear octane diamine with a chain length of 11.2 Å, that was the closest match of all investigated homologues for the cavity length, also exhibited the highest binding affinity (3.0×10^7 and 4.8×10^7 M^{-1} for WSP5A and WSP6A, respectively), which was a further stability improvement by 2 orders of magnitude compared to the complexes with the same guests discussed above (Table 5). Spermine as an example of naturally occurring (poly) alkyl amines was also investigated in the course of the study regarding its affinity. K_a value was increasing with the increasing cavity size from 2.7×10^6 (WSP5A) to 1.9×10^7 M^{-1} (WSP7A), which can be explained by the size matching effect: with 12-atomic chain between the two NH_2 end-groups spermine is longer than the optimum (8 atoms), therefore, a perfect size match can be achieved, for instance, by taking coiled conformation. Since the cavity of WSP7A is the most spacious, it offers the most volume for coiling and, hence, maximization of interactions between host and guest. These values are, however, still lower than the K_a reported for the ammonium salt of WSP6A: 2.58×10^7 M^{-1}.[153] Finally, to ultimately highlight the dominating character of electrostatic interaction contribution to the complex stability, the authors used ethylene bis(*N*-methylpyridinium) moiety as a guest species. Due to two positively charged pyridinium faces (analogous to paraquat cation) and the ethylene linker between them to match the cavity size this dication was demonstrated to form an outstandingly stable inclusion complex with WSP7A: $K_a = 3.8\times10^{11}$ M^{-1}, which is the highest-reported association constant value for a PnA complex.

Table 7. Binding affinities of water-soluble PnAs with various ionogenic guest molecules.

Host, counter-ion	Guest	Solvent	Method	K_a, M^{-1}	Ref.
WSP5A, Na^+	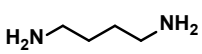	Na phosphate buffer	Dye displacement	6.3×10^5	[150]
	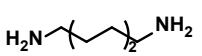	Na phosphate buffer	Dye displacement	1.8×10^6	[150]
	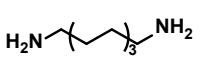	Na phosphate buffer	Dye displacement	1.1×10^7	[150]
	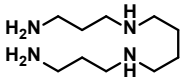	Na phosphate buffer	Dye displacement	2.7×10^6	[150]

Host, counter-ion	Guest	Solvent	Method	K_a, M^{-1}	Ref.
WSP6A, Na^+	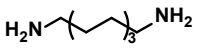	Na phosphate buffer	Dye displacement	1.5×10^7	[150]
	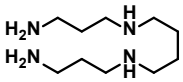	Na phosphate buffer	Dye displacement	3.8×10^6	[150]
WSP7A, Na^+	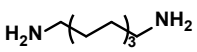	Na phosphate buffer	Dye displacement	4.7×10^6	[150]
	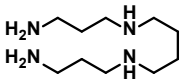	Na phosphate buffer	ITC	1.9×10^7	[150]
	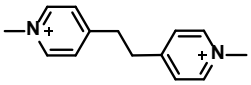	Na phosphate buffer	Indicator displacement	3.8×10^{11}	[150]
WSP6A, NH_4^+	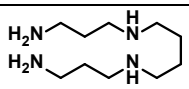	Phosphate buffer	ITC	2.58×10^7	[153]
WSP5A, NH_4^+	Arginine	D_2O	NMR	5.9×10^3	[154]
	Lysine	D_2O	NMR	1.8×10^3	[154]
	Histidine	D_2O	NMR	1.5×10^3	[154]

Furthermore, due to the efficient complexation of anionic WSP5A with organic amines, it can serve as a molecular receptor for basic amino acids lysine, arginine, and histidine. As demonstrated by Li, Jia and co-workers[154] (Table 7), due to the charge delocalization at the guanidine fragment, arginine exhibits the highest binding affinity ($K_a = 5.9\times10^3$ M^{-1}), which by more than 3 times exceed that of lysine and histidine ($K_a = 1.8\times10^3$ and 1.5×10^3 M^{-1}, respectively). None of the other naturally occurring amino acids (neutral and acidic) showed affinity to the host implying the electrostatic interactions between amino and carboxylate to be the driving force for the complexation.

Lastly, inclusion complex formation with acids can be enabled by functionalization of the macrocycle with cationic moieties. As an example, the combination of electrostatic and hydrophobic interactions provided a highly stable ($K_a = 1.33\times10^4$ M^{-1}) host–guest complex between cationic P5A decorated with 10 quaternary ammonium groups and sodium 1-octanesulfonate in water.[121]

2.3 Smart gels

2.3.1 Polymers and polymerization

Macromolecular chemistry was born in the works of Hermann Staudinger, who could demonstrate the existence of polymers—molecules of a very high molecular weight consisting of a high number of repeating units.[155]

Monomers can be reacted with each other to obtain macromolecules in the process of polymerization (Figure 6), which can be conducted as a chain reaction or in a stepwise manner.[156] Unlike small molecule synthesis, polymerization is an inherently statistical process, therefore, one of the crucial challenges is to find ways to control this process in order to obtain products with tailored structure and, hence, properties. Major breakthroughs in this field were achieved in the last decades with the introduction of controlled polymerization protocols such as atom-transfer radical polymerization (ATRP)[157] or reversible addition−fragmentation chain-transfer polymerization (RAFT).[158,159]

Since their discovery, polymer chemistry has not only been firmly established as a scientific branch.[160] Over time, polymers of various origins, both natural and synthetic, became one of the most important industrial products due to their unique properties as materials, such as light-weight, fatigue resistance, inertness, elasticity, insulation, *etc*.[161]

2.3.2 Chemical and physical crosslinking

Crosslinking is one of the common ways to chemically alter the properties of the polymeric materials, in which polymer chains are bound together forming a three-dimensional network. Hence, if placed into a solvent, a crosslinked polymer can only swell without dissolving. Such system consisting of a spatial network and a liquid phase confined inside it, is called gel.[1,8] Usually, one discriminates between hydrogels, if an aqueous solution is used as a liquid phase, and organogels, if an organic solvent is used.

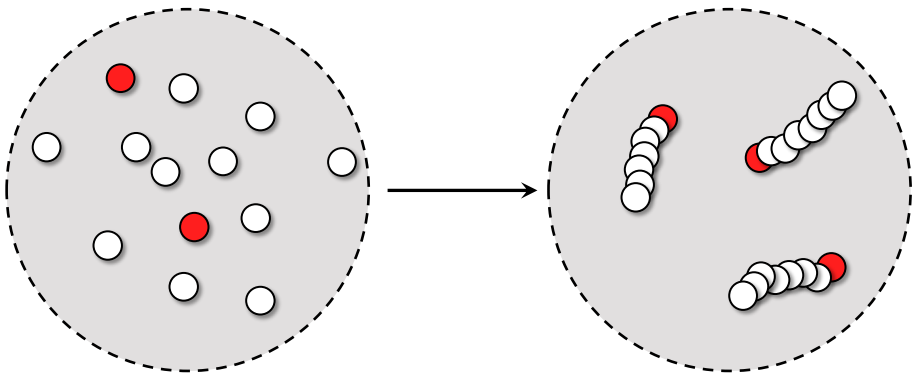

Figure 6. Schematic image of a polymerization reaction. The monomer units (white circles) are combined into long-chain molecules upon activation of the initiator (red circles).

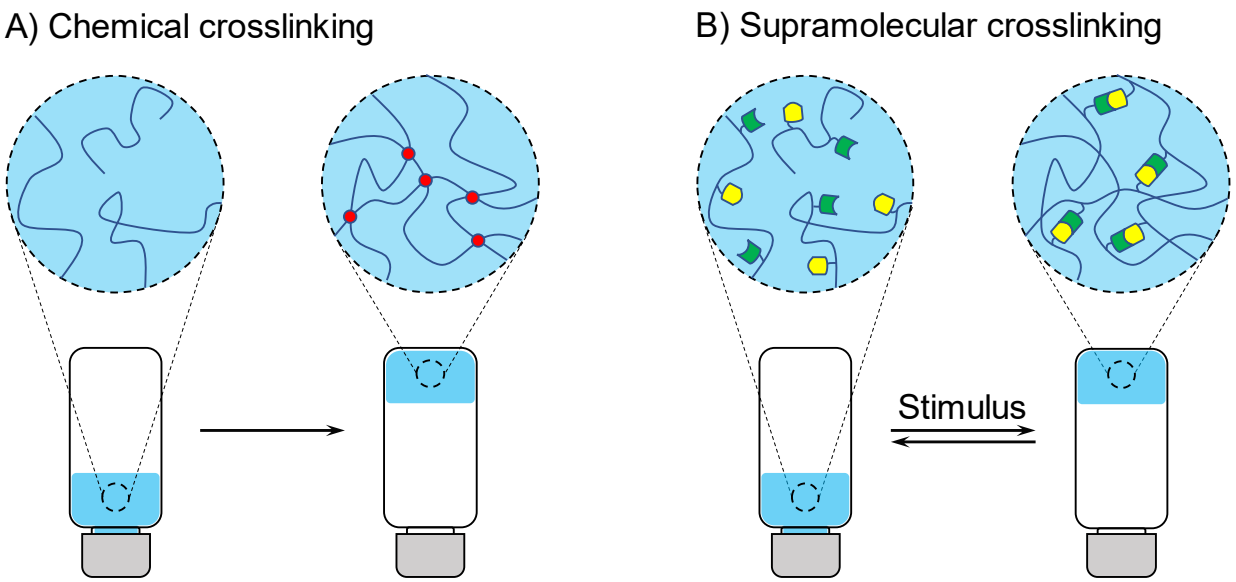

Figure 7. Two different types of crosslinking: A) Chemical (irreversible) crosslinking; B) Supramolecular (reversible) crosslinking. The latter type is reversible under action of a stimulus.

It is curious that crosslinking approach had been known and applied for polymer modification before the Staudinger's works on macromolecules: in 1830–40s rubber vulcanization by reacting with sulfur was discovered by Charles Goodyear, which paved the way for the production of elastic and durable tires.[162] This was one of the first examples of chemical crosslinking, *i.e.*, when the polymer chains are connected by covalent bonds (Figure 7, A). This way, mechanical properties of the networks can be tailored by adjusting the concentration and the nature of a crosslinking agent. As was discussed earlier in Chapter 2.1.1, these bonds are highly stable in a wide range of conditions, which leads to covalently crosslinked polymeric networks exhibiting improved mechanical properties at the expense of irreversibility.[163,164]

Polymer chains can as well be bound by non-covalent, supramolecular bonds, thus introducing reversible physical crosslinks into the networks (Figure 7, B), which renders materials susceptible to the surrounding environment.[165] The behavior of a system, at which the system changes its properties under the influence of an external stimulus, is known as stimuli-responsiveness.[2,166] The reversible networks with supramolecular crosslinks are often called "smart" gels due to their inherently stimuli-responsive nature and ability to undergo macroscopic changes in their properties upon controlled application of external triggers such as pH, temperature, light, oxidation/reduction, or chemical composition of the medium.[3,167]

Over the years, numerous architectures were implemented for the construction of smart gels, which involve different types of supramolecular bonds as crosslinks, and the choice of an interaction type is heavily influenced by the desired gel properties as well as the application area with an arsenal

of possible triggers.[168] Selected examples of responsive materials containing various supramolecular crosslink types and employed in various fields are presented in Table 8.

Table 8. Selected stimuli-responsive supramolecular gels with various crosslink types.

Supramolecular crosslink type	Stimulus	Property change	Application	Ref.
Metal–ligand complexes	Redox	Sol–gel transition	—	[21]
	Temperature, shear stress	Sol–gel transition	Self-healing materials	[169]
Hydrogen bonds	Temperature	Increased chain mobility	Ultra-tough, self-healable materials	[170]
	Temperature, humidity	Surface energy	Adhesives	[171]
Host–guest interactions	Redox	Sol–gel transition	Self-healing materials	[172]
	UV	Sol–gel transition	Drug delivery	[173]
	Redox, competitive guest	Sol–gel transition	—	[174]
Hydrophobic interactions	Temperature	Sol–gel transition	Drug delivery, tissue engineering*	[175]
	Temperature	Sol–gel transition	Injectables, drug delivery	[176]

*Suggested by authors

2.3.3 Dually crosslinked gels

One remarkable point about the supramolecular gels summarized in Table 8 and simultaneously one of the main limitations is that the property change observed in response to an external stimulus is almost exclusively a sol–gel transition, which implies that such responsive system loses all of its mechanical properties by turning into sol, therefore, becoming virtually useless as a material. On the other hand, from the practical point of view, it is beneficial to possibly combine different properties in a single "multitalented" material, such as: high toughness and self-healing ability, flexibility and chemosensitivity, high elastic modulus and degradability, multi-shape memory. To challenge this, materials with a higher level of complexity are required. One of the ways[177] to devise such versatile materials is *via* introducing a second crosslink into the system, thus, obtaining dually crosslinked single gels.[4] Based on the nature of crosslinks, three different categories of

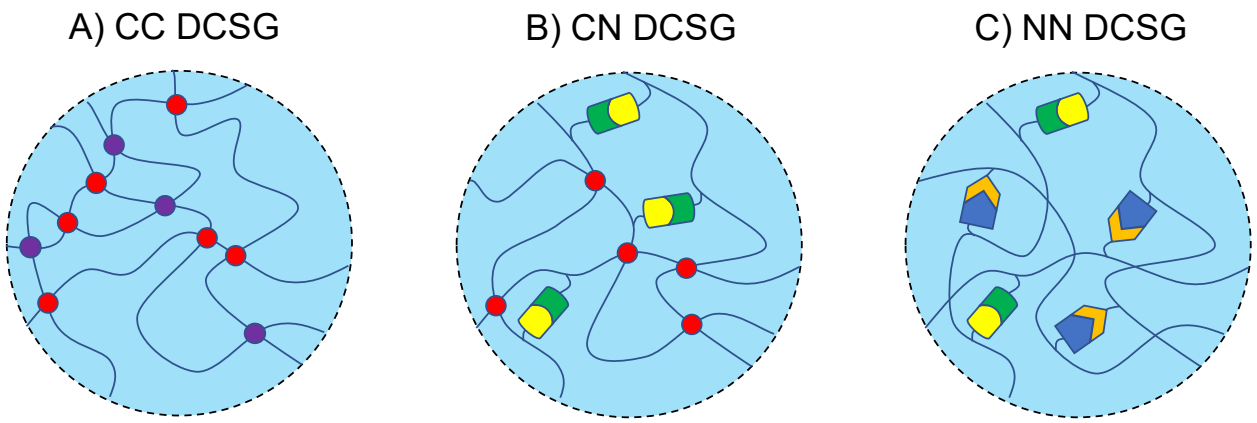

Figure 8. Types of dually crosslinked architectures: A) Covalent-covalent gel; B) covalent-non-covalent gel; C) non-covalent-non-covalent gel.

DCSG can be implemented: covalent-covalent (CC), covalent-non-covalent (CN) and non-covalent-non-covalent (NN) systems (Figure 8).

2.3.3.1 Covalent-covalent dually crosslinked gels

The gels from the first category, in which two different types of covalent crosslinks are utilized to achieve a polymer network, are mostly designed to improve mechanical properties compared to gels with only one crosslink type. For instance, cellulose was crosslinked with epichlorohydrin and PEG-diglycidyl ether to obtain short and rigid bonds with the former and long and flexible bonds with the latter crosslink.[163] This endowed the hydrogel with greatly increased strength at stretching and at compression (by 26 and 84 times, respectively) in comparison with the cellulose crosslinked only with epichlorohydrin. A gel layer with two-dimensional network density gradient was devised[178] by employing a terpolymer with two of the comonomers susceptible to two different stimuli—light (photo responsive methacrylyloxybenzophenone) and temperature (thermally responsive styrene sulfonyl azide). The authors demonstrated that the swelling ratio in such gradient network varies in both dimensions.

Despite the advantages in mechanical performance, dual covalent networks exhibit the same disadvantages as gels with a single type of covalent crosslinks, namely, lack of reversibility and adaptability.

2.3.3.2 Dually crosslinked gels with non-covalent linkages

Incorporation of supramolecular bonds as crosslinks between polymer chains renders smart, dynamic, and adaptable systems.[4] Generally, both CN and NN networks possess properties characteristic for physically crosslinked systems, such as stimuli responsiveness and self-healing ability. Moreover, reversible bonds often contribute to the improvement of their mechanical properties in two ways: firstly, by increasing the crosslink density; secondly, by acting as

"sacrificial bonds", *i.e.*, providing a pathway for energy dissipation while being under mechanical stress.[179] This results in materials with outstanding toughness and reversibility.[27,180]

CN DCSGs uniquely combine one reversible and one irreversible crosslink, which results in materials that are simultaneously mechanically strong and dynamic.[4] The amalgamation of responsiveness (due to the physical bonds) with stability of the network (due to the chemical bonds) yields reusability—the property anticipated for numerous applications (Table 9).

Introduction of a second supramolecular crosslink into the material leads to double or, in some cases, multiple stimuli-responsiveness. NN DCSGs are fully reversible implying arguably lesser stability and, therefore, usually inferior mechanical performance. This disadvantage is compensated by enhanced resistance to fatigue and total recoverability and self-healing ability owing to the dynamic nature of both constituting crosslinks. In addition, if a network is assembled *via* a pair of linkages susceptible to stimuli, which do not affect the other one in the pair (*i.e.*, orthogonal stimuli responsiveness[181]), such design can pave the way to (multi-)shape-memory materials.[4]

Various combinations of covalently and/or non-covalently crosslinked DCSGs with respect to their applications are presented in Table 9.

Table 9. Selected DCSGs with at least one reversible crosslink type and their applications published in literature.

Crosslink 1	Crosslink 2	Application	Particularity	Ref.
CN DCSGs				
Covalent (norbornene)	Host–guest (α-CD–azobenzene)	Drug delivery	Burst release of a drug upon UV exposure	[182]
Covalent (thiol–ene)	Host–guest (β-CD–adamantane)	Injectables, tissue engineering	Covalent crosslink is promoted *in vivo* after injection	[183]
Covalent (thiol–ene)	Hydrophobic	Injectable gels	Covalent crosslink is promoted *in vivo* after injection	[34]
Covalent (MBA)	Ionic interactions	Self-healing materials	Recovery of > 99 % of tensile strain and > 92 % of tensile strength within 20 h	[184]
Covalent (MBA)	H-bonds (tannic acid–alcohol/amide)	Self-healing materials, adhesives	Recovery up to 58 % strain and up to 40 % stress; adhesion to materials of diverse nature	[185]
Covalent (divinylbenzene)	Host–guest (β-CD–Fc)	Adhesives	Switching adhesion on/off by redox or electrical current	[186]

Crosslink 1	Crosslink 2	Application	Particularity	Ref.
Covalent (MBA)	Hydrophobic interactions	Shape-memory materials	Multi shape memory	[187]
Covalent (MBA/PEG diacrylate)	H-Bond (Glycinamide)	Shape-memory materials	Triple shape memory	[188]
Covalent (MBA)	Host–guest (β-CD–Fc)	Actuators	Different shapes of assemblies *via* mechanical stresses between parts	[189]
Covalent	H-bond (DMAAm–AAc)	Actuators	Time-dependent relaxation of different parts of an assembly	[190]
Covalent (DMIEA dimers)	Host–guest (β-CD–Fc)	Sensors	Ovarian cancer biomarker detection with LOD of 0.122 μM	[7,191]
NN DCSGs				
Dynamic covalent (Boronic acid)	Metal–ligand (Ca^{2+}–COO^-)	Tissue engineering	Cell proliferation; formation of a new cartilage within 3 months	[192]
Metal–ligand (Fe^{3+}–COO^-)	H-bonds (Cellulose nanofibrils–AAc)	Self-healing materials	94 % rupture stress recovery after 48 h	[193]
H-Bonds (Urea stacking)	Host–guest (α-CD–PEG)	Self-healing materials	Recovery of 93 % strain after 48 h at 55 °C	[194]
H-Bonds (UPy)	Metal–ligand (Fe^{3+}–COO^-)	Self-healing, shape memory materials	Increased strength	[27]
Metal–ligand (Ca^{2+}–COO^-)	Host–guest (α-CD–azobenzene)	Shape memory materials	Triple stimuli-responsiveness	[195]
Ionic interactions	Hydrophobic interactions	Motion sensor, adhesives	Underwater motion detection; adhesion to surfaces of different nature	[196]

2.3.4 Gels as sensors

As devices transforming physical, chemical or biological input into a measurable signal, sensors play a vital role for precise and accurate detection of species of various nature in many fields such as biomedicine, environmental monitoring, forensic studies, *etc*.[5,197] In order to perform such detection, a sensor must contain an element which specifically binds to the analyte, thus, implementing recognition, and a transducer element, which is responsible for the translation of a

binding event into a signal. Supramolecular interactions present a rich toolbox for the design of sensing platforms due to a broad range of natural and synthetic receptors possessing selective binding affinity to a vast variety of analytes.[198] Moreover, the library of recognition elements continues to grow as new, tailored receptors are designed, as was demonstrated in Chapter 2.1, which offer even higher affinity and selectivity towards desired analytes. Hereby, systems involving macrocyclic host molecules play an increasingly important role.

Gels have the advantage of combining both recognition and transducing components in their network, which makes them potential materials of choice for fabrication of physical, chemo- and biosensors.[5,199] Firstly, supramolecular recognition moieties can be integrated into chemically crosslinked polymer chains. The signal in such case can be, *e.g.*, fluorescence emission or quenching resulting from formation of a supramolecular complex in the bulk of the gel. Secondly, if these moieties serve as reversible crosslinks, a system with analyte-dependent shape or volume modulation is obtained, which translates a number of binding events into a macroscopically measurable parameter, such as gel volume. In this regard, CN DCSGs are among the most promising architectures due to their ability to exhibit volume expansion/contraction while maintaining general integrity of the system.[4]

Due to the rising concerns about quality of life in industrial countries, there is an increased demand for sustainable industry and production, healthy environment for living as well as effective medical treatment. Therefore, gel-based sensors for the detection of biomedically and environmentally relevant agents move into focus of research of various scientific groups worldwide.[199]

2.3.4.1 Gels for environmental monitoring

In the field of environmental monitoring, sensors have been developed for the detection of various chemical pollutants, such as heavy metals, pesticides, and organic waste as well as for measuring parameters such as temperature, humidity and pH.[200] In this part, application of gels as sensors for environmental contaminants will be elucidated in detail.

Heavy metal ions such as Hg^{2+} or Pb^{2+} circulating in the water bodies are extremely toxic even at low concentrations and pose a serious threat to the environment and to human life.[201] Therefore, design of sensors for such metals capable of precise detection of ion concentrations with low LOD is of utmost ecological importance. In the design of Liu group[202], pendant thymine-reach DNA strands were covalently incorporated into an acrylamide-based hydrogel to obtain a highly sensitive Hg^{2+} sensor. Each of the DNA strands can accommodate up to 7 mercury ions, and such aggregates induce green fluorescence upon addition of a SYBR Green I dye (Figure 9). Specificity of the detector is provided by the fact that the fluorescence turns yellow in the absence of Hg^{2+}. When soaked in a water sample spiked with mercury ions, the hydrogel absorbs Hg^{2+} ions from

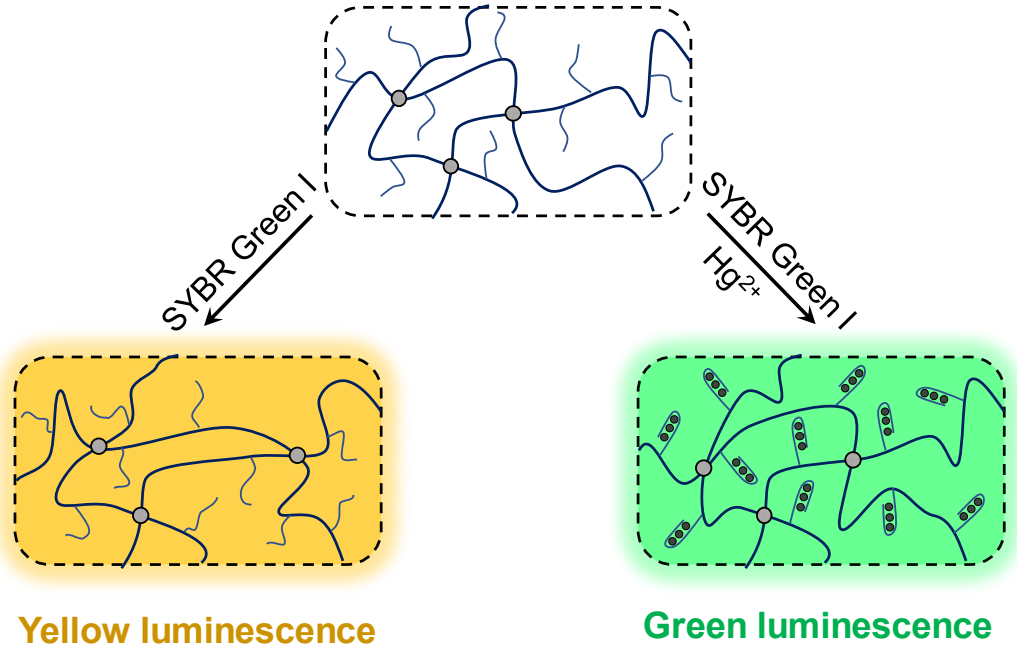

Figure 9. Supramolecular sensor for detection of mercury ions. Pendant DNA strands form complexes with Hg^{2+} by forming a hairpin structure. Upon presence of fluorescent dye SYBR Green I, the complex exhibits green luminescence. Yellow luminescence is observed without Hg ions.

the solution due to their binding to the acrylamide, which drastically increases the concentration of mercury within the hydrogel. Hence, it was possible to increase the sensitivity resulting in detection of Hg^{2+} at a concentration as low as 10 nM. Further, the same approach was applied by the group for the detection of Pb^{2+} ions.[203] For this purpose, a Pb-selective DNA sequence AGRO100 was selected in combination with thiazole orange dye for fluorescence imaging, whereby visual observation of 20 nM Pb^{2+} solutions was achieved. It was demonstrated that the combination of mercury and lead-sensitive gels paves the way for fabrication of shape-encoded multi-ion detecting sensor arrays.

Another design of Pb ion sensor was developed by the group of Tang.[204] A purely DNA-based hydrogel was designed, whose scaffold was formed by two DNA strands: a Pb-sensitive DNAzyme and a substrate strand. Ion-sensitive DNAzymes contain a region for metal ion docking, which acts as a trigger for cleaving the substrate strand by the DNAzyme. This, in turn, leads to a collapse of the hydrogel and a release of DNA fragments, which can be directly detected by fluorescence method. The resulting UV/Vis sensor platform was highly specific and sensitive with a determined LOD of 7.7 nM of Pb^{2+}.

Various precursors used in chemical and polymer industry to produce, *e.g.*, plastics or dyes, can be dangerous if found in wastewater or products. Bisphenol A (BPA) is a common monomer employed in the production of polycarbonate plastics that act as a material for numerous products of daily use in modern life. In recent years, BPA was demonstrated to cause severe adverse effects

on human health, including endocrine disruption, and impairment of fertility.[205] Hence, to minimize exposure to BPA, its levels in products must be monitored. For this purpose, a sensor was developed by Xiao group[206] based on DCSG with a chemical (MBA) and a supramolecular (β-CD–*tert*-butyl) crosslink. The pendant CD moieties function as recognition element of the sensor due to the affinity of β-CD to BPA, which acts as a competitive guest moiety. Upon its presence the β-CD–*tert*-butyl complex is disrupted leading to decrease of the crosslink density and, hence, to gel expansion. The role of the transducer element in this system is played by photonic crystals in the form of monodisperse polystyrene microbeads (d = 600 nm) embedded into the hydrogel. Photonic crystals possess long-range spatially ordered, evenly distributed structure, which diffracts light with wavelengths corresponding to the photonic band gaps, thus, yielding structure coloration.[207] In the sensor designed by Xiao group, the photonic crystals were arranged in the hydrogel in a two-dimensional fashion. The expansion of the DCSG led to the increased distance between the microspheres and, therefore, to the shift in gel coloration from blue to red upon increasing the BPA concentration. Such architecture provided an LOD of 1 μg/mL. The peculiarity of this sensor is the existence of the second transducing mode, which is the intrinsic fluorescence of BPA. Upon inclusion of the analyte into the cavity of β-CD, the fluorescence is enhanced, yielding its intensity as the second concentration-dependent parameter, which is characterized by an even lower LOD of 0.001 μg/mL. Together, both modes provide a significant range of linearity for quantitation of BPA concentrations.

A hydrogel with embedded photonic crystals was employed by Yu, Cheng and coworkers[208] as a sensor platform for 2-naphtol, a precursor for various dyes. Fe_3O_4 nanoparticles (d = 104 nm) were arranged in 1D arrays by external magnetic field and incorporated into acryl amide–NIPAAm-based covalently crosslinked hydrogel with pendant β-CD moieties, which are known to form host–guest complexes with 2-naphtol and act as recognition components. Similarly to the previously discussed sensor architecture, upon presence of the analyte, the gel expands, leading to the red shift in its color due to the increased distance between the nanoparticles. The determined LOD of the sensor was 0.01 μM. Due to the pH-dependent reversibility of the 2-naphtol–β-CD complexes, the sensor exhibited complete reusability.

2.3.4.2 Gel-based sensors for biomedicine

In biomedical milieu, sensors are practical solutions for diagnostics of severe diseases, the detection of which at early stages is crucial for the success of the treatment. In this regard, the role of biomarkers cannot be underappreciated, which are defined as measurable biological and biomolecular characteristics that can be objectively assessed to determine the state (stable/disease state) an organism is in.[209] Among all, the group of molecular biomarkers is especially interesting

since the analysis can be done on a sample of bodily fluids using an external, highly sensitive instrumentation.

One of such molecular biomarkers is a polyamine spermine (SP), which is shown to be an indicator of tumor growth in prostate cancer (see Chapter 4.1.1).[210] In the group of Serpe,[211] a hydrogel sensor for the detection of SP involving host–guest interactions with CB7 was devised (Figure 10). Incorporated into the NIPAAm backbone of the microgel, fluorescent dye Nile blue (NB) was used as an anchor for embedding CB7. Upon host–guest complex formation ($K_a = 2.5\times10^5\ M^{-1}$), nonfluorescent NB dimers were disrupted, which led to a fluorescence response and an increase in microgel diameter, since NB dimerization acted as a secondary crosslink. Upon presence of SP in the system, it replaced the dye in the cavity of CB7 due to a higher stability of SP@CB7 complex ($K_a = 2.0\times10^6\ M^{-1}$), which resulted in fluorescence quenching *via* NB dimer reformation and slight shrinkage of the gel due to partial removal of CB7 from the bulk. Under optimized conditions (C_{CB7} = 100 µM), the LOD of the sensor in Na_2HPO_4/HCl buffer, diluted serum und diluted urine were determined 0.6 µM, 0.6 µM, and 0.5 µM, respectively, with linear concentration dependence over 3 orders of magnitude. The hydrogel sensor was demonstrated to be selective towards SP in the presence of various cations as well as amine-containing biomolecules except spermidine (SD), which is a precursor for SP and is often considered a biomarker along with SP.

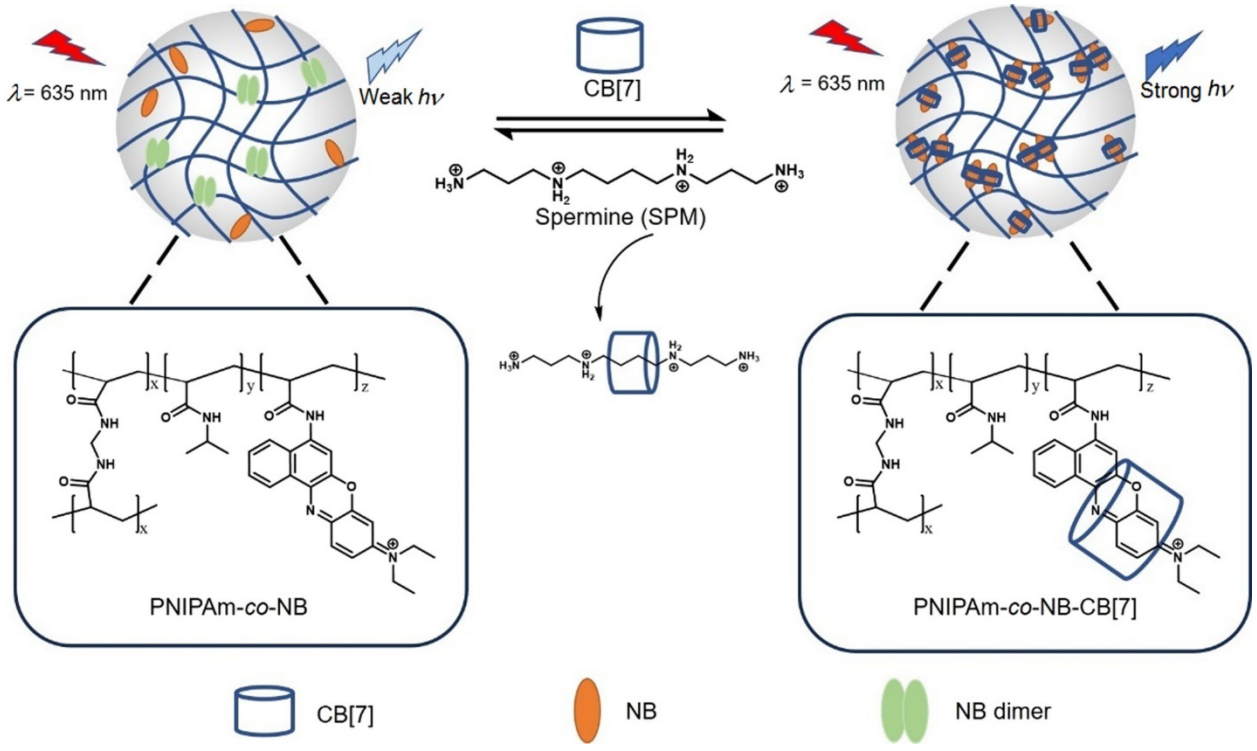

Figure 10. Sensing mechanism of a hydrogel sensor for detection spermine. Upon immersion in CB7 solution, 1:1 host–guest complexes are formed resulting in enhanced fluorescence of NB. Presence of the analyte leads to replacement of the dye from the CB7 cavity and decrease of fluorescence through Nile blue dimer reformation. Reprinted from Ref. [211]

In our working group, hydrogel-based sensors were developed with hydrogel volume acting as a transducer element, the alteration of which was monitored using SPR spectroscopy technique (see Chapter 2.5). Firstly, taking advantage of an extraordinary high affinity between biotin and streptavidin (SAV) ($K_a \approx 2.5\times10^{13}$ M^{-1})[212], a DMAAm-based chemically crosslinked gel with pendant biotin moieties was obtained on a gold surface of an SPR chip.[213] When SAV was injected into the flow cell, it could enter the hydrogel volume and bind to the biotin leading to an increase in hydrogel layer thickness, which was reflected in the SPR spectrum. The sensor exhibited linear response in the streptavidin concentration range 0.5–200 µM.

Further, a DCSG architecture was adopted involving a chemical crosslink and a supramolecular host–guest interaction between β-CD and Fc as a reversible second crosslink (Figure 11). Due to a moderate stability of the $Fc^{polymer}$@β-$CD^{polymer}$ complex ($K_a = 2.5\times10^3$ M^{-1}), it can be disrupted by molecular analytes with higher binding affinity to β-CD, such as adamantane[191] or lysophosphatidic acid (LPA).[7] LPA was found to be a biomarker for ovarian cancer, which shows significant differences in expression already at early stages of tumor development compared to healthy patients.[214] DCSG was assembled by mixing Fc- and β-CD-containing polymers and immobilized on an SPR chip by spin-coating and curing under UV light. Upon presence of the analyte in the soaking solution, analyte@β-CD complexes were preferably formed disrupting the secondary crosslink and leading to hydrogel expansion, which was recorded by SPR. DCSG

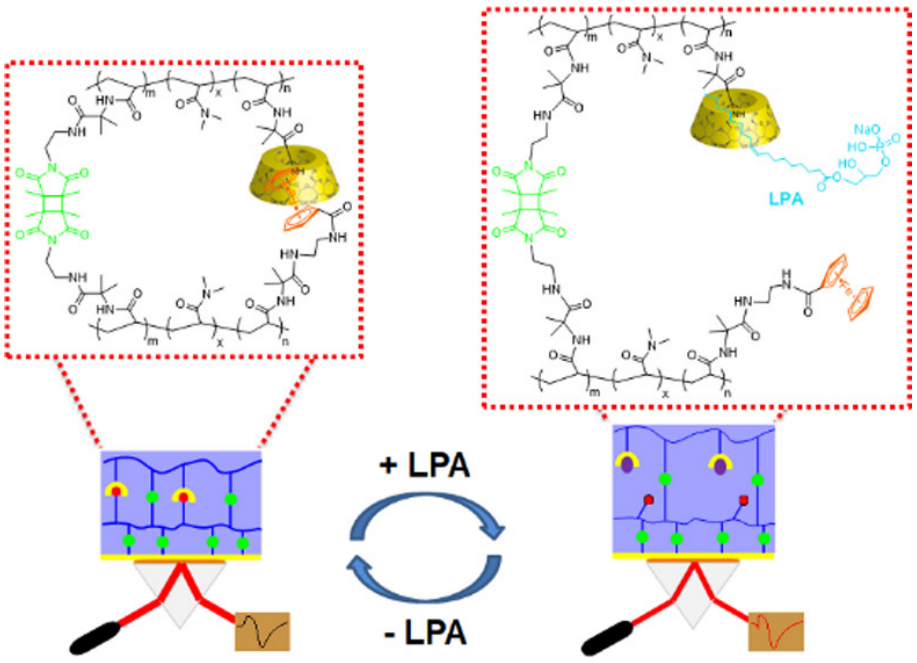

Figure 11. Dually crosslinked hydrogel for detection of ovarian cancer biomarker LPA. Fc@β-CD complex is disrupted upon presence of LPA in the medium, which leads to decrease in crosslinking density and to gel layer expansion. The change of layer thickness is monitored by SPR spectroscopy. Reprinted with permission from [7]. Copyright 2020 American Chemical Society.

sensor's LOD for adamantane was 24.3 μM. In case of LPA, LOD was calculated to be 0.122 μM in water and 2 μM for mimicked plasma conditions, which in both cases was lower than the cutoff value for ovarian cancer, thus, proving the selectivity of the sensor platform and providing accurate and reliable diagnostics.

2.3.5 Polymer networks with pillar[n]arenes

Due to the directionality, high specificity and chemical versatility of inclusion complexes, host–guest interactions are vastly employed in the fabrication of smart gels, with some examples provided above. Since their discovery, PnAs (Chapter 2.2) have been playing an increasingly important role for the design of supramolecular materials,[136,215] and for stimuli responsive gels in particular.[216] Currently emerging polymer networks involving PnAs incorporated physically, chemically or as a host moiety in a supramolecular crosslink are applied for a palette of purposes including self-healing materials, controlled drug release, and adsorbents. In the following, an overview of various PnA-based gel architectures (formed by polymer strands) will be given, and the applications will be briefly discussed.

2.3.5.1 Chemically crosslinked networks

The groups of Lin and Wang developed hydrogels with physically embedded molecular water-soluble deca-carboxylate modified PnAs. In the first approach,[217] acrylamide was copolymerized with MBA as a covalent crosslinker and a hydrophobic Fc-containing monomer. Since a binding affinity exists between WSP5A and Fc, the gel exhibited a drastic increase in swelling degree upon immersion in WSP5A solution (up to 11-fold increase), which was due to the electrostatic repulsion. Further, the possibility to influence the swelling behavior by various stimuli was shown, such as redox, competitive guest species and pH. Importantly, an uptake and pH-controlled release kinetics of doxorubicin (with a burst-release of 80 % cargo within 0.5 h at pH 2) was demonstrated, which opens a way for a potential application of the gel as a drug delivery agent.
In the second approach,[218] trimethylammonium groups were incorporated into the network as pendant guest moieties. Initially swollen in pure water, the hydrogel shrank when immersed in a WSP5A solution, which was attributed to the host–guest complex formation between WSP5A and guest groups, enhanced by electrostatic attraction forces. WSP5A-controlled drug release was demonstrated using calcein and rhodamine B as model drugs. Using anionic calcein, a high uptake into the cationic hydrogel was reported (96.7 % *vs.* 44.3 % in case of rhodamine). The release of calcein (up to 97.4 %) from the hydrogel back into the medium was achieved only by soaking in WSP5A solution, whereas in pure water or NaCl solution the release could not be observed.A unique architecture was designed by the group of Hoogenboom, in which P5A was used as a

chemical crosslinking agent.[164] As was mentioned above, covalently crosslinked gels are fabricated as mechanically strong and stable networks. Therefore, A1/A2 carboxylic acid di-substituted P5A was reacted with pendant 2-oxazoline moieties of poly(2-isopropenyl-2-oxazoline) to obtain a high-strength chemically crosslinked gel, which was demonstrated to remain intact under up to 0.9 MPa compression. The presence of P5A fragments between the chains endowed the system with guest-dependent swelling behavior as well as with excellent adsorption abilities: 24-hour uptake of such pollutants as BPA, 2-naphtol, methylene blue and methyl red from their 0.05 mM solutions was 61–93 %. The reusability of the gel was shown by release of the pollutants by soaking in DMF.

2.3.5.2 Physically crosslinked networks

The versatility of host–guest interactions involving PnA leads to the development of a broad spectrum of various supramolecular networks. In Table 10, selected examples of such networks are presented, in which covalent polymer chains are crosslinked *via* formation of inclusion complexes with PnAs. Information whether a host or guest is covalently attached to a constituent polymer (pendant) or resembles a homoditopic "low-molecular" species, is specified for each moiety. Furthermore, for each PnA moiety, the synthetic strategy leading to the desired mono-substituted product is specified. Clearly, various species are employed as guest moieties for the construction of supramolecular gels, including Fc, pyridinium, imidazolium and ammonium cationic species as well as nitrile being the only neutral species in this row (Table 10). Fc endows the systems with redox-responsiveness,[110] while host–guest complexes with other components are mostly susceptible towards temperature and competitive agents. Importantly, the reversible character of the complexes renders networks able to undergo ultrafast self-healing: a system based on nitrile@P5A complexes was able to recover its mechanical performance within 90 s.[219]

Table 10. Architecture and responsive properties of physical networks crosslinked with PnA-based host–guest interactions.

Host moiety	Guest moiety	Responsiveness	Particularity	Ref.
P6A, pendant (monodealk.)	Fc^+, pendant	Redox, competitive host/guest	Competitive host-controlled viscosity	[110]
P5A, pendant (co-cycloolig.)	Pyridinium, homoditopic	Temperature, competitive host/guest	—	[115]
P5A, pendant (monodealk.)	C≡N 1) Homoditopic; 2) Pendant	Hydrolysis of the backbone (dynamic imine)	Self-healing (10 min)	[220]

Host moiety	Guest moiety	Responsiveness	Particularity	Ref.
P5A, pendant (monodealk.)	Me_3RN^+, homoditopic	Temperature, pH	Fatigue resistance, self-healing (30 min)	[221]
P5A, pendant (monodealk.)	Pyridinium, homoditopic	Competitive anion	—	[222]
P5A, pendant (monodealk.)	Methyl-imidazolium, homoditopic	—	—	[223]
P5A, pendant (co-cycloolig.)	C≡N, homoditopic	Temperature, competitive host/guest	Moldability, self-healing (90 s)	[219]
P5A, homoditopic (co-cycloolig.)	Pyridinium, pendant	Redox (dynamic disulfide)	Crosslink density monitoring by fluorescence color (pyrene)	[224]

2.3.5.3 Dually crosslinked networks

In the recent years, PnA inclusion complexes started to be utilized in dually crosslinked architectures for improving mechanical performance of the systems as well as to render multi-stimuli responsiveness.

Ji and coworkers[225] implemented a PMMA-based CN DCSG with enhanced mechanical properties by incorporating PEG-dimethacrylate as a covalent crosslinker and pyridinium@P5A complex as a supramolecular linkage (Figure 12, A). As opposed to singly crosslinked networks that contain either only host or only guest pendant groups, the obtained DCSG demonstrated an 8 times higher elongation at break (up to 119 %) as well as significantly improved toughness, which was attributed to the reversible crosslinks serving as sacrificial bonds under mechanical stress. Furthermore, stimuli responsiveness was demonstrated by increased swelling ratio in a solution of a competitive guest (imidazolium) compared to swelling in pure solvent ($CHCl_3$).

A NN DCSG was designed by Zhang et al.[226] in which two types of crosslinking were combined: nitrile@P5A supramolecular complex and π–π stacking of azobenzene (Figure 13, B). The non-covalently crosslinked gel obtained by mixing a host- and a guest-bearing polymers was soft and demonstrated relaxation of mechanical stress at high strains due to the ability of supramolecular bonds to break and quickly re-form. The system exhibited thermo- and chemical responsiveness (competitive guest) with sol–gel transition, whereas UV-irradiation did not lead to significant macroscopic changes, arguably because the π–π stacking was maintaining the azobenzene dimers even after the isomerization of the moieties. Furthermore, xerogel fabricated from the NN DCSG

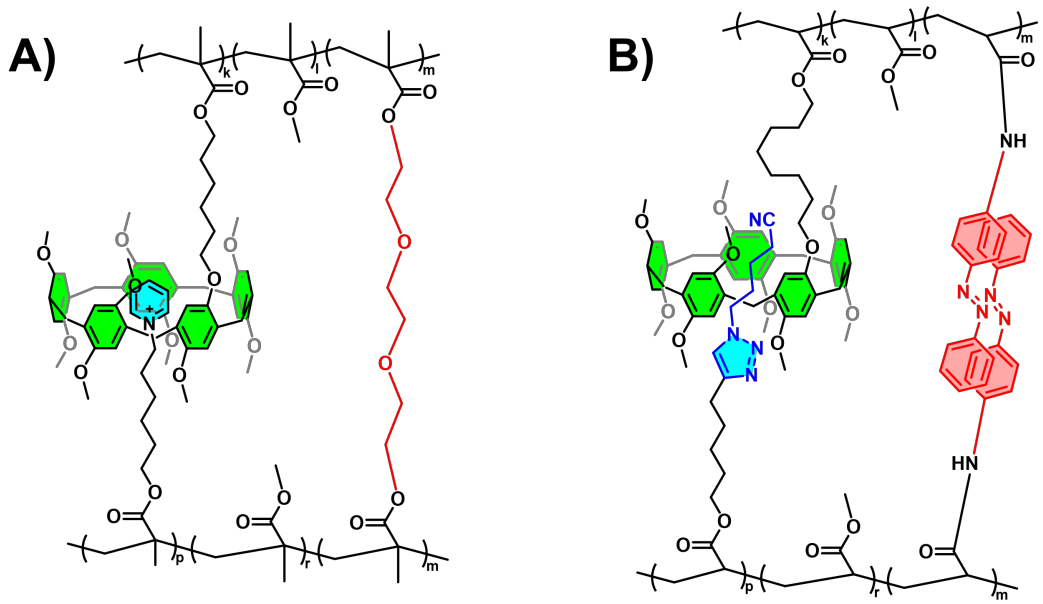

Figure 13. Dually crosslinked gels with P5A-based linkages. A) CN DCSG architecture with improved mechanical properties from Ref. [225]. B) NN DCSG architecture with azobenzene π–π stacking as secondary crosslink as per Ref. [226].

was demonstrated to effectively adsorb iodine from 1.22 mM aqueous solution with over 98 % efficiency.

2.4 Quantification of supramolecular interactions

In the field of supramolecular chemistry, being able to quantify the strength of interactions between host and guest molecules is as vital as the affinity of an enzyme to a substrate in biochemistry or of a drug to a receptor in pharmacological chemistry. In the previous chapters, complexes of various macrocycles with guest molecules were compared in terms of their binding affinity. The current chapter will provide an explanation of the principles underlying the quantification of binding affinity and a brief overview of the available techniques for the determination of complexation strength.

2.4.1 Supramolecular equilibrium[227–230]

2.4.1.1 Association constant

Since, as discussed above, supramolecular interactions are intrinsically reversible, a supramolecular "reaction" is always an equilibrium process. In the example provided in equation (1), a host (or receptor) H interacts with a guest (or ligand) G to form a complex of a stoichiometry m:n H_mG_n.

$$mH + nG \rightleftarrows H_mG_n \quad (1)$$

The measure of this process is change in Gibbs free energy ΔG (equation (2)), which can be determined at a given temperature T using equilibrium (association) constant K_a expressed for the reaction (1) as shown in equation (3).

$$\Delta G = -RT\ln K_a \tag{2}$$

$$K_a = \frac{[H_m G_n]}{[H]^m [G]^n} \tag{3}$$

In the equation (3), [H], [G] and $[H_mG_n]$, are the equilibrium concentrations of the free host, free guest, and the complex, respectively. Hence, in principle, knowing these concentrations in the system (solution) as well as the stoichiometry of the interaction (*m*, *n*) is sufficient for calculating the constant and, therefore, drawing a conclusion about the strength of the interaction under investigation or, in other words, about the stability of the complex. In real experiments, however, it is often impossible to obtain these values because of, *e.g.*, overlapping signals or one of the species being "silent", *i.e.*, not producing signals in the method used. Since the total host and guest concentrations, H_0 and G_0, are normally set in the experimental design by the researcher, it is possible to reduce the number of unknown variables by substituting [H] and [G] according to equations (4) giving equation (5), in which the equilibrium complex concentration is the only unknown parameter.

$$\begin{aligned} [H] &= H_0 - m[H_m G_n] \\ [G] &= G_0 - n[H_m G_n] \end{aligned} \tag{4}$$

$$K_a = \frac{[H_m G_n]}{(H_0 - m[H_m G_n])^m \cdot (G_0 - n[H_m G_n])^n} \tag{5}$$

2.4.1.2 1:1 equilibrium[227,228]

In the simplest case of a 1:1 equilibrium (*i.e.*, when $m = n = 1$), the expression for K_a is expressed as (6).

$$K_a = \frac{[HG]}{[H] \cdot [G]} = \frac{[HG]}{(H_0 - [HG]) \cdot (G_0 - [HG])} \tag{6}$$

By rearranging the parameters, a quadratic equation for [HG] can be formulated (equation (7)), solving which an expression for [HG] is obtained (equation (8)).

$$[HG]^2 - [HG] \cdot \left(G_0 + H_0 + \frac{1}{K_a}\right) + H_0 G_0 = 0 \tag{7}$$

$$[HG] = \frac{1}{2}\left(\left(G_0 + H_0 + \frac{1}{K_a}\right) - \sqrt{\left(G_0 + H_0 + \frac{1}{K_a}\right)^2 - 4 \cdot H_0 G_0}\right) \tag{8}$$

The expression (8) is helpful in cases where direct determination of [HG] is not possible and a change in physical property (*e.g.*, spectral absorbance) dependent on the concentration [HG] is used instead. If such physical property Y can be represented as a linear combination of contributions of single components (Y_H, Y_G, Y_{HG}), the expression (9) is obtained.

$$\begin{aligned} Y &= Y_H \cdot [H] + Y_G \cdot [G] + Y_{HG} \cdot [HG] = \\ &= Y_H \cdot (H_0 - [HG]) + Y_G \cdot (G_0 - [HG]) + Y_{HG} \cdot [HG] = \\ &= Y_H \cdot H_0 + Y_G \cdot G_0 + (Y_{HG} - Y_H - Y_G) \cdot [HG] \end{aligned} \tag{9}$$

If the terms in (9) are defined according to (10)–(12) and [HG] is substituted with the expression in (8), equation (13) is obtained.

$$Y_0 = Y_H \cdot H_0 \tag{10}$$

$$Y - Y_0 = \Delta Y \tag{11}$$

$$Y_{HG} - Y_H - Y_G = Y_{\Delta HG} \tag{12}$$

$$\Delta Y = Y_G \cdot G_0 + \frac{Y_{\Delta HG}}{2}\left(\left(G_0 + H_0 + \frac{1}{K_a}\right) - \sqrt{\left(G_0 + H_0 + \frac{1}{K_a}\right)^2 - 4 \cdot H_0 \cdot G_0}\right) \tag{13}$$

The equation (13) demonstrates how the physical property Y changes from the host solution ($G_0 = 0$) to a host–guest mixture solution with total guest species concentration of G_0. Furthermore, if a titration is conducted, in which the guest is stepwise added to the host (the concentration of which is kept constant, H_0), this dependence describes a generalized binding isotherm, in which Y_G can in principle be obtained from a separate experiment, and the only unknown parameters are

K_a and $Y_{\Delta HG}$. By applying the equation (13) for a non-linear fitting to the titration curve, the equilibrium constant K_a can be derived as one of the fitting parameters. This method, as pointed out by Thordarson[227], produces the most accurate results for the determination of binding affinity in a supramolecular system with 1:1 stoichiometry because it does not contain any simplifications. Further in the chapter, the applicability of the dependence (13) for different analytical techniques will be discussed.

2.4.2 Experimental design and limitations

As mentioned above, performing a titration experiment, and fitting the obtained titration isotherm with (13) using non-linear regression can deliver the binding constant value K_a. However, it is as important to set the experimental conditions (that is, selecting the host concentration H_0 and concentration range for G_0) accordingly in order to avoid large uncertainties and systematic errors. In the works of Hirose[229] and Thordarson,[227] the conditions for minimization of possible systematic errors are defined.

According to Hirose, for a reliable experiment condition (14) must be fulfilled since otherwise the difference between binding isotherms becomes less distinguishable, which leads to small experimental errors being increasingly magnified.

$$H_0 \cdot K_a < 1 \tag{14}$$

Thordarson makes the abovementioned condition less strict (condition (15)) by taking into account simulated errors, at the same time, however, pointing out that no reliable results can be obtained above this limit.

$$H_0 \cdot K_a < 100 \tag{15}$$

This condition not only sets an upper limit for the host concentration, but also shows that in order to conduct a proper titration experiment, a prior information (an educated guess or a comparison with similar known systems) about the binding strength K_a of the investigated complex is required. Moreover, it implies that the prior knowledge of the magnitude of K_a is crucial even for a selection of an appropriate analytical technique, since different methods require different working concentrations (*e.g.*, 10^{-3}–10^{-2} M in case of NMR).

The product $H_0 \cdot K_a$ is furthermore important for setting the guest concentration range G_0. Hirose[229] derives upper and lower limits for the G_0 that also depend on the magnitude of the association constant (condition (16)).

$$\frac{1}{10 \cdot K_a} \leq G_0 \leq \frac{10}{K_a} \tag{16}$$

According to Thordarson,[227] several cases can be considered, each implying its own range for G_0, within which 15–20 data points should be obtained:

1. In case of $H_0 \cdot K_a < 1$ (K_a is small) the guest moiety must be taken in an excess (up to 50 equivalents and more) in order to complete the titration curve.
2. In case of $H_0 \cdot K_a \approx 1$ up to 10 equivalents of guest are required, which is regarded as an optimal regime.[228]
3. In case of $H_0 \cdot K_a > 1$ (K_a is large) the range between 0 and 1 eq. of guest must be thoroughly investigated for a reliable determination of K_a.

To sum up, for a proper titration experiment that yields reliable data, prior knowledge or estimation of K_a is vital because it defines the possible ranges for H_0 and G_0, which, in turn, influences the choice of an appropriate analytical technique.

2.4.3 Determination of complex stoichiometry

The previous discussion was based for simplicity on the assumption of a 1:1 binding stoichiometry. However, for a supramolecular system it is not uncommon to exhibit stoichiometries of a higher order, *e.g.*, 1:2, 2:1 or 2:2 and higher,[228,230] which require different models for data evaluation. Hence, the initial determination of the binding stoichiometry is one of the essential steps in the investigation of supramolecular interactions, which ensures that a correct model is applied to the experimental data. Thordarson[227] elaborates on available ways that allow proving that the selected binding model corresponds to reality, including comparison of the parameters obtained by different techniques, evaluation of structural information, robustness of the data (invariability of the parameters at different host concentrations).

A technique vastly employed for the stoichiometry determination in supramolecular chemistry is the method of continuous variations, or Job's method.[231] Continuous variations method relies on the fact that the dependence of the host–guest complex concentration $[H_mG_n]$ from a component's (typically, host's) mole fraction X_H reaches its maximum, which can be shown[229] to correspond to the host's fraction in the complex, if in the course of the experiment the total concentration (C_{tot}, equation (20)) is maintained constant (Figure 13). The graphical representation of the method known as Job plot not only serves a visualization purpose but can as well deliver quantitative information about the supramolecular system. Since the curve is described, in a general case, implicitly with equation (5), association constant can theoretically be obtained by non-linear

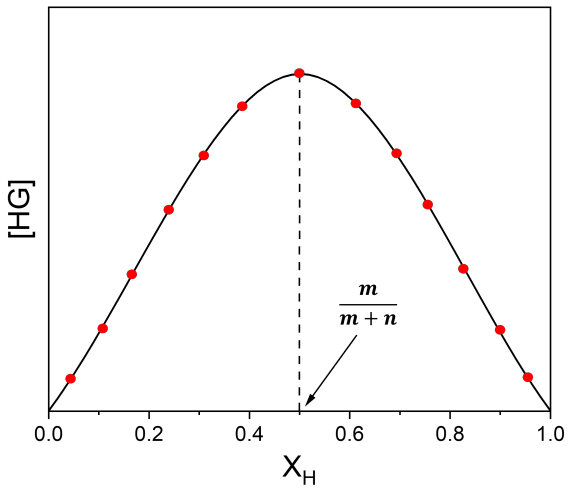

Figure 13. Example of a Job plot. Red dots resemble experimental data, the solid line is a theoretical curve. The position of the curve's maximum on the x axis corresponds to the host fraction in the complex. Instead of [HG] any physical value proportional to it can be used.

regression. For the 1:1 complexation, the Job plot is described explicitly (equation (18)).[231,232] Moreover, the plot allows one to qualitatively estimate the binding constant K_a (at a given C_0) by its shape: sharper or more angular shape of the maximum indicates a higher affinity between the reactants than a smoother one.[233]

$$C_{tot} = H_0 + G_0 \tag{17}$$

$$[H_m G_n] = \frac{C_{tot} \cdot K_a + 1 - \sqrt{(C_{tot} \cdot K_a + 1)^2 - 4 \cdot C_{tot}^2 \cdot K_a^2 \cdot X_H \cdot (1 - X_H)}}{2K_a} \tag{18}$$

In practice, since the $[H_mG_n]$ often cannot be measured directly, a physical property proportional to it is used instead.

Job's method is, however, prone to disadvantages that significantly limit the applicability of the technique for reliable data evaluation to the point that it was proclaimed "dead" for analytical applications by Brynn Hibbert and Thordarson.[234]

Firstly, the obvious disadvantage of the continuous variations technique is that, since the maximum of the dependence corresponds to the mole fraction of the host X_H, the method does not distinguish between complexes, in which $m = n$. Although the Job's plot curves of different stoichiometries of that kind are not equal in each case, they are indistinguishable in a practical experiment.[232]

Secondly, the method is demonstrated to reliably prove the stoichiometry only in the case where the process yields a single species as a product.[234,235] In a real experiment, however, if more than two molecules are expected to form a complex, the aggregates of lower stoichiometries may as well produce a signal. The group of Jurczak[235] utilized simulated titration curves to show how

the magnitude of C_0 and K_2 (defined by (19)) affects the appearance of the Job plot of the HG_2 complex formation.

$$K_2 = \frac{[HG_2]}{[HG] \cdot [G]} \tag{19}$$

Astonishingly, in the simulated experiments ($K_1 \cdot C_0 \leq 100$, $K_2/K_1 \leq 0.25$) none of the plots exhibits its maximum at X_H =0.33. Therefore, the authors restrict the method usage only as a qualitative analytical tool. Deviations of the maximum from $X_H = 0.5$ recorded at higher concentrations can signal presence of higher binding stoichiometries, which, still, cannot be predicted based on the actual shape of the curve or its maximum.

Ultimately, in order to find the true binding model for the system under investigation, different models can be sequentially applied to the experimental data, as suggested by Thordarson[227] and Jurczak,[235] with increasing number of parameters until no more significant improvement of the fitting is observed. As an indicator of a model correctness the residual distribution is considered, which resembles a random scatter around the average in case of a correct model and a regular, typically, sigmoidal distribution, if the chosen model is inappropriate. Furthermore, the correctness of a model selection can be shown in a robustness experiment, *i.e.*, by repeating the titration at another H_0 (it is recommended to use a concentration which differs by at least 5 times from the initial one).[235]

2.4.4 Analytical techniques for the determination of binding affinity

Despite the vast variety of the tools for binding affinity investigations (including fluorescence measurements[228] and mass spectrometry[236]), NMR, UV/Vis and ITC will be in the focus of the further discussion.

2.4.4.1 NMR spectroscopy

2.4.4.1.1 Method overview

Nuclear magnetic resonance (NMR) spectroscopy is an analytical method that allows chemical structure elucidation and investigation of molecular dynamics based on their interaction with a magnetic field.[237] NMR is a particularly valuable technique for investigation of supramolecular interactions because of the amount of information it can deliver: from the quantification of the association equilibrium by observing chemical shifts in ^{1}H spectra to the insights about the spatial structure and geometry of the complexes by studying spectra arising from nuclear Overhauser effect.[238,239]

NMR spectrometers routinely operate with solution concentrations of 10^{-3}–10^{-2} M, which makes this technique practically suitable for complexes with $K_a < 10^5$ M^{-1}, according to the condition (15) as discussed above.[227,228]

NMR signals are characterized by two parameters, chemical shift δ, reflecting the chemical environment of the corresponding nucleus, and integral *I*, in case of ^{1}H NMR proportionate to the amount of the nuclei of this sort. In the course of a titration the ratio of the components changes, which influences *I*, and/or a new environment is created upon complex formation affecting δ. For looking into a supramolecular equilibrium using NMR spectroscopy, it is crucial to consider kinetics of this process: the association constant K_a can be expressed with complexation and decomplexation reaction rates (k_{com} and k_{dec}, respectively) as shown in equation (20).

$$K_a = \frac{k_{com}}{k_{dec}} \tag{20}$$

Relative to the timescale of the NMR experiment, the investigated system can be, therefore, in a fast or slow regime depending on the complexation/decomplexation rates. Strictly speaking, one can define the fast regime, if condition (21) is fulfilled.[240] Here, ν_{free} and ν_{bound} are signal frequencies of the host in free and bound states, respectively, τ_{free} and τ_{bound} are the lifetimes of these states, and $\tau_{bound} = 1/k_{dec}$.

$$2\pi\left|\nu_{free} - \nu_{bound}\right| \ll \left(\frac{1}{\tau_{free}} + \frac{1}{\tau_{bound}}\right) \tag{21}$$

If, instead, the system behaves according to the condition (22), it is in a slow regime.

$$2\pi\left|\nu_{free} - \nu_{bound}\right| \gg \left(\frac{1}{\tau_{free}} + \frac{1}{\tau_{bound}}\right) \tag{22}$$

Interestingly, expressions (21) and (22) imply that the change in the chemical shift Δδ of a host signal caused by complexation is dependent on the lifetime of the corresponding nucleus in the free and complexed states.[227]

In this concern, it is important to outline complex stability. Although it may intuitively seem valid that a high association constant, *i.e.*, high complex stability, automatically implies a slow exchange on the NMR time scale, this implication is in fact not correct.[241] Since the lifetime of the bound

state τ_{bound} is reciprocal decomplexation rate constant, k_{dec} the complex stability is higher, if k_{dec} is smaller. However, the association constant K_a is a ratio of the rate constants according to (20); therefore, its value can be low if the rate constants are comparable in magnitude (both high or both low implying a fast or slow exchange complex, respectively), or high if $k_{com} > k_{dec}$ (depending on the magnitude of k_{dec}, both exchange regimes can take place).

2.4.4.1.2 Slow exchange

The regime of the exchange influences the appearance of the signals on the spectrum and the approach for evaluation thereof (Figure 14).[230] If the system is in the truly slow exchange regime, the lifetime of free and bound species is longer than the time scale of the NMR measurement meaning two different signals (δ_H of the free host and δ_{HG} of the complexed host) are observable simultaneously (Figure 14, A). Since, as mentioned before, the signal intensity *I* is proportional to the number of corresponding nuclei (and therefore, to the number of molecules), this method theoretically allows obtaining equilibrium concentrations [HG] directly. Because [HG] is connected to the total host concentration H_0, it can be calculated according to the equation (23), where *m* is host stoichiometry in the complex, I_H and I_{HG} and the integrals of the free and bound host signals, respectively.[229]

$$[HG] = \frac{1}{m} \cdot \frac{I_{HG}}{I_H + I_{HG}} \cdot H_0 \qquad (23)$$

Further, calculation of K_a is proceeded according to (5). Normally, in case of 1:1 complexes the spectrum of a solution is evaluated, in which $H_0 = G_0$. This evaluation procedure is then called "single-point method".[242,243]

To determine the stoichiometry at a slow exchange regime, a Job plot is obtained using $I_{host,complex}/(I_{host,free} + I_{host,complex}) \cdot H_0$ as a value proportional to the equilibrium complex concentration [HG].[229]

2.4.4.1.3 Fast exchange

In case of a fast exchange complex according to the condition (21), the time scale of an NMR measurement is significantly longer than the complexation/decomplexation event. Therefore, the signals of a free and complexed host species are superposed as a single peak with a constant integral value (since the host concentration is kept constant) and its observed chemical shift δ_{fact} is expressed as a weight average of signals of the two "extreme" cases (equation (24)).[229]

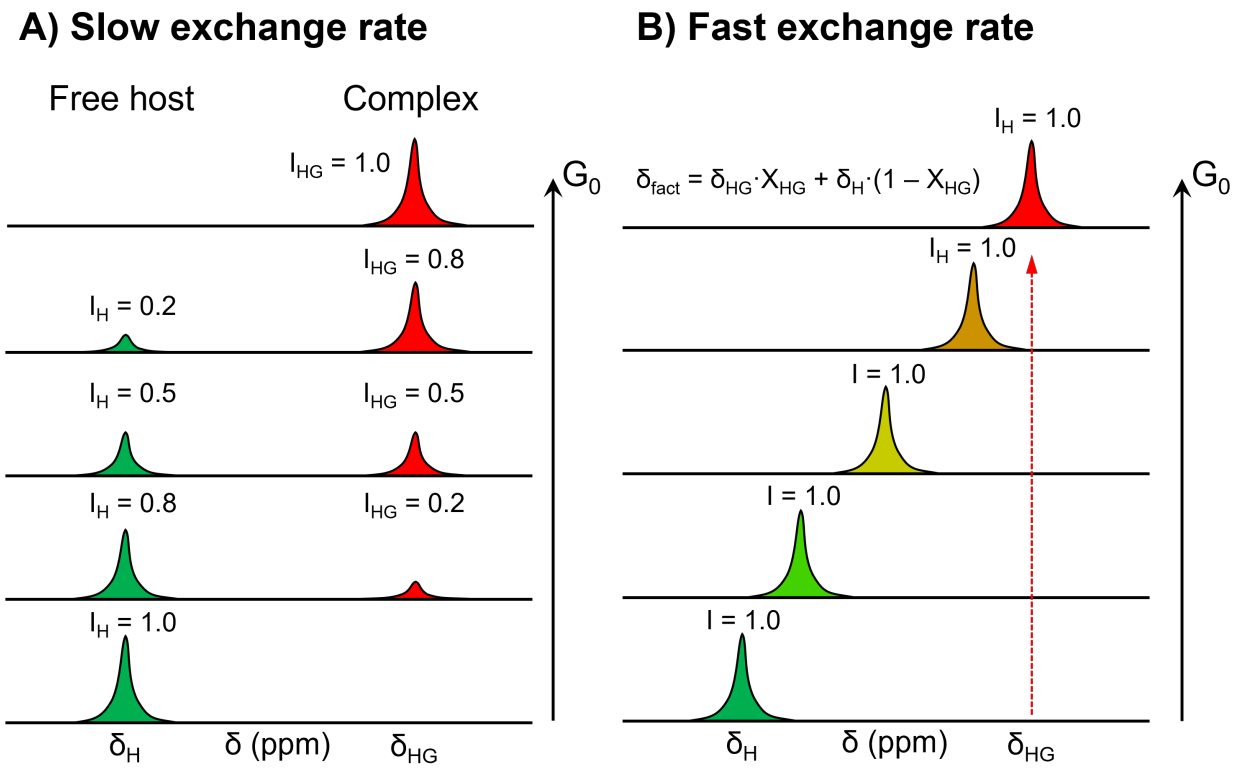

Figure 14. Evolution of the NMR spectra of a supramolecular system in the course of NMR titration. A) For the system with a slow exchange rate a separate complex peak is observed. Upon addition of the guest G, the complex peak intensity I_{HG} increases whereas the host peak intensity I_H gradually decreases. B) For the system with a fast exchange rate the host signal undergoes gradual shift from δ_H towards δ_{HG}. The intermediate chemical shift values are weight average between the free and bound states.

$$\delta_{fact} = \delta_H \cdot \left(1 - \frac{m \cdot [HG]}{H_0}\right) + \delta_{HG} \cdot \frac{m \cdot [HG]}{H_0} \tag{24}$$

For the case of a 1:1 complex stoichiometry, the equation (24) can be rearranged into the binding isotherm (13) in its form for NMR titration (25).[227,228]

$$\Delta\delta = \delta_{fact} - \delta_H = \frac{\delta_{\Delta HG}}{2H_0} \cdot \left(\left(G_0 + H_0 + \frac{1}{K_a}\right) - \sqrt{\left(G_0 + H_0 + \frac{1}{K_a}\right)^2 - 4 \cdot H_0 \cdot G_0}\right) \tag{25}$$

At constant host concentration, the equation (25) contains two unknown parameters K_a and $\delta_{\Delta HG}$ resembling the chemical shift of the investigated nucleus in a fully complexed state. Therefore, the association constant K_a of a fast-exchange complex can be obtained by fitting of the experimental data using the non-linear regression method.

To determine the complex's stoichiometry, a Job plot is obtained for a fast exchange system by plotting X_H against $\Delta\delta \cdot H_0$.[229]

2.4.4.1.4 Intermediate exchange

The methods for K_a determination were demonstrated for the systems characterized by a slow or a fast exchange rate. In case if the difference between the resonance frequencies of the free and bound host is comparable to the sum of inversed lifetimes of these states (equation (26)), the intermediate regime is observed.

$$2\pi\left|\nu_{free} - \nu_{bound}\right| \approx \left(\frac{1}{\tau_{free}} + \frac{1}{\tau_{bound}}\right) \tag{26}$$

The intermediate exchange regime may cause significant signal broadening accompanied by significant distortion of the Lorentzian shape of the peaks.[240] This may lead to enormous errors in K_a estimation if one of the models discussed above is applied for data treatment. Therefore, this regime cannot be utilized for a reliable NMR titration.[229]

2.4.4.1.5 Sample preparation

One of the assumptions that were made for deriving the isotherm (25) was that the total host concentration is kept constant. Since the titration is conducted in the way that aliquots of the guest solution are added in a stepwise manner to the stock host solution, dilution correction must be considered to obtain reliable data. There are several ways how to arrange an NMR titration in order to assure a constant H_0 throughout the complete experiment.[230]

1. Each of solutions with different H_0:G_0 ratios can be prepared in a separate tube. Although in this case the H_0 may slightly vary between the tubes, this method has an advantage of lower systematic error arising from multiple pipette/syringe usage.
2. The experiment is conducted in a single tube. The guest solution is prepared by dissolving the guest moiety in the host stock solution (H_0). This solution is then added into the tube with the host stock solution (with the concentration of H_0) used to record the initial spectrum ($G_0 = 0$).
3. A highly concentrated guest solution is added to the host solution. High guest concentration allows the aliquots to be small enough to keep the dilution of a minimal level. Alternatively, special software can be employed to take the dilution into account at the data evaluation step.

2.4.4.1.6 NOESY NMR

Undoubtedly, ^{1}H NMR spectroscopy is a powerful tool for the investigation and quantification of supramolecular processes. However, other NMR techniques can provide valuable complementary information for further understanding of structures of supramolecular complexes.

Nuclear Overhauser enhancement spectroscopy (NOESY NMR) utilizing nuclear Overhauser effect is a highly useful method for elucidation of a compound's or complex's geometry and spatial orientation. The effect describes the change of a resonance intensity of a nucleus upon saturation of another nucleus, which is located in a close proximity to the first one, with radio frequency irradiation.[238,239,244] Interestingly, the magnitude of the resonance change depends on molecular weight of the species: whereas for small molecules an increase up to 38 % is observed, the resonance of the macromolecules can appear completely inversed (–100 % decrease) with an inversion point at which the resonance reaches zero at around 600–2000 Da.[245]

For the effect to take place, two nuclei must be < 5 Å away from each other, which is especially beneficial for clarification of complex bio- and macromolecule structures. In case of supramolecular complexes, the method allows determining the positioning of the guest molecule in the host by considering the NOE cross-peaks corresponding to both species, which is vital for the complex structure clarification.

2.4.4.1.7 DOSY NMR

Diffusion-ordered spectroscopy (DOSY NMR) is a technique developed in the early 1990s,[246] which allows the determination of translational diffusion of components in a sample quantified using diffusion coefficient D. This is possible by applying magnetic field gradients within a pulse sequence varying gradient strength *G*. By using a set of different *G*, a set of one-dimensional ^{1}H NMR spectra is obtained with peaks of different components decaying at different rates. These signal intensity changes are analyzed with Stejskal–Tanner equation (27), in which $I(G)$ and I_0 are signal intensities at the magnetic field gradient of strength *G* and without gradient, respectively; γ is the gyromagnetic ratio of a nucleus; δ^{grad} is the duration of the gradient; Δ^{grad} is a delay between two gradient pulses, or in other words, the diffusion time.[247] The diffusion coefficient D can be obtained as a parameter by fitting the dependence of signal intensity $I(G)$ *versus* gradient strength *G*.

$$I(G) = I_0 \cdot \exp\left[-D \cdot (\gamma \cdot G \cdot \delta^{grad})^2 \cdot (\Delta^{grad} - \delta^{grad}/3)\right] \quad (27)$$

Not only does DOSY offer the analysis of complicated substance mixtures by discriminating between the components' diffusion, but it can also deliver vital information for investigating the supramolecular complex formation.

The diffusion coefficient D of a particle depends on the particle size r according to Stokes–Einstein equation (28), where k_B is the Boltzmann constant, T is a temperature, and η is the viscosity of the solvent. Therefore, if one assumes that the guest molecule is small enough to be fully encompassed by the host molecule, the size of the guest, and, accordingly, its diffusion coefficient should become equal to the ones of the host species.

$$D = \frac{k_B \cdot T}{6\pi \cdot \eta \cdot r} \tag{28}$$

However, the ultimate reduction of the guest's D to the host's value can only be expected in the case of a slow exchange complex, *i.e.*, when the species in the system remain in one state during the measurement. If the complex is characterized by fast exchange, then the obtained D value corresponds to the weighted average between the free and bound states, which, therefore, opens a new way for the determination of the binding constant, namely, from the diffusion experiments.[241]

2.4.4.2 UV/Vis spectroscopy

UV/Vis spectroscopy is suitable for the investigation of the systems, the components of which have characteristic absorption bands in the ultraviolet and/or visible region of the spectrum, *i.e.*, when they are chromophores.[248] The absorbance A at a given wavelength λ is proportional to the species' concentration C according to the Lambert–Beer law (29), where *ε* is molar absorptivity of the species at this wavelength and *l* is beam path length. Importantly, reliable linearity is provided in the concentration range where A < 1.

$$A(\lambda) = \varepsilon(\lambda) \cdot l \cdot C \tag{29}$$

Because the typical duration of the UV/Vis relevant transitions is much shorter than the lifetime of the complexes, the supramolecular equilibria are always in the slow regime.[228] Therefore, the absorbance of all the chromophores present in the solution is observed simultaneously, and absorbance at a given wavelength A (λ) can be expressed as a linear combination of the components' absorbances respective their equilibrium concentration in solution (equation (30)).

$$A(\lambda) = \varepsilon_H(\lambda) \cdot l \cdot [H] + \varepsilon_G(\lambda) \cdot l \cdot [G] + \varepsilon_{HG}(\lambda) \cdot l \cdot [HG] \tag{30}$$

The general binding isotherm (13) for host–guest complexes of 1:1 stoichiometry is applicable for UV/Vis spectroscopy and the change in the observed absorbance ΔA between the system without guest and containing total guest concentration of G_0 is expressed in the form of (31) where $\varepsilon_{\Delta HG}$ is defined by equation (32).[227,228]

$$\Delta A = \varepsilon_G \cdot G_0 + \frac{\varepsilon_{\Delta HG}}{2}\left(\left(G_0 + H_0 + \frac{1}{K_a}\right) - \sqrt{\left(G_0 + H_0 + \frac{1}{K_a}\right)^2 - 4 \cdot H_0 \cdot G_0}\right) \quad (31)$$

$$\varepsilon_{\Delta HG} = \varepsilon_{HG} - \varepsilon_H - \varepsilon_G \quad (32)$$

Equations (31) and (32) imply that, for the more pronounced increase in the titration curve, species and/or a wavelength has to be chosen so that the difference between the molar absorptivities of the interacting components $\varepsilon_{\Delta HG}$ is large in value. On the other hand, since the expression (31) should be valid regardless of the wavelength, a binding isotherm for each λ can be obtained and fitted using K_a as a common parameter. Therefore, a much more reliable value for the complexation constant can be obtained.[230]

For the stoichiometry determination, value ($A - \varepsilon_H \cdot H_0 - \varepsilon_G \cdot G_0$) can be used due to its proportionality to [HG] to obtain a Job plot.[229]

Typically, concentrations in the micromolar range[227,229,230] (10^{-4}–10^{-6} M) are employed for UV/Vis spectroscopy, which according to the abovementioned condition (15) affords accurate determination of association constants as high as 10^8 M^{-1},[228] implying that this technique is suitable for the investigation of complexes whose stability is out of the NMR accuracy range.

2.4.4.3 ITC

2.4.4.3.1 Method overview

Since its first development in the 1960s,[249] isothermal titration calorimetry (ITC) was established as another powerful technique for the investigation of intermolecular interactions. This method relies on measuring heat that is produced or absorbed in a course of the addition of guest solution to host solution in order to monitor the equilibrium in the system.[250] Since almost all processes in physics,[251] chemistry, supramolecular chemistry[252] as well as biochemistry[253] are characterized by a heat (Q) or enthalpy (ΔH) change, ITC is a universal method that is suitable for interactions which involve either non-chromophores (as in case of UV/Vis spectroscopy) or species that are too complex to be able to distinguish and monitor signals of single protons (in case of NMR). The importance of this technique is underlined by the fact that within a single titration

one can obtain all the thermodynamic parameters of the process:[254] stoichiometry *n*, association constant K_a, process enthalpy ΔH —from the non-linear fitting of the experimental data; Gibbs free energy of the process ΔG and process entropy ΔS—from equations (2) and (33).

$$\Delta G = \Delta H - T\Delta S \tag{33}$$

2.4.4.3.2 ITC instrumentation

Modern calorimeters mostly employ power compensation method for producing the signal in the course of an experiment.[255] This means that an instrument has a sample cell and a reference cell surrounded by an adiabatic jacket to maintain isothermal conditions. Constant cooling is applied to both cells, and a constant heating power is applied to the reference cell by a reference heater, whereas a heater on the sample cell is controlled by a temperature sensor. During the titration, the rise (exothermic reaction) or drop (endothermic reaction) in temperature is sensed and the power of the sample cell heater is decreased or increased, respectively, to keep the temperature equal to the reference cell. The difference in the heating powers between the sample and the reference cells is the resulting time-dependent signal Q of such instrument. The sample cell is equipped with a stirrer to ensure proper mixing of the components, and the guest solution is injected into the cell in precise volume increments using a syringe.

2.4.4.3.3 Experimental design

As with other analytical techniques discussed above, it is essential to determine the conditions for the controlled parameters (H_0 and G_0) in order to produce reliable *n*, K_a and ΔH values. The experimental conditions have to be chosen in such a way that 1) the heat produced by the addition of each guest aliquot is large enough to be accurately measurable, and 2) the heat changes of subsequent aliquots must yield a distinguishable curvature of the binding isotherm.[255,256]

To describe the steepness of the isotherm, Wiseman parameter *c* equal to the product of the number of non-interacting binding sites *n* (stoichiometry), association constant K_a and starting (total) host concentration H_0 (equation (34)) is employed.[257] It was demonstrated that the most accurate determination of the binding constant from the non-linear regression is achieved for $c = 40$[258], however, conditions (35), which bear similarities to the condition (15), are considered to be acceptable for obtaining reliable data with minimized error (< 1 %).[255,256,259]

$$c = n \cdot K_a \cdot H_0 \tag{34}$$

$$10 < c < 100 \tag{35}$$

Therefore, for each system, the host concentration must be selected according to (35) but large enough to produce measurable heat signal.[259] The sensitivity of the instrument is, thus, a defining factor for upper K_a limit: calorimeters with sub-μJ sensitivity allow determination of K_a as high as 10^8–10^9 M^{-1}.[255] It is recommended for G_0 to be set as 20–50-fold H_0,[256] however, it was demonstrated that optimal ratio between the total guest and total host concentrations depends on the *c* parameter and can as well contribute to the minimization of experimental error.[259]

A further critical factor in the design of the experiment is the heat of mixing that can arise from unequal host and guest solution compositions. Because of the sensitivity of modern calorimeters and since, as mentioned above, due to the universality of the ITC, processes of different nature can cause signals in the experiment, it is crucial for a correct evaluation to eliminate the contributions of the components' dilution, which is done by conducting blank experiments. Hence, the true interaction heat $Q_{corrected}$ is obtained by subtraction of dilution heats of host $Q_{host,dil}$ and guest $Q_{guest,dil}$ and the instrument blank (titration of the pure solvent into the pure solvent, Q_{instr}) from the observed signal Q_{obs} (equation (36)).[255]

$$Q_{corrected} = Q_{obs} - Q_{host,dil} - Q_{guest,dil} - Q_{instr} \quad (36)$$

Because studied interactions can include (de-)protonation of the species (*e.g.*, in biochemical systems), buffer solutions are often used to control the process. Interestingly, the magnitude of the ionization enthalpy can be manipulated by buffer system selection.[256]

2.4.4.3.4 Data treatment

Normally, the guest solution is added into the sample cell filled with the host solution in precise aliquots, and signals arising on the time-dependent thermogram upon addition of each guest aliquot have shape of spikes because for a valid quantification, the difference between the sample and reference heater powers must reach zero before the next aliquot can be injected. Integration of the corrected signal and plotting the integral heat *versus* the total amount of guest added yields the titration curve, which, when a correct model applied for a non-linear fitting thereof, can deliver the desired thermodynamic parameters of the interaction (Figure 15).

The simplest model for a system of interest is a 1:1 binding, or more general, a single set of *n* identical (since biologically relevant macromolecules are often act as hosts/receptors) binding sites (it is assumed that a binding event at one site has no influence of another site).[255,256] Based on equation (6), the binding constant can be expressed as (37), where *f* is a fraction of bound host sites (or host molecules) defined by (38).[228]

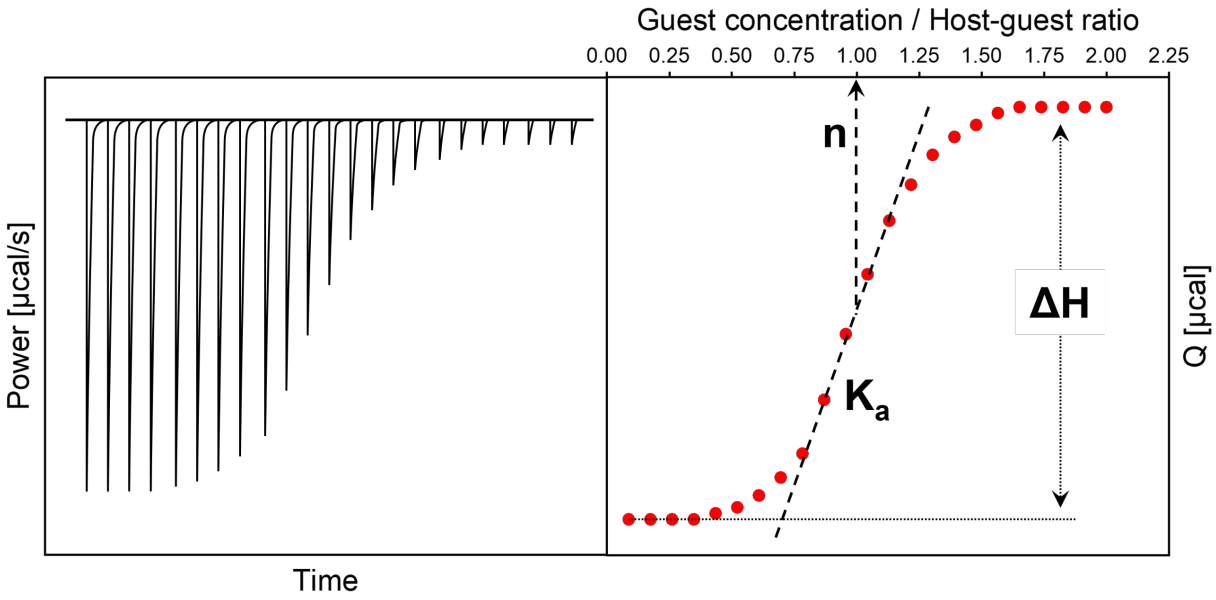

Figure 15. Hypothetical ITC experimental data. Left graph shows raw signal, right graph depicts a titration isotherm, in which each data point is an integral of a peak on the left graph. From the curve the thermodynamic parameters can be obtained: process enthalpy ΔH as a difference between the maximum and minimum heat; association constant K_a corresponds to the steepness of the curve; stoichiometry n is the x-coordinate of the inflection point of the isotherm.

$$K_a = \frac{f}{(1-f)\cdot[G]} \tag{37}$$

$$f = \frac{[HG]}{H_0} = \frac{[HG]}{[H]+[HG]} \tag{38}$$

In this case, the heat of the supramolecular process is connected to the parameters *n*, K_a, and ΔH using adjusted equation (13) in the form of (39).[228] Equation (39), however, only describes the total heat content of the system Q_i after the *i*-th guest aliquot addition.[255] Therefore, the total host ($H_{0,i}$) and guest ($G_{0,i}$) concentrations are changing upon each injection. In order to describe the heat change in each spike and, further, the binding isotherm, the heat of the previous injection Q(i−1) must be subtracted and the exemption of the solution volume equal to the aliquot volume ΔV_i from the sample cell must be considered (equation (40)).

$$Q_i = \frac{\Delta H \cdot V_0}{2}\left(\left(G_{0,i} + n\cdot H_{0,i} + \frac{1}{K_a}\right) - \sqrt{\left(G_{0,i} + n\cdot H_{0,i} + \frac{1}{K_a}\right)^2 - 4n\cdot H_{0,i}\cdot G_{0,i}}\right) \tag{39}$$

$$\Delta Q_i = Q_i + \frac{\Delta V_i}{2V_0} \cdot (Q_i + Q_{i-1}) - Q_{i-1} \tag{40}$$

This model can be extended to two or even multiple independent sets of identical binding sites, each with its own association constant $K_{a,i}$ (equation (41)).[255]

$$K_{a,i} = \frac{f_i}{(1 - f_i) \cdot [G]} \tag{41}$$

Sequential binding sites model take into consideration that the following binding events are affected by the previous ones resulting in stepwise association constants (Chapter 2.4.3). For a host molecule having *n* binding sites, each constant is expressed according to equations (42)–(44).[255]

$$K_1 = \frac{[HG]}{[H] \cdot [G]}, \; K_i = \frac{[HG_i]}{[HG_{i-1}] \cdot [G]}; \; 2 \leq i \leq n \tag{42}$$

$$H_0 = [H] + \sum_{i=1}^{n} [HG_i] \tag{43}$$

$$G_0 = [G] + \sum_{i=1}^{n} i \cdot [HG_i] \tag{44}$$

The correctness of the data evaluation can be estimated by the stoichiometry value *n* obtained from the non-linear fit. Clearly, *n* should be integer and, therefore, serious deviations from integer values are a sign of wrong host or guest concentration. Importantly, the determination of a correct value of G_0 is more crucial, since, as pointed out by Lewis and Murphy,[256] if the deviation is caused by incorrect H_0, the other obtained parameters—K_a and ΔH—are still determined accurately and represent the true values, and otherwise, if the G_0 is incorrect.

2.4.4.4 Summary of the techniques

A brief summary of the analytical methods for the determination of the binding affinity in supramolecular systems discussed in this chapter is given in Table 11.

Table 11. Summary of the discussed methods for binding affinity determination.

Technique	Suitable for	Concentration range	K_a range	Disadvantages
NMR	Organic molecules, polymers	$10^{-3} – 10^{-2}$ M	$< 10^5$ M^{-1}	Intermediate exchange conditions and many-component mixtures are not suitable. Relatively low K_a range
UV/Vis	Chromophores	$10^{-6} – 10^{-4}$ M	$10^4 – 10^8$ M^{-1}	Not applicable for non-absorbing systems
ITC	Everything	$> 10^{-7}$ M	$< 10^8 – 10^9$ M^{-1}	Sensitive towards side processes involving heat

2.5 Surface plasmon resonance spectroscopy

Surface plasmon resonance (SPR) spectroscopy is a highly sensitive optical method of analyzing the composition of thin films and studying processes occurring on metal surfaces.[6,260] The technique relies on the phenomenon of surface plasmons—electromagnetic surface waves excited at an interface between two media, whose dielectric constants ε_i have opposite signs, such as a metal–dielectric interface—which can be excited by light. The theory behind this phenomenon, first observed by Wood[261] on grating metal surfaces, was described decades later by Fano,[262] and developed further for the case of systems with attenuated total reflection in works of Otto[263] as well as Kretschmann and Raether[264] in 1968.

2.5.1 Excitation of surface plasmons

Surface plasmon is a TM-polarized evanescent wave propagating along the interface, meaning that the magnetic vector ***H*** is parallel to the interface and the intensity of the wave exponentially decreases with distance from the interface (Figure 16).[260] As a condition for the light to excite such plasma wave, the light wave vector's parallel component must match the one of the surface plasmon, thus inducing the resonance.[6] Furthermore, to achieve the coupling, the incident light must be p-polarized.

As already mentioned, it is possible to observe a surface plasmon at the interface of two media: metal and dielectric characterized by dielectric constants (of opposite signs) ε_m and ε_d, respectively. From the Maxwell's equations for a wave propagating along such interface, the parallel wavenumber component $k_x(\omega)$ is determined by the equation (45), where ω is the angular

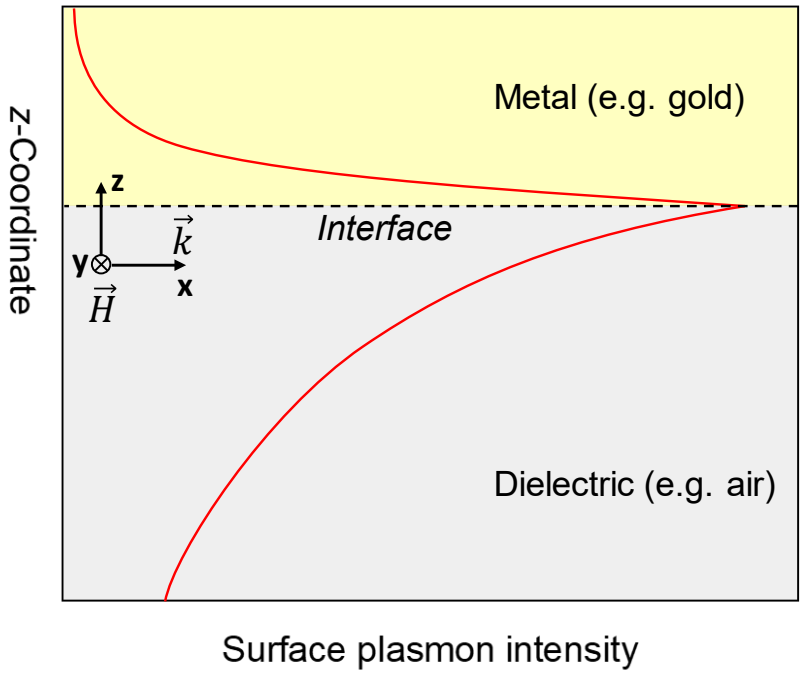

*Figure 16. A perpendicular profile of a metal–dielectric interface. The surface plasmon wave propagates along the x coordinate (vector k) in a TM-mode: Magnetic vector is orthogonal to the propagation vector and parallel to the interface plane (vector **H** is directed into the plane). The red curves represent the distribution of the plasmon intensity along the z axis.*

frequency of the electromagnetic wave and c is the speed of light in vacuum. For such mode to exist, the two media's dielectric constants must comply with the condition (46).[265] Usually, for a dielectric, $\varepsilon_d > 0$, which implies that ε_m must be negative.

$$k_x(\omega) = \frac{\omega}{c} \cdot \sqrt{\frac{\varepsilon_m \cdot \varepsilon_d}{\varepsilon_m + \varepsilon_d}} \tag{45}$$

$$\varepsilon_m < -\varepsilon_d \tag{46}$$

Clearly, the wavenumber of the surface plasmon (equation (45)) is higher than the wavenumber of light in vacuum (or dielectric) (equation (47)), therefore, it must be increased, *e.g.*, by passing the light beam through a coupler, *i.e.*, medium with a higher refractive index ε (equation (48)). Then the resonance condition of the surface plasmon excitation for a light beam falling onto the surface at an incidence angle θ_{SPR} is expressed as equation (49). Hence, the resonance can be achieved by adjusting the angle of incidence θ.

$$k(\omega) = \frac{\omega}{c} \tag{47}$$

$$k_x(\omega) = \frac{\omega}{c} \cdot \sqrt{\varepsilon} \cdot \sin\theta \tag{48}$$

$$\sqrt{\varepsilon} \cdot \sin\theta_{SPR} = \sqrt{\frac{\varepsilon_m \cdot \varepsilon_d}{\varepsilon_m + \varepsilon_d}} \tag{49}$$

In case the matching condition is fulfilled, a part of the energy of the incident light is transformed into surface plasmon (and further dissipated in the metal) leading to a loss of light intensity in the reflected light compared to the incident light.

2.5.2 Otto and Kretschmann configurations

If a glass prism is used as a coupler, one can work under the conditions of total internal reflection of the light beam from the inner wall of the prism, thus obtaining an evanescent wave, which can induce the surface plasmon through a layer of a dielectric or a metal. The former configuration where a glass prism is separated from a metal film by a layer of air (Figure 17, A) was designed by Otto.[263] The latter one was implemented by Kretschmann (Figure 17, B).[264] In this configuration, a thin metal layer is grown directly on the prism wall, and the evanescent wave produced by the total internal reflection of the incident light couples with the surface plasmon on the "outer" surface of the metal, *i.e.*, on the metal–air (or any other dielectric) interface. Due to a

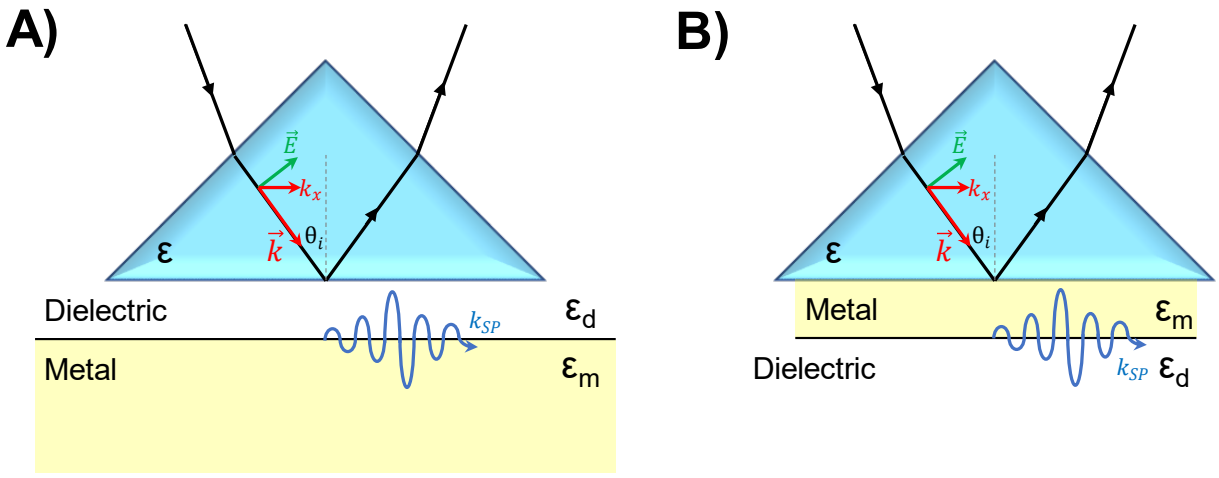

Figure 17. Configurations for surface plasmon excitation using (attenuated) total internal reflection. A) Otto configuration. The incident light is passed through a prism with dielectric constant ε, which is separated from metal with a dielectric layer, and is reflected from the back wall of the prism. Through the dielectric layer, the evanescent wave excites a surface plasmon at the metal–dielectric interface. B) Kretschmann configuration. The incident light is passed through a prism and reflected from a prism–metal interface. The evanescent wave penetrates the metal layer and excites a surface plasmon on the outer surface, i.e., metal–dielectric interface.

significantly easier practical implementation, the Kretschmann configuration is the one employed in modern SPR systems.

2.5.3 Penetration depth and sensing principle

The surface plasmon as an electromagnetic wave reaches its highest intensity at the surface and exponentially decays with increasing distance from it. Therefore, plasmons are characterized by penetration depth L_{pd} (*i.e.*, distances from the interface, at which the intensity decays by a factor of *e*), which depends on the wavelength λ as well as on the dielectric constants of the media.[6] Typical intensity distribution perpendicular to the interface plane is shown in Figure 16. Due to the fact that $|\varepsilon_m| > |\varepsilon_d|$ the intensity decay is significantly slower in the dielectric compared to the metal leading to a considerably higher concentration of the field and penetration depth L_{pd} in the dielectric. In case of metals such as gold and silver, typical L_{pd} values for a surface plasmon with λ = 630 nm are 24–29 nm into the metal and 160–220 nm into the dielectric.[260]

Thus, a propagating plasma wave can effectively "probe" a dielectric layer of about 400 nm in depth. Any changes occurring in the layer lead to a change in ε_d, which affects the plasmon wavenumber according to (45), and therefore, the resonance angle θ_{SPR}. This dependence underlies the working principle of SPR-based bio- and chemical sensors: the angular spectrum of the reflected light intensity depends on the composition and optical behavior of the dielectric layer and can be analyzed using Fresnel equations to obtain the information about dielectric constant (or, similarly, refractive index n_d) as well as thickness d of the layer.

An example of angular dependence of the relative intensity of the reflected light beam from incidence angle is presented in Figure 18. Here, a system is assumed, in which a thin gold layer (d = 50 nm; ε_{real} (real part of dielectric constant) = −12.3; ε_{imag} (imaginary part) = 1.29) is located between two semi-infinite media: air as a dielectric (ε = 1) and N-LaSF9 quartz (ε = 3.4036) as coupler. Two distinct features are clearly recognizable on the curve: an intensity increase at the critical angle (angle of total internal reflection) θ_{TR} and a minimum of intensity corresponding to the resonance at the angle θ_{SPR}. For given coupler's and dielectric medium's parameters, the shape of the spectrum around the critical angle and the position of the plasmon resonance depend on both the layer thickness d_{rec} and the refractive index (RI) $n_{d,rec}$ of a receptor (polymeric gel/biofilm/etc.) layer on the surface of the gold. Typically, the angle θ_{SPR} increases with increased d_{rec} and $n_{d,rec}$. However, if the layer thickness exceeds a critical value (in practice, around 400 nm), the plasmon wave cannot discriminate between different thicknesses anymore, and the position of the resonance minimum becomes solely dependent on the RI, whereas the area around θ_{TR} is susceptible to variations in both d_{rec} and $n_{d,rec}$ even for much thicker layers.[266]

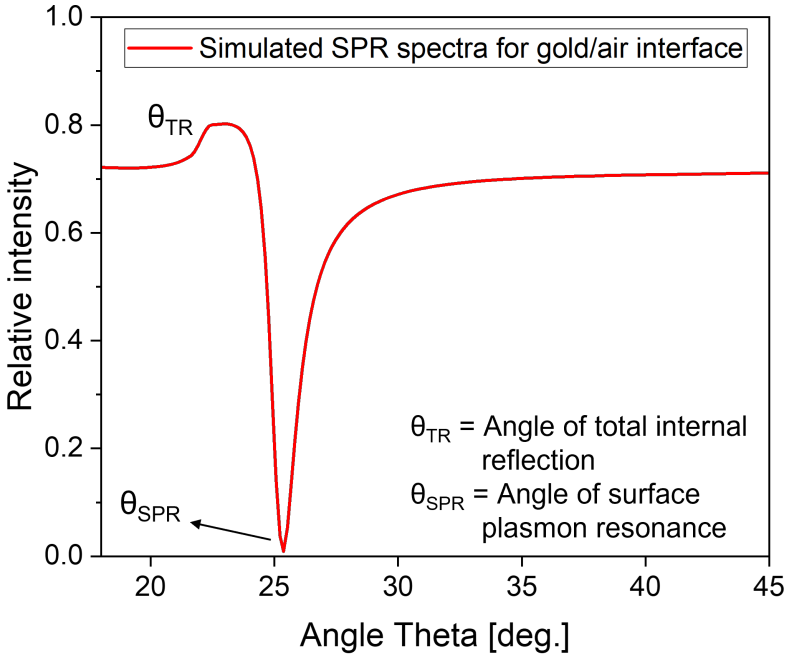

Figure 18. Simulated angular SPR spectrum at the interface 50 nm gold layer/air. As a coupler a N-LaSF9 (ε = 3.4036) quartz prism was assumed. Angle of total internal reflection and angle of the surface plasmon resonance are marked accordingly.

2.5.4 Experimental setup

A typical SPR-sensor setup in Kretschmann configuration for angular modulation measurements is shown in Figure 19. A light beam of a constant wavelength is excited by a laser. A chopper mounted after the laser generates rectangular modulation, which suppresses the noise and leads to a better signal-to-noise ratio. By an optical system, the beam is guided through two polarizers. The first one is responsible for the intensity of the incident beam, the second one endows the beam with p-polarization, which is, as mentioned above, one of the coupling conditions. Further, the light is passed through a quartz prism in a sample holder. Within the prism, the light's momentum is increased to match the momentum of the surface plasmon in accordance with the conditions (48). Normally, the metal layer is grown or deposited on a separate quartz wafer rather than directly on the prism, therefore, to eradicate possible undesired reflections at the wafer–prism interface, both are brought in contact using an immersion oil (index match) which has a refractive index close to that of the prism and wafer. A receptor (*e.g.*, a gel) is immobilized on the metal layer on the outer surface of the wafer and covered with a flow cell, by means of which an analyte can be injected or a medium (*e.g.*, air or a buffer solution) can be changed. The whole sample mount is set on a goniometer equipped with two stepper motors, the purpose of which is concerted as well as individual rotation of the sample and the detector (by θ and 2θ, respectively) around the vertical

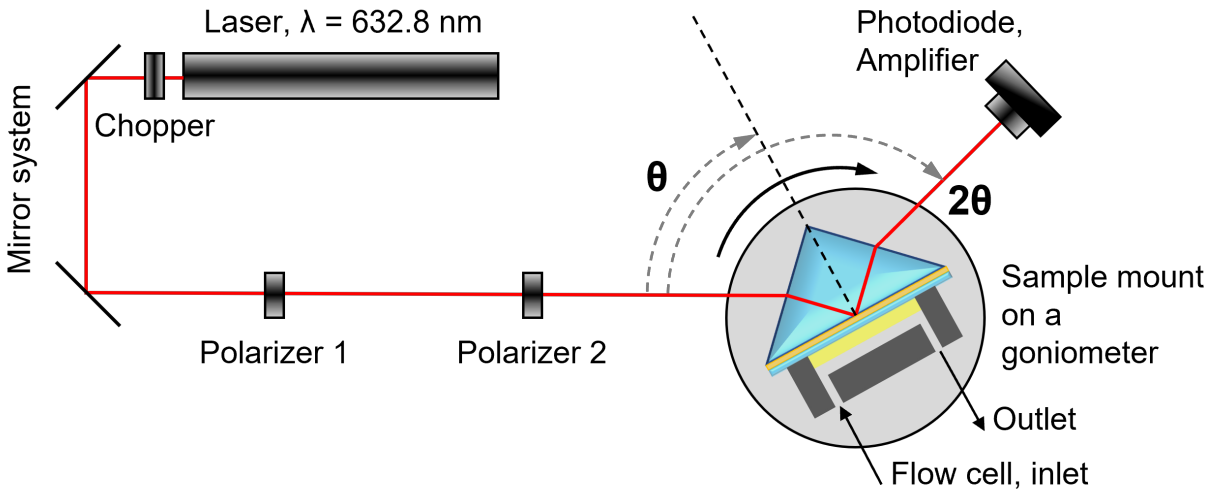

Figure 19. A setup for an SPR-sensor based on Kretschmann configuration. A detailed description is given in the text.

axis, and various screws for adjusting the incidence and reflection of the beam. After the reflection inside the prism, the beam reaches the detector coupled with an amplifier, which transforms the light intensity into an electric signal to obtain angular spectra as the one shown in Figure 18.

2.5.5 Applications of SPR spectroscopy

The possibility to conduct a highly sensitive, selective, and label-free analysis of systems accounts for the fact that SPR spectroscopy—an optical analytical technique based on the effect of SPR—is irreplaceable in many fields including chemistry, microbiology, medicine, and environmental monitoring.[6]

From the perspective of chemical applications, SPR is a powerful tool for studying processes occurring in hydrogels. So, the technique was employed for the investigation of swelling and de-swelling of hydrogels based on copolymers containing responsive units, such as NIPAAm, which is well-known to exhibit a LCST behavior. It was demonstrated that the transition temperature is such gels is dependent on the thickness of the initial dry gel, and two swelling behavior regimes are distinctly observable with a critical thickness d_{crit} = 280–500 nm.[267,268] Furthermore, SPR spectroscopy allows investigating the formation of hydrogel bilayers by applying a two-layer fitting model. The layers of a bilayer system comprised of a non-responsive and a responsive hydrogel were shown to maintain their swelling behavior compared to individual states.[269]

By immobilizing various receptor materials on the surface of gold, a sensor array can be constructed with high selectivity towards the desired analyte. This approach can be applied to environmental monitoring for the detection of various contaminants. A sensor for simultaneous detection of multiple pesticides (DDT, carbaryl and chlorpyrifos) was obtained *via* immobilization of analyte–protein conjugates of the gold surface with self-assembled alkanethiolates.[270] An

antibody binding inhibition principle was employed for the detection of the pesticides to achieve LOD in the range of 18–54 ng/L. A similar binding inhibition principle was applied for the detection of BPA, where BPA-modified sensor chip was treated with BPA solution containing a certain amount of a BPA-antibody.[271] Under such conditions, an elevated BPA concentration in the solution inhibited binding of the antibody to the surface. The LOD of such immunosensor was estimated around 10 ppb.

Further, SPR-based biosensors are utilized in medical diagnostics. Such immunoassays were devised for the detection of various cancer types at early stages using disease-specific biomarkers, such as RNAs, exosomes, proteins or antibodies.[272,273] An SPR-sensor for breast cancer diagnostics was developed by Sina, Vaidyanathan et al.[274] Using biotin–SAV binding motif, a gold surface was modified with exosomal markers exhibiting affinity towards different types of exosomes. Therefore, exosomes were captured from the injected solutions, and the cancer-specific ones, HER2, were detected from the population using HER2-antibody. This approach showed remarkable sensitivity with LOD as low as 2070 exosomes/µL.

To highlight the medicinal applications of the SPR spectroscopy, the technique was recently widely employed for the detection of corona viruses. SARS-CoV-2 is an RNA virus capable of causing a respiratory illness COVID-19, which caused a worldwide pandemic in early 2020. Since then, efforts have been made to develop a cure to the disease as well as methods for reliable and accurate detection of SARS-CoV-2 in humans. Since the COVID-19 outbreak, various SPR-based assays were devised for the said purpose.[275] One of the most recent biosensors was designed by the groups of Jia and Liu, in which spike protein antibodies were immobilized on Au surface as a bioreceptor for SARS-CoV-2.[276] The SPR sensor was demonstrated to be highly sensitive with LOD of 1 ag/mL in pharyngeal swab solution. Astonishingly, by employing antibodies attached to gold nanoparticles as an additional layer, the authors could improve the sensitivity even further reaching the LOD for SARS-CoV-2 as low as 0.1 ag/mL.

Last but not least, SPR can be used along with the methods discussed in Chapter 2.4 to calculate the association constant K_a between the receptor and the ligand/guest/analyte.[277] At a given incidence angle θ_i, the value of the equilibrated signal R_{eq} in the presence of the analyte in a concentration of G_0 can be expressed according to (50), where R_{max} is a signal at complete complexation. Plotting R_{eq} against G_0 and fitting the resulting isotherm yields binding constant as a fitting parameter.

$$R_{eq} = \frac{G_0 \cdot R_{max}}{G_0 + {}^{1}/_{K_a}} \tag{50}$$

3 Pillar[5]arene-based dually crosslinked supramolecular gel as a sensor for the detection of adiponitrile[1]

3.1 Introduction

3.1.1 Polymeric gels

Gels, *i.e.*, polymer chains interconnected via covalent crosslinking moieties into three-dimensional networks, represent one of the most important classes of synthetic materials.[1,279] Despite their versatility for numerous applications, such networks exhibit often insufficient mechanical properties and poor reversibility, which drastically limits the applicability of the gels. However, their fusion with supramolecular chemistry paved the way for numerous opportunities to enhance the properties of the gels, or even to endow the gels with unprecedented ones.[280] The introduction of supramolecular interactions (such as ionic interactions[281], metal/ligand complexes[282], hydrogen bonding[283] or host-guest inclusion complexes[284,285]) into the network results in the reversible crosslinks between the polymer chains. This, in turn, bestows the systems with improved mechanical properties[286] and susceptibility towards the changes in the medium and thus with stimuli-responsiveness. This feature is the key for the fabrication of smart materials that can be utilized in diverse areas ranging from tissue engineering[287], bioelectronics,[288] and drug delivery[289] to self-healing materials[290], actuators[291], and sensors.[59,285,292]

Lately, the focus of various research groups has been shifted onto polymeric networks that combine multiple types of crosslinks in one system[4,293]. Utilization of dual reversible crosslinking, for instance, was shown to endow the networks with multi-stimuli-responsiveness as well as shape memory behavior[294]. Furthermore, incorporation of a covalent and a non-covalent linkage types in a single gel was demonstrated to be highly promising since it receives the advantages of both types[295]: the former provides an integrity of structure to the system, whereas the latter is responsible for the reversibility and responsiveness. Such combination proved to be beneficial for the fabrication of reusable devices, which is especially important in sensing applications. Recently, dually cross-linked hydrogel sensors were developed in our working group for the detection of small molecules[191] and ovarian cancer biomarker[7] LPA. Reversible crosslinks in a form of a host-guest complex with β-CD were disrupted in the presence of an analyte—a compound with a higher binding affinity to CD—which led to a decrease in the crosslink density and, therefore, to an increased swelling. The swelling behavior was monitored

[1] Parts of this chapter were published in [278].

by SPR spectroscopy[273], the sensitivity of which offered a limit of detection of the LPA as low as 0.122 μM.

3.1.2 Nitriles

Nitriles comprise a chemical substance family which is of high importance in various areas such as chemical industry (where they are extensively used as precursors for plastics, fibers, etc.[296,297]), or medicine (*e.g.*, as biomarkers of chemotherapy-related kidney damage in cancer patients[298]). In the field of chemical industry adiponitrile is one of the key members of the nitrile family. It is used in the synthesis of nylon-6,6, which is the reason for a very high demand for it (annual production over 1.5 million tons[297]). Despite being crucial for market, nitriles can exhibit high toxicity[299], and adiponitrile can pose a risk for human health (hence being listed in the List of Extremely Hazardous Substances by the US Environmental Protection Agency), especially at high concentrations.[12,300] The studies conducted on fish revealed the lethal concentration of AN LC_{50} between 670 and 2140 mg/L[12] (corresponding to 6.2 to 19.8 mM; the values are dependent on the species and the exposure duration), therefore, making it crucial to introduce a reliable method of monitoring AN levels in the environment.

3.1.3 Aim of the current project

In the current work, we aimed at designing a supramolecular sensor chip for the detection of adiponitrile. Benefiting from a stable complex formation between P5A and AN, a gel-based sensor was developed bearing two types of crosslinks: chemical (irreversible) and supramolecular (labile), the latter based on a host-guest complex with P5A. Upon the presence of the analyte in the medium around a pre-swollen gel, the competitive complexation takes place with the analyte displacing the original guest species, which leads to disruption of the crosslinks and, thus, to the decrease in the crosslink density. This change can be measured by change in the swelling using a sensitive SPR technique (Figure 20).

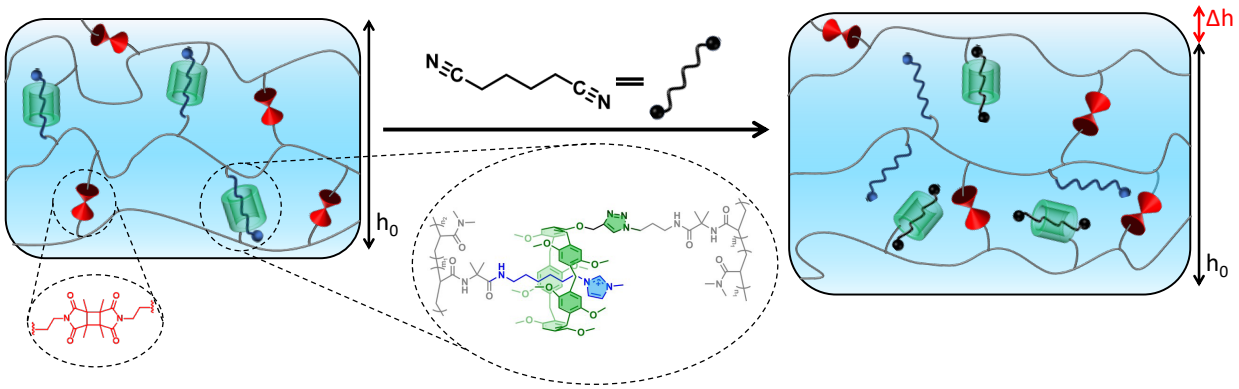

Figure 20. The concept of a pillar[5]arene-based dually crosslinked gel sensor for the detection of adiponitrile.

3.2 Synthesis and general considerations

3.2.1 Synthetic strategy

For a fabrication of a dually crosslinked system, it can be very beneficial to obtain separately host and guest polymers (*i.e.*, polymers with pendant host and guest groups) which upon mixing would produce a supramolecular gel. Introduction of a photo-crosslinking moiety, such as dimethylmaleimide[191,213,301,302], brings an advantage of on-demand chemical crosslink formation, which can be used to form a chemical gel in any form upon irradiation with light after conveniently processing the polymer blend as a solution. Such host, guest and crosslinker groups can be embedded into polymer chains either as comonomers in a copolymerization process or in course of post-modification of polymers containing reactive groups. The former approach is not free from disadvantages: firstly, the monomers might not have similar reactivities, thus, leading to an uneven distribution of functional groups along the chain; secondly, this approach is less flexible towards the composition of the resulting copolymers. Therefore, we chose the post-modification approach, since it requires less components for the polymerization step (which means a higher adjustability), and the initial polymer can be used for both host and guest polymers implying a similar distribution of pendant moieties. As mentioned above, such post-modification requires a presence of a reactive comonomer, such as 4,4-dimethyl-2-vinylazlactone (VDMA).[303] VDMA has been gaining an increasing attention as a comonomer possessing an electrophilic ring, which can be opened in a "click"-manner at a high rate and efficiency by various nucleophiles, especially by amines.[304] Recently, the advantages of this versatile monomer were employed to create adjustable and smart co- and block-copolymers.[213,305,306,307] Hence, the utilization of a copolymer containing VDMA allows highly efficient post-modification by a species possessing an amine functionality, which serves as a foundation for the design of host and guest moieties.

One of the features of PnAs that make them highly versatile host species is the possibility of their functionalization *via* rim-group substitution.[10,97] Hence, various strategies were developed which paved the way for selective substitution of one, two or more alkyl rim groups as well as for achieving regioselectivity thereof (see Chapter 2.2.2).[97,98,308] For a fabrication of host polymers with pendant P5A groups a selective mono-substitution is required, which can be implemented by two major approaches: 1) by co-cyclooligomerization (the functionality is introduced directly during the macrocycle formation) and 2) by forming "homo"-P5A followed by mono-dealkylation and subsequent etherification. We chose the second pathway for several reasons. DMP5A in the first step can be produced in a relatively high yield (> 70 %) and on a gram scale without complex purification. For the selective mono-demethylation using BBr_3 it is crucial to find the perfect conditions, however, the unreacted P5A can be recovered from the mixture, which minimizes

losses and makes this procedure effective considering the overall yield. P5AOH containing a single hydroxyl group can be easily converted into a mono-functionalized P5A, for instance, by Williamson etherification. In the current work, we sought to improve the versatility of this method by introducing a propargyl function as a side chain. This allows utilizing azide-alkyne [2+3]-cycloaddition for further functionalization. As a result, P5A with a single triazole-containing amine-terminated side chain (HT) was synthesized with a yield of 17 % over 5 steps (Chapter 5.2.2). The intermediates and the product were characterized by ^{1}H, ^{13}C and 2D NMR as well as by MS. ^{1}H NMR spectrum of the HT is demonstrated in Figure 21.

3.2.2 Choice of a solvent

For the binding studies as well as for AN detection using the gel sensor chloroform was selected as a solvent for several reasons. Firstly, solubility of the investigated host and guest species is high enough for performing NMR titration experiments in this solvent. Secondly, the combination of relative low polarity as well as bulkiness of $CHCl_3$ stimulates the binding between P5A and guests in comparison to high-polarity solvents (such as in acetone or DMSO) or solvents that act as guest species themselves (for instance, CH_3CN or acetone).[309] High binding affinity is, in its turn, beneficial for both stability of the second crosslink in the gel and its sensitivity upon presence of the analyte. Thirdly, the fabricated polymers (as discussed further) were as well soluble in

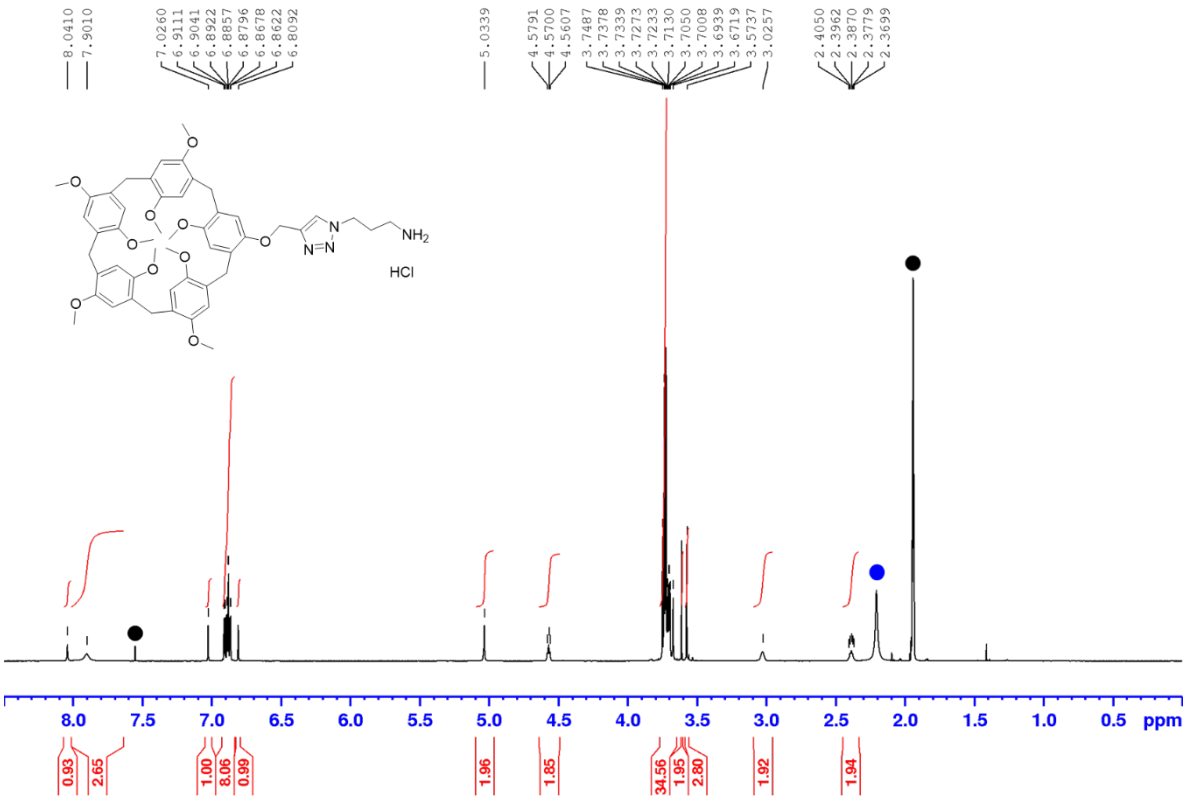

Figure 21. ^{1}H NMR (700 MHz) spectrum of HT in $CDCl_3$: CD_3CN (1:3). Solvent peaks are marked with black circles, water peak – with a blue circle.

chloroform, therefore, providing an adequate estimation of the system behaviour already on the low-molecular stage of investigations.

3.2.3 DMP5A–AN complexation

In order to create a chemoresponsive gel with supramolecular crosslinks which would break upon the presence of the analyte, a thorough selection of a host-guest system is required. The complex should possess a binding affinity in a certain range. On the one hand, it should not exceed (actually,

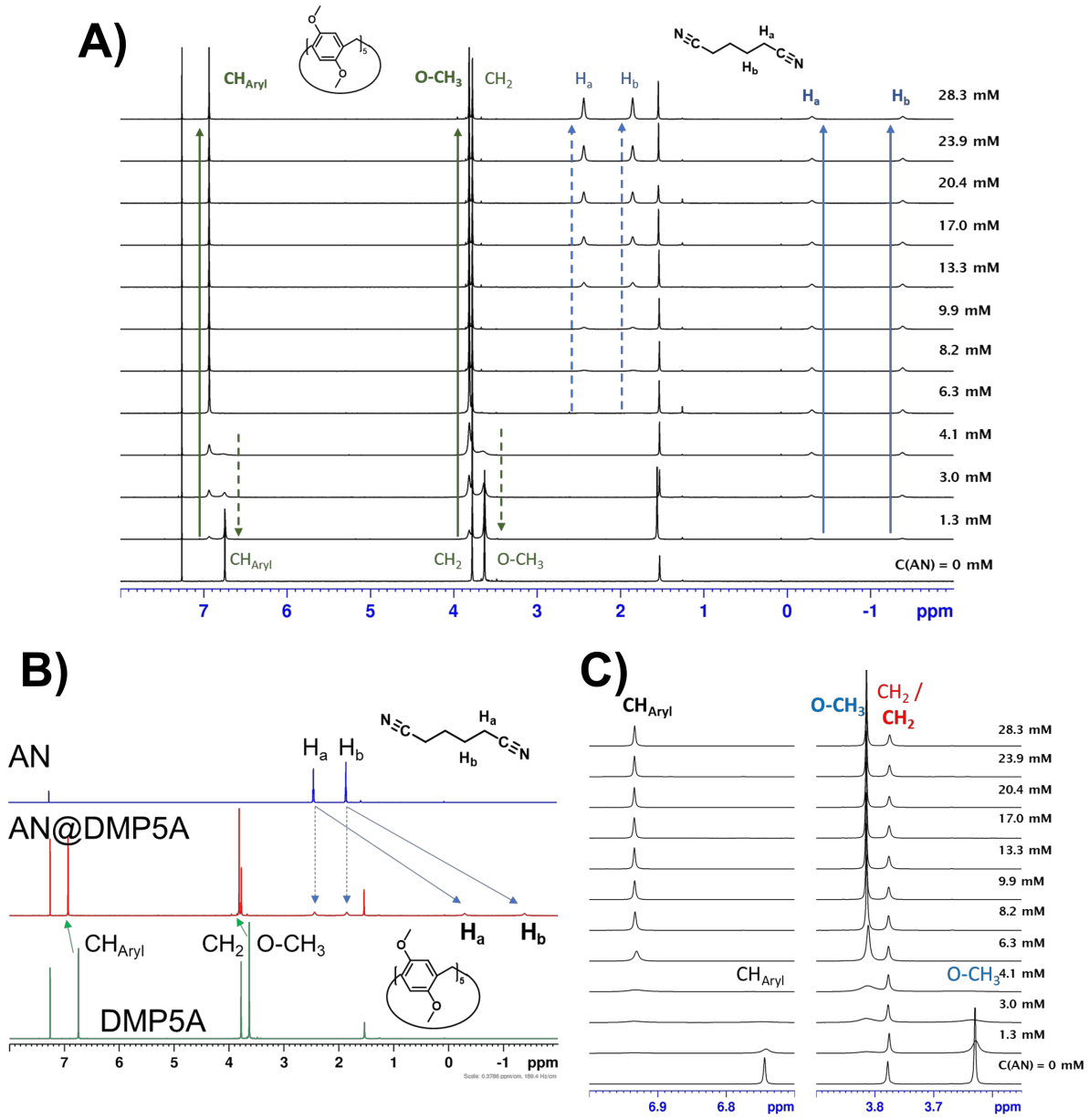

Figure 22. A) NMR titration of DMP5A with AN in $CDCl_3$ ($[H]_0$ = 6 mM). Green arrows and letters refer to the DMP5A, blue ones – to the AN. Solid and dashed lines demonstrate the evolution of the peaks belonging to the complexed and free species, respectively. B) NMR spectra of (from the bottom) DMP5A, AN@DMP5A complex (at $[G]_0 : [H]_0$ = 2.2:1), AN. The change in peak shifts of host and guest is presented by the green and blue arrows, respectively. C) Fragments of the NMR titration (AN@DMP5A), with only DMP5A peaks shown. The peaks of the complexed host are depicted in bold.

be at least one order of magnitude lower) the affinity between the analyte and the host moiety, otherwise the analyte in the solution would not have any effect on the crosslink density and, therefore, on the swelling behavior. On the other hand, if the binding affinity is too low, the crosslinking might not be formed at all, which, again, means a drastic decrease in responsiveness. As shown by Shu et al., [11] AN is capable of forming particularly stable pseudorataxanes with P5A (Chapter 2.2.3.2, Table 3) due to the combination of C–H···π and dipole-dipole interactions. In the paper, the authors were unable to deliver any value for K_a for the system per-*O*-alkyl-P5A/AN in $CDCl_3$ because of the limitations of the NMR titration technique. [227–229] A similar trend is observed in the case of the AN@DMP5A complex. The NMR titration was conducted in $CDCl_3$ at the constant host concentration $[H]_0 = 6$ mM (Figure 22, A and B) and the results are in accordance with previously reported ones.[11] In the spectra, peaks of both complexed and uncomplexed species are observable indicating a slow exchange. Noticeably, the peaks of the free AN do not appear until the 1:1 host:guest ratio is reached, and upon further addition of the guest species the complete disappearance of the free host peaks was observed (Figure 22, C). All these facts speak in favor of a highly stable binding between both species.

Further details of the complexation equilibrium can be provided by 2D NOESY NMR (Figure 23, A). Notably, the strong negative cross-peaks demonstrate that the peaks of both free and "threaded" AN belong to the same molecule, which implies that although the pseudorotaxane exhibits slow equilibrium, the guest molecules still exchange in a cavity within the time of an

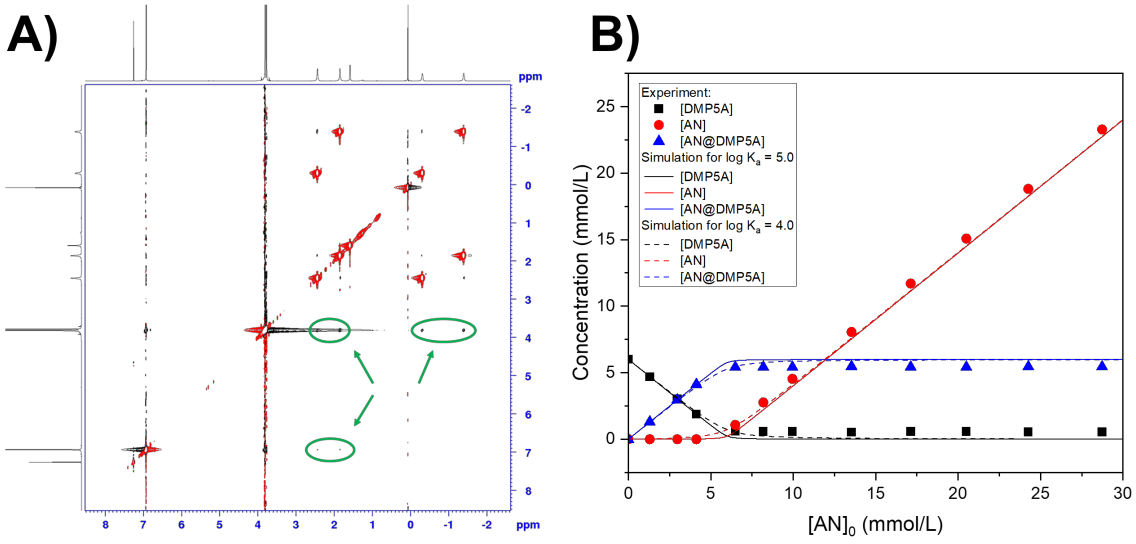

Figure 23. A) 2D NOESY spectrum of the system DMP5A–AN (1:2 eq.). NOE cross-peaks indicating proximity between AN and the macrocycle are marked green. B) Titration curves for DMP5A–AN system. Scattered plots: experimental data, line plots: simulated curves for the corresponding species (solid lines: log K_a = 5.0; dashed lines: log K_a = 4.0).

experiment. This is further proved by NOE cross-peaks (marked green) which appear for all AN protons.

To have an insight into the complexation strength the titration curves were simulated using HySS 2009 (Version 4.0.31) software[310] for a two-component system of 1:1 stoichiometry and two different binding constants. The resulting curves (Figure 23, B, solid lines: log K_a = 5.0; dashed lines: log K_a = 4.0) resemble the evolution of free host [DMP5A], free guest [AN] and complex [AN@DMP5A] concentrations depending on the total guest concentration $[AN]_0$. As can be seen from the figure, for both K_a values the curves align almost perfectly with the experimental data (the discrepancies taking place because of the AN and AN@DMP5A peak broadening, which results in an addition integration error) and with each other, therefore, demonstrating that log K_a (AN@DMP5A) is exceeding 4.0 but cannot be precisely determined using NMR titration.

3.2.4 Candidates for a guest moiety

From these considerations, as well as taking into account possible sensitivity issues, the upper limit for the binding affinity of the desired guest moiety to DMP5A can be set at around log K_a = 3.5. It is known that pillar[5]arenes can form stable pseudorataxanes with various neutral and positively charged heterocycle-capped axles,[138,143,144,311] such as imidazole, 1,2,3- and 1,2,4-triazoles (Table 4), methylimidazolium and pyridinium-substituted species (Table 6). The complexes of PnAs with various guests in relation to the stability of the supramolecular entities is discussed in detail in Chapter 2.2.3. Furthermore, methylimidazolium[223] and pyridinium[115,222,225] derivatives have been successfully used by various working groups as guest moieties for the preparation of pillar[n]arene-based gels. Final condition, since the host and guest moieties are designed as pendant groups on the polymer chains, the desired axles should only have one side substituted.

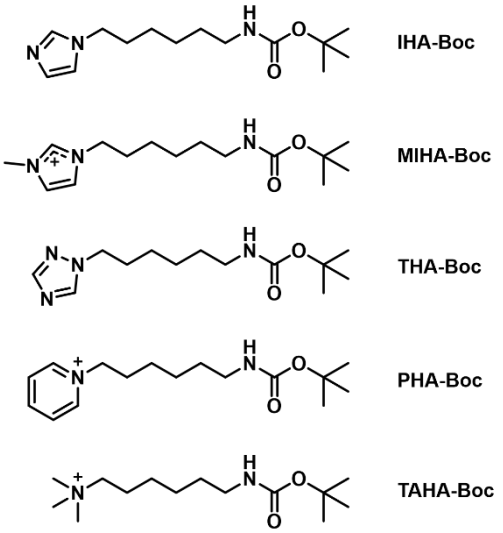

Scheme 8. Investigated guest moieties

In this work, with regard to the polymer post-modification arrangement, 6-aminohexan-1-ol was chosen as a basic building block for the guest moieties. After substitution of OH group with a bromine by refluxing in a concentrated HBr and subsequent Boc-protection of the amino group (Scheme 11), it was reacted with various nitrogen-containing species to obtain corresponding guests (Scheme 8). We chose the following axle substituents as potential candidates for the role of

the guest in the gel sensor: imidazol-1-yl, (3-methyl)imidazol-1-yl, 1,2,4-triazol-1-yl, pyridinium and trimethylaminium moieties.

3.3 NMR investigations of host-guest interactions[1]

In order to choose the best candidate, NMR titrations were conducted using Boc-protected aminohexane bearing the corresponding groups on the other end of the alkyl chain: IHA-Boc, MIHA-Boc, THA-Boc, PHA-Boc and TAHA-Boc (Scheme 8). Boc-protected moieties are much closer chemically to the pendant group structure in real gels (compared to the deprotected ones which are required for polymer modification), hence they were selected for the NMR titration. From the investigated guest moieties, MIHA-Boc (Figure 24 and 25), PHA-Boc (Figure 26 and 27) and THA-Boc (Figure 28 and Figure 29) exhibited fast exchange, while IHA-Boc (Figure 30 and 31) and TAHA-Boc (Figure 32 and 33) showed slow exchange on the NMR time scale, which is indicated by the presence of separate peaks of free and complexed species. For each complex Guest@DMP5A the titration was conducted up to 3.25–4.7 guest moiety equivalents. In case of the fast-exchange systems, the assignment of the proton signals of complexes was conducted by the analysis of the corresponding peak shifts evolution in the NMR titration spectra as well as using 2D COSY NMR, whereas for the systems exhibiting slow exchange, 2D NOESY spectra were analyzed to assign the signals.

3.3.1 Fast exchange complexes

3.3.1.1 MIHA-Boc@DMP5A

For the system DMP5A–MIHA-Boc the concentration of the guest moiety in the range of 0 to 14.4 mM (corresponding to host:guest ratios from 1:0 to 1:3.6) was used (Figure 24). On the spectra the shift of the peak positions can be traced. Firstly, the protons of the MIHA-Boc alkyl chain undergo an upfield shift, which is induced by the inclusion of the guest molecule into the macrocycle. It can be noticed that the closer a methylene group is located to the imidazole fragment, the more pronounced the shielding effect is (Figure 24, A; peak assignment according to 2D COSY NMR, Figure 25, B): whereas for the proton H_a (for $[H]_0$:$[G]_0$ = 1:0.83) the $\Delta\delta$ = – 2.26 ppm and a strong broadening is observed, for the proton H_e $\Delta\delta$ = –0.14 ppm, and for H_f even a slight deshielding takes place: $\Delta\delta$ = +0.04 ppm with almost no broadening of the signal. The protons of the imidazole fragment exhibit different trends. H_g which is normally the most deshielded due to the positive charge of the MIHA-Boc shows a very strong upfield shift and signal broadening in the presence of DMP5A ($\Delta\delta$ = –2.47 ppm). The proton H_h, however, demonstrates

[1] The discussion of this chapter is based on results from Ref. [312].

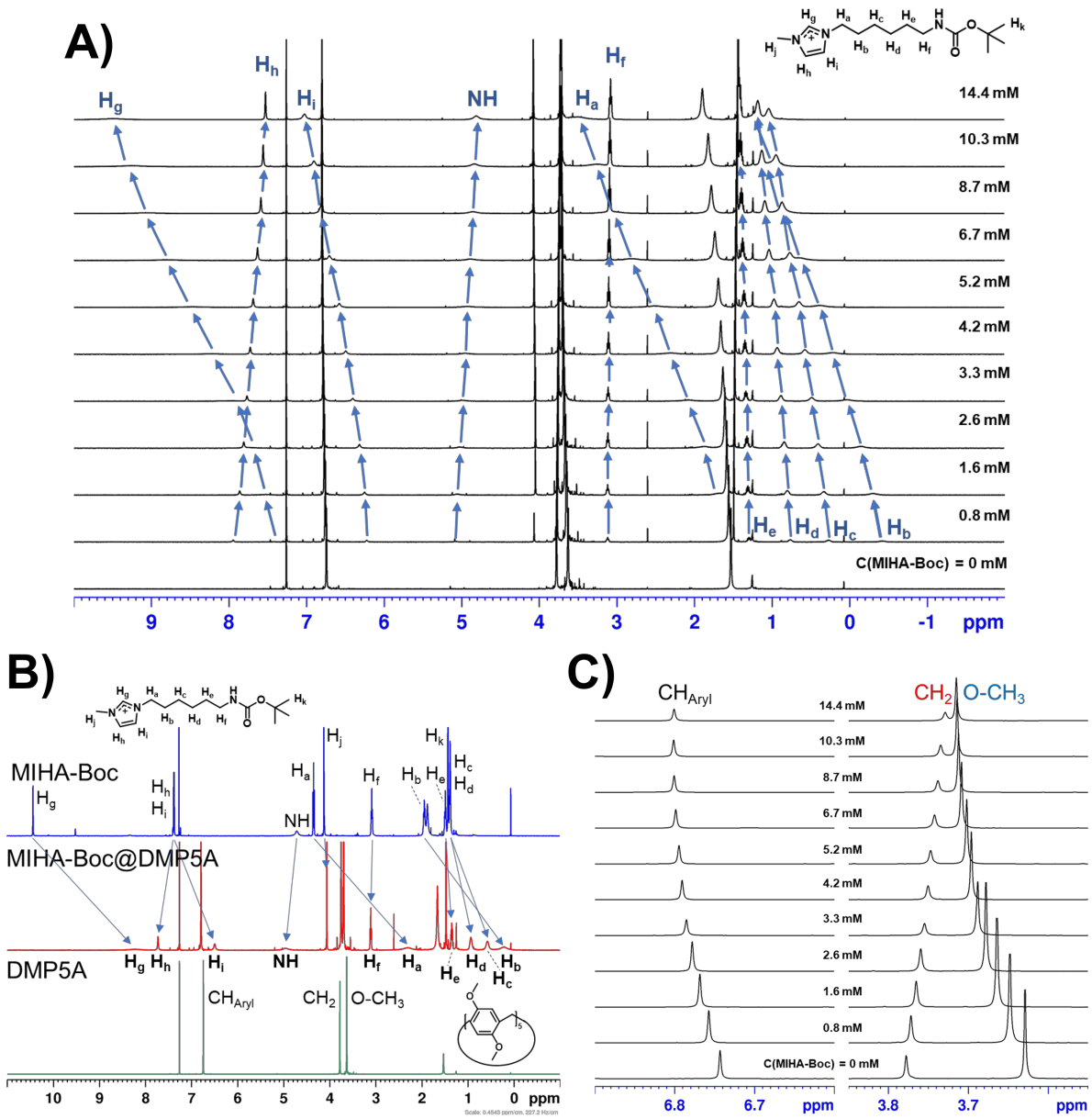

Figure 24. A) NMR titration of DMP5A with MIHA-Boc in $CDCl_3$ ($[H]_0$ = 4 mM). B)) NMR spectra of (from the bottom) DMP5A, MIHA-Boc@DMP5A complex (at $[G]_0$ = 3.3 mM), MIHA-Boc. The change in peak shifts of the guest molecule is presented by the arrows. C) Fragments of the NMR titration (MIHA-Boc@DMP5A), with shifts of only DMP5A peaks shown.

an opposing trend with a downfield shift: $\Delta\delta = +0.40$ ppm. 2D NOESY spectrum, however (Figure 25, A), does not reveal any cross-peaks that might be indicators of the inclusion complex geometry.

As for DMP5A signals (Figure 24, C), a clear trend can be noticed that deshielding takes place for methoxy groups and aromatic protons, which is in accordance with earlier literature reports for DMP5A.[149] Interestingly, the protons of methylene bridges exhibit slight shielding in all fast exchange systems.

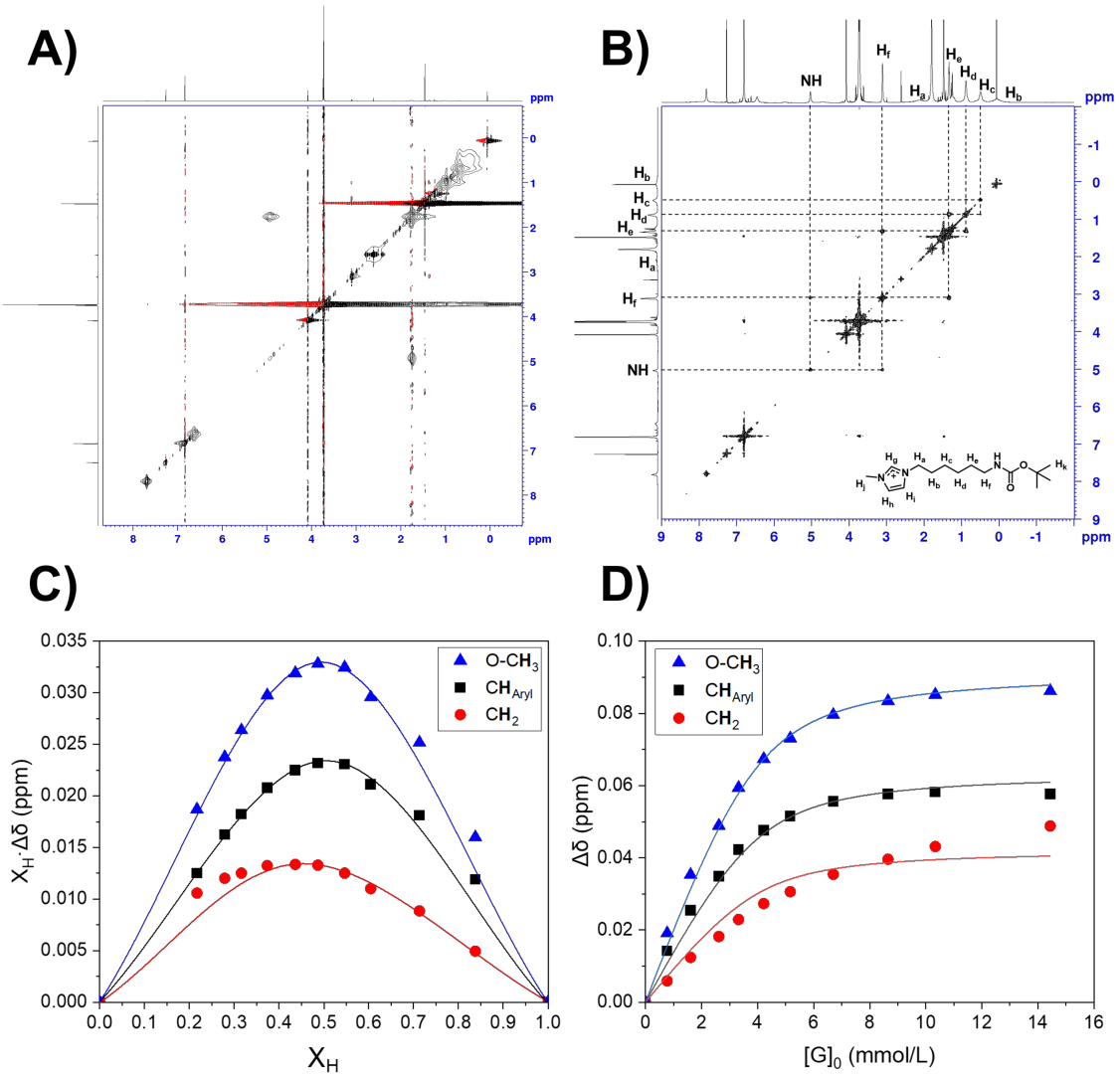

Figure 25. A) 2D NOESY spectrum of the system DMP5A–MIHA-Boc (1:1 eq.). B) 2D COSY spectrum of the MIHA-Boc@DMP5A complex. C) Job plot of the DMP5A–MIHA-Boc titration. The maximum of all three peaks of DMP5A lie around 0.5, which proves a 1:1 stoichiometry of the complex (The lines serve as guides for the eye). D) Titration curves corresponding to the DMP5A protons. The fit curves are obtained using a non-linear least square method with K_a as a common parameter for all dependencies.

From the DMP5A peak shifts, the stoichiometry of the MIHA-Boc@DMP5A complex and its binding constant was calculated. Job plots obtained from the shifts of each proton (Figure 25, C) indicate a 1:1 stoichiometry of the pseudorataxane due to the maximum of all the curves lying at approx. 0.5. Using the non-linear regression method for the 1:1 complexation model (Figure 25, D), the constant K_a as a global parameter and the chemical shift at full complexation $\Delta\delta_{max}$ for each of the peaks were obtained (Table 12). For the complex MIHA-Boc@DMP5A, the obtained value of $K_a = (2150 \pm 470)\ M^{-1}$ ($\log K_a = 3.32 \pm 0.10$).

3.3.1.2 PHA-Boc@DMP5A

The NMR titration was conducted in the PHA-Boc concentration range of 0 to 13.0 mM (1:0 to 1:3.25 host:guest ratio, respectively; Figure 26). Similar to the MIHA-Boc@DMP5A complex, the upfield shift of the alkyl protons H_b–H_e (Figure 26, A, B) can be traced with decreasing shielding effect strength ($\Delta\delta$ = –2.49 ppm and –0.07 ppm for H_b and H_e, respectively; assignment is performed using 2D COSY spectrum, Figure 27, B). The shielding effect on the proton H_a is so strong that its signal is not observed in the spectrum of the pseudorotaxane. In contrast to the other protons of the alkyl chain, H_f undergoes a slight deshielding upon DMP5A presence

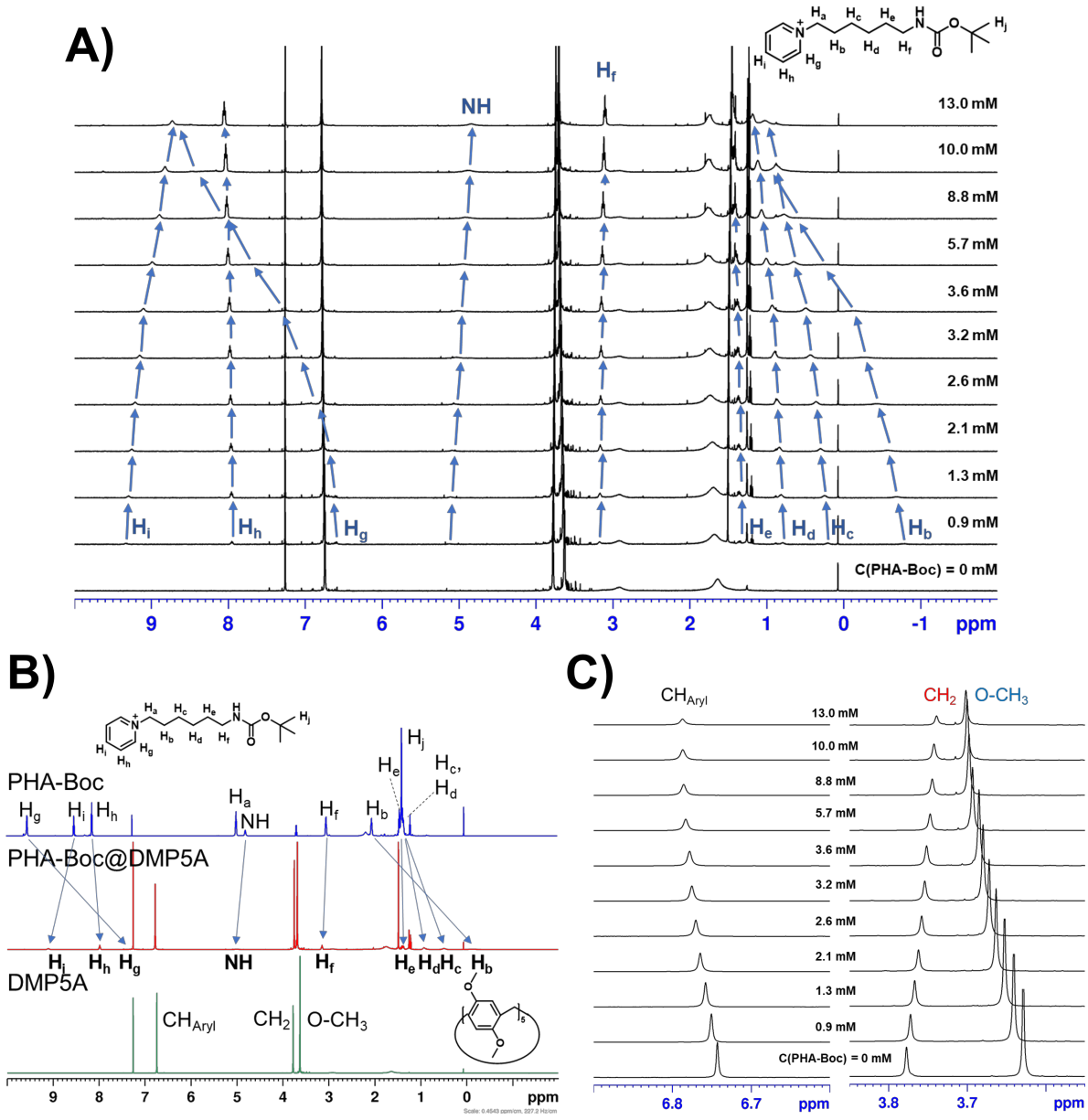

Figure 26. A) NMR titration of DMP5A with PHA-Boc in $CDCl_3$ ($[H]_0$ = 4 mM). B) NMR spectra of (from the bottom) DMP5A, PHA-Boc@DMP5A complex (at $[G]_0$ = 3.6 mM), PHA-Boc. The change in peak shifts of the guest molecule is presented by the arrows. C) Fragments of the NMR titration (PHA-Boc@DMP5A), with shifts of only DMP5A peaks shown.

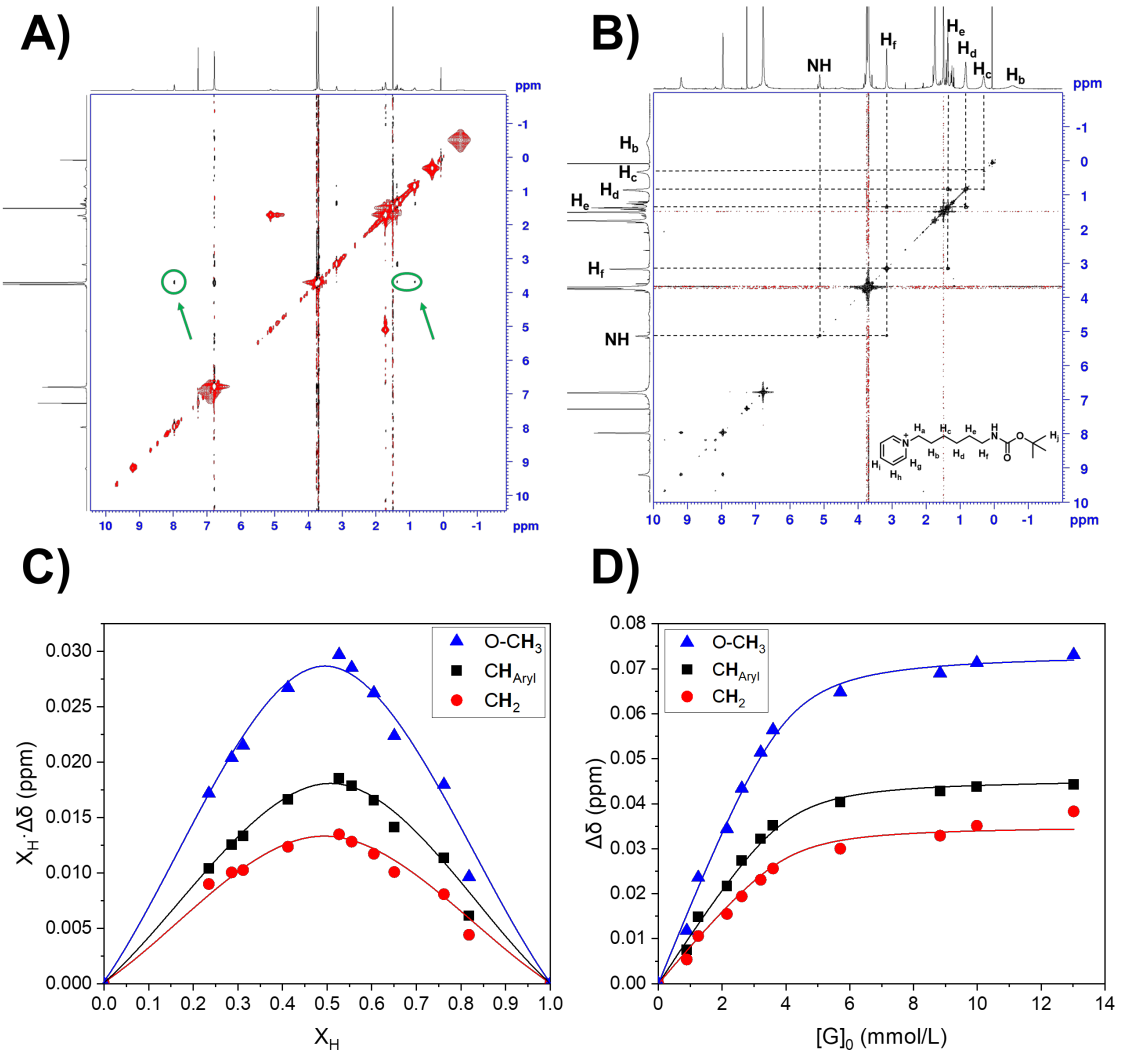

Figure 27. A) 2D NOESY NMR of the complex PHA-Boc@DMP5A. The NOE cross-peaks between host and guest species are marked green. B) 2D COSY spectrum of the PHA-Boc@DMP5A complex. C) Job plot of the DMP5A–PHA-Boc titration. The maximum of all three peaks of DMP5A is around 0.5, which proves a 1:1 stoichiometry of the complex (The lines serve as guides for the eye). Titration curves corresponding to the DMP5A protons. The fit curves are obtained using a non-linear least square method with K_a as a common parameter for all dependencies.

($\Delta\delta$ = +0.12 ppm). From the aromatic peaks of the PHA-Boc the significant upfield shift and broadening is exhibited by the *ortho*-proton H_g, suggesting a pronounced shielding due to the inclusion into DMP5A and coulomb interaction with the electron-rich cavity thereof. Interestingly, even the "outer" *para*-proton H_i exhibits a slight upfield shift whereas the *meta*-proton H_h shifts to the low field. The inclusion complex formation was further supported by 2D NOESY NMR (Figure 25, A). The spectrum shows cross-peaks corresponding to the interactions between H_h as well as H_d and H_e of PHA-Boc with methoxy groups of DMP5A.

The peaks of the host molecule shift similarly to the MIHA-Boc@DMP5A complex (Figure 26, C). The maximum of the Job plots (Figure 27, C) indicates a 1:1 stoichiometry of the pseudorotaxane. The binding constant $K_a = (4580 \pm 980)\ M^{-1}$ ($\log K_a = 3.66 \pm 0.09$) determined

using to the non-linear method (Figure 27, D) is higher than for MIHA-Boc@DMP5A implying a more stable complex.

3.3.1.3 THA-Boc@DMP5A

The DMP5A titration with THA-Boc was conducted with the guest concentrations ranging from 0 to 19.2 mM (corresponding to host:guest ratios from 1:0 to 1:3.8; Figure 28). Unlike the previously discussed complexes, the formation of THA-Boc@DMP5A can be demonstrated[313] by broadening but no significant shift of the protons of the guest moiety (Figure 28, A, B). Interesting to note the different behavior of the 1,2,4-triazole fragment protons: H_h situated closer to the alkyl chain exhibits strong broadening whereas H_g on the outer side of the heterocycle does

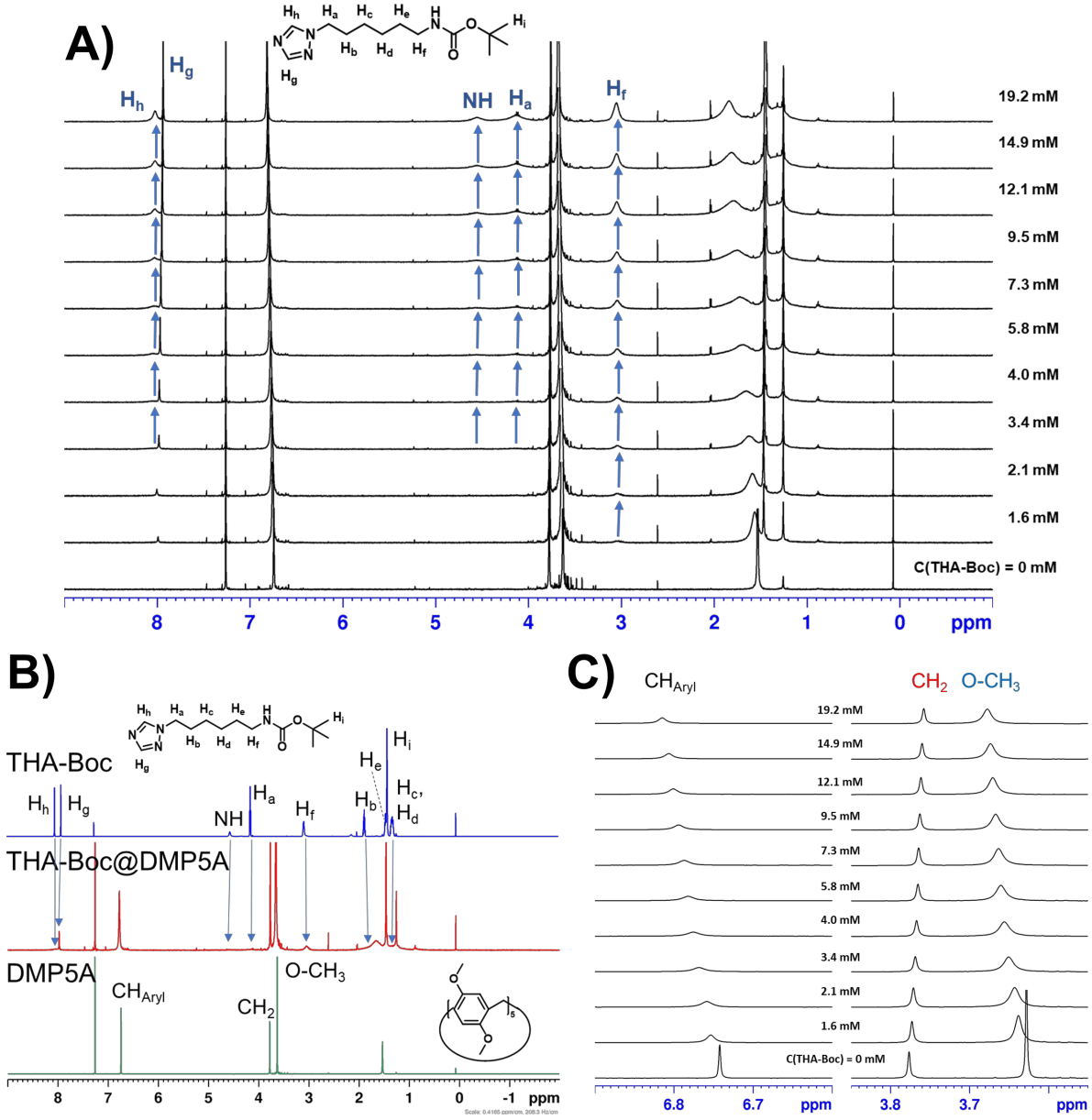

Figure 28. A) NMR titration of DMP5A with THA-Boc in $CDCl_3$ ($[H]_0$ = 4 mM). B) NMR spectra of (from the bottom) DMP5A, THA-Boc@DMP5A complex (at $[G]_0$ = 4.0 mM), THA-Boc. C) Fragments of the NMR titration (THA-Boc@DMP5A), with shifts of only DMP5A peaks shown.

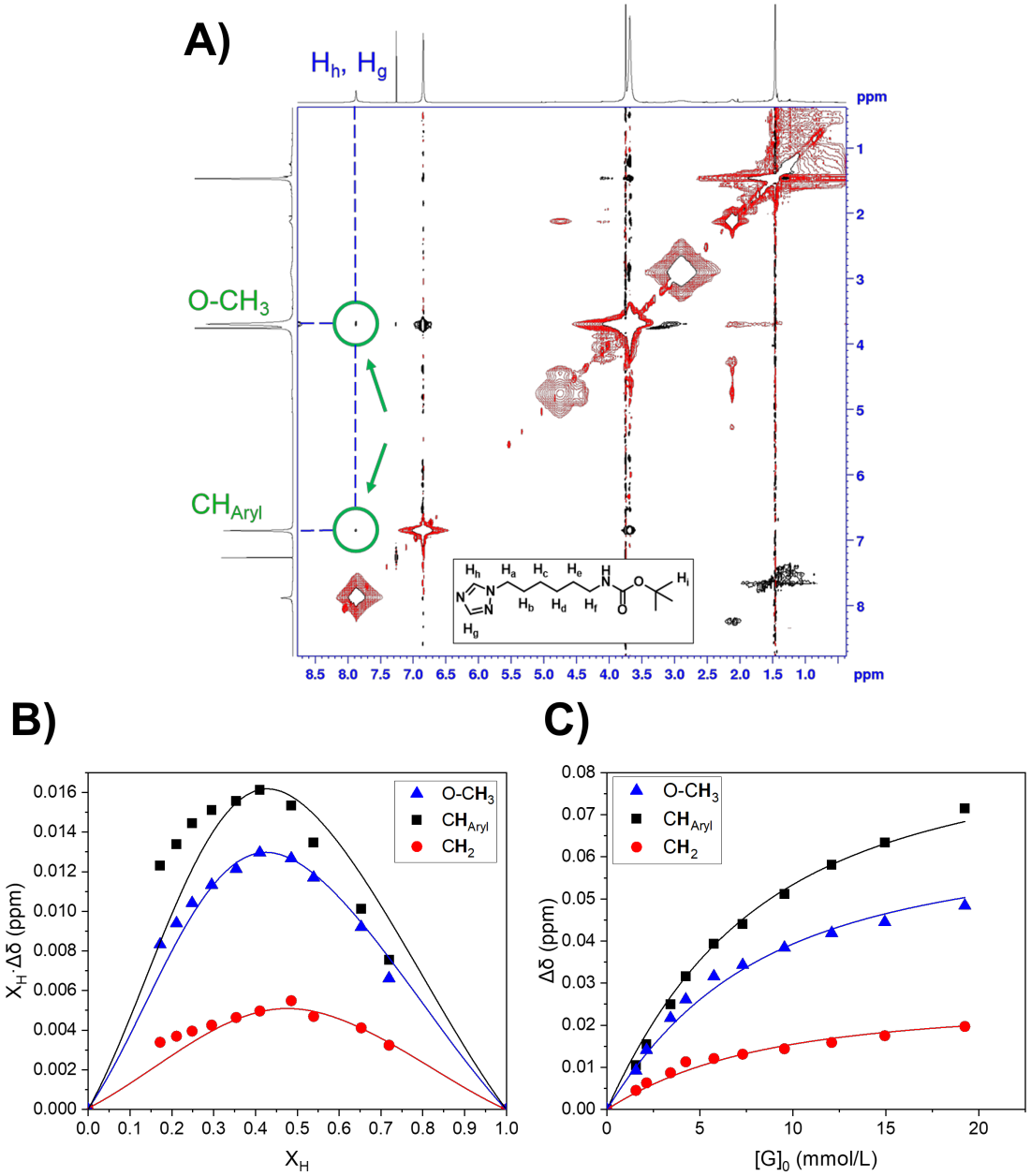

Figure 29. A) 2D NOESY NMR of the complex THA-Boc@DMP5A. The NOE cross-peaks between host and guest species are marked green. B) Job plot of the DMP5A–THA-Boc titration. The maximum of all three peaks of DMP5A is around 0.5, which proves a 1:1 stoichiometry of the complex (The lines serve as guides for the eye). C) Titration curves corresponding to the DMP5A protons. The fit curves are obtained using a non-linear least square method with K_a as a common parameter for all dependencies.

not. This might be attributed to the positioning of the guest molecule in the DMP5A with triazole peeking outside of the cavity. Due to such placement the outer proton H_g is not screened by the macrocycle and, therefore, its relaxation proceeds slower compared to the proton H_g, which results in a sharp peak even in a complexed state.

The host-guest complex formation was further proven by NOESY NMR (Figure 29, A). The cross-peaks between triazole protons and the methyl as well as aromatic protons of DMP5A (highlighted

green), demonstrate that the triazole tail of the THA-Boc are in proximity to the protons of the cavity. However, since H_g and H_f overlap in the investigated ^1H NMR spectra, it is not possible to determine which of the protons interacts with DMP5A.

The stoichiometry of the pseudorotaxane is determined with the Job plot (Figure 29, B) to be 1:1, which allows the application of the 1:1 binding model to calculate the complexation constant: $K_a = (185 \pm 18)\ M^{-1}$ ($\log K_a = 2.27 \pm 0.04$) (Figure 29, C). This value is by an order of magnitude lower than the ones of MIHA-Boc@DMP5A and PHA-Boc@DMP5A indicating a relatively weak complex in $CDCl_3$.

It can be observed that from the systems with fast exchange on the NMR timescale the charged species (MIHA-Boc and PHA-Boc) have a significantly (by one order of magnitude) higher binding affinity (and therefore, more stable complexes) than neutral THA-Boc: $\log K_a = 3.32 \pm 0.10$, 3.66 ± 0.09 and 2.27 ± 0.04, respectively, see Table 12. The absence of THA-Boc signal shifts can be hence explained by too weak interactions between the guest and DMP5A in $CDCl_3$.

Table 12. Binding constants and chemical shift at full complexation determined by NMR-titration

Complex	log K_a	O-CH_3		CH_{Aryl}		CH_2	
		$\Delta\delta_{max}$, ppm	R^2	$\Delta\delta_{max}$, ppm	R^2	$\Delta\delta_{max}$, ppm	R^2
MIHA-Boc @DMP5A	3.32 ± 0.10	0.092 ± 0.002	0.9853	0.064 ± 0.002	0.9926	0.042 ± 0.002	0.9680
PHA-Boc @DMP5A	3.66 ± 0.09	0.074 ± 0.001	0.9950	0.046 ± 0.001	0.9947	0.035 ± 0.001	0.9813
THA-Boc @DMP5A	2.27 ± 0.04	0.066 ± 0.003	0.9853	0.090 ± 0.003	0.9926	0.026 ± 0.001	0.9680

3.3.2 Slow exchange complexes

As mentioned before, the results of this work suggest that the complexes IHA-Boc and TAHA-Boc exhibit slow exchange on the NMR timescale, which is indicated by the presence of separate peaks of free and complexed species.

3.3.2.1 IHA-Boc@DMP5A

For the IHA-Boc@DMP5A this finding correlates with an extensive studies of P5A complexes with imidazole-substituted alkanes performed by Li, Jia et al.[149] According to their investigations, bis(imidazolyl)-containing guest molecules are characterized by a slow exchange with the DMP5A (Table 4). Although IHA-Boc in the present work contains an imidazole moiety only on the one end of the axle, the complex still exhibits a slow exchange (Figure 30) arguably due to a higher number of methylene groups of the alkyl chain and a carbamate group on the other end. As is the

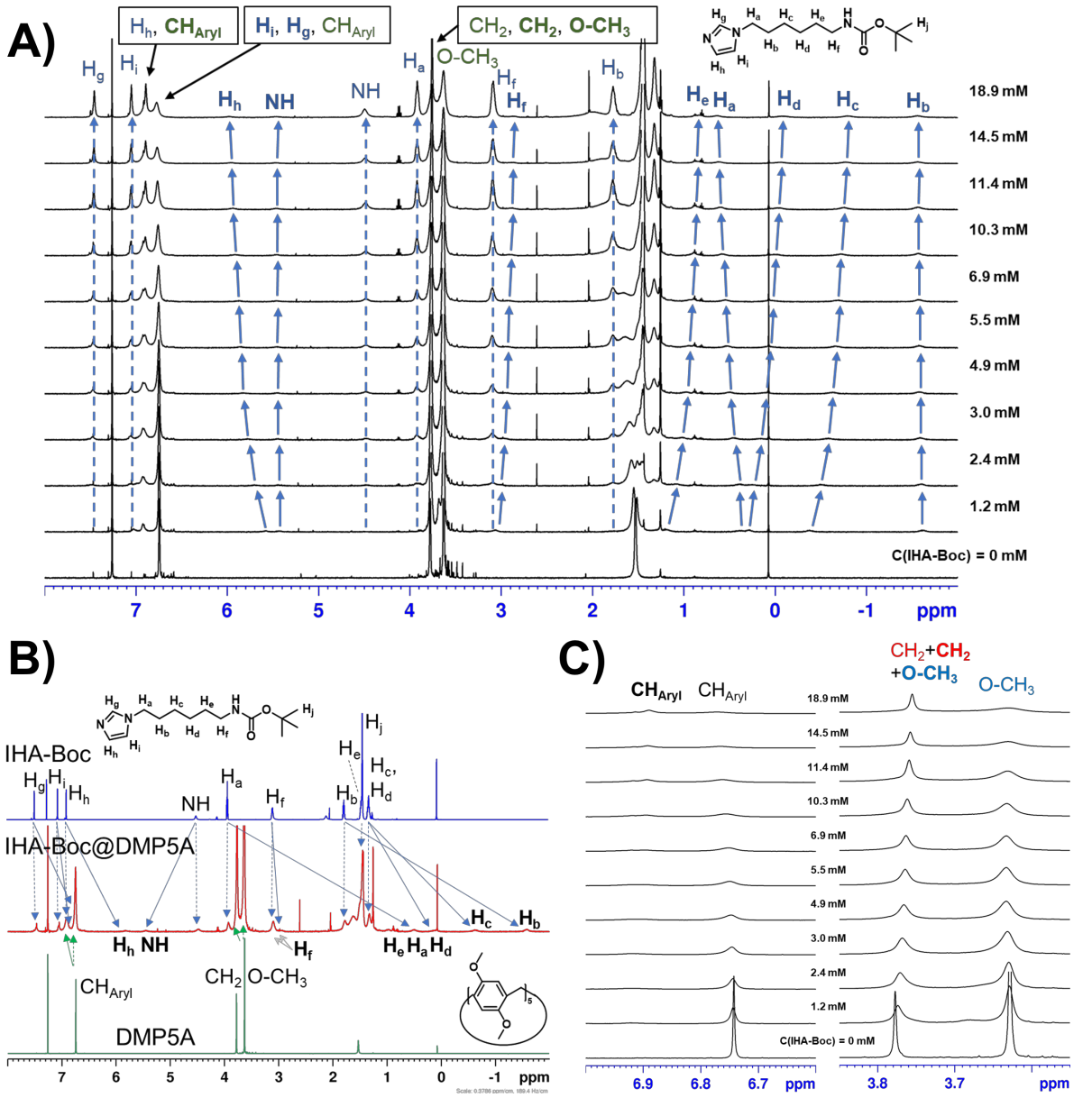

Figure 30. A) NMR titration of DMP5A with IHA-Boc in $CDCl_3$ ($[H]_0$ = 4 mM). Normal and bold designations refer to free and complexed species. B) NMR spectra of (from the bottom) DMP5A, IHA-Boc@DMP5A complex (at $[G]_0$ = 4.9 mM), IHA-Boc. The change in peak shifts of the molecules is presented by solid arrows; dashed arrows demonstrate the peaks of the free species. C) Fragments of the NMR titration (IHA-Boc@DMP5A), with shifts of only DMP5A peaks shown.

case with other host-guest complexes in this work, the methylene protons of the hexane chain undergo a strong shielding with a difference in chemical shift for the proton H_a reaching $\Delta\delta$ = -3.43 ppm (Figure 30, B).

The stoichiometry is determined by the integration of the peaks corresponding to the complexed DMP5A and IHA-Boc which interestingly revealed a 1:2 (DMP5A:IHA-Boc) geometry for the whole range of titration ratios. Although the spectra contain only one set of peaks belonging to complexed species, the peaks of alkyl protons of IHA-Boc shielded by the complexation

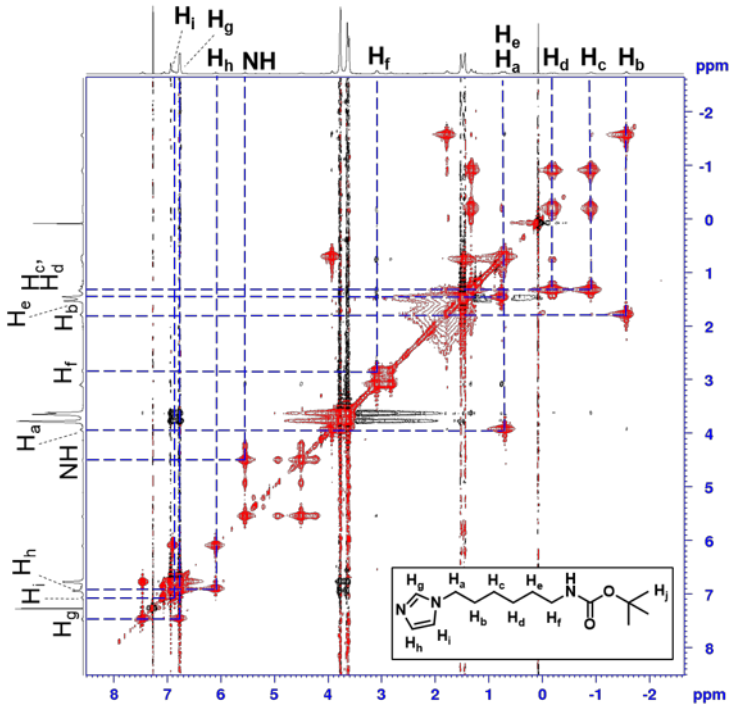

Figure 31. 2D NOESY NMR of the complex IHA-Boc@DMP5A. The blue dashed lines represent the relation between the peaks of the free and bound guest. On the horizontal and vertical projections, the peaks of a bound and free (respectively) guest signals are marked.

noticeably shift upon increasing IHA-Boc concentration (Figure 30, B). The assignment of the alkyl chain signals was performed using 2D NOESY (Figure 31, which, however, does not provide any cross-peaks characteristic for a host–guest complex). Surprisingly, unlike aforementioned MIHA-Boc@DMP5A or PHA-Boc@DMP5A whose alkyl peaks exhibit deshielding upon guest addition due to an increasing uncomplexed species ratio, the peaks of IHA-Boc (H_c and H_d) shift upfield suggesting an enhanced shielding and, therefore, a higher ratio of guest molecules taking part in the pseudorotaxane formation. This implies a three-state equilibrium between free host, free guest and two complex species in the solution (equation (51)).

$$H + 2G \overset{K_1}{\leftrightarrow} HG + G \overset{K_2}{\leftrightarrow} HG_2 \tag{51}$$

From these processes taking place in the system the first equilibrium (K_1) is plausibly slow on NMR timescale, whereas the second one (K_2) is fast, hence, the positions of peaks of H_c and H_d resemble the weighted average between two- and three-component complexes. The in-depth determination of the parameters underlying the interaction between IHA-Boc and DMP5A requires further investigations which are out of the scope of the present study.

The complexation constant K_a was calculated using the following equation (52), where $[HG_2]$ is the concentration of the complex $(IHA\text{-}Boc)_2$@DMP5A, [H] and [G] are the concentrations of free DMP5A and IHA-Boc, respectively, from the spectrum of 1:2 (host:guest) mixture.

$$K_a = K_1 \cdot K_2 = \frac{[HG_2]}{[H][G]^2} = 7900\ M^{-2} \quad (52)$$

3.3.2.2 TAHA-Boc@DMP5A

In the case of TAHA-Boc the interaction between host and guest is also slow on the NMR timescale (Figure 32). Alkyl peaks belonging to the axle included into the DMP5A cavity are strongly shifted upfield compared to the free TAHA-Boc, and similar to the other complexes the upfield shift and, hence, shielding of the protons decreases from H_a to H_e ($\Delta\delta$ = –3.15 ppm and +0.01 ppm, respectively). The protons of the methyl groups of the quaternary ammonium tail exhibit likewise a shift to the high field as well as a significant broadening. These protons are further shown by the NOE cross-peak on the 2D NOESY spectrum to be in a proximity of DMP5A methoxy groups (Figure 33, A). These findings suggest the placement of the guest moiety with its ammonium tail inside of DMP5A. The stoichiometry of the pseudorotaxane was determined by the peak integration to be 1:1 (host:guest), and the binding constant was calculated from the 1:1 mixture to be $K_a = 336 \pm 20\ M^{-1}$ ($\log K_a = 2.53 \pm 0.03$). The titration curves simulated for a system with $\log K_a = 2.53$ align well with the experimental data for the beginning of the titration, as shown on the Figure 33, B.

The equilibrium constants obtained in the course of the NMR titration experiments for the complexes of 1:1 stoichiometry are summarized in Figure 34.

3.3.3 DOSY NMR

A further insight into the complex formation between DMP5A and the guest moieties was provided by the diffusion-ordered NMR in $CDCl_3$ (Figure 35). Since DMP5A is a large molecule, its diffusion coefficient D can be expected to be lower than that of smaller and, hence, intuitively more mobile guest molecules. Moreover, after the formation of the inclusion complex, the coefficient D should become comparable to D_{DMP5A} because the dimensions of the pseudorotaxane are mostly determined by the dimensions of DMP5A if the guest moiety is fully encompassed by the host.[144] The graph in Figure 35 demonstrates the clear difference between neutral and positively charged guest molecules: the former have higher D values than the latter roughly divided by the coefficient value of the DMP5A ($D_{DMP5A} = 6.4\times10^{-10}\ m^2/s$), the reason being arguably the

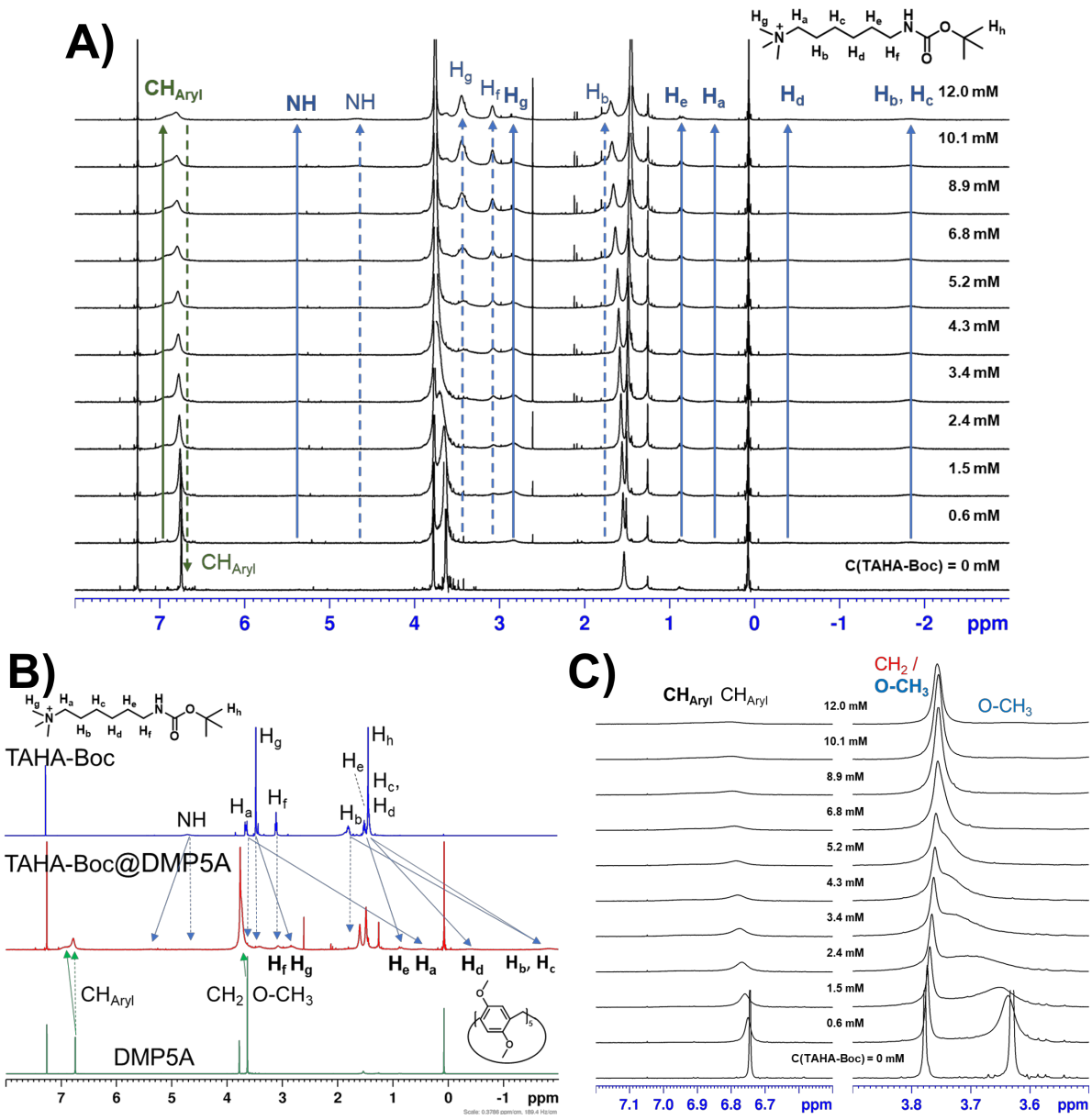

Figure 32. A) NMR titration of DMP5A with TAHA-Boc in $CDCl_3$ ($[H]_0$ = 4 mM). Normal and bold designations refer to free and complexed species. B) NMR spectra of (from the bottom) DMP5A, TAHA-Boc@DMP5A complex (at $[G]_0$ = 4.3 mM), TAHA-Boc. The change in peak shifts of the molecules is presented by solid arrows; dashed arrows demonstrate the peaks of the free species. C) Fragments of the NMR titration (TAHA-Boc@DMP5A), with shifts of only DMP5A peaks shown.

solvation that occurs because of the polarity of the chloroform, which increases the size of the molecule in the solution, thus, hindering the mobility.

Being the smallest molecule among the investigated species, AN has by far the highest diffusion coefficient ($D_{AN} = 1.48\times10^{-9}$ m^2/s). Upon presence of DMP5A, the D_{AN} value drops down to 1.02×10^{-9} m^2/s for the peaks of the "threaded" AN and to 1.20×10^{-9} m^2/s if calculated for the peaks of "free" AN. This highlights the finding made with NOESY NMR that although the interaction is considered "slow" on the NMR timescale, the two states are not fully separated.

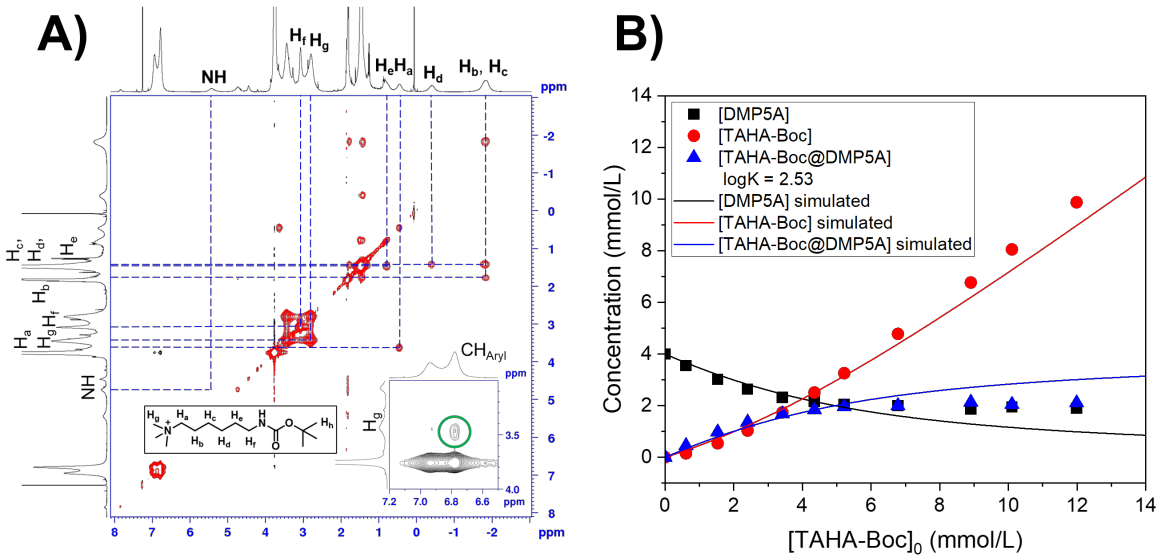

Figure 33. A) 2D NOESY NMR of the complex TAHA-Boc@DMP5A. The blue dashed lines represent the relation between the peaks of the free and bound guest. On the horizontal and vertical projections, the peaks of a bound and free (respectively) guest are marked. Inset: The NOE cross-peak between host and guest species is marked green. B) Titration curves for DMP5A–TAHA-Boc system. Scattered plots: experimental data, line plots: simulated (HySS 2009 software) curves. Calculated assuming 1:1 (host : guest) stoichiometry of the complex with log K_a = 2.53.

Therefore, the diffusion coefficients of both free and complexed AN in solution are average values between the isolated and fully threaded AN. It is worth noting that due to the strength of the binding affinity of AN@DMP5A these two states are distinguishable, which is not the case for other guest species as will be shown further. Moreover, AN@DMP5A is the only pseudorotaxane by which the mobility of DMP5A slightly increases up to 6.9×10^{-10} m^2/s.

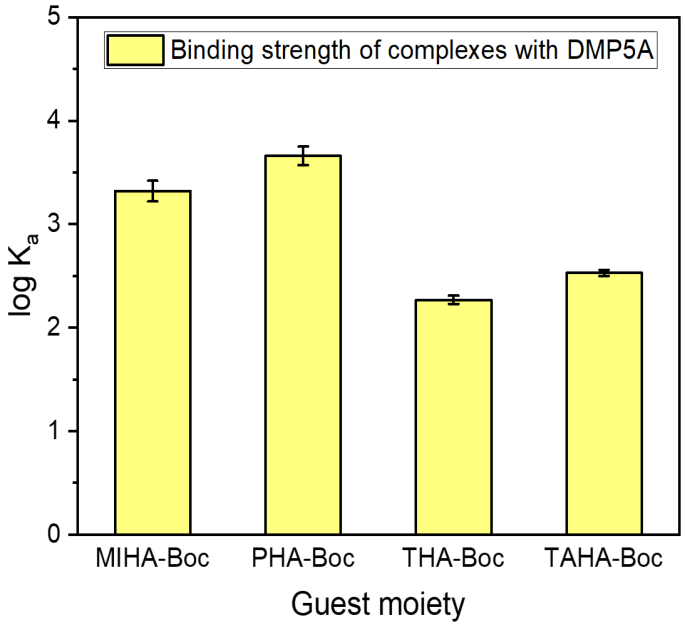

Figure 34. Comparison of the binding affinities of DMP5A with various guests, as obtained in this work.

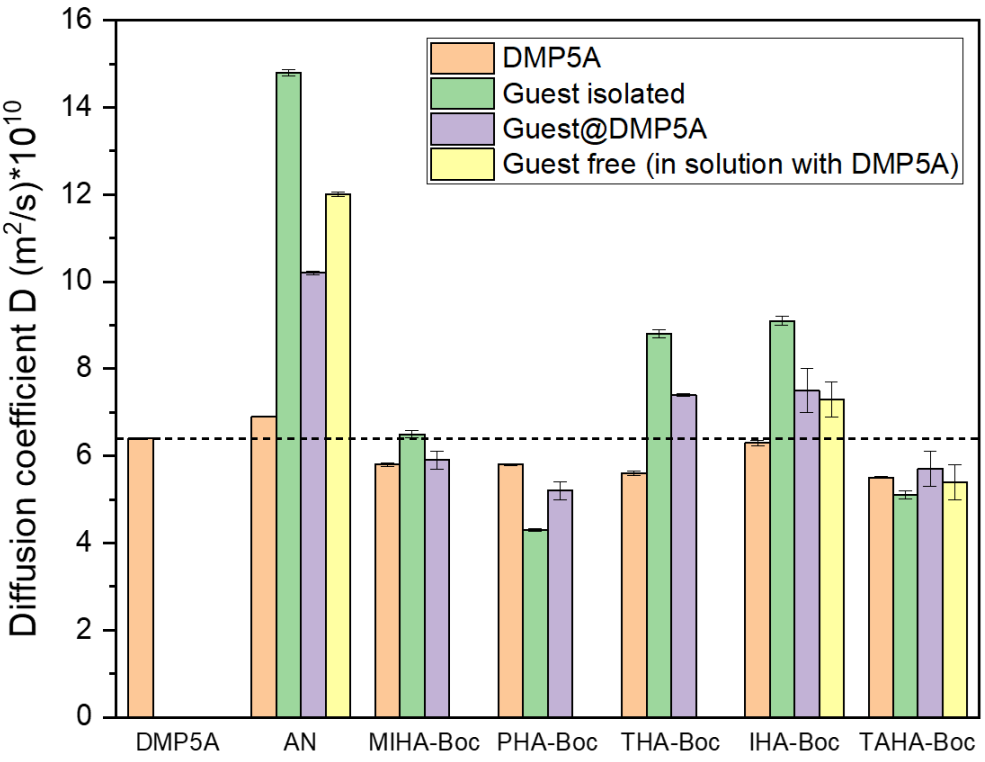

Figure 35. Diffusion coefficients D for DMP5A and the discussed guest molecules alone and as parts of the host-guest inclusion complexes. In case of the complexes with a slow exchange, peaks of free and complexed species were evaluated separately. The dashed line represents a D value for DMP5A ($D = 6.4\times10^{-10}$ m²/s).

Other guest molecules are larger in size and, therefore, possess smaller D values than AN. The diffusion coefficients of neutral THA-Boc ($D_{THA\text{-}Boc} = 8.8\times10^{-10}$ m²/s) and IHA-Boc ($D_{IHA\text{-}Boc} = 9.1\times10^{-10}$ m²/s) decrease upon presence of DMP5A in the system. The value of $D_{THA\text{-}Boc@DMP5A} = 7.4\times10^{-10}$ m²/s as expected for a fast exchange complex, lies as an average between pure guest and pure host. DMP5A diffusion is noticeably hindered as well, which implies a size increase of the macrocycle upon threading with THA-Boc. The same behavior is observed in case of the pseudorotaxane IHA-Boc@DMP5A, where the differences in mobility between "free" and complexed guest molecules is within the error and, therefore, insignificant ($D_{IHA\text{-}Boc@DMP5A} \approx 7.4\times10^{-10}$ m²/s). The diffusion coefficients of the isolated charged guests are comparable to ($D_{MIHA\text{-}Boc} = 6.5\times10^{-10}$ m²/s) or lower than that of DMP5A ($D_{PHA\text{-}Boc} = 4.3\times10^{-10}$ m²/s, $D_{TAHA\text{-}Boc} = 5.1\times10^{-10}$ m²/s). As was with THA-Boc@DMP5A, for the complexes exhibiting fast exchange the D value resembles an average between D values for host and guest (for MIHA-Boc the values are within an error from each other). In case of TAHA-Boc@DMP5A because the diffusion coefficient of the isolated guest ($D_{TAHA\text{-}Boc} = 5.1\times10^{-10}$ m²/s) is close to the D of the complexed DMP5A, the values of the complexed TAHA-Boc do not change much upon presence of the host species.

Hence, using DOSY NMR it could be demonstrated that the formation of the host-guest assemblies studied in the current work is affecting their mobility and size. Furthermore, alteration of the mobility upon complexation was found to follow the pattern of fast exchange complexes, *i.e.*, where the resulting diffusion coefficient of the guest was an average value rather than completely reduced to the mobility of DMP5A, which is in agreement with the previously discussed NOESY results.

3.3.4 Guest moiety selection

From the investigated guest moieties two candidates—MIHA and PHA—demonstrated the highest binding affinity towards DMP5A. Despite the K_a of the complex MIHA-Boc@DMP5A being lower than that of PHA-Boc@DMP5A, they are of the same order of magnitude, and both moieties were used to construct supramolecular gel systems by various research groups.[115,222,223,225] Nonetheless, lower binding affinity means a slightly higher lability in the presence of competitive guests, therefore, a higher sensitivity towards AN, which is beneficial for the fabrication of a sensor with a detection mechanism based on competitive complexation. Based on this, we have selected MIHA as a guest moiety for further fabrication of a guest polymer.

3.4 Polymer synthesis and modification

VDMA as "click"-modifiable monomer was synthesized in two steps form 2-methyl alanine by a slightly modified procedure from Levere *et al*.[306] (see Chapter 5.2.5 for the synthetic procedure and Chapter 4.6.1 for a detailed discussion). DMIEA was obtained according to a known literature procedure (Chapter 5.2.6).[191] Since DMIEA contains a 3,4-maleimide fragment, as mentioned above, it is capable of UV-light-induced [2+2]-dimerization for the subsequent gelation of the polymer blends. VDMA was copolymerized with dimethyl acrylamide (DMAAm; DMAAm to VDMA ratio 80:20) using RAFT polymerization with DMP as chain transfer agent and AIBN as initiator (Scheme 19). Controlled radical polymerization was selected for achieving a regular distribution of monomers in the copolymer (however, VDMA is known to have a higher copolymerization rate than DMAAm, see Li *et al.*[213] and Chapter 4.6.2). The copolymer poly(DMAAm-co-VDMA) (P20) was characterized by ^{1}H NMR and GPC. The results are presented in Figure 36, A and Figure 38 and summarized in Table 13. Because of the susceptibility of VDMA groups towards hydrolysis, the fresh copolymer was stored under inert atmosphere in a tightly closed vial in a freezer.

P20 was used for further post-modification to obtain a host polymer (P20HTP, containing HT and DMIEA as pendant groups, Figure 37, A), a guest polymer (P20MIHAP, containing MIHA and DMIEA, Figure 37, B), and a photo-crosslinker-modified polymer (P20PC, containing only

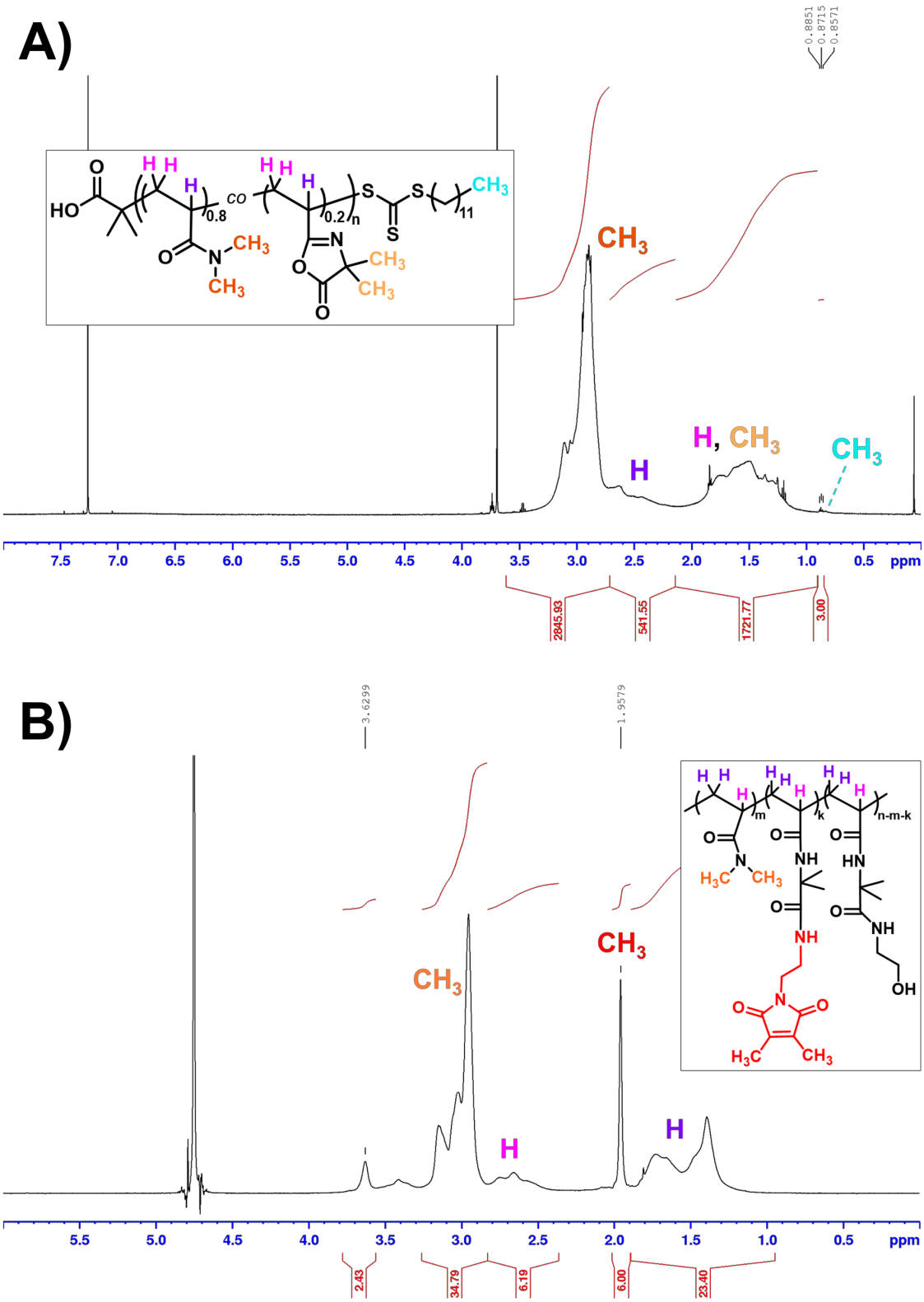

Figure 36. ^{1}H NMR spectra of P20 in $CDCl_3$ (A) and P20PC in D_2O (B).

DMIEA groups, Figure 36, B). All moieties (HT, MIHA and DMIEA) were attached to the polymer chains by mixing them with P20 in DMF in the presence of DBU. Because VDMA undergoes the ring opening with nucleophiles, DBU was used to deprotonate the amine hydrochlorides thus increasing the nucleophilicity. By the devising the modified polymer

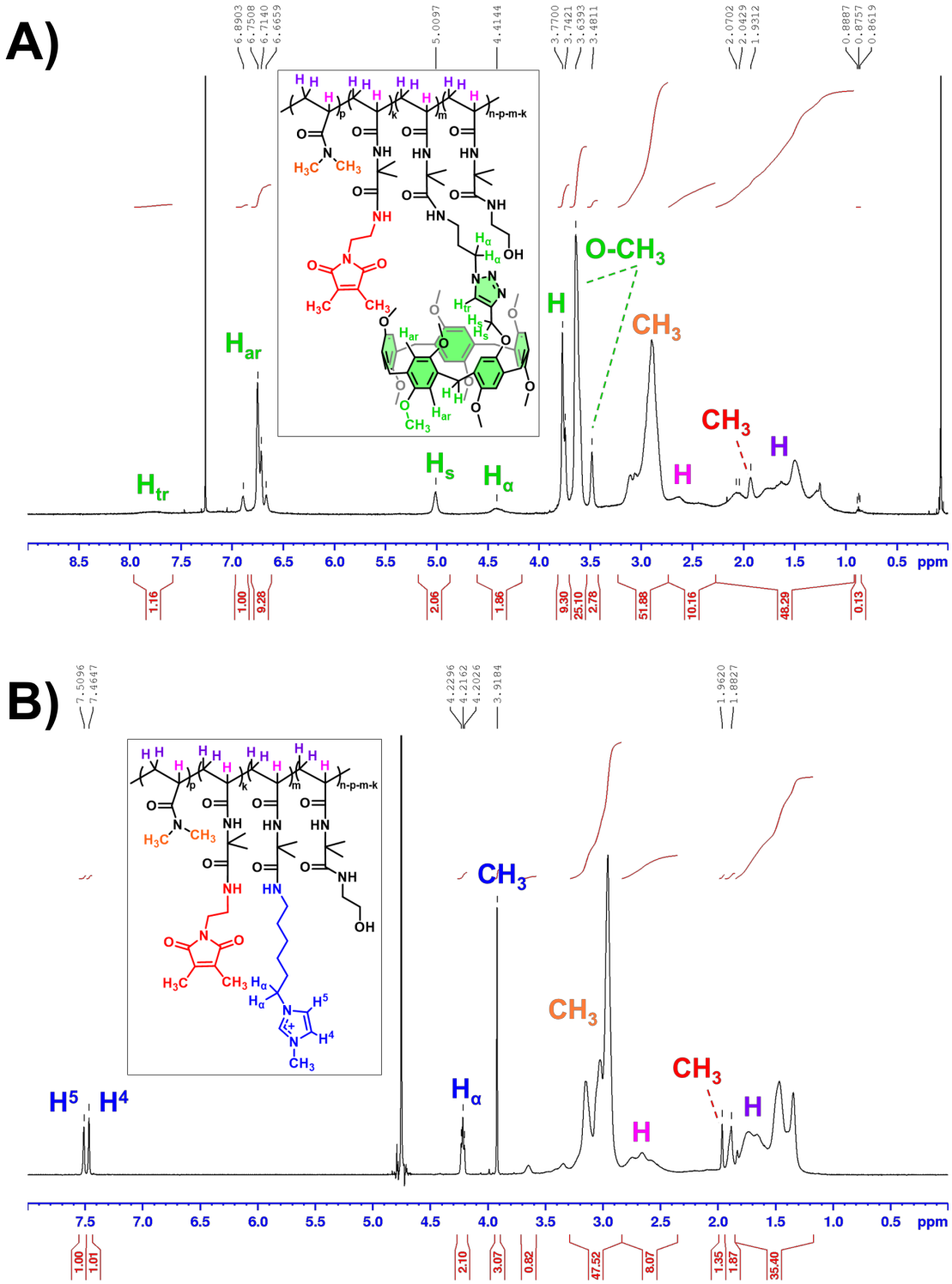

Figure 37. ^{1}H NMR spectra of P20HTP in $CDCl_3$ (A) and P20MIHAP in D_2O (B).

composition, the amount of the photo-crosslinker DMIEA was aimed at 3 mol% since it was demonstrated earlier in our working group that the DMIEA monomer ratio of as low as 2.3 % allows a stable gel formation.[191] Furthermore, preliminary studies showed that at the host and guest modifier ratio of 5–6 % the responsivity and sensitivity of the system towards AN is insufficient, thus, their content was increased up to 11 % and 12 % for HT and MIHA, respectively.

It is worth mentioning that all polymers including P20HTP were water-soluble, therefore, it was possible to purify them by dialysis in water.

The effectiveness of the polymer modification, *i.e.*, the functional groups content in the resulting polymers was calculated (Table 13) by integration of the corresponding NMR signals (equations (53)–(55)).

$$X_{HT}(\%) = \frac{0.1 \cdot \int(HT, 7.0 - 6.4\ ppm) \cdot 79\%}{{}^{1}/_{6} \cdot \int(DMAAm, 3.2 - 2.8\ ppm)} \tag{53}$$

$$X_{MIHA}(\%) = \frac{{}^{1}/_{3} \cdot \int(MIHA, 3.9\ ppm\ ) \cdot 100\%}{\int(backbone, 2.85 - 2.35\ ppm)} \tag{54}$$

$$X_{DMIEA}(\%) = \frac{{}^{1}/_{6}\ \int(DMIEA, 1.9\ ppm) \cdot 100\%}{\int(backbone, 2.85 - 2.35\ ppm)} \tag{55}$$

GPC results (Table 13 and Figure 38) demonstrate that upon modification the increase in M_n of the polymer is observed, which is almost double as high in the case of P20HTP compared to P20. This is expected due to a high molecular mass of the attached pendant groups (HT). Noticeably,

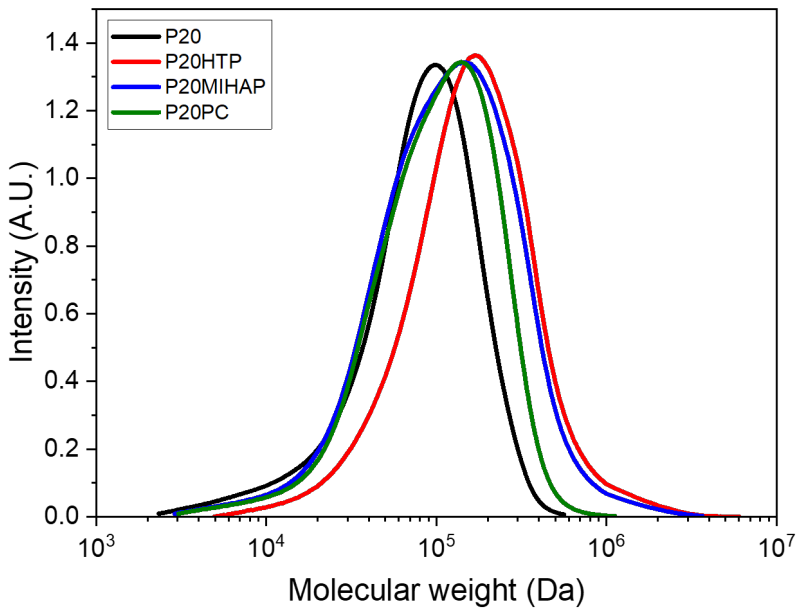

Figure 38. The GPC chromatograms of the co-polymer P20 and its modification products. The elution conditions are discussed in the text and the results are presented in Table 13.

the M_n of P20PC is also significantly higher than that of the unmodified polymer. This can be explained by DMIEA moieties dimerizing during the polymer work up or storing leading to the crosslink formation between chains. This possibility is supported by a remarkably increased polydispersity of the sample.

Table 13. Properties of the obtained polymers.

Polymer	Functionality	Host or guest group, %[a]	Photo-crosslinker, %[a]	M_n[b]	Đ[b]
P20	–	–	–	48400	2.08
P20HTP	HT, DMIEA	11%	2.8%	103200	2.21
P20MIHAP	MIHA, DMIEA	12%	2.8%	68900	2.57
P20PC	DMIEA	–	16%	92700	4.45

[a]Determined by 1H NMR spectroscopy. Per cent of total number of monomer units.

[b]Determined by size-exclusion chromatography.

3.5 Supramolecular gelation experiments

Prior to using the dually cross-linked system for the fabrication of sensor chips, interaction between host and guest groups attached to the polymer backbone was investigated by the inverted vial test with the intention to prove the concept of the sensor, namely, the formation of the supramolecular crosslinks as well as their responsiveness towards AN. This investigation was done by D. Helle in the framework of his Bachelor thesis.[312]

P20 was modified with 6-aminohexyl-substituted P5A (P5AHA) to obtain a host polymer (P20P5AHA) containing 7.2 % P5AHA pendant groups. Furthermore, a guest polymer P20MIHA without DMIEA units was obtained (Figure 39). Each polymer was weighed in a 2 mL GPC vial and dissolved in $CHCl_3$ on a stirring plate. Figure 39 A, B demonstrates that the solutions of a host and guest polymers in chloroform separately are low-viscous liquids which flow down if the vial is inverted.

In the next step, the solutions were combined at such volume ratio that the resulting concentration of both P5A and MIHA groups was equal (0.184 M). Since it was done at constant stirring, a dramatic increase in solution viscosity could be noted due to the hindered rotation of the stirring bar. Figure 39, C shows that the mixed solution does not readily flow down upon vial inversion indicating a formation of a supramolecular gel. The reversibility of the formed crosslinks and, thus, the responsiveness of the gel was demonstrated by adding 20 µL AN into the mixture. The disruption of the crosslinks by the competitive guest led to a drastic decrease in the viscosity upon

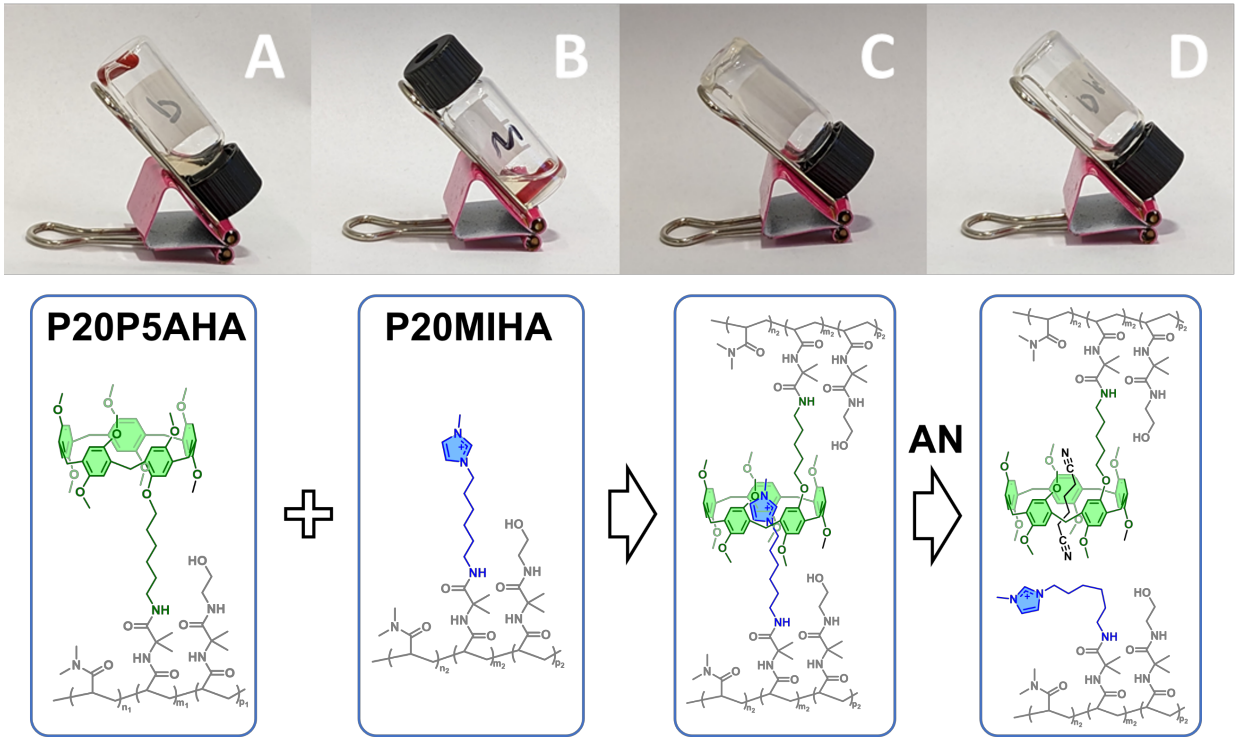

Figure 39. Reversible gel formation upon mixing polymers with pendant P5AHA and MIHA groups. A) P20P5AHA solution in $CHCl_3$. B) P20MIHA solution $CHCl_3$. C) Upon mixing both solutions, a supramolecular network is formed, therefore, the solution does not readily flow during the inverted vial test. D) Upon addition of 20 µL AN the host–guest complexes are disrupted resulting in transition into sol.

transition into sol, which can be illustrated by Figure 39, D depicting solution freely flowing down the vial after its inversion.

The demonstrated reversible sol–gel transition proved the responsiveness of the devised system and the feasibility of the sensor concept. Therefore, P5A- and MIHA-modified P20 can be used for chip fabrication, which will be discussed further.

3.6 SPR studies: adiponitrile responsiveness

Although for the environmental monitoring it is beneficial to be able to determine AN concentration directly from wastewater samples, we consider water to be a poor solvent for the sensing platform in its current design because of, on the one hand, its high polarity which leads to a highly energetic solvation of the charged MIHA pendant groups, thus, hampering the initial host-guest complex formation. On the other hand, considering an exceptional hydrophobicity of P5A groups, water as a solvent promotes their aggregation, which not only hinders the possibility of MIHA@P5A formation even further, but also it decreases the number of P5A units available for binding with AN. As discussed above, $CHCl_3$ was selected for the detection studies due to a good solubility of unmixed host and guest polymers as well as proven high binding affinities of the participating species, which implies a high sensitivity of the designed sensor.

3.6.1 Experimental setup and sample preparation

The sensor chip was prepared as shown in Figure 40. Host and guest polymer solutions were prepared at a concentration of 4 wt.% in DMF separately. After stirring both solutions for 1 h they were mixed at a 1:1 ratio of host and guest groups. The mixture was stirred overnight in a dark place followed by filtering through a Chromafil® PTFE syringe filter (0.45 µm) prior to spin-coating. Spin-coating was carried out using a G3P-8 spin coater by Specialty Coating Systems. The polymer solution (ca. 80 µL) was applied onto the wafer by static dispense method and coated with a two-step program:

1. 1200 rpm (20 s ramp) for 180 s;
2. 1500 rpm (10 s ramp) for 60 s.

After the completion of the coating process the sample was dried *in vacuo* overnight in dark to remove the rest of the solvent. Further, the polymer layer on the wafer was photo-crosslinked by UV-irradiation for 300 s. The crosslinked gel layer was measured by SPR (dry layer thickness) after equilibrating in an anhydrous $CHCl_3$ overnight.

Here, the gel swelling behavior was studied in $CHCl_3$ and in the presence of the analyte—AN. The scan measurement of a golden layer and a dry gel are demonstrated on Figure 41. The plasmon resonance minimum is strongly shifted to higher angles ($\theta_{PR} \approx 90°$) indicating a high refractive index and, accordingly, high gel density. The parameters of the gel layer, obtained by a fit simulation are given in Table 14. The fit is not matching the experimental SPR curve perfectly because of the inhomogeneities on the gel surface, however, it is possible to draw conclusions about the parameters of the gel by fitting the area around the angle of total internal reflection (20°– 25°) and the plasmon resonance minimum.

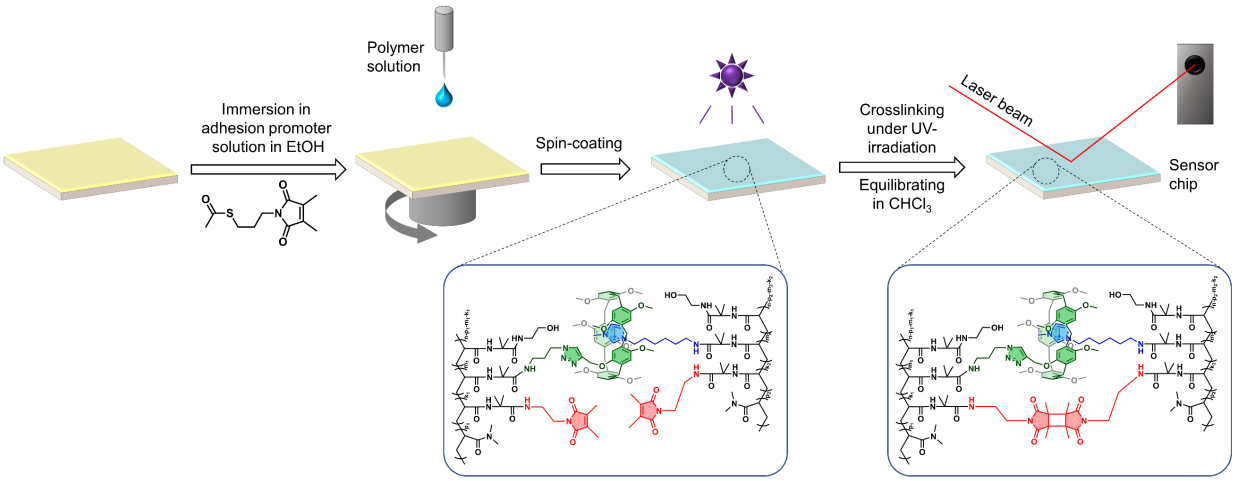

Figure 40. SPR sample preparation. Gold-coated N-LaSF9 wafer is immersed in an adhesion promoter solution overnight. Then, a polymer (mixture) solution is spin-coated onto the wafer, followed by drying in vacuo and crosslinking by UV-irradiation. After equilibrating in $CHCl_3$ overnight the sensor chip can be measured

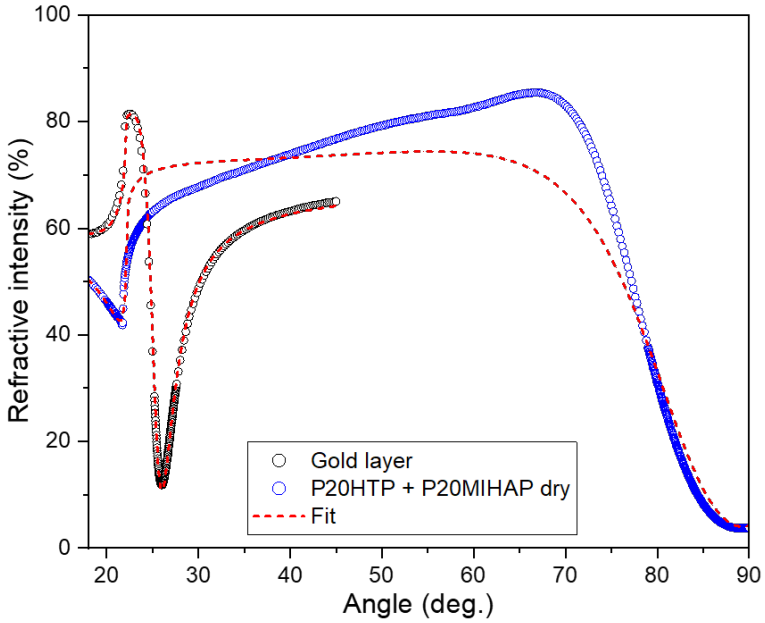

Figure 41. SPR scan measurement of a gold-coated wafer (black circles), P20HTP+P20MIHAP gel in a dry state (blue circles) and the fit by Winspall software (red dashed lines).

Table 14. Parameters of the polymeric gel sensor in different mediums.

Medium	d^{in}, nm	d^{out}, nm	d, nm	*Q*	n_d^{in}	n_d^{out}	Refractive index n_d
Gold layer			33.92				–11.6448 (ε_{real}) 1.3854 (ε_{imag})
Air	–	–	187.2	–			1.5595
$CHCl_3$	269.6	482.7	752.4	4.02	1.4998	1.4771	1.4853
AN 1 µM	269.2	489.9	759.1	4.06	1.5000	1.4765	1.4848
AN 5 µM	267.6	491.3	758.9	4.05	1.5002	1.4764	1.4848
AN 10 µM	262.5	500.3	762.8	4.07	1.5000	1.4762	1.4844
AN 20 µM	266.2	497.7	763.9	4.08	1.4998	1.4760	1.4843
AN 50 µM	271.2	501.0	772.2	4.12	1.4998	1.4754	1.4840
AN 100 µM	272.5	507.1	779.6	4.16	1.4999	1.4749	1.4836
AN 200 µM	269.6	515.8	785.4	4.20	1.4996	1.4745	1.4831
AN 500 µM	262.3	543.5	805.8	4.30	1.4988	1.4732	1.4815
AN 1 mM	262.6	557.9	820.5	4.38	1.4987	1.4723	1.4808

3.6.2 Responsiveness of the sensor chip towards AN

Through the flow cell 1 ml $CHCl_3$ was pumped using a syringe and the gel was equilibrated for 2 h. Then, the gel layer was treated with AN solutions of increasing concentrations (in each case, 1 ml of the corresponding solution was injected into the flow cell and the gel was equilibrated for 10 min): 1 µM, 5 µM, 10 µM, 20 µM, 50 µM, 100 µM, 200 µM, 500 µM and 1 mM. Between

every two injections the flow cell was purged with 1.5 ml $CHCl_3$. The gel behavior was investigated using kinetic measurement at 76°. As can be seen from Figure 42, A, the system P20HTP+P20MIHAP exhibits almost no responsiveness up to $C_{AN} = 20$ µM, followed by a decrease of intensity at a constant angle with an increasing concentration resulting in a linear dependence from log C_{AN}. It is worth noting that the system exhibits almost complete recovery of the intensity upon rinsing with $CHCl_3$, which proves the reusability of the constructed sensor chip. To determine the sensitivity of the chip, scan measurements were performed after each AN solution injection and equilibration. The angular spectra of the swollen gels are presented on Figure 42, B. In the spectra, two features are clearly recognizable and the changes in the system affect these regions the most: the plasmon resonance around 82° and the waveguide (56° – 58°). For layers of high thickness (> 300 nm) in a one-layer model the former is affected by the refractive index n_d, whereas the latter by both the refractive index and the layer thickness (see

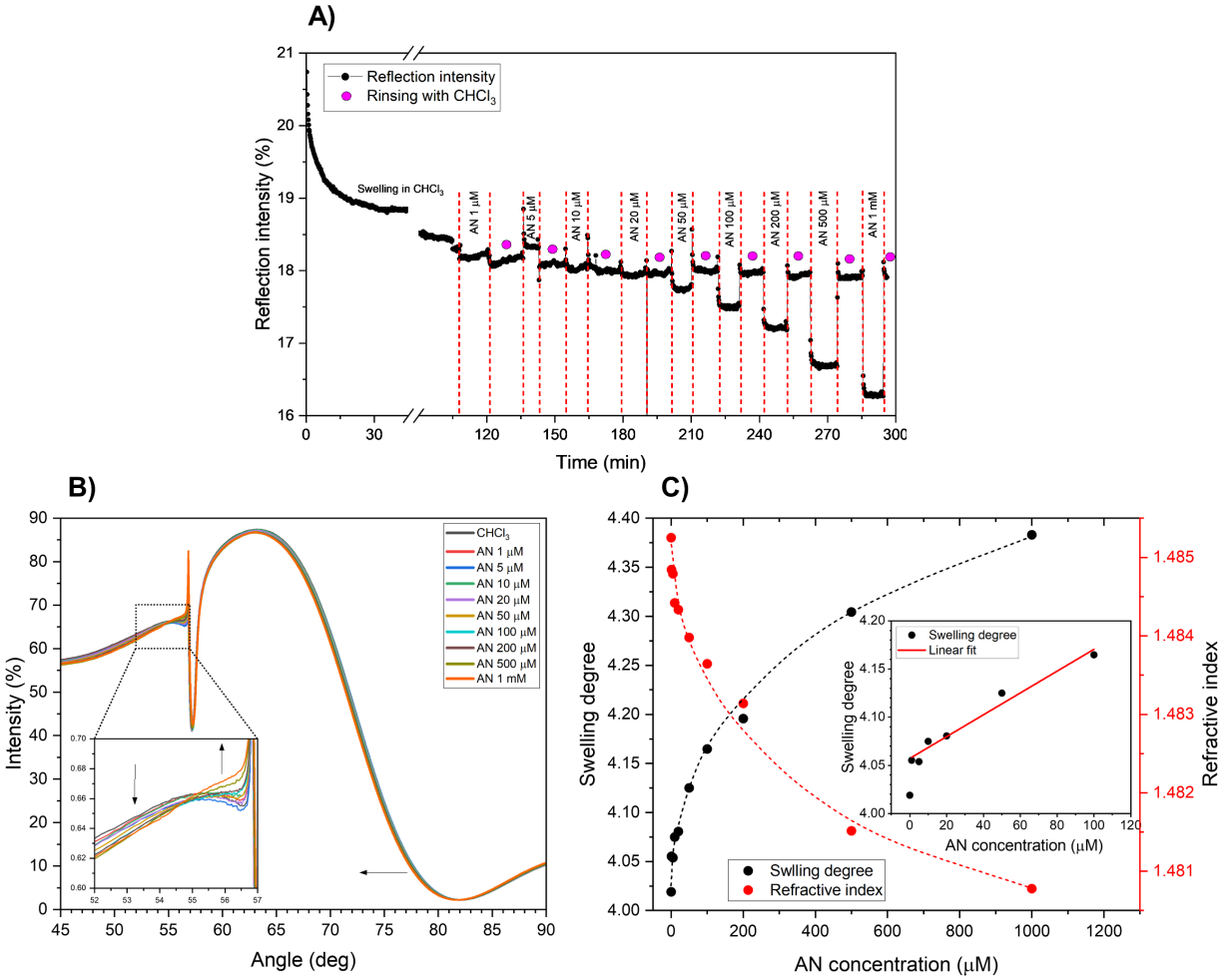

Figure 42. SPR measurement of the P20HTP+P20MIHAP sensor chip with different concentrations of AN in $CHCl_3$. A) Kinetic studies at 76°. Between swelling in AN solutions the gel was rinsed with $CHCl_3$, which led to the gel returning to its initial state. B) SPR scan measurements of the gel swollen in AN solutions. C) Dependence of swelling degree and refractive index with increasing AN concentration (dashed lines serve as guides for the eye). Inset: Linear fit of the first section of the graph.

Chapter 2.5).[268] The shift of the plasmon minimum to the lower angles observed in Figure 42, B and implies a decrease in n_d and, therefore, evidence of the decreasing gel density upon the addition of AN, which is expected due to the crosslinks being broken because of the competitive complex formation.

Simultaneously, the change in the waveguide region can be noted, serving as a hint about gel thickness changes. For the determination of the gel layer thickness the curve simulation based on Fresnel equations is required. Unfortunately, for the obtained spectra, the one-layer model failed to deliver a precise curve fit. Thus, a two-model simulation was utilized, which considers the anisotropic character of the gel swelling.[268,314] In this model, the parameters of the inner layer affect the plasmon minimum region the most, and the waveguide region can be precisely fitted by optimizing the parameters of the outer layer. Layer thicknesses d as well as refractive indexes n_d were determined using a 2-layer model as follows.

The entire spectrum (45° – 90°) was simulated and fitted iteratively by optimization of the x-minimum, *i.e.*, the plasmon resonance; only the parameters of the inner layer were varied during the iterative process. Further, d and ε_{real} of the inner layer were fixed for the second iterative process where parameters of the outer gel layer were varied. This was performed using the full curve optimization. The resulting d value was calculated as a sum of the thickness of both simulated layers, and the average refractive index $<n_d>$ was obtained according to the equation (72), Chapter 5.1.2.5.1.

From the Figure 42, C and Table 14 it is clear that the sensor chip developed in this work shows responsiveness towards AN. With an increasing concentration of the analyte the gel thickness d (and, therefore, swelling degree *Q*) increases and the n_d value decreases, indicative of a reduced density likely caused by breaking of the supramolecular host-guest crosslinks through a competitive complex formation. It is worth noting that according to the obtained parameters the inner layer does not undergo significant changes upon increasing AN concentration with the layer thickness d^{in} staying between 262–273 nm, whereas the outer layer thickness d^{out} increases from 483 up to 558 nm with a significant decrease in refractive index.

It can also be noticed in linear coordinates that saturation of the supramolecular system is occurring with increasing AN concentration. Thus, a linear section of the swelling degree dependence (Figure 42, inset of C), was chosen for the calculation of the limit of detection for the fabricated sensor chip (Table 15, equations (73) and (74)):[315] LOD = 25 µM.

The achieved limit of detection is significantly lower than the concentration limit in the toxicity evaluation against fish as discussed earlier.[12] This proves that the sensitivity of the devised sensor chip is sufficient for the detection of AN concentrations that can pose a threat to the environment.

Nevertheless, the value can be improved further, in our view, by optimizing the designed sensing platform on chemical and/or methodological levels for further fabrication of sensing devices.

Table 15. Parameters for the calculation of the LOD according to equations (73) and (74)

AN concentration (µM)	$(Q_i - Q_{r,i})^2$	n	$s_{y/x}$	Slope A (μM^{-1})	LOD (µM)
1	9.99E-06	6	0.00851	0.00113	24.86
5	8.24E-05				
10	3.98E-05				
20	4.23E-07				
50	1.23E-04				
100	3.39E-05				

3.6.3 Negative control: swelling experiments with P20PC

To prove that the responsiveness of the gel sensor is based on the built-in host-guest interactions and to separately evaluate the influence of the other polymer components (DMIEA and DMAAm) on the interaction with AN, an SPR measurement was conducted using a wafer coated with P20PC, *i.e.*, not containing any host or guest groups (Figure 43). The gel was measured in a dry state as well as swollen in $CHCl_3$ and in 1 mM AN solution (therefore, exposing it to a high concentration). Figure 43 shows that no difference is noticeable between the two curves, and Table 16 reveals that upon presence of the analyte the P20PC gel even exhibits a very slight shrinking, thus confirming the expected mechanism of AN interaction with P20HTP+P20MIHAP gel sensor.

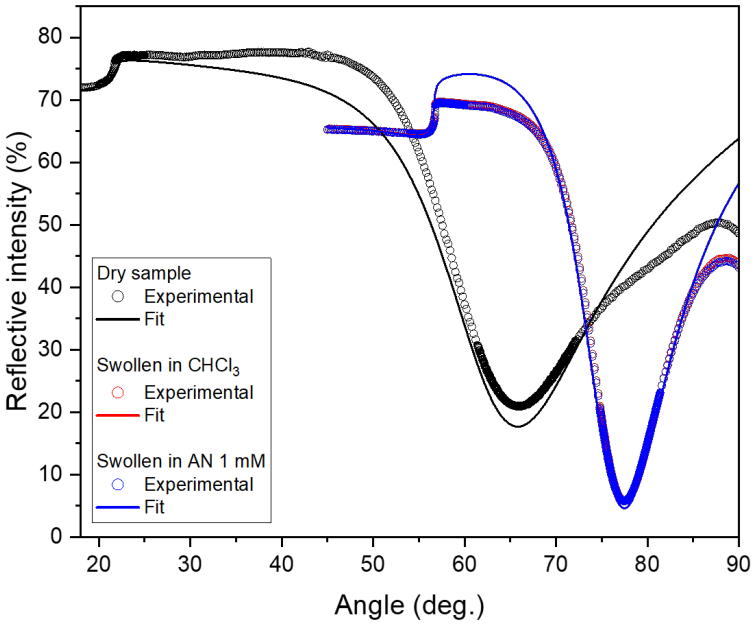

Figure 43. SPR curves of the P20PC gel: dry (medium: air; black curves), swollen in $CHCl_3$ (red curves) and in 1 mM AN solution (blue curves).

Table 16. Parameters of the P20PC gel in different mediums.

Medium	d, nm	*Q*	n_d
Air	122.0	–	1.4750
$CHCl_3$	461.6	3.78	1.4732
AN 1 mM	457.8	3.75	1.4738

3.7 Summary and outlook

In this work, we constructed a sensor chip for the detection of adiponitrile based on a dually crosslinked supramolecular gel. Chemical crosslinks formed by dimerization of DMIEA endowed the network with stability, whereas supramolecular host–guest complexes with P5A acted as reversible crosslinks disrupted upon presence of AN, due to the competitive complexation between the moieties. For the design of the gel MIHA was selected as a guest moiety from various neutral and positively charged amine- and heterocycle-substituted aminohexanes. The selection was conducted by the evaluation of the binding affinity of Boc-protected axles with DMP5A. NMR titration revealed that K_a of MIHA-Boc ($\log K_a = 3.32 \pm 0.10$) and PHA-Boc ($\log K_a = 3.66 \pm 0.09$) with the macrocycle are by one order of magnitude higher than those of THA-Boc ($\log K_a = 2.27 \pm 0.04$) and TAHA-Boc ($\log K_a = 2.53 \pm 0.03$) complexes, while still being lower than K_a of the AN@DMP5A complex. IHA-Boc was found to form complex of 1:2 (H:G) stoichiometry with DMP5A. Additionally, it was demonstrated using 2D DOSY NMR that for neither fast nor slow exchange complexes the mobility of the bound species is fully reduced to the mobility of DMP5A. The diffusion coefficient D, therefore, stays an average between free and "completely bound" states. HT as a host moiety was synthesized by a mono-demethylation of DMP5A and further etherification of the phenolic OH-group.

Host and guest polymers were synthesized by modification of a P20 copolymer containing VDMA as a comonomer with HT, MIHA (which was our guest moiety of choice) and a photo-crosslinker. By spin-coating and subsequent curing under UV-irradiation, a thin gel layer was fabricated, which was treated with $CHCl_3$ and AN solution of different concentrations (1 μM up to 1 mM). By measuring the change in swelling degree and refractive index using SPR technique, a limit of detection was estimated as a sensitivity parameter of the sensor chip (LOD = 25 μM).

Thus, the designed polymeric gel system can serve as a starting point for the development of a sensor for adiponitrile as well as other small molecules capable of forming stable complexes with pillar[n]arenes. We believe that further tuning of the polymer parameters as well as methodology

will help improve the performance of the sensing platform for the fabrication of sensors in a form of devices.

4 Spermine detection using water-soluble pillar[5]arene

4.1 Introduction

4.1.1 Polyamines and their functions

Polyamines such as putrescine (PUT), spermidine (SD) and SP are ubiquitous in eukaryotic cells and vital for cell proliferation and growth.[316] Due to their cationic nature, at physiological pH the polyamines are fully protonated, which leads to the interaction and complex formation with anionic species present in the cell such as nucleic acids, therefore, being involved in modulation of the functions of DNA and RNA.[317,318] Hereby, since its charge density is higher than for other polyamines (4 cationic groups *versus* 2 and 3 in case of PUT and SD, respectively), SP is bound stronger and, thus, plays a more important role in the nucleic acid modulation.

Intracellularly, the polyamines are synthesized from the amino acid ornithine.[317,319] In the first step, PUT is produced from ornithine under the action of the enzyme ornithine decarboxylase (ODC), then, catalyzed by spermidine synthase, PUT is converted into SD, which is transformed further into SP by spermine synthase (Figure 44). Because the polyamines support regulatory function in cell proliferation, overexpression of ODC and, as a result, the polyamines are known as markers of tumor growth and carcinogenesis.[320] Various types of cancer including leukemia,[321] pancreatic[322] and breast cancer[323] were demonstrated to be accompanied by higher levels of PUT, SD and SP in bodily liquids such as urine, blood, or saliva. As was demonstrated

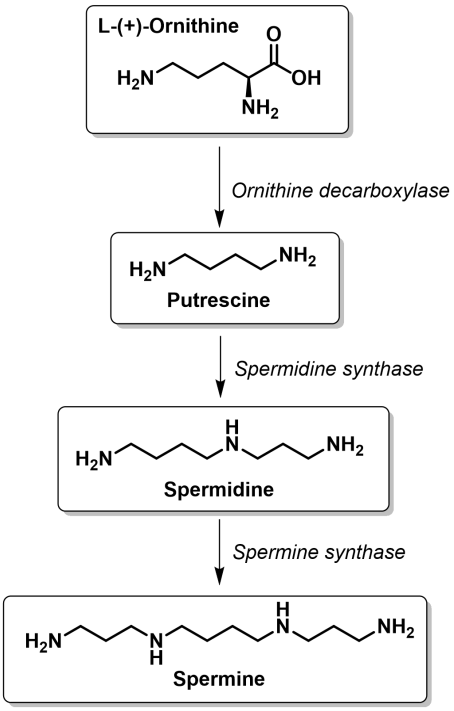

Figure 44. Biogenic pathway of polyamines synthesis.

by the group of Chung,[324] in serum of breast cancer patients the concentration of the polyamines is elevated (40.02 ± 4.49, 15.72 ± 2.09, and 6.23 ± 0.79 mg/L for PUT, SD and SP, respectively) compared to healthy control group (analogously, 30.44 ± 2.89, 11.76 ± 1.2, and 3.19 ± 0.41 mg/L). This rendered estimation of the polyamine concentrations in bodily fluids of cancer patients in the range of 1–10 μM in further works.[325]

Prostate cancer is one of the leading causes of cancer-related mortality among the male population in developed countries.[326] In 2023 in the USA, prostate cancer comprised the most new cases and was the second-deadliest after lung cancer.[327] Importantly, prostate tissue is the one producing the highest amounts of SP and unlike other types of cancer, the prostate tumor progression leads to the reduction in levels of excreted SP possibly as a result of malfunctioning metabolic processes including polyamines with increased expression of SP-consuming enzymes.[14,328,329] In the work of Wong, Ng, Wong and co-workers,[329] a possibility to use polyamines in urine as prostate cancer biomarkers was demonstrated. The results obtained with ultra-high performance liquid chromatography coupled with mass spectrometer showed that SP concentration in urine of prostate cancer patients (normalized by creatinine) were lower (1.47 ± 0.22 μmol/g) than those of healthy control (5.43 ± 1.17 μmol/g) or benign prostatic hyperplasia patients (5.87 ± 0.71 μmol/g). At the same time, no significant differences in PUT or SD concentrations were detected. In another work,[330] a significantly higher distribution of the detected SP concentrations in prostate cancer patients' urine compared to control group was demonstrated: 0.07–7.01 μM *versus* 0.46–2.86 μM. Although this data somewhat contradicts the findings of the previous study, it provides the range of SP concentrations in human urine for the design of an analytical experiment.

4.1.2 Spermine detection using macrocycles

In the discussed studies, the detection of polyamines was conducted mainly by chromatographic methods. Although accurate and sensitive, chromatographic methods are not free from drawbacks, such as long and tedious sample preparation and long analysis duration. The use of supramolecular interactions and host–guest complexes specifically can help overcome these limitations and create a platform for accurate, precise and, at the same time, express detection of the analytes. In particular, such platforms can benefit from the utilization of CBns and PnAs, since these macrocycles were shown to form stable complexes with polyamines.[150,331] In the literature, multiple examples of macrocycle-based supramolecular polyamine sensors can be found, which will be discussed in the following.

4.1.2.1 Detection with CBns

A sensor array for SP detection based on the immobilized CB6 monolayer was devised by the groups of Biedermann and Hirtz.[332] Initially incubated with an indicator tetramethylrhodamine cadaverine, the array exhibited fluorescent properties. Upon incubation in a 10 μM SP solution in PBS buffer, fluorescence intensity dropped almost instantly due to replacement of the dye in the CB6 cavity with SP as a more affine guest species.

An example of a hydrogel-based detection of SP employing host–guest interaction of CB7 with incorporated dye moieties[211] is discussed in detail in Chapter 2.3.4.2.

4.1.2.2 Detection with PnAs

Unlike CBn-based sensors, which solely rely on fluorescent probes, sensors based on PnAs reported in the literature utilize various detection mechanisms: fluorescence, colorimetry, and voltammetry.

4.1.2.2.1 Fluorescence-based detection

The first fluorescence-based molecular sensor for alkylamines and polyamines (including PUT, SD, and SP) was devised in the group of Stoddart.[13] In their design, a fluorescent pyrene group was attached to the P5A *via* azide-alkyne coupling (Figure 45, A). The signal was quenched upon complexation with alkylamines in 1:1 MeCN/H_2O mixture, which allowed determining the binding affinity.

Ma and co-workers[333] presented a unique WSP6A-based probe, in which pyrene moieties are attached to alternating methylene bridges of the macrocycle (Figure 45, B). Such architecture provided, in contract to the previous example, an increased fluorescence intensity upon SP addition with a linear range between 22 and 50 μM. Importantly, the molecular detector possessed high selectivity towards the analytes with SP and SD being the only polyamines able to induce the enhanced emission. Nevertheless, the authors could not reliably determine the complexation stoichiometry presuming that the interaction occurs both inside and outside the host molecule.

Recently, the group of Biedermann[334] suggested fluorescent dye replacement technique for the detection of polyamines in artificial and natural bodily fluids. For this purpose, host–guest complexes between per-sulfonic P5A (Figure 45, C) and two diazapyrenium dyes containing either two methyl or two bromobutyl groups were applied. Whereas the first dye had somewhat lower binding affinity to P5A in PBS buffer ($K_a = 1.5\times10^7\ M^{-1}$) and could be replaced by all the investigated polyamines (SP, SD and cadaverine), the second dye exhibited significantly higher binding ($K_a = 6.0\times10^8\ M^{-1}$) with only SP being a more beneficial guest ($K_a = 5.9\times10^9\ M^{-1}$). Therefore, by applying both dye@host complexes the combined polyamine as well as selective SP content could be determined. The robustness of the method was shown by conducting the analysis

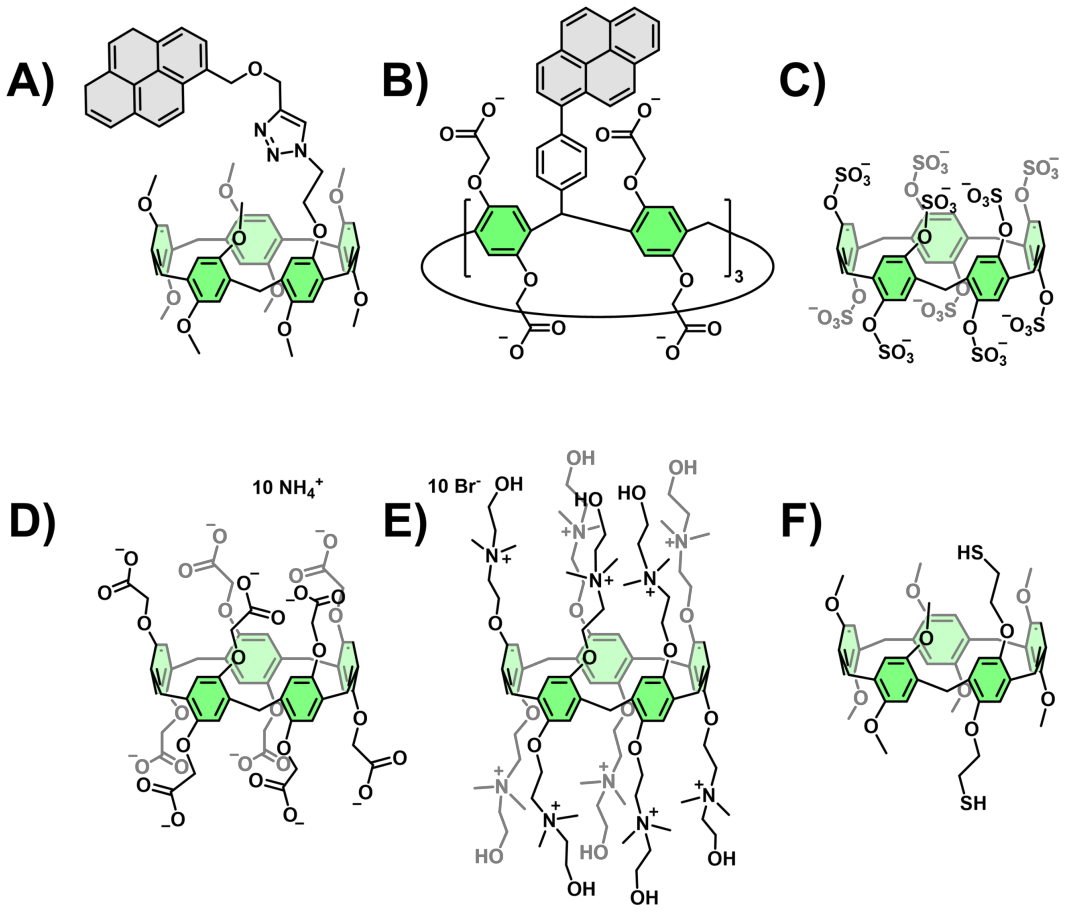

Figure 45. PnA derivatives used for polyamine detection as reported in literature. A) Mono-pyrene modified P5A from Ref.[13] B) WSP6A with pyrene moieties on methylene bridges.[333] C) Per-sulfonate P5A from Ref.[334] D) WSP5A used for Ag nanoparticle stabilization.[335] E) Per-cationic P5A derivative utilized for Au nanoparticle synthesis and stabilization.[336] F) Bis(2-mercaptoethyl)-P5A for electrochemical detection.[337]

in artificial urine, human urine as well as human saliva spiked with the amounts of polyamines typical for healthy individuals and cancer patients (Table 17). Furthermore, the method proved to be highly sensitive with practical limit of detection as low as 1 µM.

Table 17. Spiking concentrations (µM) of polyamines corresponding to healthy and diseased levels in human urine according to Ref.[334]

	Cadaverine	Putrescine	Spermidine	Spermine
Healthy individuals	17.1	15.5	10.7	8.8
Cancer patients	62.2	59.5	25.3	46.6

4.1.2.2.2 Colorimetric-based detection

The Xue group was the first to develop colorimetric detection of SP.[335] *In situ* produced silver nanoparticles were stabilized in aqueous solution using WSP5A (Figure 45, D). Due to the inherent surface plasmon resonance of Ag, the nanoparticle solution was yellow-colored with absorption

maximum at ~400 nm. Upon addition of millimolar SP solution, the nanoparticle aggregation occurs leading to the coupling of plasmon absorbances and, therefore, to a color change from yellow to black. Interestingly, only analytes with polyamine chain long enough to penetrate two WSP5A macrocycles belonging to different Ag nanoparticles were causing such change, which proves a certain degree of selectivity in the sensor.

This approach found further advancement in the work of Tan, Zhao and co-workers.[336] According to their design, gold nanoparticles were generated *in situ* from $HAuCl_4$ solution via reduction using positively charged per(*N*-(2-hydroxyethyl)-*N*,*N*-dimethyl-aminiumethyl)-substituted P5A (Figure 45, E). Through oxidation of the terminal OH-group, a carboxylate is obtained, and the resulting zwitter-ionic P5A forms a monolayer on the surface of the Au nanoparticles, thus, stabilizing them. The plasmon resonance band of such nanoparticles at 520 nm endows the solution with wine red color. The color is gradually turned to black upon SP addition-caused aggregation of the nanoparticles. The absorption intensity decrease is linearly dependent on the SP concentration in the range of 0.1–4.0 μM, with LOD 0.034 μM, which covers well the physiological concentration range. Similarly to the Ag-based detection, shorter alkyl- and polyamines do not induce a color change in Au nanoparticles.

4.1.2.2.3 Electrochemical detection

Finally, electrochemical detection involving A1/A2-bis(2-mercaptoethyl)-P5A (Figure 45, F) was introduced by Cragg's group.[337] Two thiol groups at the opposite portals of P5A served as anchors for attaching to the surface of a gold electrode. When polyamines (pentylamine, PUT, SD and SP) were present in the solution, inclusion complex formation with P5A facilitated the electron transfer between the amines and the gold surface. Cathode and anode peak currents were demonstrated to be linearly dependent on SP concentration with LOD = 113 μM. Although this value is too high for the analysis of real patients' samples, it was found that the method can discriminate between the polyamines based on their voltametric responses, which is unique among the discussed sensors.

4.1.3 Novel hydrogel-based design for the sensor

All things considered, it is of utmost importance for the treatment of cancer patients to be able to detect polyamines and SP particularly at early stages in bodily liquids. The existing detection possibilities are prone to disadvantages, *e.g.*, they are time-consuming, not sensitive enough or lacking reusability.

Herein, a hydrogel sensor for the detection of SP is proposed based on the polyDMAAm strands with pendant guest moieties as well as dimerizable DMIEA groups as photoactivated crosslinkers. When immersed in a WSP5A solution, the pre-swollen hydrogel changes its thickness (depending on the charge of the guest moiety) due to the WSP5A macrocycles being attached to the polymer *via* inclusion complexation with guest anchor groups. After the gel is pretreated this way, it can detect SP in the analyte solution according to the mechanism graphically presented in Figure 46. If the complexation constant of SP@WSP5A is higher than that of Guest@WSP5A, SP replaces the pendant guest group from the WSP5A cavity leading to the newly formed complex being removed from the gel volume. This, in turn, results in a reverse change in hydrogel layer thickness. In order to utilize SPR spectroscopy as a highly sensitive technique to monitor the evolution of the gel thickness, the hydrogel should be immobilized on a surface of a gold-coated quartz chip. The washed off host moieties can be re-introduced by subsequent immersion in WSP5A solution, thus, establishing the reusability of the detection platform.

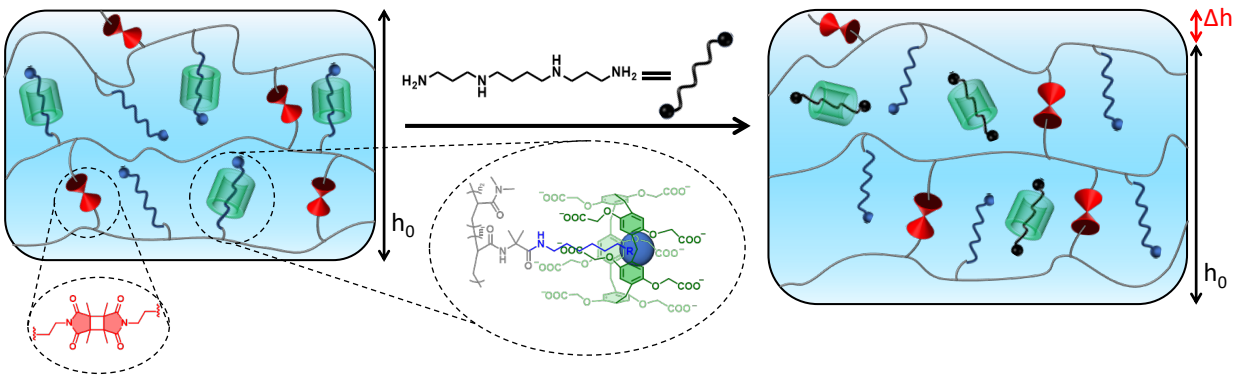

Figure 46. The concept of the hydrogel sensor for spermine based on water-soluble pillar[5]arene.

4.2 WSP5A host molecule

4.2.1 Synthesis of WSP5A

The host macrocycle WSP5A containing negatively charged carboxylate groups was synthesized in 5 steps from 1,4-dimethoxybenzene[338] (in our working group, this strategy was established in René Probst's Bachelor thesis[339]). In the first step, DMP5A was obtained by cyclopentamerization with paraformaldehyde in the presence of an acid.[88] Then, the obtained macrocycle was reacted with an excess of BBr_3 to remove all methyl groups providing decahydroxy-pillar[5]arene (DHP5A). DHP5A showed a very high sensitivity towards oxidizers such as atmospheric oxygen resulting in it turning from white to black after few hours on air (according to literature data,[340] it can be stored for several days if submerged under deionized water immediately after isolation). From multiple attempts to synthesize DHP5A, in only one it

could be isolated and characterized; in the other cases it was used for the next step without isolation. In the further step, ester functionalities were introduced to the macrocycle by the etherification of the phenolic groups of DHP5A an excess of ethyl bromoacetate. The synthesized deca-ester DECMP5A was hydrolyzed using NaOH followed by acidification to collect DCMP5A containing 10 carboxylic acid functionalities. On the final step, an acid-base reaction with NH_3 led to the formation of the decaammonium salt WSP5A.

4.2.2 Investigation of the WSP5A structure

Since it is challenging to obtain sufficient information on the formation of the decasalt (*i.e.*, the actual number of cations per molecule) using NMR spectroscopy, MS and elemental analysis were utilized for this purpose. The mass spectrum of a WSP5A sample is presented on Figure 47. The spectrum contains peaks corresponding to the negatively charged macrocycle (denoted as An^{10-}) with different number of protons (see the insets): from six-fold to nine-fold protonated species. Moreover, species with Na^+ as cations are also present on the spectrum due to the ionization method. Such species are responsible, for instance, for repeating peaks with an interval of ~11 m/z in the case of doubly negatively charged species (Figure 47, middle inset). No evidence of ammonium cations was found, the reason for which might be the protonation of the species in the aqueous solution. Hence, the MS only provided information about the presence of anions and because no NH_4^+ cations were found, this information is insufficient for the determination of the molecular weight of the product.

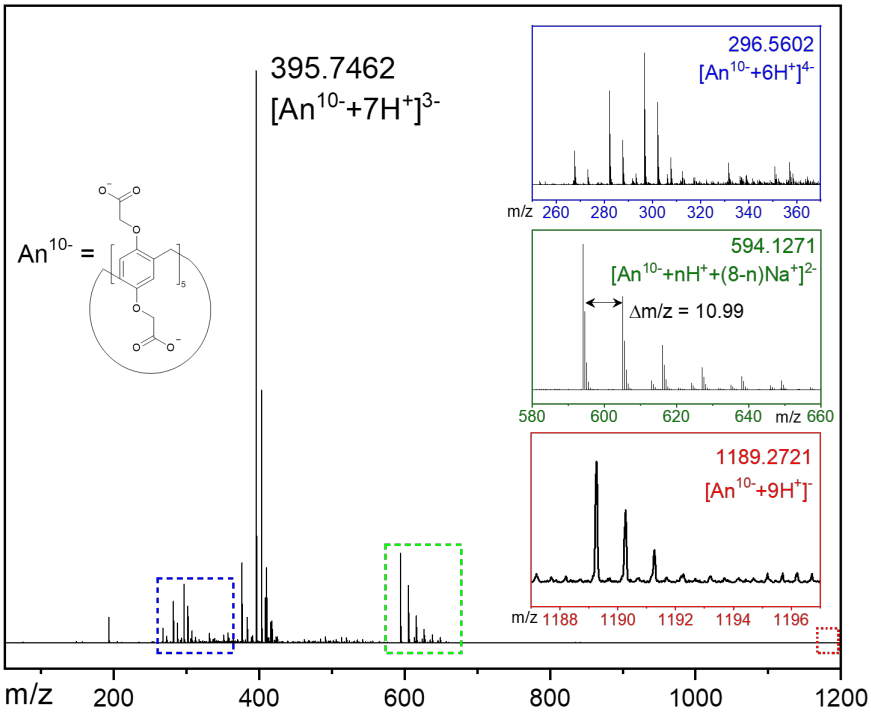

Figure 47. Mass spectrum of WSP5A. Insets represent spectrum excempts with ions of interest.

Therefore, elemental analysis was conducted to elucidate the composition of the compound (Table 18). The analysis was conducted twice, and the average value was used for the evaluation. For the determination of the amount of ammonium cations per macrocycle the ratio between N and C atoms was compared. The experimentally obtained N/C ratio was found to be less than the theoretical one, which corresponds to 8.8 NH_4^+-cations per macrocycle. However, since the calculated elemental composition for the species with 8.8 NH_4^+ still does not fit the experimental data, it was supposed that there are still water molecules present in the sample. Indeed, with 9 H_2O molecules per macrocycle the calculated values correspond to the obtained data.

Table 18. Elemental analysis of WSP5A.

	C, %	H, %	N, %	O, %	N/C
Found	43.89	6.24	8.18		0.1865
Calculated (10 NH_4^+)	48.53	5.92	10.29	35.26	0.2120
Calculated (8.8 NH_4^+, no H_2O)	49.26	5.70	9.20	35.83	
Calculated (8.8 NH_4^+, 9 H_2O)	43.95	6.29	8.20	41.56	

Thus, it is assumed that the sample contains 8.8 ammonium cations and 9 H_2O molecules per macrocycle, and the effective molecular mass is therefore M = 1501.6 g/mol. Since the drying overnight *in vacuo* was shown to be insufficient, the product was stored in a desiccator under reduced pressure.

4.3 Investigation of WSP5A–SP interaction

4.3.1 NMR titration

The interaction between WSP5A and SP was evaluated in terms of binding affinity and the complexation constant K_a was determined using NMR titration in D_2O in the course of R. Probst's Bachelor thesis [339] (Figure 48). To the solution of WSP5A in D_2O (13.6 mM) SP solution in D_2O (76 mM) was added in portions (corresponding to 0.13, 0.51, 0.83, 0.96, 1.24, 1.65, 1.93, 2.17, 3.22, and 4.10 equivalents of WSP5A) followed by sonication for 10 min prior to NMR analyses. An almost linear downfield shift of aryl (6.77 ppm) and methylene (3.89 ppm) protons of the WSP5A was observed until the ratio reached 1:1 and a slight upfield shift upon increasing the concentration of SP.

Such trends in the NMR titration may imply a highly thermodynamically beneficial 1:1 complex formation so that almost all the WSP5A molecules in the solution are bound into complex as soon as a sufficient amount of SP molecules are available. A Job plot was used to confirm the stoichiometry of the complex (Figure 49, A). As one can observe, the maximum of the dependence

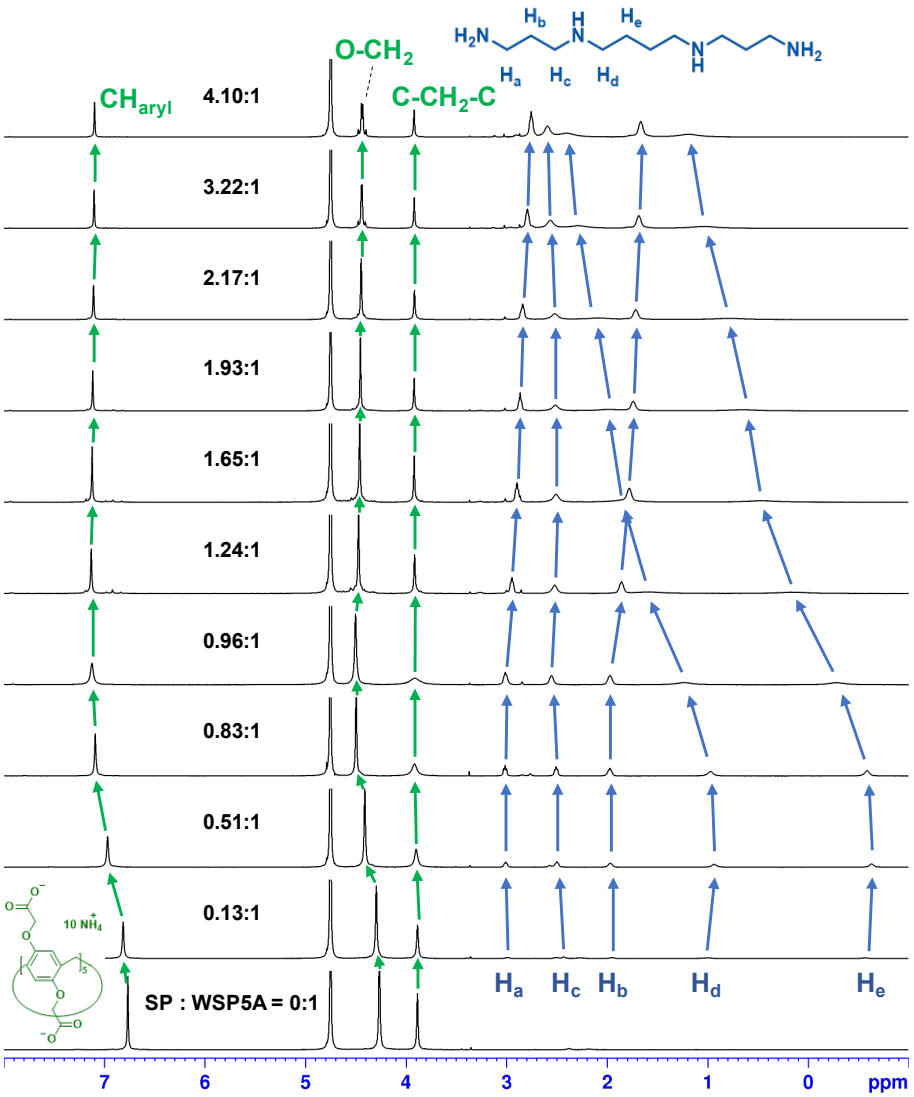

Figure 48. NMR titration of WSP5A with SP. Green and blue arrows mark shifts of host and guest peaks, respectively.

lies close to the mole fraction of the host X(WSP5A) ≈ 0.5, which suggests a 1:1 stoichiometry of the SP@WSP5A complex. The sharp triangle-like form of the Job plot furthermore indicates high stability of the SP@WSP5A complex.[232]

As one can deduct from the trends of the NMR titration, the exchange between WSP5A and SP is fast (see Chapter 2.4.4.1.3) and therefore for 1:1 inclusion complex the binding affinity can be calculated using the equation (25) (Chapter 2.4.4.1).

Unfortunately, the determination of the K_a according to the 1:1 model failed in the case of the WSP5A–SP system, which might be due to the binding affinity which exceeds the applicability range of the NMR titration.[227–229] Indeed, the equilibrium constants determined for complexes of SP with carboxylated PnAs reported in literature well exceed 10^5 M^{-1}.[150,153] Particularly in the case of WSP5A the K_a value was determined by indicator displacement assay to be 2.7×10^6 M^{-1}.

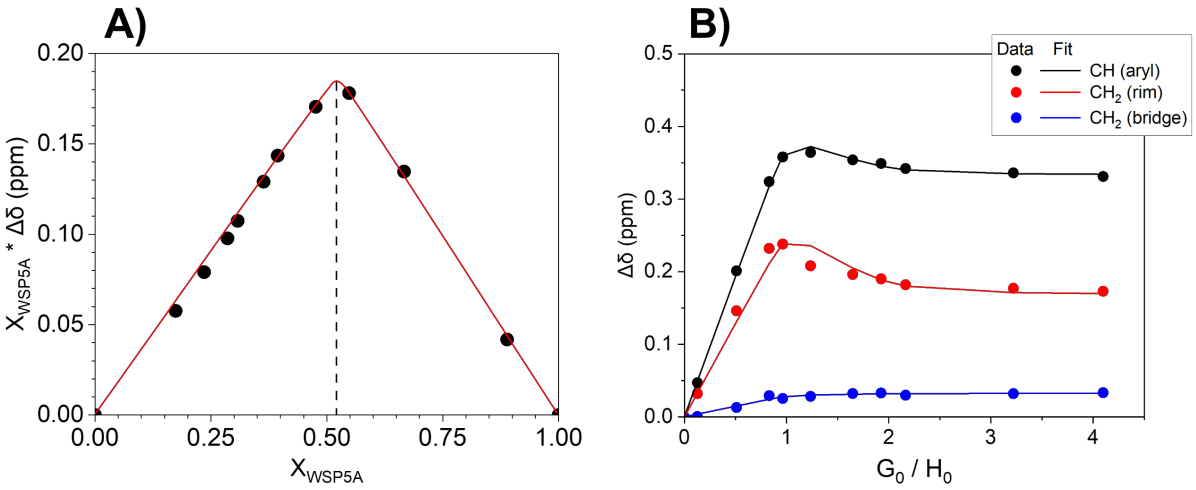

Figure 49. NMR titration data of the system WSP5A–SP corresponding to the evolution of the signal of the aromatic protons: A) Job plot indicates that the complex is supposed to have a 1:1 stoichiometry. The red line serves as a guide to the eye. B) Scatter plot: titration curves of each of the WSP5A proton peaks plotted against guest:host ratio. Lines: fitting of the titration curves by BindFit v.0.5.[234,341]

Another possible reason might be the presence of other equilibria. Although the stoichiometry determined by the Job plot is 1:1 for the SP@WSP5A complex, the upfield shift occurring at higher SP:WSP5A ratios as well as splitting of the O-CH_2 signal of the macrocycle imply that some other process might take place in the system.[234,235] Firstly, this can be accounted to increasing pH and, therefore, deprotonation of the carboxylic acid groups of the WSP5A that might be left protonated during the last synthetic step. Secondly, formation of a trimolecular complex HG_2 might take place according to equation (56).

$$SP@WSP5A + SP \rightleftarrows (SP)_2WSP5A \quad (56)$$

This possibility was tested by applying a 1:2 complexation model to the experimental data using BindFit software.[234,341] The obtained fit (Figure 49, B) confirms a decrease in Δδ value with increasing SP concentration due to a presence of a second equilibrium, which supports the assumption about $(SP)_2$@WSP5A complex formation. However, the K_{12} (1.8×10^3 ± 118 %) value is by 2 orders of magnitude lower than K_{11} (7.84×10^5 ± 191 %) implying a low concentration of trimolecular complexes in the solution in the considered range of SP concentrations. The high residual standard deviation values (118 % and 191 %) can be explained by insufficient amount of data points (especially around the area where $G_0 = H_0$) to provide correct fitting of the data. Therefore, the K_{11} value can be used as an estimation of a binding affinity for comparison with other host–guest systems. Furthermore, such difference in magnitudes of the both equilibrium

constants might be accounted for the "invisibility" of the second equilibrium on the Job plot[234,235] (see Chapter 2.4.3).

Additional information of the inclusion complex formation was delivered by 2D NOESY NMR spectroscopy (Figure 50). The spectrum demonstrates the NOE cross-peaks between the protons H_b, H_c, and H_d of the SP axle and aryl as well as methoxy protons of the WSP5A macrocycle, proving the host–guest complex formation.

4.3.2 Mass-spectrometry

SP@WSP5A complex formation was confirmed by MS (Figure 51). As in the case of the unbound WSP5A, the mass spectrum of the complex contains the peaks of the protonated deca-anion without ammonium cations. In the highlighted regions of the spectrum (see insets) the peaks corresponding to the SP@WSP5A complex species are observed, which are, similarly, protonated (m/z = 1931.4402 and 695.2171) or in which a proton is exchanged for a Na^+ (m/z = 706.2092) in the course of the ionization process.

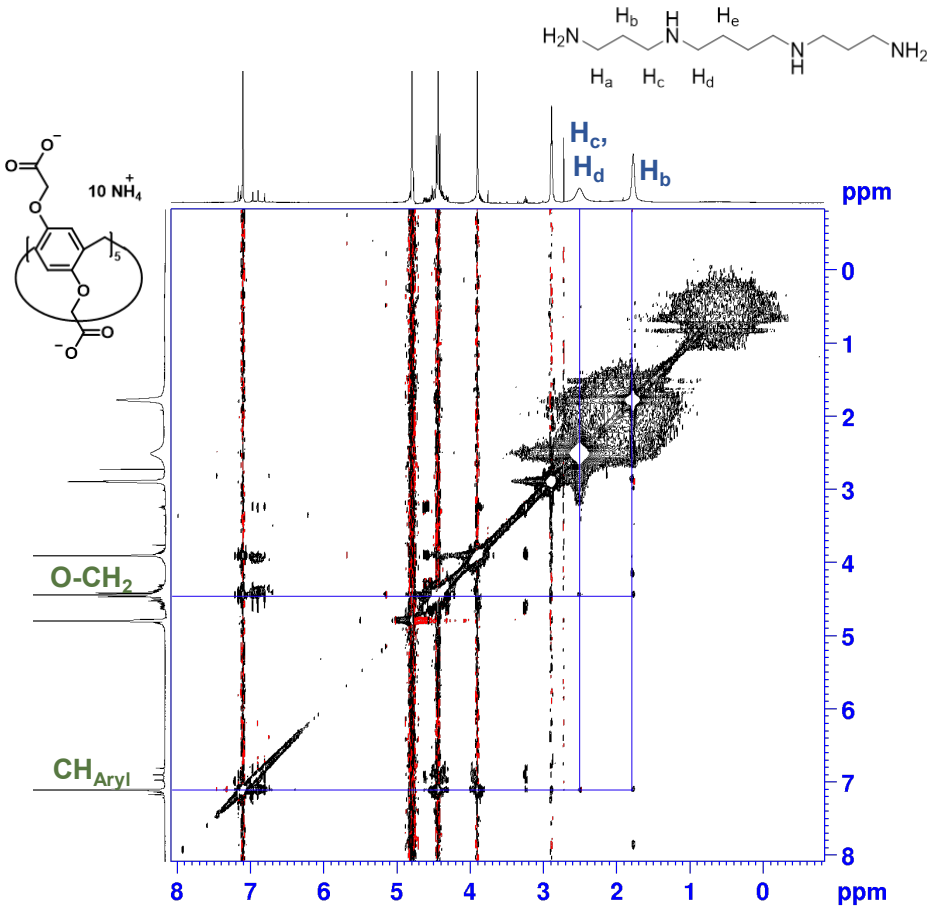

Figure 50. 2D NOESY NMR spectrum of a SP@WSP5A sample. The NOE cross-peaks are highlighted by blue lines.

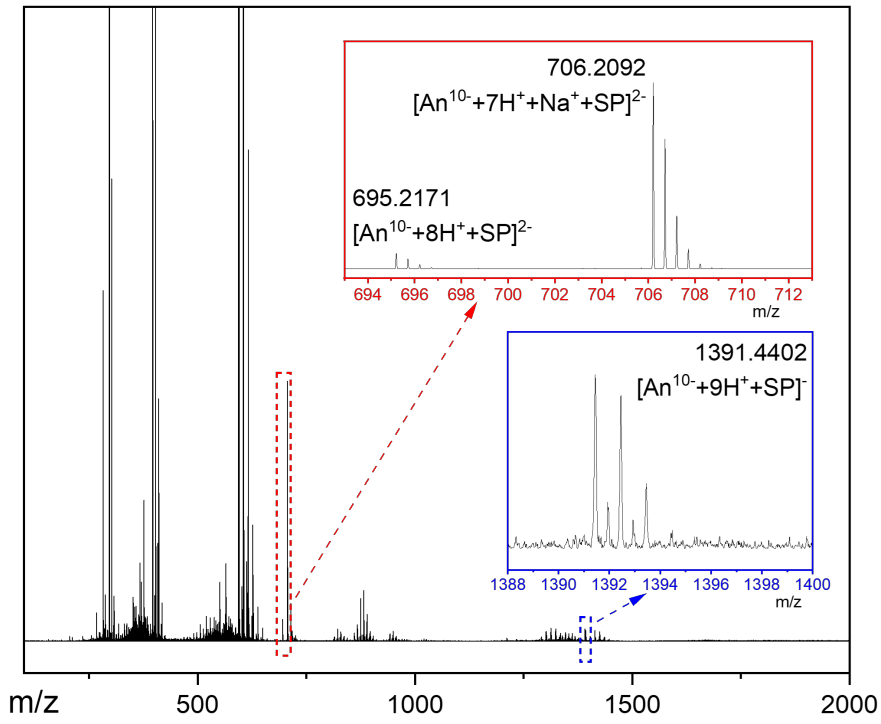

Figure 51. Mass spectrum of the mixture WSP5A and SP. The highlighted regions contain the peaks corresponding to the complexed species.

4.3.3 Isothermal titration calorimetry

Further, the SP@WSP5A complex formation was investigated by the ITC. The analysis was conducted by working group of Prof. Dr. Schönhoff in WWU Münster. For all the complexes, the data fitting was performed using a model of single set of equal binding sites (see Chapter 2.4.4.3.4). Preliminary experiments in water proved a significant binding affinity between the WSP5A and SP (Figure 52, A and Table 19). According to the results, the forming complex has an association constant of $K_a = 7.1 \times 10^5$ M^{-1}, implying a highly stable complex. The experimental stoichiometry is, however, surprisingly low: n = 0.24, meaning that one SP molecule binds with 4 macrocycles in an equilibrium state, which is not plausible considering the dimensions of both host and guest molecules. Moreover, the standard enthalpy of the observed process ($\Delta H° = -181$ kJ/mol) is quite high for inclusion complex formation: for cyclodextrins with various guest molecules including drug formulations[342], for neutral pillar[5]arene in organic solvents[309], and for cationic pillar[5]arene with acids in aqueous solutions[343,344] the ΔH value does not exceed 50 kJ/mol. Because of this remarkable ΔH value, the entropy ΔS calculated using equation (33) appears unprecedentedly low as well. Such decrease in entropy would imply a drastic reduction of degrees of freedom upon complexation, which was observed for charged PnAs in organic (*e.g.*, MeOH/$CHCl_3$ [116]) but not in aqueous medium.

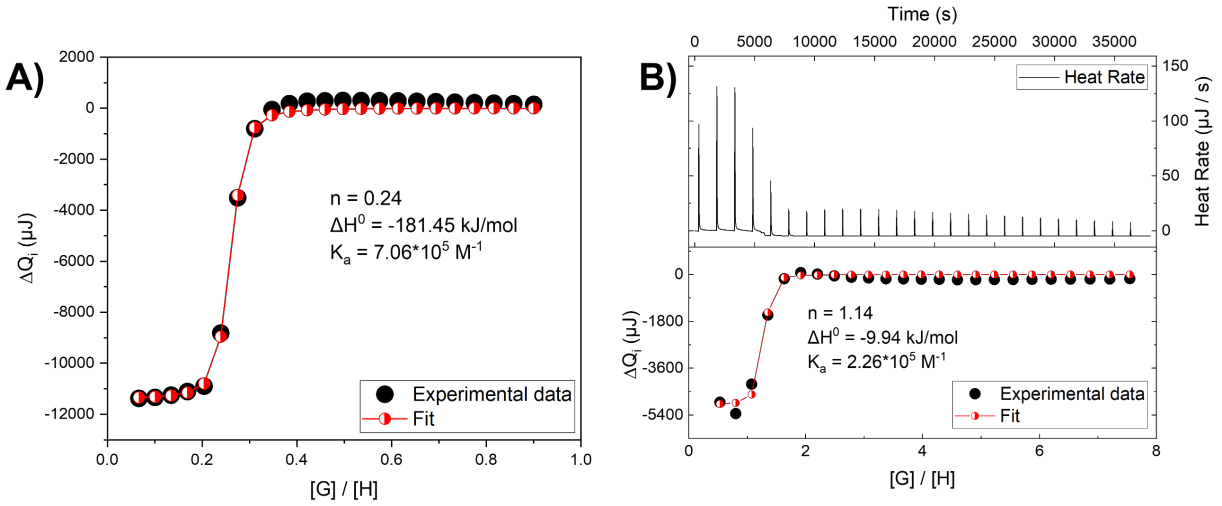

Figure 52. ITC experimental results A) Titration isotherm of WSP5A (2 mM) titrated with SP solution (6 mM) in water. B) Raw ITC data (top) and titration isotherm of WSP5A (2 mM) titrated with SP4HCl (50 mM) in MOPS (0.2 M) buffer.

Table 19. Thermodynamic parameters of the systems WSP5A–SP in water and WSP5A–SP4HCl in MOPS buffer obtained by ITC at 298.15 K. ΔG° and ΔS° are calculated according to equations (2) and (33).

System	K_a, M^{-1}	ΔH°, kJ/mol	ΔG°, kJ/mol	ΔS°, J/(mol·K)
WSP5A–SP/H_2O	7.1×10^5	−181.45	−33.38	−497
WSP5A–SP4HCl/MOPS	2.3×10^5	−9.94	−30.56	+69.2

It was supposed that the addition of SP could have a drastic effect on the pH of the solution. Indeed, the pH measurement of a 1 mM SP solution revealed that at these concentration levels the solution is significantly basic (pH = 10.1) at RT, whereas pH value of a 1 mM WSP5A solution is close to neutral (pH ≈ 6.5). Therefore, there must be a neutralization reaction occurring in the system upon dropwise addition of SP. Heat of such neutralization reaction will contribute to the overall heat consumption/production during the process, which will distort the results presented on a enthalpogram.[345] Interestingly, the obtained value for a "reaction" enthalpy is significantly above the heat values reported for amine protonation (≈ –50 kJ/mol)[346] which might be due to a manifold of ionogenic groups in both host and guest species.

Hence, two measures were taken in order to exclude the abovementioned neutralization reaction from the overall process. Firstly, instead of pure SP, which is considerably basic, its salt, spermine tetrahydrochloride (SP4HCl) was used. Unlike SP, the pH of a 1 mM solution of SP4HCl was determined to be ~6.5, which is close to the pH value of WSP5A. Secondly, a buffer solution was used for the process investigation to ensure that changes of concentration or ionic strength of the solution do not affect the process significantly. Since the ultimate goal of the project was to devise

a sensor for the detection of spermine/spermidine in human urine samples, the buffer should provide a comparable pH of the medium (pH 6–7[347]). At first, a phosphate buffer (K_2HPO_4 + KH_2PO_4) was used. However, it was soon discovered that insoluble salts are formed during the measurements. Therefore, a Good's buffer, MOPS[348] containing 3-(*N*-morpholino)-propanesulfonic acid, was used instead. The pH of the buffer was adjusted at 6.01 and a SP solution in the buffer was confirmed to be stable for at least several months. The pH values of 1 mM WSP5A and SP4HCl solutions in the buffer were 5.98 and 6.00, respectively (the inconsistency was most probably due to the fluctuations of room temperature).

With these points considered, a new ITC experiment was conducted using SP4HCl as a titrant and the experiment was conducted in a MOPS buffer as a medium (Figure 52, B, Table 19). As one can observe, the stoichiometry of the interaction became very close to unity (n = 1.14), *i.e.*, to the results of the NMR titration and mass spectrometry. In comparison to the earlier result, the K_a value ($K_{a,\,MOPS} = 2.3\times10^5\ M^{-1}$) decreased although stayed in the same order of magnitude (which is also reflected in comparable ΔG values), also confirming the value obtained using NMR titration. The drastically reduced enthalpy of the process is noteworthy: $\Delta H° = -10$ kJ/mol. Although the absolute value is less than the one obtained for the titration of water soluble P7A macrocycle with SP (~42 kJ/mol)[150] or for the abovementioned system cationic PA–acid[343,344], it is plausible that suppression of protonation reactions led to a further decrease in the interaction enthalpy. Furthermore, the ΔS value increased and even changed its sign to the positive: +69 J/(mol·K), which is in accordance with the data for PnA–guest complexes in aqueous medium.[150,343] Such behavior can be explained by the release of water molecules electrostatically bound to the WSP5A and SP4HCl upon complex formation, therefore, illustrating the significant contribution of entropic forces for the affinity between host and guest.

4.4 Synthesis of the guest moieties and complexation with WSP5A

4.4.1 Initial considerations

With the aspects considered, it is clear that the SP forms a highly stable complex with WSP5A with binding constant exceeding $10^5\ M^{-1}$. For the proposed mechanism of the detection based on the competitive complexation a guest moiety must be found, whose affinity to WSP5A is lower than that of SP, and due to a high value of K_a of SP@WSP5A even complexes yielding relatively stable aggregates ($K_a \sim 10^3 - 10^4\ M^{-1}$) present lower binding affinity than that between SP and WSP5A.

As guest moieties, molecules based on end-capped hexyl chains were selected: capped with 1,2,4-triazole (THA) and with trimethylamine (TAHA). The former was chosen as a neutral species with

a moderate K_a value[138] (additionally, see Chapter 3.3.1). Moreover, the neutrality of the triazole fragment is anticipated to lead to a considerable difference in the swelling degree after WSP5A is added to the preswollen hydrogel in water, the principle underlying a high sensitivity of the gel sensor.

The choice of TAHA relies on the data from the Chapter 3.3.2 and from the literature, where WSP5A is shown to exhibit a significant binding affinity towards trimethylalkylammonium salts: $K_a = 1.75\times10^6\ M^{-1}$ as determined by ITC.[349] Although this K_a value exceeds the one that was obtained in the current work for SP@WSP5A, which might contradict to the envisioned design, it is believed that additional substituents at quaternary ammonium group will lead to a decrease of binding strength, since trimethylhexylammonium bromide used in the aforementioned work[349] has an alkyl tale, which endows the system with an additional hydrophobic binding mode. Furthermore, WSP5A was shown to bind multiple guest moieties simultaneously based on hydrophobic and electrostatic interactions causing a hydrogel to shrink in its presence.[218] This finding suggests a mechanism of detection, which is opposite to the one involving THA as a guest species: namely, a TAHA-containing gel shrinks in the presence of WSP5A and swells back to its original state upon SP injection.

4.4.2 Synthesis of the guest moieties THA and TAHA

THA and TAHA (Scheme 9) were synthesized for further polymer modification according to the described procedures (Chapter 5.2). Because the products are highly hygroscopic, they were stored in a desiccator over $CaCl_2$.

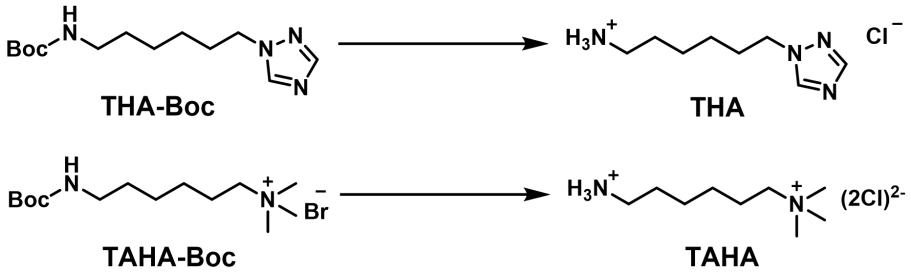

Scheme 9. Guest moieties used in the present work. For the full synthetic pathways and experimental conditions, see experimental part (Chapter 5.2).

To prove their applicability for the gel sensor fabrication, binding affinity towards WSP5A must be evaluated and compared to that of the analyte. In order to make a plausible assumption about the interaction between WSP5A and a guest moiety as a pendant group within the gel, Boc-protected molecules (THA-Boc and TAHA-Boc) can be used instead of deprotected ones, since they are chemically closer to the amides formed upon VDMA ring-opening and do not bear an additional positive charge (which will lead to an overestimated affinity determination). Yet there

is an obstacle in the case of the triazolyl-substituted guest moiety: THA-Boc, unlike TAHA-Boc, is insoluble in water, which is the reason for using THA-modified polymers for the estimation of the complexation, as discussed further.

4.4.3 TAHA-Boc@WSP5A

4.4.3.1 NMR titration

Complex formation between WSP5A and TAHA-Boc was investigated by NMR spectroscopy in D_2O as well as by ITC and MS. In Figure 53 NMR spectra of WSP5A solution in D_2O containing 0 to 4.8 equivalents of TAHA-Boc are shown (total host concentration was held constant at 4 mM). NMR-Titration proved a complex formation with a slow to intermediate exchange on the NMR time scale, which is demonstrated, on the one hand, by the presence of peaks of both free and bound species, on the other hand, the gradual shifts of the WSP5A peaks: CH_{aryl} (6.8 ppm) and O-CH_2 (4.2 ppm). The peaks of the guest molecule's methylene groups are shielded upon binding to

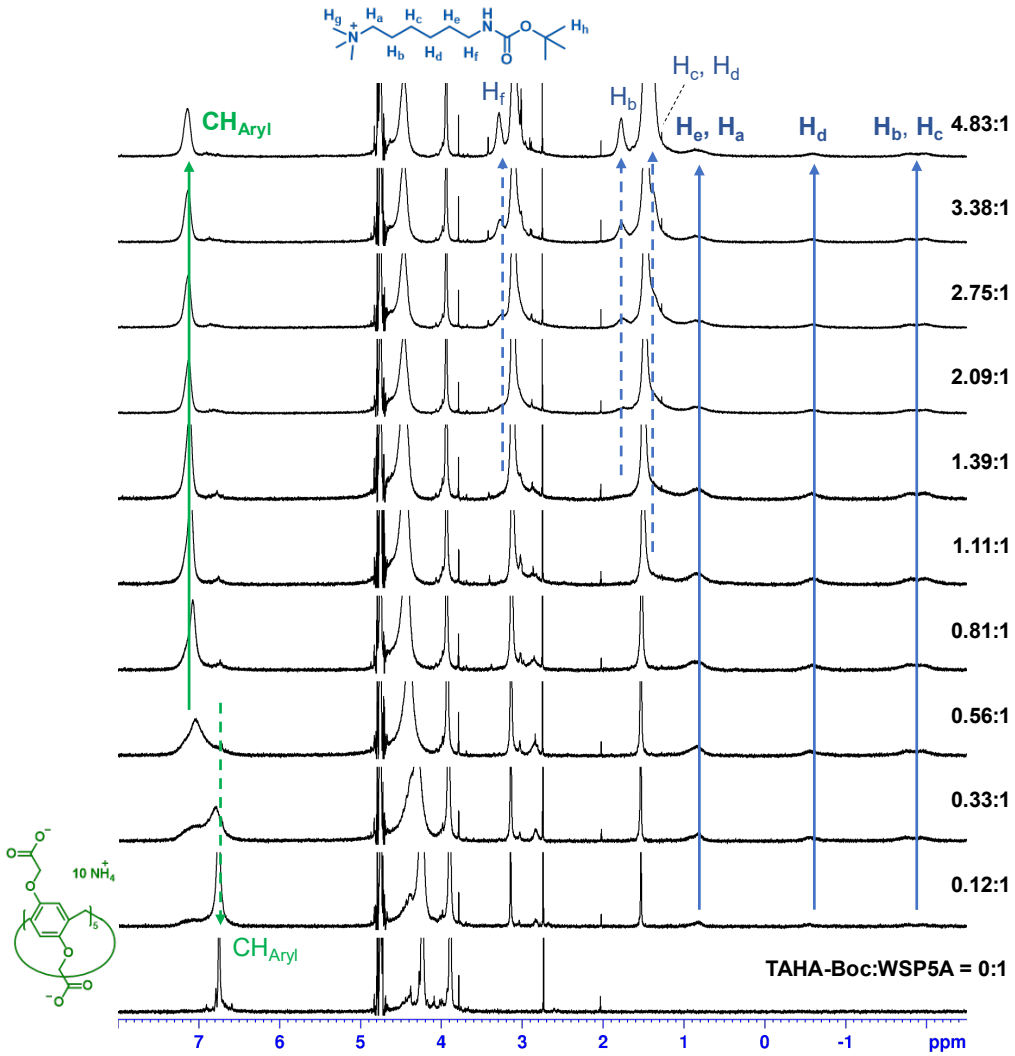

Figure 53. NMR titration of WSP5A with TAHA-Boc. $[WSP5A]_0$ = 4 mM. Green and blue arrows mark shifts of host and guest peaks, respectively. The peaks of bound species are shown in bold.

the host (Figure 54, A). Here, H_b exhibits the most pronounced upfield shift ($\Delta\delta = -3.85$ ppm), and for other protons the shift and, therefore, the shielding effect decreases in both directions along the alkyl chain. At the same time, the peaks of WSP5A (CH_{aryl} and O-CH_2) are shifted downfield. The complex stoichiometry was determined by integrating signals of host CH_{aryl} (7.52 – 6.41 ppm), free and bound guest (1.90 – 0.50 ppm) and complex (H_b+H_c, −1.45 – −2.30 ppm) peak integration (Table 20) revealing a 2:1 (H:G) complexation, which can also be a reason behind the appearance of both slow and fast exchange features on the NMR spectra of the titration points (Figure 53).

Table 20. NMR signals used for TAHA-Boc@WSP5A stoichiometry determination.

NMR signal/area, ppm	Protons corresponding to the signals
7.52 – 6.41	10H ($WSP5A_{free}$) + 10H ($WSP5A_{bound}$)
1.90 – 0.50	17H (TAHA-Boc_{free}) + 13H (TAHA-Boc_{bound})
−1.45 – −2.30	4H (TAHA-Boc_{bound})

With the aim to clarify this outcome, 2D NOESY spectrum of the complex was recorded. In a spectrum in Figure 54, B cross-peaks are only observed corresponding to the proximity between the trimethylammonium tail of the guest molecule (methyl groups, H_g, and methylene groups adjacent to the nitrogen, H_a) and the host (protons of the methylene bridges of the macrocycle). Considering that the protons of the methylene groups connecting aromatic rings of the macrocycle

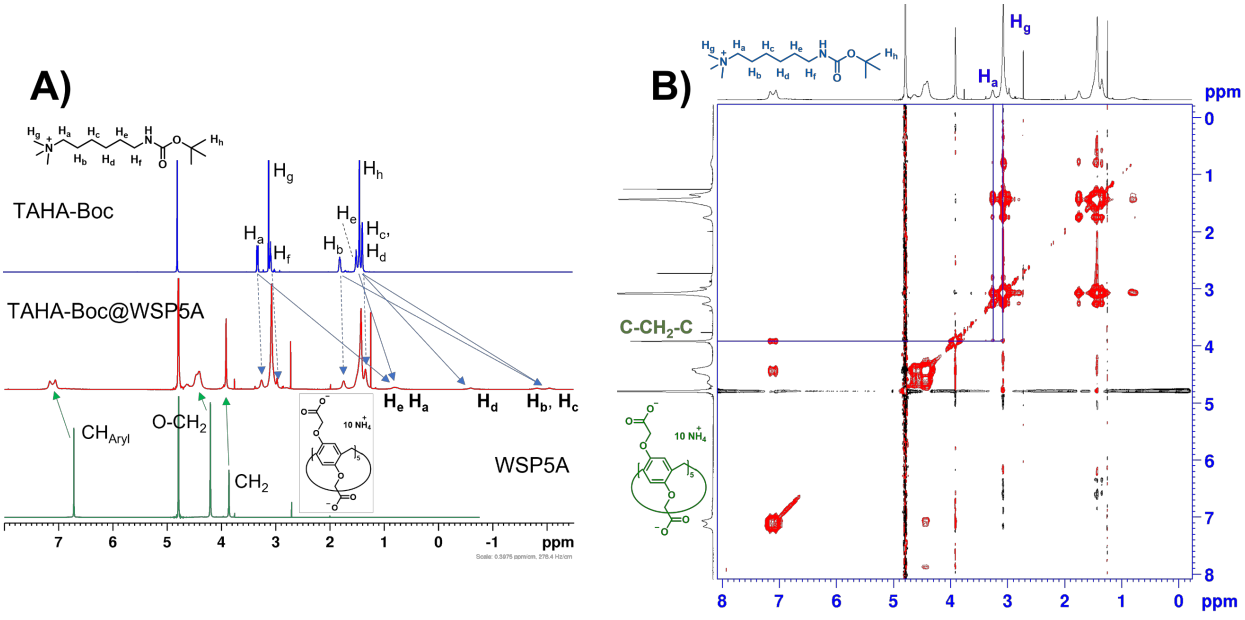

Figure 54. A) NMR spectra of (from the bottom) WSP5A, TAHA-Boc@P5A complex (at $[G]_0/[H]_0 = 3.9$), TAHA-Boc. The change in peak shifts of the guest molecule is presented by the arrows. The signals of bound species are depicted in bold. B) 2D NOESY NMR spectrum of a TAHA-Boc@WSP5A sample (1 : 2.1 G : H ratio). The NOE cross-peaks are highlighted by blue lines.

are facing outwards (Chapter 2.2, Figure 3), these NOE signals might be a hint of an outer complex formation, which could explain the determined stoichiometry. However, the CH_2 peak did not change its chemical shift in the course of the NMR titration (Figure 53) implying negligible interaction with the guest molecule, which contradicts with these considerations.

Nonetheless, strong broadening of the peaks and relatively low complex signal intensity do not allow accurate quantification of the spectra. A similar inclusion complex, in which trimethylhexylammonium was used as a guest moiety, was demonstrated to have 1:1 stoichiometry and fast exchange kinetics.[349] Therefore, it is feasible that the intermediate exchange regime is the factor hampering correct evaluation of WSP5A–TAHA-Boc titration.

4.4.3.2 Mass-spectrometry

To further validate the possibly of a ter-complex formation, an MS measurement was conducted in ESI positive mode (Figure 55). Unfortunately, it was unable to provide any indication of that because the complex was apparently not stable enough to be ionized as a single species. Therefore, no HG or H_2G peaks are observed on the spectrum. The peak at $m/z = 259.2367$ can be assigned to the TAHA-Boc molecule whereas the signals in the areas between $m/z \approx 1213$ to 1347 and 618 to 729 belong to singly and doubly charged WSP5A species, respectively, in which 1 to 7

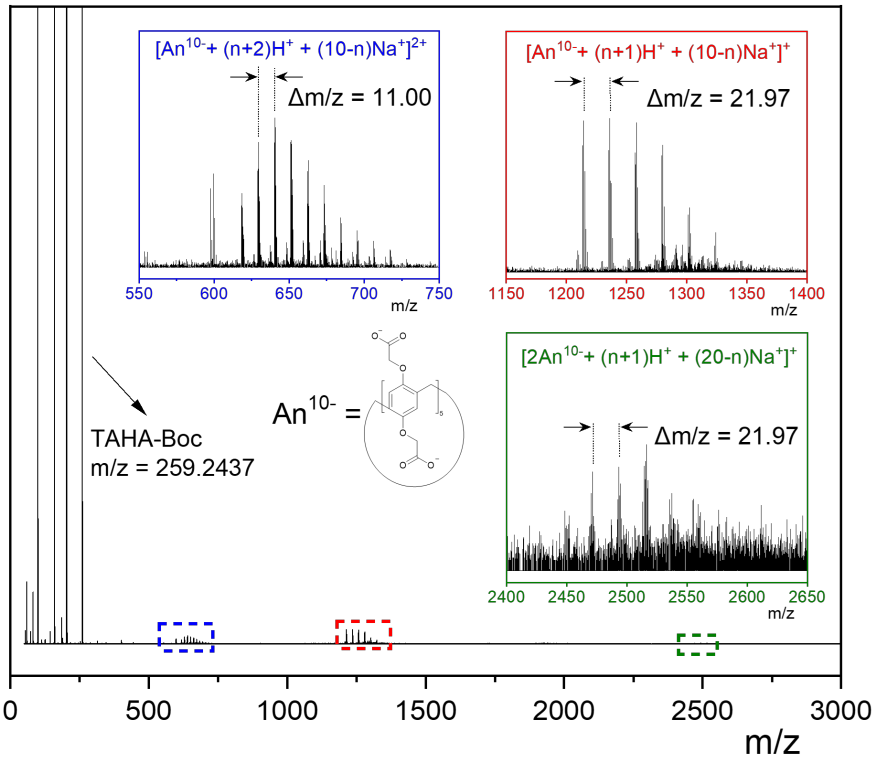

Figure 55. Mass spectrum of a sample containing WSP5A and TAHA-Boc. A strong TAHA-Boc peak as well as various areas of WSP5A signals (singly, doubly charged and dimerized) are observable. Peaks corresponding to the complexes TAHA-Boc@WSP5A or TAHA-Boc@$(WSP5A)_2$ were not found.

carboxylic protons are replaced with Na atoms (implied by the difference of approx. 22 *m*/*z* units between the corresponding peaks in neighboring groups of signals). Interestingly, another area with signal groups (ca. 2450–2620 *m*/*z*) was found to possess a similar pattern arguably suggesting aggregates of Na salts of $(WSP5A)_2^+$ being present as ionized species.

4.4.3.3 Isothermal titration calorimetry

Further, ITC was carried out to shed light on the complex stoichiometry and binding affinity. In the experiment, a 2 mM WSP5A solution in the buffer was titrated with 50 mM solution of TAHA-Boc. The results are presented in Figure 56 and Table 21. First, the isotherm demonstrates only one "step", which implies either a single equilibrium existing in the system or, if there are two different equilibria (*e.g.*, a stepwise 1:2 complex formation), both steps have similar binding energy, from which the weakest affinity can be determined.[255] Regrettably, the portion volumes of the guest solution are revealed to be too large, which makes the number of data points before the saturation is settled was too low to analyze the titration accurately. The parameter *n* reflecting the guest to host ratio in the complex deviates from unity, which, again, might be an experimental error because of the low number of data points or a further indication of multiple equilibria. Therefore, a K_a value obtained from the fitting of the titration isotherm (a single set of equal binding sites model): 8.77×10^4 M^{-1} can be either a measure of the affinity of a 1:1 system or

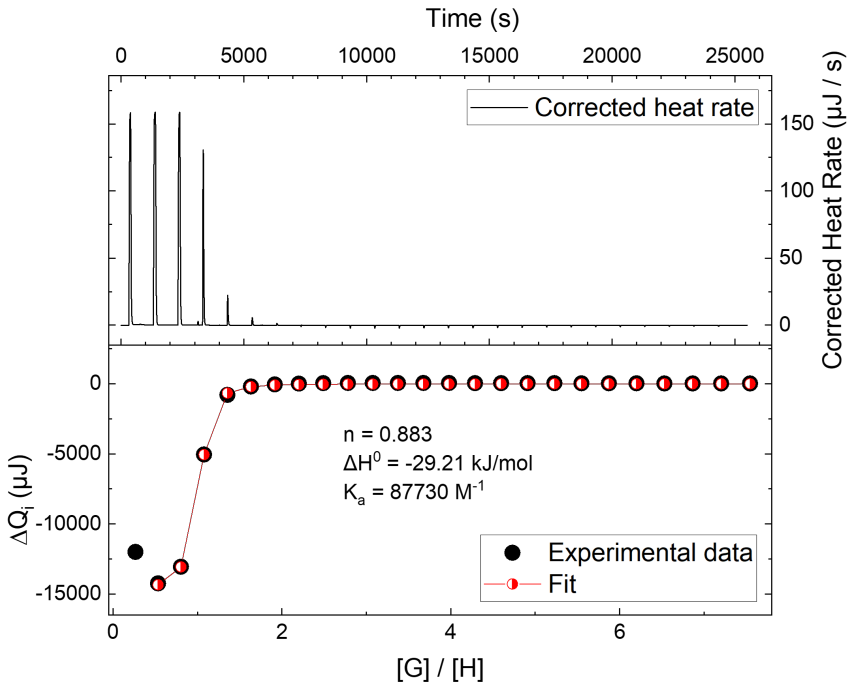

Figure 56. Calorimetric titration of WSP5A (2 mM solution in MOPS) with TAHA-Boc (50 mM solution in MOPS). Top: Raw heat rate data; Bottom: titration isotherm, i.e., integral heat release after each portion of the titrant.

approximately each of the stepwise complexation constants (equations (39) and (40)) in the process of TAHA-Boc@$(WSP5A)_2$ complex formation.

Table 21. Thermodynamic parameters of the systems WSP5A–TAHA-Boc in MOPS buffer obtained by ITC at 298.15 K. ΔG° and ΔS° are calculated according to equations (2) and (33).

System	K_a, M^{-1}	ΔH°, kJ/mol	ΔG°, kJ/mol	ΔS°, J/(mol·K)
WSP5A–TAHA-Boc/MOPS	8.8×10^4	−29.21	−28.21	−3.3

Nonetheless, the heat of the complex formation recorded for TAHA-Boc and WSP5A (−29.2 kJ/mol) is comparable to the ΔH° of the trimethylhexylammonium@WSP5A complex, which was shown to be ~33.9 kJ/mol and dominated by electrostatic interaction contribution.[349] The negative (−3.3 J/(mol·K)) entropy value can be interpreted as a strong decrease in conformational degrees of freedom in the guest molecule, which is not compensated by the release of affine H_2O molecules. This serves as a further demonstration of the strong affinity between the host and guest species, which is beneficial for the sensor design because it proves the possibility of secure incorporation of the WSP5A in the hydrogel.

4.5 DOSY NMR

Diffusion-ordered NMR spectroscopy can give further information about the structure of the complex by comparing the mobility of the free and bound species in the solution. It is envisioned that if a guest species is completely encompassed by the macrocycle, its mobility expressed in terms of diffusion coefficient D should become similar or equal to the mobility of the host, which, in turn, should not undergo any significant changes. Figure 57 demonstrates the comparison between D values of free WSP5A and guest molecules (SP and TAHA-Boc) as well as complex species, recorded in D_2O. For the investigation of the SP@WSP5A and TAHA-Boc@WSP5A systems solutions were used containing [H]:[G] ratios of 1:2.5 and 1:4, respectively.

As one can observe, the mobility of WSP5A ($D_{WSP5A,\ free} = 2.3\times10^{-10}$ m^2 s^{-1}) remained practically unchanged even when bound to guest molecules, whereas the mobility of SP and TAHA-Boc becomes reduced. Notably, because the stability of the SP@WSP5A complex is high, as was discussed before, the diffusion coefficient of SP ($D_{SP,\ free} = 4.2\times10^{-10}$ m^2 s^{-1}) decreased by almost 45 % down to the value of the host moiety. This illustrates the expected behavior in case of an inclusion complex formation. TAHA-Boc, on the other hand, exhibits a less drastic drop in mobility upon complexation ($D_{TAHA\text{-}Boc,\ free} = 4.4\times10^{-10}$ m^2 s^{-1}; $D_{TAHA\text{-}Boc,\ bound} = 3.4\times10^{-10}$ m^2 s^{-1}). This might be elucidated by the fact that for the determination

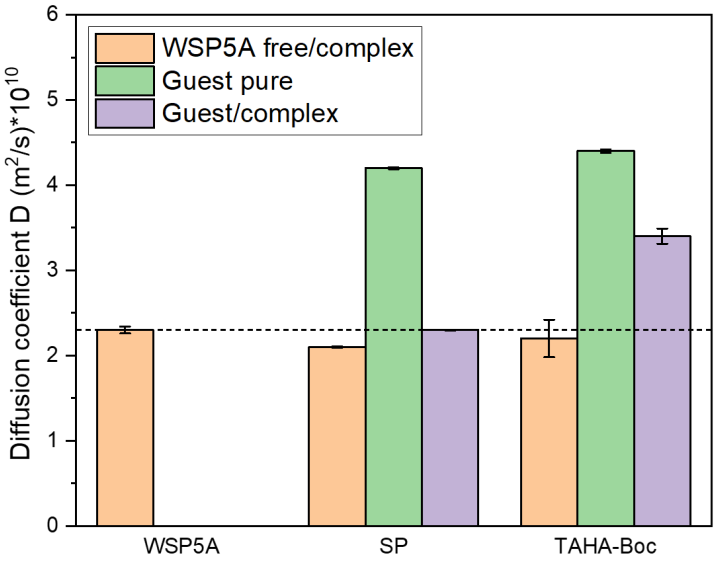

Figure 57. Diffusion coefficients of the host, guest moieties and their complexes obtained using DOSY NMR. The dashed line is given as a comparison for a free WSP5A.

of the diffusion coefficient signals with high intensity are required. Such peaks in case of TAHA-Boc correspond to the protons H_g and H_h (Figure 54, A), which do not undergo any significant shift in the presence of the host. Therefore, both free and bound species are arguably taken into account for the DOSY analysis. Nevertheless, the mobility of WSP5A is not affected by the presence of the guest species implying that its hydrodynamic radius and, thus, its size, is not affected, which could be an argument against a 2:1 complex formation. Nonetheless, an inclusion complex formation, indeed, occurs and serves as reason for the decrease in diffusion coefficient of TAHA-Boc.

4.6 Polymer synthesis

4.6.1 Synthesis of VDMA

VDMA was used as a comonomer that is capable of "click"-modification via ring-opening under nucleophilic attack. The azlactone moiety was synthesized according to a two-step procedure (Chapter 5.2.5) described in the literature[306] with a slight adjustment in the work-up of the second step. Because of insufficient power of the vacuum pump and lack of control over the pressure, the purification by vacuum distillation required elevated temperatures (up to 95 °C), which was constantly leading to the crude product polymerizing in the flask as a result of its high reactivity. Attempts were made to purify the VDMA by other methods including column chromatography or precipitation (according to the literature[350], the product can be crystallized by cooling down the hexane solution on a dry ice/acetone bath, which was implemented using EtOAc/N_2 bath). Chromatography failed to provide a pure product presumably because of the interaction with the

silica in the column, whereas hydrolysis during the filtration is supposed as a source for impurities in case of precipitation method. Delightfully, the highest purity was achieved by multiple cycles of dissolving in hexanes, filtration and evaporating the filtrate *in vacuo*. Upon addition of hexanes, a white precipitated formed, presumably consisting of the residual triethylamine hydrochloride and poly-VDMA particles. After three cycles, no precipitation was observed implying the product achieved the purity, which was also confirmed by ^{1}H NMR.

4.6.2 Kinetics of DMAAm and VDMA co-polymerization

The polymer P10 was synthesized by RAFT polymerization using AIBN as an initiator and DMP as a chain transfer agent. Since the reversible chain transfer mechanism determines that all the chains in the system grow simultaneously, RAFT was used to achieve a uniform distribution of monomers among the polymer chains.

Kinetic experiments were conducted to give insight into the reactivities of the monomers which therefore define the distribution of the units within chains. For the kinetic investigations, the components (DMAAm, VDMA, AIBN and DMP) were dissolved in 3 mL 1,4-dioxane in a ratio n(DMAAm):n(VDMA):n(AIBN):n(DMP) = 90:10:1:0.5 at a DMAAm concentration of 0.33 g/mL. Then the mixture was degassed by purging Ar through the solution for 30 min and a sample was taken for the NMR analysis (t = 0 min) followed by placing the mixture into a pre-heated oil bath at 70 °C. The conversion was controlled in 15 min interval, the aliquots (~50 µl) of the reaction mixture were quenched by freezing in liquid nitrogen and then dissolved in 0.5 mL $CDCl_3$ for NMR analysis (Figure 58). The monomer concentration was calculated according to equation (57) from the corresponding integrals of vinyl protons (multiplet at 5.89 ppm for VDMA and 5.62 ppm for DMAAm) normalized by the total number of protons involved[351] (excluding the signal of 1,4-dioxane).

$$[Monomer] = \frac{\int vinyl\ protons}{\int total\ protons} = \frac{\int vinyl\ protons}{\int (6.9 - 5.3\ ppm) + \int (3.3 - 0.5\ ppm)} \qquad (57)$$

The conversion was calculated by equation (58) from the concentration relations ($[M]_0$ and $[M]_t$ are monomer concentrations at the starting point and t min after the reaction start, respectively).

$$Conv\ (t) = 1 - \frac{[M]_0}{[M]_t} \qquad (58)$$

Hereto, the degree of polymerization P_n (equation (59)) as well as number-average molecular weight M_n (equation (60)) were determined for each time point, where [*end groups*] is a concentration of end groups determined according to (61), and mole fractions of the comonomers in the copolymer are defined by equations (62) and (63). For the calculations, following molecular weights of the reactants were used: M_{DMAAm} = 99.13 g/mol; M_{VDMA} = 139.15 g/mol; M_{CTA} = 364.63 g/mol.

$$P_n(t) = \frac{[DMAAm]_t^{pol} + [VDMA]_t^{pol}}{[end\ groups]} = \frac{Conv(t) \cdot ([DMAAm]_0 + [VDMA]_0)}{[end\ groups]} \quad (59)$$

$$M_n(t) = P_n(t) \cdot \left(M_{DMAAm} \cdot X_{DMAAm}^{pol}(t) + M_{VDMA} \cdot X_{VDMA}^{pol}(t) \right) + M_{CTA} \quad (60)$$

$$[end\ groups] = \frac{\int triplet\ 0.82\ ppm}{3 \cdot \int total\ protons} \quad (61)$$

$$X_{DMAAm}^{pol}(t) = \frac{[DMAAm]_t^{pol}}{[DMAAm]_t^{pol} + [VDMA]_t^{pol}} \quad (62)$$

$$X_{VDMA}^{pol}(t) = \frac{[VDMA]_t^{pol}}{[DMAAm]_t^{pol} + [VDMA]_t^{pol}} \quad (63)$$

4.6.2.1 Co-monomer reactivities and co-polymer composition considerations

The results of the kinetic studies are shown on the Figure 59, A and Table 22. First, monomer concentration in logarithmic coordinates is linearly dependent on time for both comonomers, which demonstrates that the reaction in both cases proceeds with pseudo-first order kinetics typical for various RAFT systems.[352–354] The slopes of the dependences correspond to the apparent rate constants *k* according to the equation (64).

$$\ln\left(\frac{[M]_0}{[M]}\right) = kt \quad (64)$$

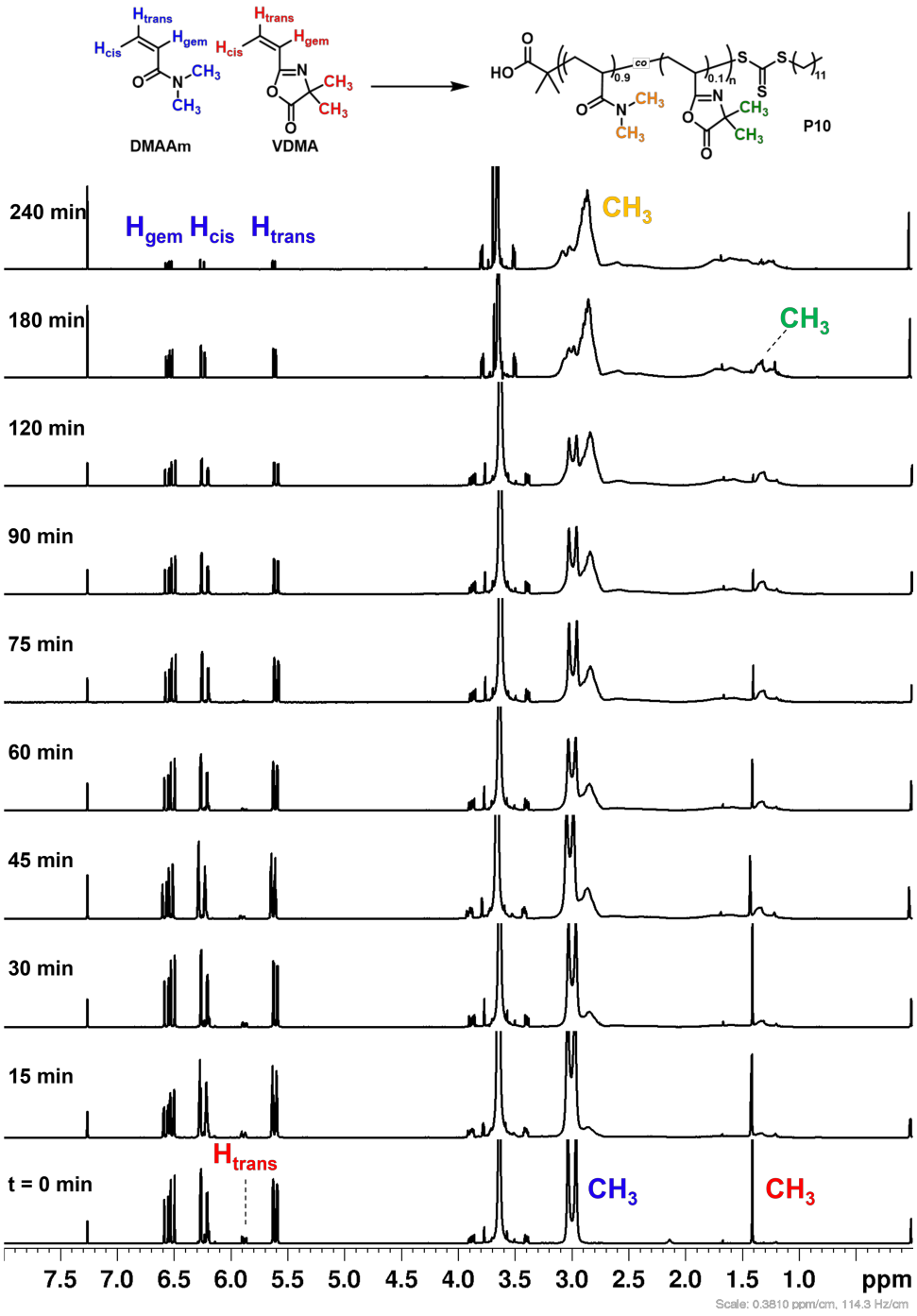

Figure 58. NMR spectra of the reaction mixture of DMAAm and VDMA in the course of RAFT copolymerization. The conversion of monomers is demonstrated by decrease of their signals' intensities over time.

where [M] and $[M]_0$ are current and initial monomer concentrations, k is the rate constant and t is time. The apparent constants obtained for each of the monomers are: k^{app} (DMAAm) = 0.75 h^{-1}, k^{app} (VDMA) = 1.51 h^{-1}, implying that VDMA in the given system (copolymerization with DMAAm in 1,4-dioxane) is twice as reactive as DMAAm. Further, by extrapolating the regression until $\ln([M]_0/[M]) = 0$ induction times t_{ind} of both monomers could be calculated. The kinetic plots show that the polymerization proceeds with a short induction period indicating a proper selection of CTA. It can be noticed that VDMA (t_{ind} = 5.9 min) starts to polymerize slightly earlier than

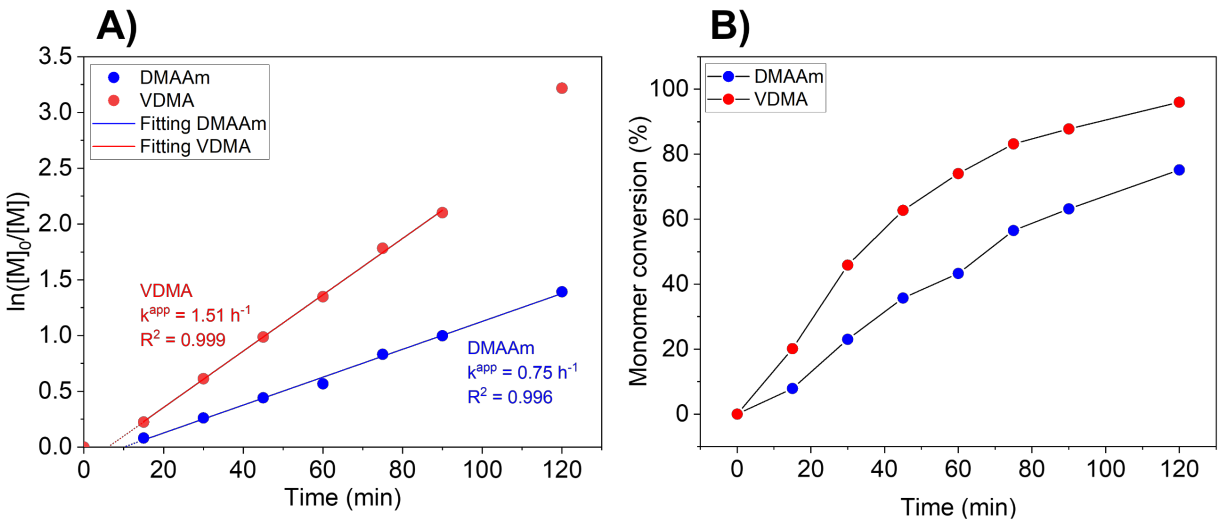

Figure 59. Kinetic studies of the RAFT copolymerization of DMAAm and VDMA as determined by NMR. A) Pseudo-first order kinetic plots of DMAAm and VDMA and linear fit of the kinetic curves; B) Monomer conversion vs. time.

DMAAm (t_{ind} = 9.8 min), which suggests that during the initial period of the reaction of copolymerization azlactone homopolymer is formed. Seeming growth in reaction rate of VDMA at high conversions can be attributed to the increasing error in the NMR peak integration as peak intensities become too low.

Table 22. Apparent rate constants and induction times of DMAAm-VDMA copolymerization.

Monomer	k^{app}, h^{-1}	t_{ind}, **min**
DMAAm	0.75	9.8
VDMA	1.51	5.9

Since VDMA is approximately 2 times more reactive than DMAAm, it is also the reason behind it reaching 95 % conversion in under 2 hours, whereas DMAAm only reaches ~75 % conversion (Figure 59, B).

Because of the different reactivities, the comonomer distribution within the polymer chains has a gradient, rather than statistical, character. In the beginning of the reaction the VDMA content in the chains is higher than DMAAm by almost 100 % (at 60 min mark), then the content decreases gradually until 120 min mark after which practically only DMAAm contribute to the polymer chain. After 4 h the VDMA is completely consumed and conversion of DMAAm exceeded 96 % (Figure 58), whereas after 15 h it was higher than 99.5 %.

If the conversion is plotted against number-average molecular weight (Figure 60), it can be noticed that the M_n determined by two different methods (GPC and NMR spectroscopy) exhibits linear increase with increasing conversion indicating that the polymerization proceeds under controlled conditions.[352,353,355] However, the evolution of the M_n shows negative deviation from the

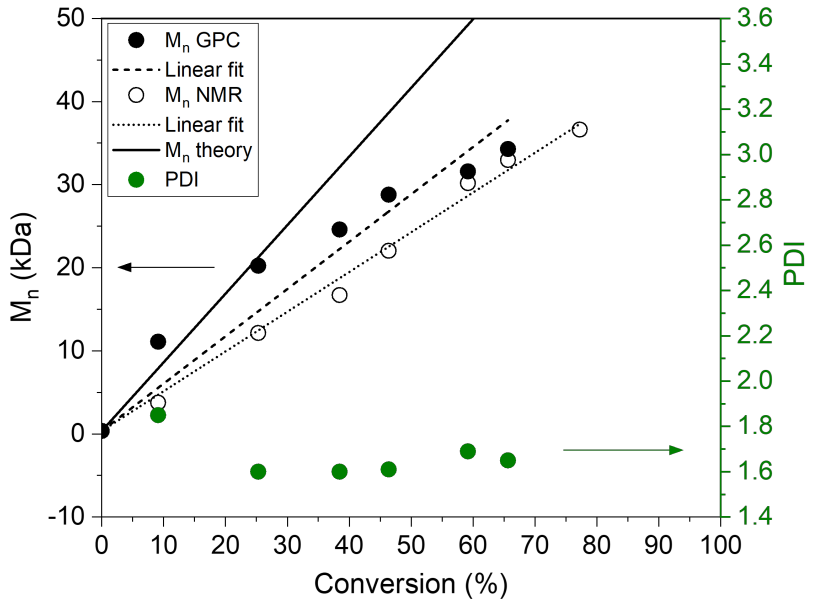

Figure 60. The evolution of molecular weight and the polydispersity of the polymer in the course of the reaction.

theoretical values at a given conversion. The reason for the deviation in the GPC results is arguably the standard used for calibration (PMMA), which does not structurally resemble the investigated polymer. Furthermore, error arising from the NMR peaks integration is increasing since the intensity of the peaks of end groups as well as monomer peaks is drastically reduced with an increasing conversion, hence the deviation of the M_n calculated using NMR spectra (equation (65)).

4.6.2.2 Polydispersity considerations

In a polymerization under controlled conditions, the PDI stays on a constant low level or slightly decreases in the course of the reaction.[159,356] In case of the investigated polymerization, the PDI of the copolymer drops within the first 30 min, further remaining at the value of ~1.65 (Figure 60), which is relatively high for controlled radical polymerization and can signal the occurrence of chain terminations, especially at early stages of the reaction.[357]

Two main reasons are accounted for this high value. Firstly, the ratio between monomer and CTA amounts are relatively high (800:1), and diffusion starts to be an important rate-determining factor at high conversions. Secondly, this anomaly may be caused by the GPC conditions, namely, an inappropriate selection of elution conditions with the solvent and/or stationary phase interacting with polymer's functional groups.

It was originally supposed that the use of two different monomers could be the source for the high PDI, however, a homopolymerization of DMAAm in the same conditions provided in a product with polydispersity of 1.88 (as determined in HFIP with PMMA standard), whereas elution in THF

resulted in too low peak intensities so that the M_n values were not reproducible (Table 23). When DMAc was used as an eluent, the PDI of PDMAAm amounted to 1.39 at M_n = 43800, which is significantly lower, proving the elution conditions might be the source of the high polydispersity. Nevertheless, since the main objective of utilizing RAFT was to achieve a uniform monomer distribution, and the polymers are aimed for further modification and gelation, the non-ideal parameters (molecular weight distribution) were not optimized further.

Table 23. Molecular weight and polydispersity of the PDMAAm obtained by GPC with different elution conditions

GPC elution conditions		**M_n, Da**	**PDI**
Eluent	Standard		
HFIP	PMMA	46500 ±1600	1.88 ± 0.02
THF	PMMA	7200 ± 2900	1.73 ± 0.15
THF	PS	11400	1.53
DMAc	PS	43800	1.39

4.6.3 Poly(DMAAm-co-VDMA) molecular weight and its distribution after the completion of polymerization

The molecular weight of the co-polymer P10 determined by GPC in HFIP using PMMA calibration and BHT as an internal standard as well as by NMR spectroscopy in $CHCl_3$ after 15 h is presented in Table 24. Notably, the PDI is (compared to the kinetic studies) further increased up to 1.82, which can be explained by the occurrence of termination processes at high conversions.[354] In addition, the ratio between the comonomers was also calculated using ^{1}H NMR (conversion after 15 h): n(DMAAm):n(VDMA) = 8.96:1.04. For the determination of M_n by ^{1}H NMR an integral of a triplet around 0.8 ppm corresponding to the polymer end group (CH_3 group of the DMP dodecyl chain) was set to 3, therefore, an integral of the area of the tertiary backbone protons (2.62–1.97 ppm) was equal to the P_n of the polymer. M_n was calculated according to the equation (65), where $\langle M_{mon} \rangle$ is an average molecular weight of monomers in the copolymer as defined in equation (66).

$$M_n = \left[\int (2.62 - 1.97\ ppm)\right] \cdot \langle M_{mon} \rangle + M_{DMP} \tag{65}$$

$$\langle M_{mon} \rangle = 0.896 \cdot M_{DMAAm} + 0.104 \cdot M_{VDMA} = 103.3\ {}^{g}/_{mol} \tag{66}$$

Table 24. Chemical composition and molecular weight of P10

[DMAAm], %	[VDMA], %	M_n (NMR), g/mol	M_n (GPC), g/mol	M_w (GPC), g/mol	PDI
89.6	10.4	60800	46500	84700	1.82

4.7 Polymer modification

The polymer P10 was "click"-modified using hexylamine-functionalized guest moieties: THA with a terminal 1,2,4-triazole group and TAHA with a trimethylammonium as a terminal group (for the structures of the guest moieties see Scheme 9). The reactions were conducted in DMF in the presence of DBU for the initial deprotonation of guest moieties, which could be observed by dissolution of the solids in DMF upon DBU addition. Both guest polymers were obtained in two versions: with (denoted P10THAP and P10TAHAP) and without DMIEA (denoted P10THA and P10TAHA) as a photo-crosslinker. Since VDMA moieties can undergo a ring opening as a result of a nucleophilic attack, interaction of VDMA with water according to Scheme 10 results in an acid formation. Since pendant carboxylic acid groups would add an unnecessary ionic interaction into the system and thus can disturb the targeted concept, the unreacted VDMA rings were opened using ethanolamine. The polymers were characterized by ^{1}H NMR and GPC in HFIP (Table 25).

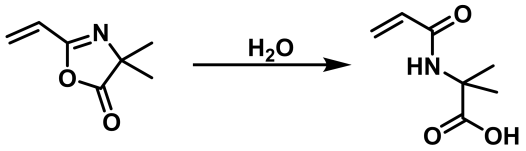

Scheme 10. Hydrolysis of the VDMA moiety.

Table 25. Molecular mass parameters and a composition of the guest polymers.

Polymer	Mole fraction of a moiety in the polymer chain				Mn, Da**	PDI**
	DMAAm, %*	Guest, %*		DMIEA, %*		
P10THA	90	THA	7.5	–	57500	1.70
P10THAP	90	THA	4.1	3.3	59800	2.04
P10TAHA	90	TAHA	6.2	–	61900	1.78
P10TAHAP	90	TAHA	6.4	3.0	66900	2.83

*Determined by NMR spectroscopy

**Determined by GPC (HFIP, PMMA calibration)

The pendant groups' content was determined by NMR spectroscopy (Figure 61) and calculated in a relation to the DMAAm or polymer backbone using formulas (53)–(55):

$$X_{THA}(\%) = \frac{\int(THA, 8.5\ ppm) \cdot 90\%}{{}^{1}/_{6} \cdot \int(DMAAm, 3.2 - 2.8\ ppm)} \tag{67}$$

$$X_{TAHA}(\%) = \frac{{}^{1}/_{9} \cdot \int(TAHA, 3.4\ ppm\ ) \cdot 100\%}{\int(backbone, 2.85 - 2.35\ ppm)} \tag{68}$$

$$X_{DMIEA}(\%) = \frac{{}^{1}/_{6}\ \int(DMIEA, 1.9\ ppm) \cdot 90\%}{{}^{1}/_{6} \cdot \int(DMAAm, 3.2 - 2.8\ ppm)} \tag{69}$$

For the calculation of THA groups an integral of the H3 proton of the triazole moiety was considered; in case of TAHA – the signal belonging to the methyl groups' protons (marked with

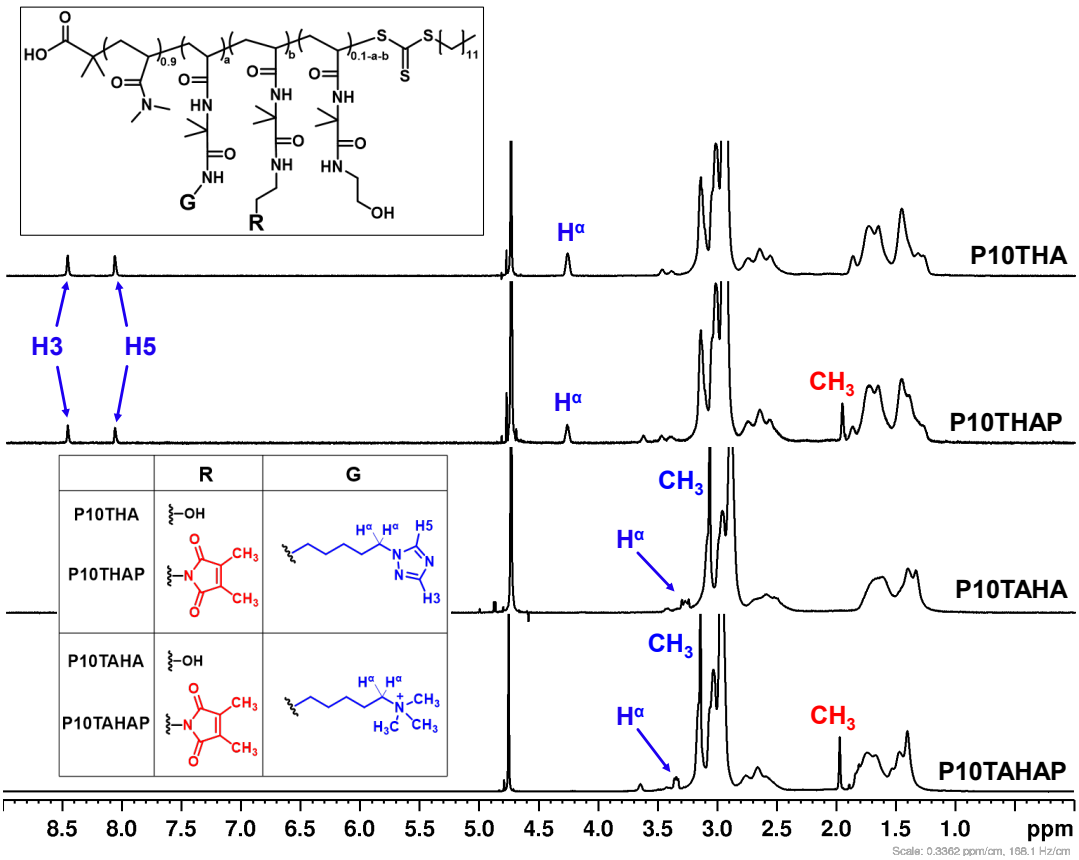

Figure 61. ^{1}H NMR spectra (D_2O) of the synthesized guest polymers: (from the top to the bottom) P10THA, P10THAP, P10TAHA, and P10TAHAP. Characteristic peaks of the functional groups are marked. Blue color corresponds to the guest moiety groups, red color – to the photo-crosslinker.

blue CH_3 symbol); for DMIEA – the signal of 2 methyl groups adjacent to the double bond (red CH_3 symbol).

Concerning GPC results, it can be noticed that the TAHA-modified polymers have higher M_n possibly due to the electrostatic repulsion by positively charged groups, which increases the hydrodynamic radius of the polymer coils. As a result, the TAHA-modified polymers are eluded faster, and a higher molecular weight is detected. Noticeably, the PDI of P10THA and P10TAHA (1.70 and 1.78, respectively) are lower than that of the unmodified polymer P10 (1.82), which is considered to be due to the dialysis as a purification step. At the same time, partial dimerization of DMIEA moieties in the samples modified with the photo-crosslinker are accounted for the increased polydispersities (2.04 and 2.83 for P10THAP and P10TAHAP, respectively).

4.8 Investigations of the interactions in the system guest polymer–WSP5A–SP

4.8.1 NMR studies

Because THA-Boc is not water-soluble, which restrains the possibilities to quantify the binding affinity using low-molecular host and guest, as a proof of the sensor concept the interaction between P10THA, which is soluble in water, and WSP5A was investigated qualitatively by NMR. Figure 62 shows that the triazolyl proton by 8.49 ppm broadens (blue arrows) upon the addition

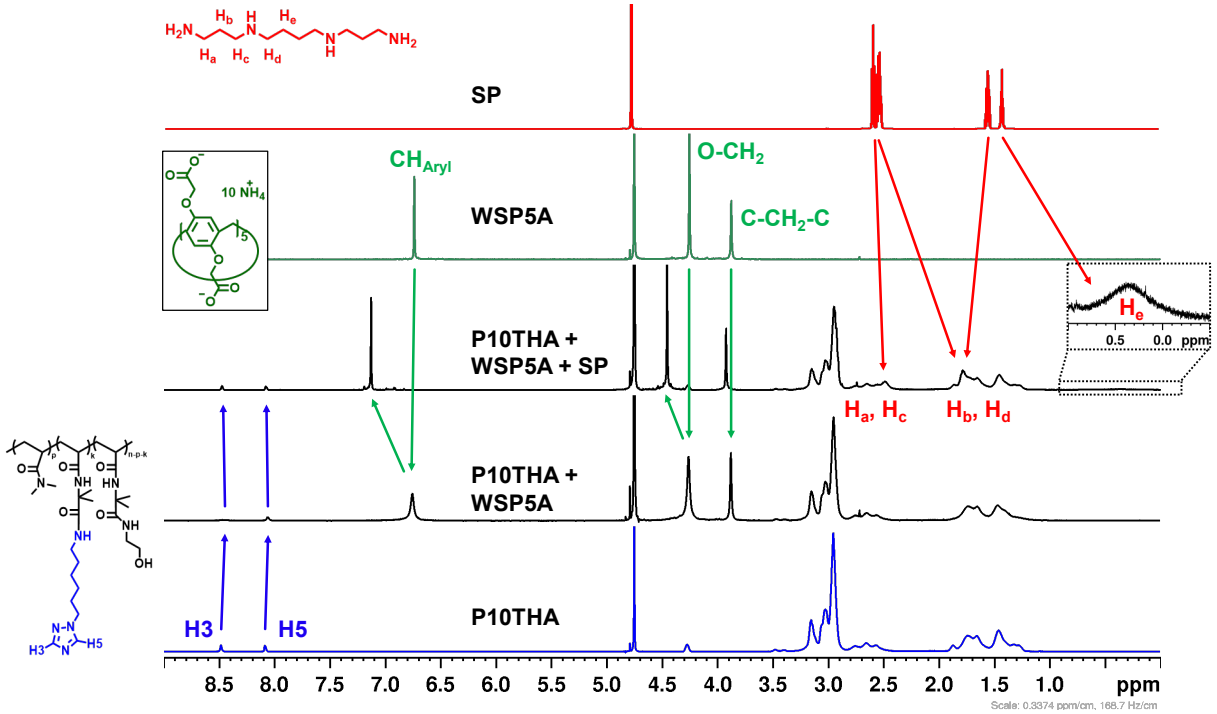

Figure 62. ^1H NMR (D_2O) spectra of (from the bottom to the top): P10THA, P10THA+WSP5A, P10THA+WSP5A+SP, WSP5A and SP. Blue arrows show the change of the peaks of the THA moiety, green arrows follow the peaks of the WSP5A, and the red arrows show the change of SP peak shifts.

of 1 eq. WSP5A and becomes sharp again after the addition of the SP. The peaks of WSP5A undergo a strong downfield shift (6.76 to 7.13 ppm and 4.26 to 4.46 ppm) in the presence of 1 eq. SP, in accordance with the WSP5A–SP NMR titration results. This behavior can be interpreted in the way that a relatively weak interaction occurring between WSP5A and P10THA is disrupted by SP due to a much stronger interaction between WSP5A and SP, which proves the concept underlying the detection principle.

The same procedure was utilized to assess the interaction between WSP5A and P10TAHA (Figure 63). In this instance, complex formation leads to a pronounced change in the chemical shift of both guest polymer and host molecule. In particular, the signals of the quaternary ammonium's CH_3 groups as well the methylene group in α-position experience significant broadening, which leads to the disappearance of the peaks in the spectrum of P10TAHA@WSP5A. The WSP5A signals, at the same time, slightly shift downfield indicating formation of an inclusion complex. The shift is significantly increased upon addition of SP4HCl to the system, and the signals of the TAHA moiety return to the positions, corresponding to the free species, demonstrating release of the quaternary ammonium groups from the WSP5A cavity.

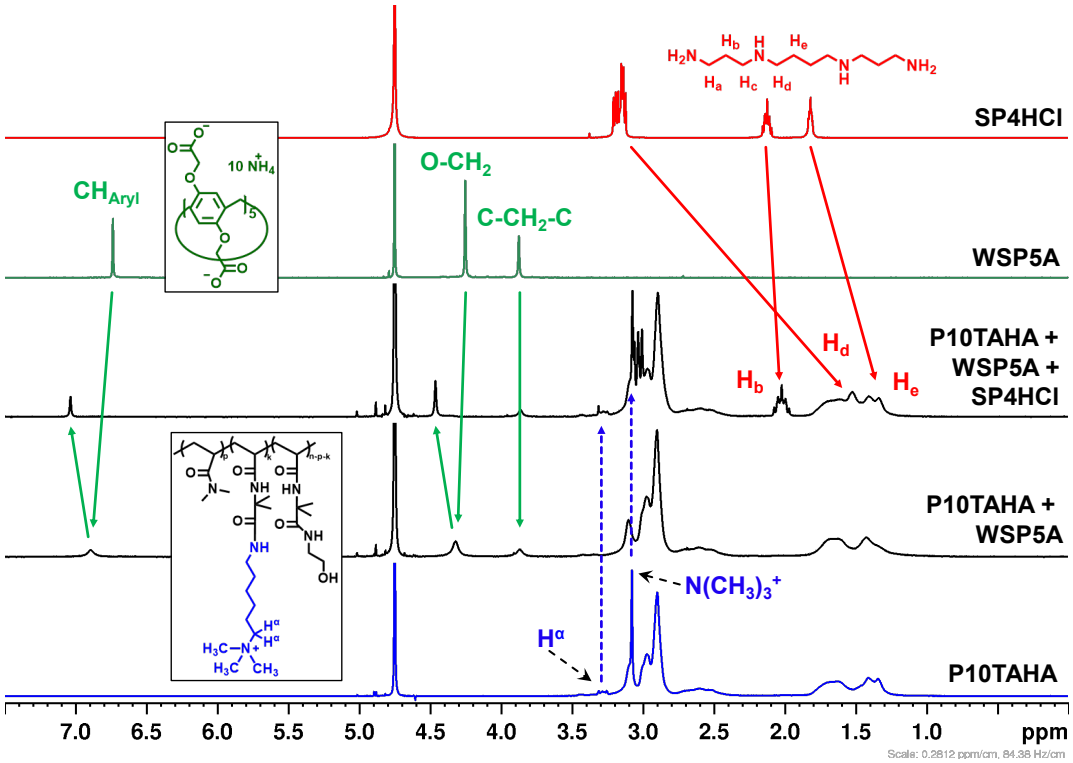

Figure 63. ^{1}H NMR (D_2O) spectra of (from the bottom to the top): P10TAHA, P10TAHA+WSP5A, P10TAHA+WSP5A+SP4HCl, WSP5A and SP4HCl. Blue arrows show the change of the peaks of the TAHA moiety, green arrows follow the peaks of the WSP5A, and the red arrows show the change of SP peak shifts.

4.8.2 ITC investigation

In order to quantitatively assess the binding affinity between THA moieties and WSP5A and, in case of TAHA, prove the results obtained with low-molecular compounds, an ITC study was carried out using P10THA and P10TAHA as guest species in MOPS buffer solution. (The study was conducted by Prof. Dr. Schönhoff's lab in WWU Münster.) The results of the analysis are presented in Figure 64 and Table 26.

Regrettably, the data obtained using a single set of equal binding sites model cannot be clearly interpreted. The obtained stoichiometry values (n = 4 and 5, respectively) suggest that 4 or 5 guest moieties per WSP5A macrocycle are required to completely saturate the host moieties. This discrepancy is rather too large to explain it by an error in sample preparation. Since the concentration for guest samples correspond to the concentration of pendant THA and TAHA groups, a plausible clarification might be given by taking the determination of guest groups content in polymers into account. The number of the groups was defined by NMR spectroscopy, and for a precise quantification it is necessary to evaluate the peaks with best possible resolution. In case of P10THA it is not a problem since the peaks of triazole protons appear separately between 8.0 and 8.5 ppm in D_2O. On the other hand, the peak corresponding to the adjacent methyl groups of the

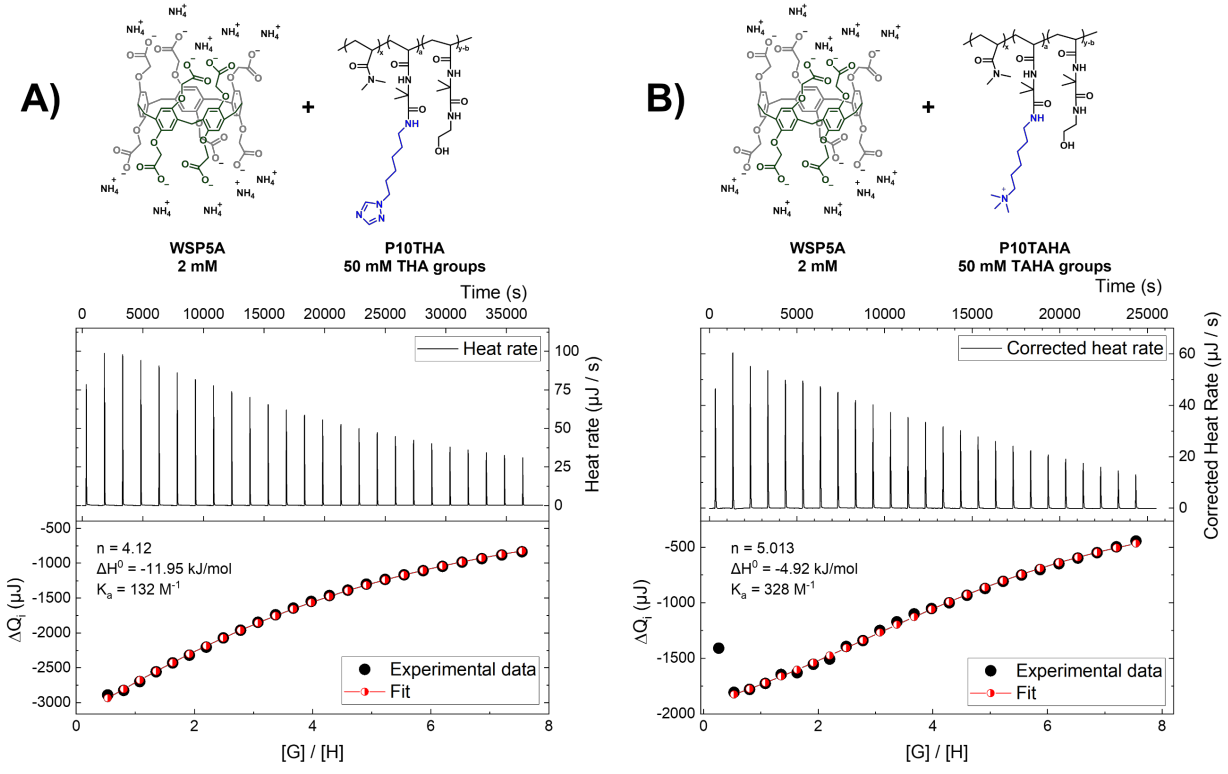

Figure 64. ITC results of WSP5A solution (2 mM in MOPS) titrated with guest polymers (see schemes on top). Graphs top: raw heat rate corrected with blank titration results; bottom: integral heat after each consecutive addition of a titrant. A) Titration with P10THA (50 mM THA groups) in MOPS; B) with P10TAHA (50 mM TAHA groups) in MOPS.

quaternary amine of TAHA is located within an area of methyl groups' peaks of DMAAm in D_2O, hence, a spectrum in $CDCl_3$ was used for determination of the TAHA groups. Another possible explanation for a deviating stoichiometry could be not complete solubility of the polymer moieties,[309] which, however, is only applicable to P10THA.

Table 26. Thermodynamic parameters of the systems WSP5A–P10THA and WSP5A–P10TAHA in MOPS buffer obtained by ITC at 298.15 K. ΔG° and ΔS° are calculated according to equations (2) and (33).

System	K_a, M^{-1}	ΔH°, kJ/mol	ΔG°, kJ/mol	ΔS°, J/(mol·K)
WSP5A–P10THA/MOPS	132	−11.95	−12.10	+0.5
WSP5A–P10TAHA/MOPS	328	−4.92	−14.36	+32

It is also important to mention that such a high stoichiometry can be also a result of intermolecular interactions in the solution. Since THA and TAHA groups are not completely free from each other but bound together as pendant groups of the same polymer chains, it is conceivable that as soon as WSP5A is bound to one of the guest groups, neighboring groups get affined to the macrocycle (in a form of an inclusion complex or from the outer side of the WSP5A, as was demonstrated for the interaction between WSP5A and TAHA moieties in Ref. [218]) or get excluded from further interactions by conformational changes of the polymer chain.

In addition, the association constant values observed from the data indirectly support the supposition that WSP5A forms more stable complexes with TAHA than with THA because the K_a value of the interaction with P10TAHA is 2.5 times higher (328 M^{-1} *vs.* 132 M^{-1}). However, it is debatable if these values can be compared or even taken into consideration at all since, in fact, such complicated equilibria as 4:1 or 5:1 are highly unlikely to occur as single process but rather a product of stepwise or cooperative reactions[358] requiring deeper analysis, which is out of scope of the current work.

Remarkable is furthermore the calculated entropy for each system. Comparing the ΔS values obtained for WSP5A titration with TAHA-Boc and with TAHA-containing polymer P10TAHA a large difference can be observed (−3.3 *vs.* +32 J/(mol·K)) suggesting another contribution in the case of polymer. This contribution might be the entropy of dilution, which might be more substantial in case of the charged P10TAHA than neutral P10THA (ΔS = +0.5 J/(mol·K)).

Despite the stoichiometry of the interactions between WSP5A and guest polymers determined by ITC being significantly higher than projected (n = 4 and 5 for experiments with P10THA and P10TAHA, respectively), the results proved qualitatively the presence of interactions between the participating species.

All things considered, according to the results of the NMR studies, even though the interaction between P10THA and WSP5A is comparatively weak, it can be concluded that the behavior of both systems aligns with the concept of the project. ITC results could only confirm that in both cases there is an interaction taking place between guest polymers and the WSP5A macrocycle. Hence, both guest polymers were used further for the fabrication of a gel sensor.

4.9 Responsiveness of sensor chips

4.9.1 Sample preparation. Spin-coating parameters

4.9.1.1 Parameters influencing the coated layers

According to the design of a sensor chip for the SPR technique, the polymer should be applied onto a substrate as a thin layer. The most effective method for obtaining polymeric thin layers is spin-coating, in which a polymer solution is delivered onto a rotating surface. Due to the centrifugal force, the solution is driven to the edges of the surface leading to a spreading of the solution around the whole surface area. In the course of further spinning, the system switches to an evaporation regime, where the excess of the used solvent evaporates leaving a thin layer of a substance.[359] The thickness of the obtained layers depends on several parameters of the polymer solution:

- Nature of the solvent;
- Initial concentration;
- Solution density;
- Solution viscosity;
- Rotation frequency.

Within the framework of the current research, three of those parameters can be varied in a controlled manner: the solvent, solution concentration and the rotation speed. The choice of a solvent is dictated by solubility of the polymers as well as by its volatility since the evaporation rate has a direct impact on the homogeneity and overall quality of the coatings.[360] Increased concentration as well as decreased rotation rate leads to an increased layer thickness. It is worth mentioning that a change in concentration has a higher impact on the thickness than a change in rotation speed (relation (70), where d_0 is a layer thickness; C is a polymer solution concentration; ω is a rotation speed).[361]

$$d_0 \sim C \cdot (1 - C)^{-\frac{1}{3}} \cdot \omega^{-\frac{1}{2}} \quad (70)$$

4.9.1.2 Influence of the polymer solution concentration

Both P10THAP and P10TAHAP are soluble in common organic solvents including ethanol, *iso*-propanol, and acetone. For the convenience of handling, EtOH was used as a solvent for polymer solution preparation. 1 wt.% and 2 wt.% solutions were prepared for the initial evaluation of concentration dependence of the layer thickness. The polymers were dissolved in EtOH and stirred at RT in darkness for 4 h, then filtered through a Chromafil® 0.45 µm PTFE syringe filter immediately prior to spin-coating.

For spin-coating, the polymer solution (ca. 80 µL) was applied onto the wafer by static dispense method and coated with a two-step program:

1. 1800 rpm (10 s ramp) for 60 s;
2. 2000 rpm (10 s ramp) for 120 s.

After the completion of the coating process the sample was dried *in vacuo* overnight in dark to remove the rest of the solvent. Further, the polymer layer on the surface of the wafer was photo-crosslinked by UV-irradiation for 300 s. The crosslinked gel layer was measured by SPR (dry layer thickness) as it is.

The dependence of the polymer solution concentration on the layer thickness is demonstrated in Table 27. The increase of the gel thickness is different for P10THAP and P10TAHAP (increase by 1.5 and 3 times, respectively), which can be explained by the fact that for the 2 wt.% P10TAHAP sample *iso*-propanol was used as a solution instead of EtOH (see Chapter 4.9.3.1). Furthermore, a problem occurred while recording a spectrum of P10THAP-1% dry layer that the signal fell to 50 % of its normal intensity, which was later found out to be the detector's battery running low. Nevertheless, the general trend of layer thickness increase is observable.

Table 27. Thickness of spin-coated layers deposited from P10THAP and P10TAHAP solutions of different concentrations

Polymer/gel	Thickness, nm	
	1 wt.%	2 wt.%
P10THAP	97.9	142.4
P10TAHAP	67.3	197.0 ± 5.3*

*Polymer was deposited from *iso*-propanol solution at 0 °C, n = 3.

To further clarify the influence of the solution concentration, in Figure 65 the angular SPR spectra of sensor chips swollen in a MOPS buffer solution are shown, prepared *via* spin-coating from P10THAP solutions of two different concentrations: 1 wt.% (P10THAP-1%, black curve) and 2 wt.% (P10THAP-2%, red curve). The distinction in the gel layer thickness in a dry state is

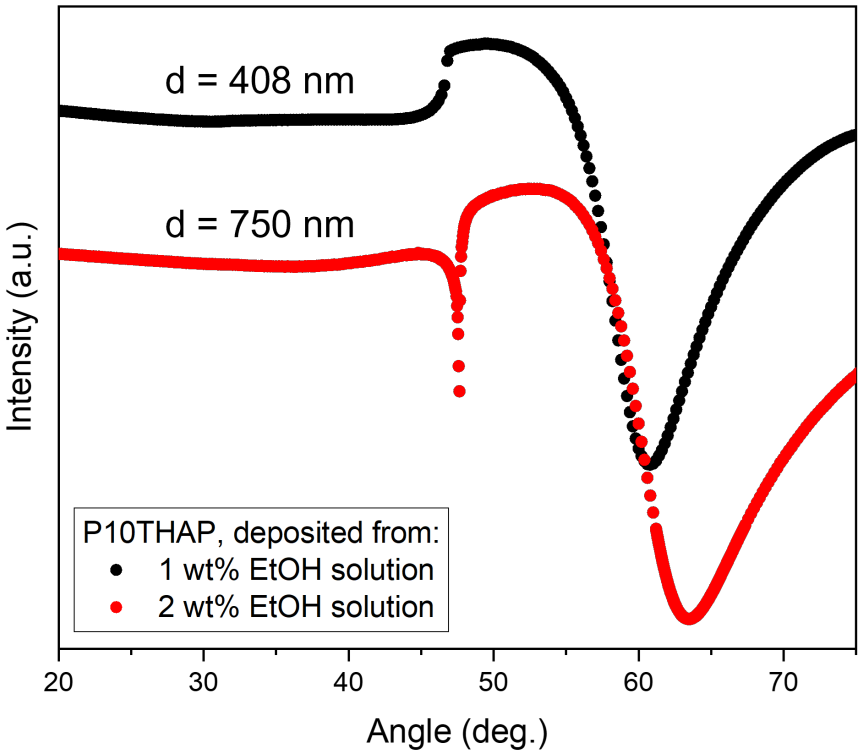

Figure 65. Comparison between two P10THAP sensor chips swollen in MOPS buffer solution: spin-coated from 1 wt.% (black curve) and 2 wt.% (red curve) EtOH solutions. An optical waveguide mode as a local minimum around 47° is clearly distinguishable for the chip prepared from the 2 wt.% solution.

magnified after swelling, leading to P10THAP-1% thickness reaching 408 nm *versus* 750 nm in case of P10THAP-2%. Therefore, on the spectrum of P10THAP-2% a new feature appears in the area around the total internal reflection angle (46–50°): an optical waveguide minimum. As discussed in Chapter 2.5, the presence of this minimum additionally to the plasmon resonance allows independent calculation of the layer thickness and refractive index,[268,314] therefore, significantly increasing the precision of the fit and of the method itself. Hence, 2 wt.% solutions were used further for spin-coating and subsequent analysis.

4.9.2 SPR investigation of P10THAP sensor chip

4.9.2.1 Experimental procedure

Onto a quartz wafer with an Au layer (44.46 nm) applied using PVD method, adhesion promoter was adsorbed *via* dip-coating and further a 2 wt.% P10THAP solution was spin-coated onto this pre-treated chip. After drying *in vacuo* overnight and cross-linking under UV-irradiation for 300 s, the spectrum of a dry gel was recorded, then the chip was equilibrated in MOPS buffer for 3 h in the SPR flow cell. The responsiveness of the chip towards SP of different concentrations was probed by a kinetic study at 61° angle (Figure 66). In this study, a gel was alternately treated with WSP5A solution (1 mM, 1.5 mL) and SP4HCl solutions (1 µM, 5 µM, 10 µM and 20 µM, 0.5 mL

per concentration). This concentration range was selected to cover the abovementioned (Chapter 4.1.1) range of SP concentrations in urine of cancer patients. Before each sample injection the cell was briefly washed with MOPS (0.5 mL) to remove unbound P5A macrocycles as well as to wash away the SP@WSP5A complex species before the next concentration cycle.

4.9.2.2 Kinetic study of the P10THAP chip's responsiveness

In Figure 66, A, a complete evolution of the signal intensity in the course of the kinetic study is presented. Noticeably, the signal intensity demonstrates a steady overall decrease trend, and intensity change upon the first cycle of WSP5A, MOPS and SP injections is more significant compared to the further injections (from the second WSP5A injection onwards). Possible reason

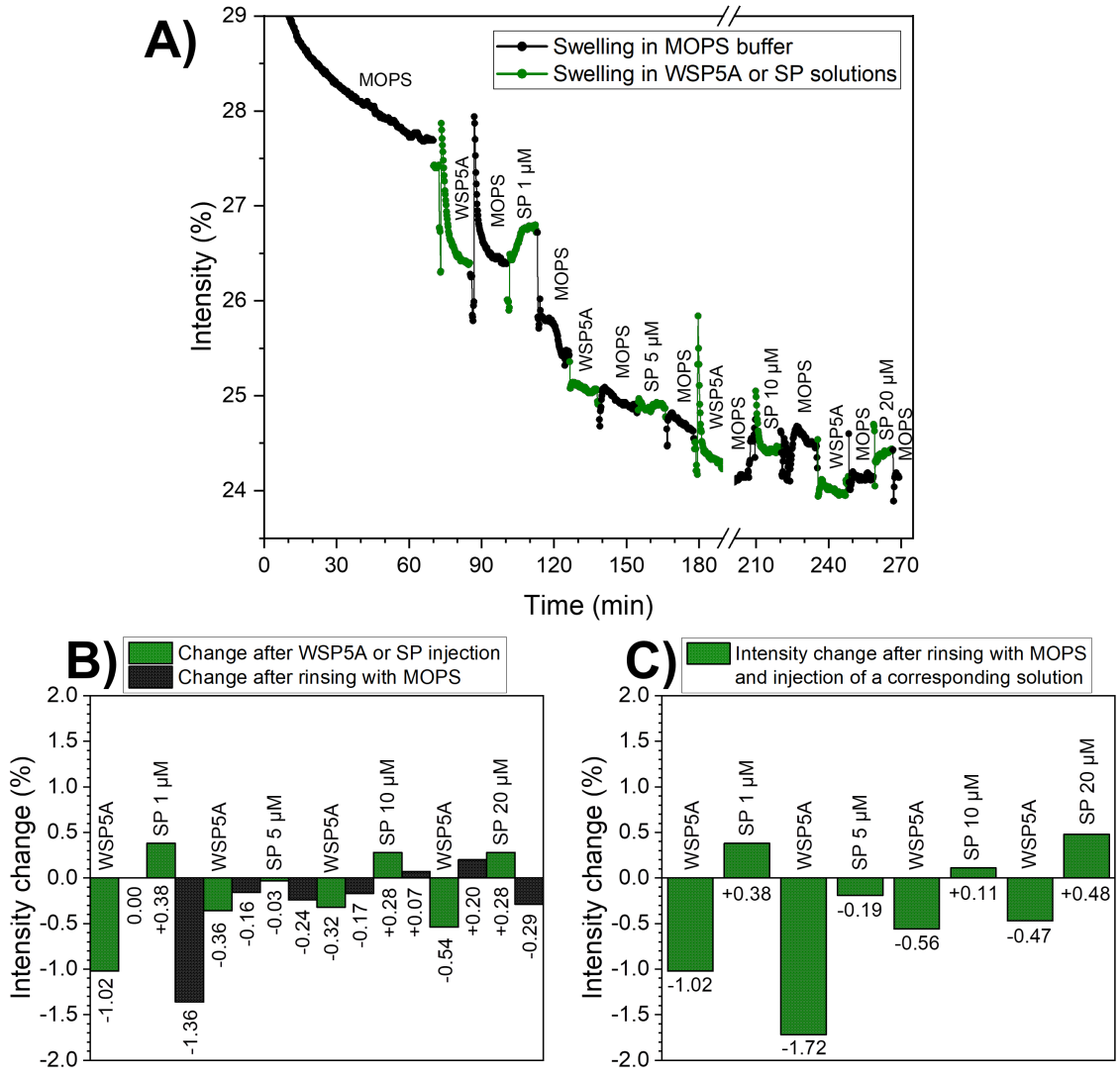

Figure 66. Kinetic studies of P10THAP-2% gel sensor. A) Evolution of signal intensity of a swollen gel upon injection of different solutions recorded at 61° angle. B) Intensity changes upon each injection. C) Intensity changes resulting after rinsing with MOPS are calculated together with the subsequent injection of a solution.

for this behavior might be an inaccessibility of the inner layers of the gel during initial swelling. During multiple exchange of the solution (which is accompanied by a solution flow through the cell upon injections) the inner chains can be reached and solvated leading to a decrease in the refractive index (and, therefore, observed intensity at 61°). On the other hand, at the first stages of the experiment, non-crosslinked chains can be washed out of the bulk of the gel as well. A relatively large drop at 110 min mark upon rinsing with MOPS is, however, out of trend and cannot be explained solely by a signal drift.

Despite a general tendency of decreasing intensity, it is possible to make a conclusion about the responsiveness by comparing the states of the gel equilibrated in different solutions. The intensity difference after each change of a solution is shown in Figure 66, B. Notably, each WSP5A injection leads to a decrease in the signal intensity, which conforms to the anticipated behavior of the system upon presence of the macrocycle – a negatively charged macrocycle is threaded onto neutral THA groups resulting in electrostatic repulsion between the chains, which, in turn, leads to a lower gel density, and thus, to a lower refractive index. An opposing tendency is observed upon spermine addition: the intensity rises suggesting an increasing refractive index, *i.e.*, a higher density of the gel layer as a result of a decreasing electrostatic repulsion, which is caused by WSP5A molecules beneficially binding to the SP axles and being washed out of the gel volume.

Nevertheless, the intensity change obtained upon injecting various concentration of SP is not consistent with the increase of the concentration. The injection of 1 μM SP solution resulted in a signal increase excessing both 10 and 20 μM solutions (+0.38 % *vs.* +0.28 %), whereas 5 μM solution injection surprisingly led to a slight decrease in intensity (–0.03 %). This inconsistency can as well be demonstrated if the intensity change resulted by rinsing with MOPS is combined with a change caused by an injection of WSP5A or SP solutions (Figure 66, C). Therefore, this preliminary result demonstrates that P10THAP gel shows insufficient responsiveness. Otherwise, it is worth noting that rinsing with MOPS did not bring any consistent changes (see Figure 66, B), which might be an indirect proof of the stability of the system's threaded and unthreaded states.

4.9.2.3 SP concentration dependencies of layer thickness and refractive index of P10THAP films

A deeper insight into the responsive behavior of the gel can be delivered by analyzing the actual layer thickness and refractive index change. For the investigated sensor system these parameters were obtained by fitting the angular spectra, recorded after each equilibration in a WSP5A or SP solution (Figure 67). The fitting using Fresnel equations was performed in Winspall 3.02 (MPI für Polymerforschung Mainz). For the fits, a 2-layered model was applied in which the inner layer thickness d^{in} was set at 200 nm and its refractive index n_d^{in} was iteratively varied to match the

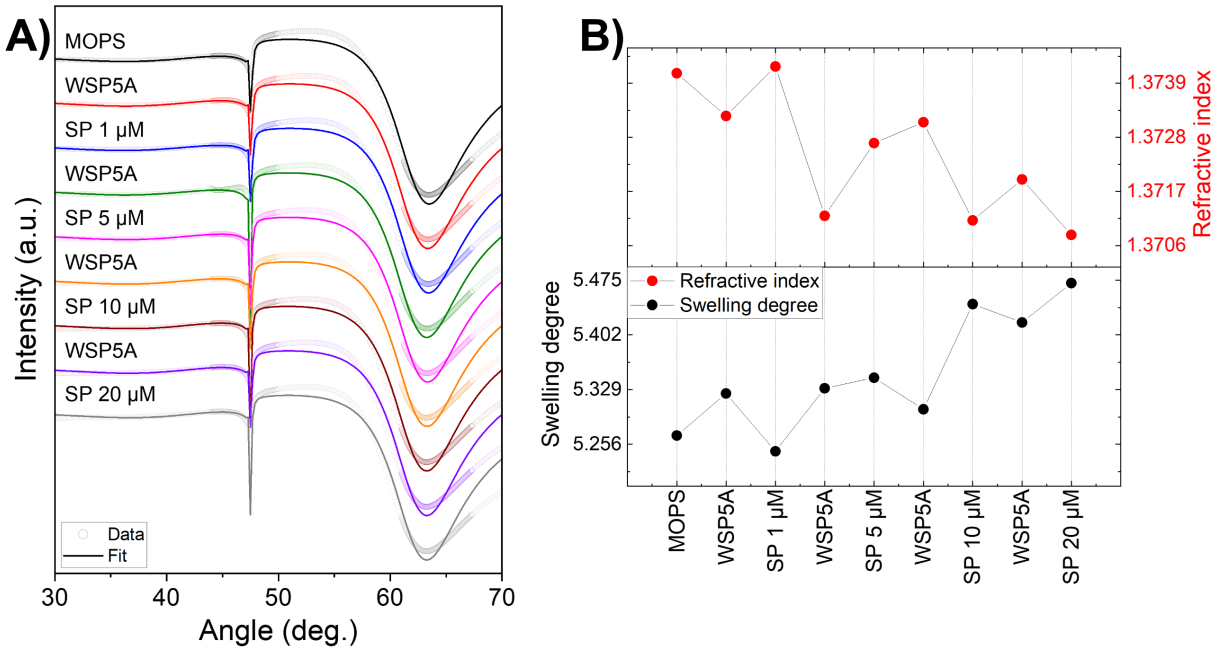

Figure 67. A) Angular spectra of P10THAP-2% after equilibration in corresponding solutions. The curves represent fitting of experimental data. B) Evolution of refractive index (on top) and swelling degree of the P10THAP gel equilibrated in different solutions.

plasmon minimum. For the outer layer d^{out} and n_d^{out} were varied manually to match the minimum of a waveguide mode. The resulting fits for P10THAP swollen in different solutions are presented in Figure 67, A) as solid lines. To characterize the polymeric gel as a whole and to trace the transformation dependent on the medium the parameters (swelling degree, Q, and average refractive index, n_d^{gel}) were calculated according to the equations (71) and (72).

The obtained data is plotted in Figure 67, B, the values of layer thickness as well as RI of the gel in different mediums are summarized in Table 28. It can be noticed that, similar to the results of the experiment in the kinetic mode, the data is not consistent and the change of the layer thickness/refractive index cannot be unambiguously explained by threading and dethreading of WSP5A units onto/from the pendant guest groups of the polymer. Furthermore, it is worth mentioning that since in a 2-layer model the plasmon minimum is mostly determined by the inner layer, and for the kinetic investigation a single layer model was assumed, the results of two analysis approaches are not harmonized. Still, this can be regarded as a further confirmation of a poor responsivity of the P10THAP gel sensor towards WSP5A and SP.

Table 28. Layer thicknesses and RI values obtained for P10THAP sensor chip in different media by fitting the angular SPR spectra. Graphical representation is shown in Figure 67.

Medium	Inner layer		Outer layer	
	d, nm	n_d	d, nm	n_d
MOPS	200	1.3853	550	1.3700
WSP5A	200	1.3842	558	1.3693
SP 1 µM	200	1.3847	547	1.3704
WSP5A	200	1.3837	559	1.3667
SP 5 µM	200	1.3842	561	1.3686
WSP5A	200	1.3837	555	1.3693
SP 10 µM	200	1.3837	575	1.3667
WSP5A	200	1.3837	572	1.3678
SP 20 µM	200	1.3837	579	1.3664

4.9.3 SPR investigation of P10TAHAP sensor chip

The responsiveness tests conducted using NMR spectroscopy have demonstrated that the interaction between the three species proceeds according to the desired scenario and the states of unbound guest, TAHA@WSP5A and SP@WSP5A+TAHA are clearly distinguishable, which implies a considerable affinity between them. Therefore, it was supposed that these host-guest interactions would have a significant impact on the states of the gel in the form of a sensor chip, *i.e.*, on its responsiveness.

4.9.3.1 Suppression of Marangoni instabilities

For SPR measurements, P10TAHAP polymer was spin-coated from a 2 wt.% solution in *iso*-propanol. The problem appeared while spin-coating, that the film obtained by this method exhibited high roughness in a form of Marangoni defects. The defects emerged in ethanol as well as in *iso*-propanol solutions. According to Fowler, et al.[362], the roughness of the film depends on the interplay between two processes: 1) spreading of the solution with eventual flattening of the surface, and 2) solvent evaporation causing solidification of the film. If the evaporation rate is too high, the film might not have sufficient time to level itself, thus, increasing its roughness. Therefore, Marangoni instabilities are provoked by surface tension gradient resulting from solvent evaporation which is associated with concentration as well as temperature gradients. The solution for getting uniform surfaces suggested by the authors was spin-coating at low temperatures, which decreases the evaporation rate and the temperature gradient within the film layer. In their work, authors demonstrated how cooling down the chamber improves the homogeneity of polystyrene films. Replacing ethanol with *iso*-propanol was the initial step in attempt to reduce the evaporation rate. Because of the limitations of the spin-coater used in this work, it was not possible to conduct

spin-coating at 0 °C by cooling down the chamber, therefore, the polymer solution was placed in an ice bath for 15 min immediately before deposition.

Figure 68 demonstrates the microscopic images of P10TAHAP films dispensed at room temperature and after preliminary cooling (at 0 °C). Comparing the structures appearing in the polymer films spin-coated at room temperature (Figure 68, A and B) and at 0 °C (Figure 68, C and D), a significant improvement of the film uniformity can be observed: both the defect wavelength and amplitude (which can be estimated by the contrast between lighter and darker regions) decrease drastically offering flattened layers. Therefore, the polymer solutions were further deposited at cooling.

4.9.3.2 Experimental procedure

Similar to the procedure described above for P10THAP chip, the P10TAHAP sensor chip was prepared by spin-coating the P10TAHAP polymer from a 2 wt.% solution on a pre-treated N-LaSF9 wafer bearing an Au layer. Prior to the measurements, the chip was equilibrated in MOPS buffer solution purged through a flow cell of the SPR sample holder, for 1–3 h. The equilibration was monitored by an SPR signal intensity measured in the kinetic mode at 61°. Further, 1 mM WSP5A solution was injected followed by rinsing with MOPS and, subsequently, SP solution

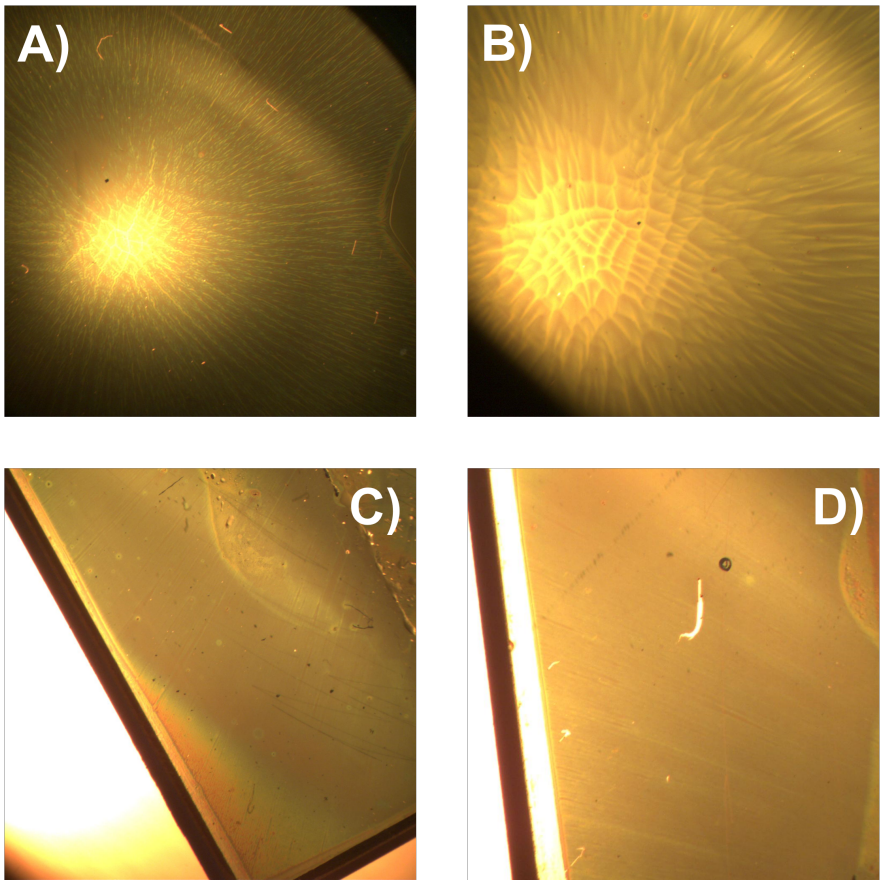

Figure 68. Microscopic images of the film layers deposited from the 2 wt.% P10TAHAP solution in iso-propanol. A) and B) deposition at room temperature; C) and D) deposition at 0 °C.

injection was performed to evaluate the responsiveness of the gel. Before the next measurement cycle, the cell was rinsed with MOPS once again to remove the formed complexes from the gel volume as well as from the medium.

4.9.3.3 Kinetic studies of the P10TAHAP chip's responsiveness

The complete kinetic investigation is presented in Figure 69. Firstly, as in case of P10THAP it is noticeable that the intensity of the light reaching the detector is decreasing in the course of the experiment presumably because of the advancing equilibration of the inner layers of the gel volume under repeating cycles of purging/swelling in different mediums (similarly to the case of P10THAP described in the Chapter 4.9.2.2). Nevertheless, the changes after individual injections reveal certain patterns. Firstly, each WSP5A injection leads to an increase in signal intensity (however, by a different increment between 1 and 2.8 %), *i.e.*, in the gel density. This increase is due to the macrocycles incorporating into the gel structure by forming the inclusion complexes with pendant TAHA groups (since the polymer strands are already charged, the WSP5A binding does not contribute to the electrostatic attraction/repulsion between the chains but to the gel mass) as well as accommodating them on the outside of the macrocycles by electrostatic interactions, which leads to WSP5A acting as a supramolecular crosslinker.[218] Secondly, the subsequent rinsing with MOPS causes a drop in intensity, albeit very unsystematic in magnitude, which might be associated with the abovementioned gradual equilibration of the gel. Thirdly, the injections of the SP solutions led consistently to the intensity decrease, however, without significant difference in the value for 1, 5 and 10 µM (0.7–1.1 %). The 20 µM SP sample shows a more pronounced reduction of intensity (3.2 %), which is particularly interesting given that the rinse with MOPS

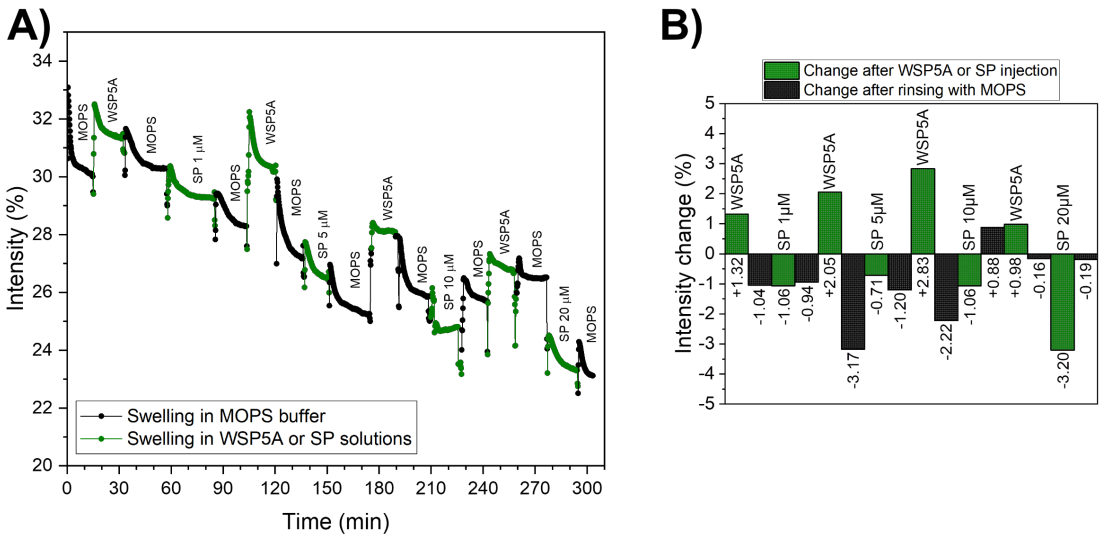

Figure 69. Kinetic studies of P10TAHAP-2% gel sensor. A) Evolution of signal intensity of a swollen gel upon injection of different solutions recorded at 61° angle. B) Intensity changes upon each injection.

one step earlier had only a negligible effect on the gel implying that the system was approaching the "overall" equilibrated state.

4.9.3.4 SP concentration dependencies of layer thickness and refractive index of P10TAHAP films

For each equilibrated state of the gel sensor (WSP5A or SP) an angular scan spectrum was recorded in order to analyze how the processes occurring between the host and guest moieties as well as the analyte in the volume affect the swelling behavior and density of the system. A 2-layer fitting based on Fresnel equations was conducted on the P10TAHAP system similar to the procedure discussed before for the P10THAP sensor. The angular scans with fits and corresponding *Q* and RI values for the gel sensor after each WSP5A or SP injection are shown in Figure 70 and the results obtained from the fitting in Table 29. It is important to point out the regular manner with which the gel shrinks in the WSP5A solution and swells back after injections of the SP solutions. As indicated for the kinetic study, the impact of the analyte of concentration between 1 and 10 µM is almost identical and minimal in magnitude suggesting that the main reason for the change in the parameters of the gel was flushing off the unbound host molecules due to the equilibrium nature of the host-guest complexation. Overall, it may be concluded that despite the P10TAHAP sensor chip being more promising that the P10THAP system, it also appears not to be

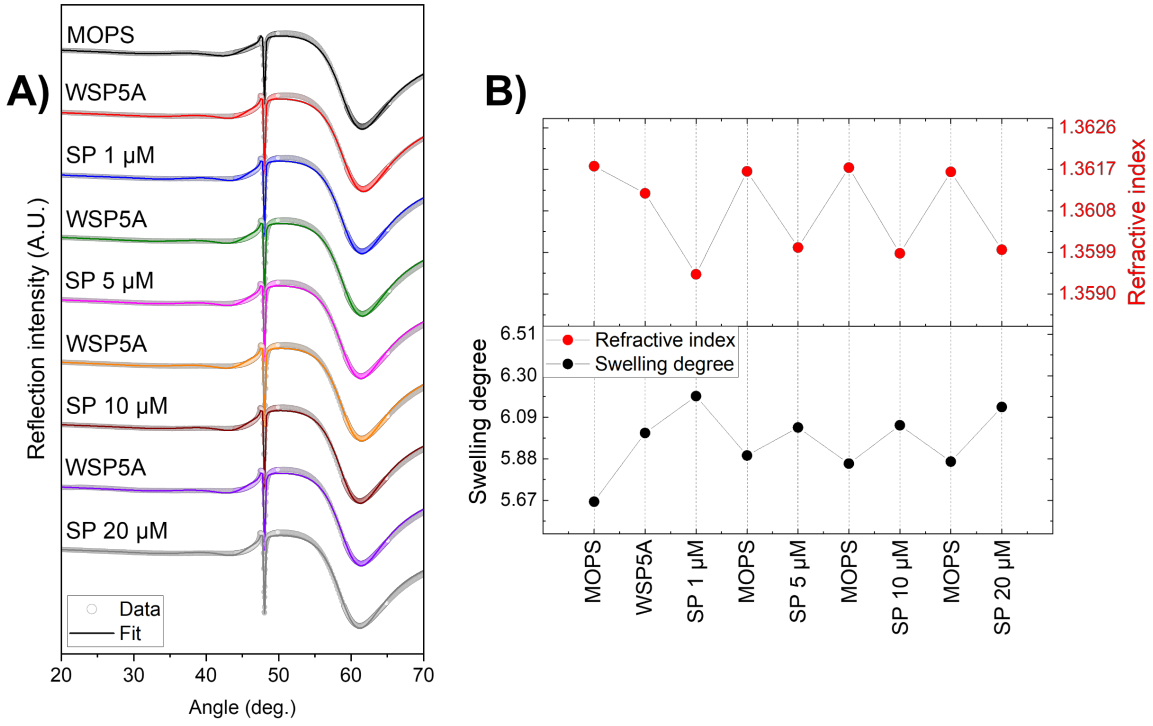

Figure 70. A) Angular spectra of P10TAHAP-2% after equilibration in corresponding solutions. The curves represent fitting of experimental data. B) Evolution of refractive index (on top) and swelling degree of the P10TAHAP gel equilibrated in different solutions.

suitable for the detection of SP at physiological and potentially pathological concentrations (~ 10 μM).

Table 29. Layer thicknesses and RI values obtained for P10TAHAP sensor chip in different media by fitting the angular SPR spectra.

Medium	Inner layer		Outer layer	
	d, nm	n_d	d, nm	n_d
MOPS	48	1.3755	1041	1.3611
WSP5A	124	1.3716	1032	1.3599
SP 1 μM	128	1.3696	1063	1.3582
WSP5A	131	1.3696	1003	1.3606
SP 5 μM	125	1.3680	1036	1.3590
WSP5A	126	1.3685	1000	1.3609
SP 10 μM	120	1.3672	1043	1.3590
WSP5A	134	1.3676	994	1.3608
SP 20 μM	120	1.3664	1061	1.3592

Notably, the 20 μM sample lead to a slightly larger gain of the swelling degree. Together with the significant decrease in the signal intensity upon injection of the 20 μM SP solution (compared to the lower concentrations) demonstrated during the kinetic studies, this might be evidence for the threshold of the system's sensitivity.

4.9.3.5 Sensor responsiveness investigations with 100 μM SP solution

With the aim of testing this hypothesis, SPR investigations of a P10TAHAP gel sensor were conducted with a SP solution of a higher concentration (0.1 mM). Both kinetic study and angular scan measurements were conducted to prove the impact on the gel's parameters (Figure 71). The monitoring of the signal intensity at 60° angle (Figure 71, A, B) demonstrated significant influence of the medium on the gel behavior. In the presence of WSP5A in the solution the system experienced increase in the density comparable to the previous studies (increase by ca. +2–3 % upon injection).

However, in the contrast to the experiments with solutions of lower SP content, the concentration as high as 100 μM caused, indeed, a substantial drop in intensity (–4.3 %). Remarkably, the resulting intensity is lower than the intensity exhibited by a gel swollen in the buffer extrapolated to the times of SP solution injection. This can be explained by the fashion of the interactions and processes occurring in the gel volume upon addition of SP. SP axles replace pendant TAHA groups from the cavity of the WSP5A leading to them being dragged into the medium between the polymer strands. Free TAHA groups provide expansion of the network *via* electrostatic repulsion,

which is plausibly further enhanced by the presence of the charged pseudorotaxanes in the medium.

Furthermore, notable is the system's response to the rinsing with MOPS. For both cases of rinsing after equilibrating in WSP5A solution the signal intensity dropped but stayed above the "pure MOPS" level indicating unbound WSP5A being partially washed out of the gel. On the other hand, rinsing after SP injection increased the intensity back to the "pure MOPS" level, which might be due to the fact that all the formed SP@WSP5A pseudorotaxanes are flushed from the SPR cell. Interestingly, this behavior contrasts with the previous experiments, where MOPS injections in each case led to a further intensity decrease. This seeming contradiction can be justified by the use of different sensor chips for the two experiments: whereas for the investigation with lower SP concentrations a freshly fabricated chip was used, the experiment with the 0.1 mM SP solution

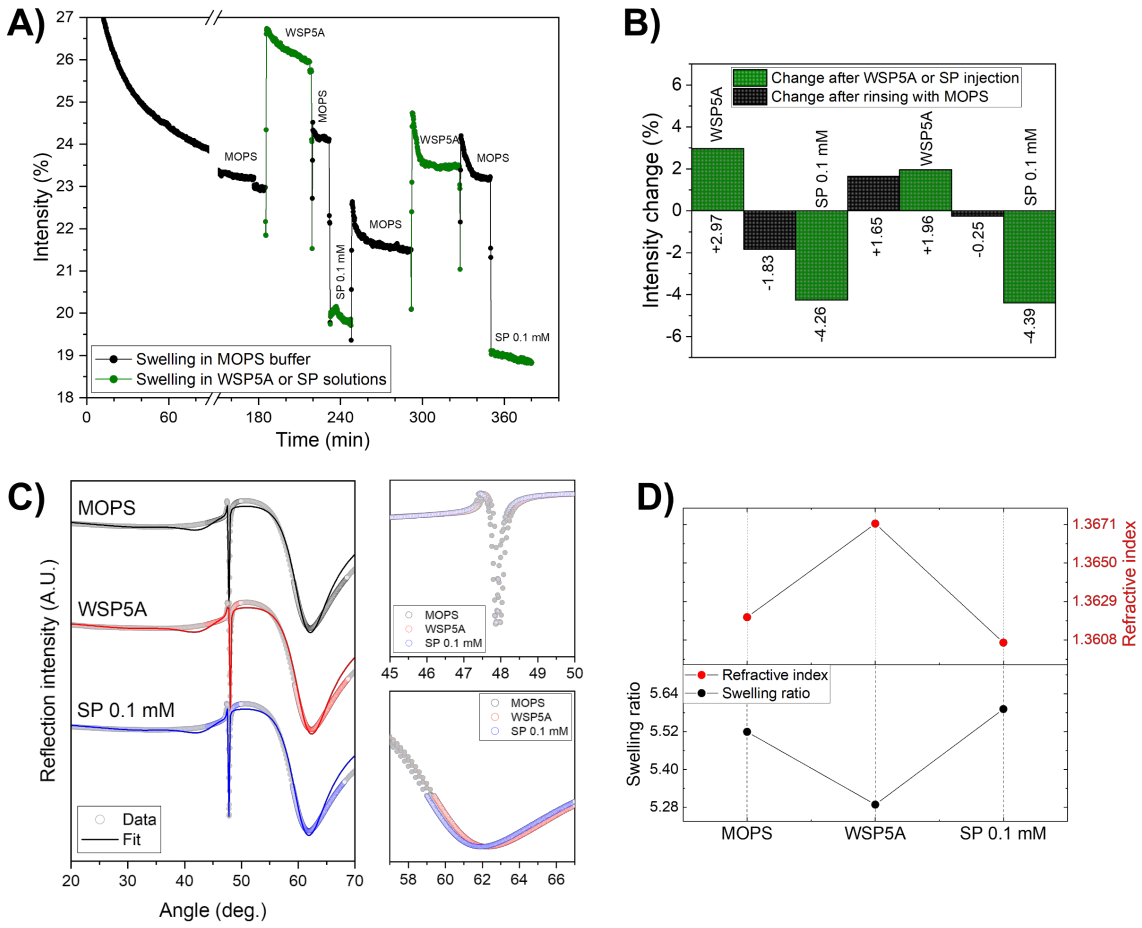

Figure 71. Responsiveness of the P10TAHAP gel sensor with higher SP concentrations. A, B) Kinetic studies: evolution of signal intensity of a swollen gel upon injection of 0.1 mM SP solution recorded at 60° angle. C) Angular spectra of the P10TAHAP gel after equilibration in corresponding solutions. D) Evolution of RI (on top) and swelling degree of the P10TAHAP gel equilibrated in MOPS and solutions of WSP5A and SP.

was conducted on a chip used for two preliminary experiments. Undoubtedly, this can as well have contributed to the considerable responsiveness of the gel to the presence of SP.

The fitting of the angular spectra (Figure 71, C, D, Table 30) further proved the influence of different solutions on the gel's parameters (similar to all the other experiments, a 2-layer gel model was assumed). Swelling in the WSP5A solution clearly caused the gel to shrink by 4 % along with raise in its density indicated by the refractive index. Subsequent SP injection led to the expansion of the gel as well as drop in the density in accordance with the process discussed earlier.

Table 30. Layer thicknesses and RI values obtained for P10TAHAP sensor chip in different media (including 0.1 mM SP solution) by fitting the angular SPR spectra.

Medium	Inner layer		Outer layer	
	d, nm	n_d	d, nm	n_d
MOPS	200	1.3806	872	1.3578
WSP5A	200	1.3822	828	1.3635
SP 100 µM	200	1.3784	886	1.3567

These results demonstrate, on the one hand, that the sensitivity of the sensor chip based on the positively charged P10TAHAP gel is still insufficient for the detection of SP when it is presented in the solution at the concentration levels corresponding to spermine content in urine of cancer patients (1–10 µM) or lower. On the other hand, it was shown that for the fabricated sensor 20 µM SP is already a distinguishable threshold, and the sensitivity is increased further at higher SP concentrations.

4.9.3.6 Responsiveness of a chip without WSP5A

Finally, in order to verify that the fluctuations in the gel's attributes are not arbitrary and occur indeed due to the interplay of host-guest interactions involving WSP5A, a kinetic study was conducted at 60° without host injections, *i.e.*, injections of the SP solutions alternated with MOPS rinsing cycles (Figure 72).

As reflected by the decreasing intensity in the whole course of the experiment, the sensor chip was still equilibrating: after each subsequent rinsing with MOPS solution, the gel density was dropping (arguably due to the swelling of the inner layers of the hydrogel), and reached its equilibrated state around 80 min mark. Hence, the signal drop after each consecutive injection (Figure 72, B) prior to this mark does not reflect the interactions which might occur in the system in the presence of SP. More representative is the second half where neither rinsing with MOPS nor the injection of 20 µM SP solution (which caused a considerable decrease in the signal in the presence of the WSP5A, see Figure 69) led to any substantial change of the intensity. Therefore, it can be

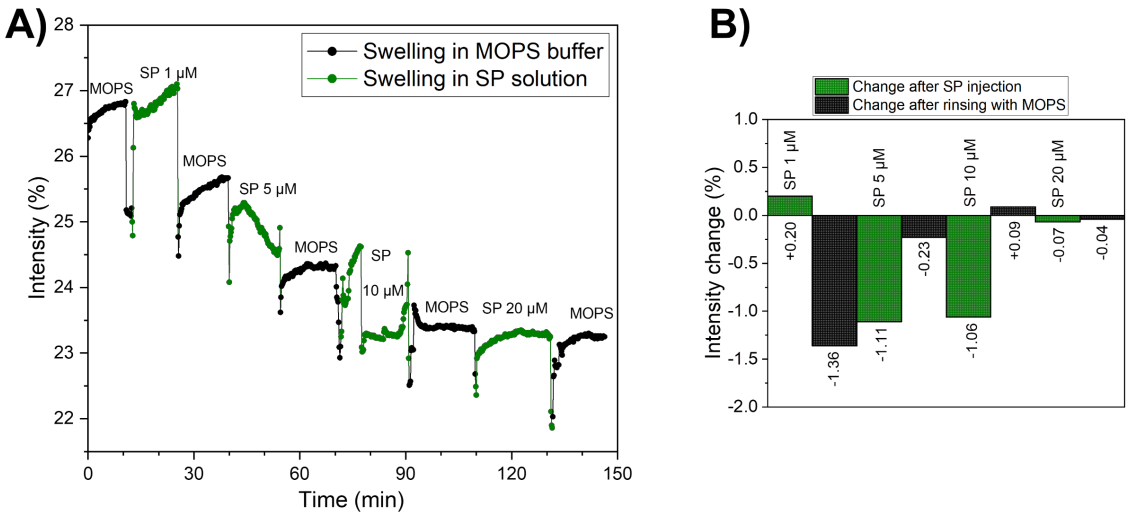

Figure 72. Kinetic studies of P10TAHAP gel sensor. A) Evolution of signal intensity of a swollen gel upon injections of different solutions recorded at 60° angle. B) Intensity changes upon each injection.

concluded that the presence of the water-soluble macrocycle in this system endows it with responsiveness towards spermine and, thus, is an essential component of the designed supramolecular sensor chip.

4.10 Summary and outlook

A hydrogel-based SPR sensor chip for the detection of spermine as a cancer biomarker was devised. The hydrogel was obtained by photo-crosslinking of copolymers synthesized using RAFT co-polymerization of DMAAm and VDMA, which was subsequently used to attach DMIEA as a photo-crosslinker and a guest moiety as anchoring points for further embedding of a host species. 1,2,4-triazole and (trimethylhexyl)ammonium containing species were selected as guest moieties for the modification of polymers. The detection concept relied on a competitive host-guest inclusion complex formation, where SP displaced a guest moiety bound to polymer network out of a cavity of WSP5A.

It was demonstrated by NMR spectroscopy, ITC, and mass spectrometry that SP exhibits an outstanding binding affinity to the host species WSP5A ($K_a \sim 10^5\ M^{-1}$), which is by one order of magnitude higher than for the complex TAHA-Boc@WSP5A, as determined by ITC ($K_a \sim 10^4\ M^{-1}$). Furthermore, for both P10THA and P10TAHA an NMR investigation of the systems guest polymer–WSP5A–SP confirmed the competitive complexation principle in case of macromolecular species implying that the anticipated systems are suitable for sensor fabrication.

Hence, P10THAP as well as P10TAHAP were used as materials for fabrication of sensor chips by spin-coating the polymers' solutions onto pretreated gold-coated quartz chips. The so-applied thin

films were photo-crosslinked under UV-irradiation. By comparing thickness of gel layers prepared from solutions of two different concentrations, conditions were found to deliver sensor chip with a gel layer thick enough to exhibit both surface plasmon and wave guide modes in SPR spectroscopy. SPR investigations in MOPS buffer using P10THAP and P10TAHAP revealed that the sensitivity of the polymeric detector was insufficient for the detection of SP at pathological concentrations (1–10 μM). However, the gel sensor based on P10TAHAP showed response upon injection of elevated concentrations of SP (100 μM) as indicated by an increase of the swelling ratio and a decrease in refractive index upon addition of the SP solution. Moreover, the behavior of the network in cycles of swelling in WSP5A, SP and rinsing with MOPS buffer arguably confirmed the outcome of the ITC investigation according to which a single host molecule is able to bind to multiple guest species.

Clearly, the devised system requires optimization in order to achieve the purpose it was designed for. Pushing down the LOD for the devised sensor can be possible if additional improvements for the sensor design are undertaken. Firstly, in order to make the bulk changes in the gel more pronounced and the swollen states more easily distinguishable, the spin-coating can be conducted with polymer solutions of higher concentrations to obtain gels with higher initial thickness. Secondly, since the detection mechanism of the system is based on the WSP5A inclusion complexes, an increased content of the host molecules threaded onto the polymer pendant groups could lead to an increased capacity of the sensor. This requires an increased TAHA-group number per chain, which can be implemented by introducing polymers with a higher VDMA content (*e.g.*, P20 from Chapter 3). It is conceivable that equilibration of the whole volume of the gel, *i.e.*, including the inner layers, prior to actual measurements, can further benefit the sensitivity due to the eliminated drift of the signal intensity level. Finally, sensitivity of the sensor towards SP (and SD as its related compound) has to be determined (as LOD) as well as selectivity by treating the sensor chip with (artificial) urine samples in order to prove its effectiveness in the presence of other substances such as urea or salts.

It is expected that the results obtained in the course of the current work will pave the way for the fabrication of the gel sensors based on water-soluble pillar[n]arenes which are covalently attached to the polymer chains. This improvement should provide the possibility of dual crosslinking and, therefore, automatic regeneration of the sensor's capacity by rinsing it or soaking it in a suitable solvent, thus, making it fully reusable.

5 Experimental section[1]

5.1 Materials and methods

5.1.1 Materials

The substances from Table 31 were purchased and used as received unless stated otherwise.

Table 31. List of materials used in the current work

Actual name	Purity	Supplier	Remarks
1,2,4-1*H*-triazole	98 %	Janssen Chimica	
1,2-Dichloroethane	99.8 %	Riedel-de Haën	
1,4-Dimethoxybenzene	99+ %	Acros Organics	
1,4-Dioxane	99.5 %	Grüssing GmbH	
1,8-Diazabicyclo[5.4.0]undec-7-en	98 %	Sigma Aldrich	
1-Methyl-1*H*-imidazole	99 %	Sigma Aldrich	
2-(Dodecylthiocarbonothioyl-thio)-2-methylpropionic acid	98 %	Sigma Aldrich	
2,3-Dimethylmaleic anhydride	97 %	Acros Organics	
2,6-Di-*tert*-butyl-4-methylphenol	99 %	Fluka	
2-Methyl alanine	98 %	TCI Chemicals	
3-Bromopropylamine hydrobromide	98 %	Sigma Aldrich	
6-Aminohexan-1-ol	97 %	Sigma Aldrich	
Acetone	technical	Stockmeier	distilled
Acetonitrile	99 %	Fisher Chemical	
Acryloyl chloride	97 %	Sigma Aldrich	
Adiponitrile	98 %	TCI Chemicals	
Allyl amine	98+ %	Alfa Aesar	
Ammonia	25 % in H_2O	Stockmeier	
Azobis(isobutyronitril)	98 %	Sigma Aldrich	rec. from EtOH
Boron tribromide	1M in DCM	Sigma Aldrich	
Chloroform	technical	Stockmeier	distilled over P_2O_5
Copper iodide	99.999 %	Sigma Aldrich	
Dichloromethane	technical	Stockmeier	distilled

[1] Parts of this chapter were published in [278].

Actual name	Purity	Supplier	Remarks
Diethyl ether	technical	Stockmeier	distilled
Di-*tert*-butyl dicarbonate	97 %	Thermo Fisher	
Ethanol	99.5 %	Grüssing GmbH	
Ethanolamine	99 %	Acros Organics	
Ethyl acetate	technical	Stockmeier	distilled
Ethyl bromoacetate	98 %	Alfa Aesar	
Ethyl chloroformate	97 %	Sigma Aldrich	
Ethylene diamine	99 %	Acros Organics	
Hexafluoroisopropanol	99 %	Carbolution	
Hydrogen bromide	48 % in H_2O	Sigma Aldrich	
Hydrogen chloride	4M in 1,4-dioxane	Thermo Fisher	
Hydrogen chloride	37 % in H_2O	Stockmeier	
Iso-hexane	technical	Stockmeier	distilled
Magnesium sulfate	anhydrous	VWR International GmbH	
Methanol	technical	Stockmeier	distilled
N,*N*-Dimethyl acrylamide	>99.0 %	TCI Chemicals	distilled *in vacuo*
N,*N*-Dimethyl formamide	99.8 %, anhydrous	Thermo Fisher	
Paraformaldehyde	95+ %	Sigma Aldrich	
Potassium carbonate	99.5 %	Grüssing GmbH	
Potassium iodide	98+ %	Lancaster	
Potassium trifluoroacetate	98 %	Sigma Aldrich	
Propargyl bromide	80 % in toluene	Alfa Aesar	
Sodium azide	99 %	Merck	
Sodium carbonate	anhydrous	VWR International GmbH	
Sodium chloride	anhydrous	Stockmeier	
Sodium hydride	60 % in mineral oil	Acros Organics	
Sodium hydroxide	anhydrous	Normapur	
Sodium sulfate	anhydrous	VWR International GmbH	
Tetrahydrofuran	99.5 %	Grüssing GmbH	
Thioacetic acid	98 %	Acros Organics	
Toluene	technical	Stockmeier	
Triethylamine	99.5 %	Sigma Aldrich	
Trifluoroacetic acid	99 %	Thermo Fisher	
Trimethylamine	33 % in EtOH	Fluka	

Deuterated solvents: $CDCl_3$ (99.8 % D, with Ag), DMSO-d_6 (99.8 % D), CD_3CN (99.0 % D) and D_2O (99.9 % D) were purchased from Deutero GmbH and used as received.
Spectra/Por® 6 dialysis membrane from Spectrum with a molecular weight cutoff value of 1 kDa was used.

5.1.2 Methods

5.1.2.1 Melting point

The determination of melting point was conducted using Büchi Melting Point B-545 apparatus at a heating rate of 1 °C/min.

5.1.2.2 Nuclear magnetic resonance spectroscopy

NMR spectra were recorded on a Bruker Avance 500 spectrometer (500 MHz for ^{1}H) and a Bruker Ascent 700 spectrometer (700 MHz for ^{1}H and 176 MHz for ^{13}C). Chemical shifts (δ) are listed in ppm (relative to the solvent peak) and coupling constants (J) in Hz. Spectra processing was conducted using Bruker TopSpin 4.1.1. software.

5.1.2.2.1 NMR titration

NMR titration was conducted using two methods described in Ref [230]. According to the first one, into a single NMR tube with 0.5 mL host solution (4 mM) aliquots of host–guest solution (4 mM host and 20 mM guest) were successively added and NMR spectra were recorded after each portion. The tube was gently shaken and sonicated for 5 min prior to each NMR measurement.
The second method implies usage of several NMR tubes with various host–guest ratios. Thus, to each of the tubes 200 μL 10 mM host solution was added. Then, 12.5 μL (0.25 eq.) to 200 μL (4.0 eq.) of guest solution (40 mM) were added to the host solutions and filled up to 0.5 mL with the solvent to ensure an equal host concentration among the tubes.

5.1.2.2.2 Determination of a binding constant

Determination of binding constants K_a for complexes exhibiting a slow exchange proceeded using a single point method.[11,138,144,149,242,243,363] The stoichiometry was determined by the integration of NMR signals, and for 1:1 (host:guest) complexes the binding constant was calculated from the equilibrium (6), Chapter 2.4.1.2.
After obtaining titration curve the data was compared to titration curves simulated for a 1:1 complex using HySS 2009 (Version 4.0.31) software.[310] For the simulation the K_a value obtained experimentally was used.

In case of the fast exchange complexes for the determination of the stoichiometry of a complex a Job plot was used, where the mole fraction of a host compound X(H) was plotted against a product X(H)·Δδ (where Δδ is a change in a chemical shift of a host peak). The shift of host peaks was monitored, and the titration curves were fitted using the equation (25). [227,228]

For each complex, the titration curves of all three pillar[5]arene signals were fitted using a general fit with the same parameter K_a.

For the fitting of titration results where formation of complexes of 1:2 (H:G) stoichiometry was anticipated, BindFit v0.5[234,341] software was used.

5.1.2.3 Mass spectrometry

High-resolution mass spectra were recorded using Synapt-G2 HDMS mass spectrometer by Waters equipped with a quadrupole-time-of-flight detector. Electron spray ionization with following parameters was used as an ionization method:

Capillary voltage: 2.62 kV

Sample peak voltage: 10 kV

Extraction peak voltage: 3.2 kV

Spectrus Processor software by ACD/Labs was used for processing of the MS spectra.

5.1.2.4 Gel permeation chromatography

For the determination of the molecular weight and molecular weight distribution HFIP + 0.05 M potassium trifluoroacetate was used as eluent with BHT as an internal standard at the flow rate of 1.000 mL/min. The system was equipped with a guard column (PSS-PFG guard 7 μm) and two consecutive columns (PSS-PFG 10^3 Å and 10^2 Å, 7 μm), a pump (Merck Hitachi L-6200) and an RI detector (Shodex RI 101). Samples were prepared with a concentration of 4 mg/mL. Molar masses were obtained according to the calibration using poly(methyl methacrylate) standards.

5.1.2.5 Surface plasmon resonance spectroscopy

SPR measurements were conducted in Kretschmann configuration using a RES-TEC RT2005 spectrometer from Res-Tec – Resonant Technologies GmbH. A monochromatic light from a He-Ne laser (λ = 632.8 nm) guided through a series of polarizers (Glan-Thompson polarizer, B. Halle) passed through a N-LaSF9 prism to reach the sensor chip. The reflected beam was further guided to a (photodiode) detector coupled to a lock-in amplifier (7265 DSP, Signal Recovery). The sensor chip was attached to the prism using an index match (Cargille Lab., $n_d^{25} = 1.8000 \pm 0.005$). From the other side, the chip was covered by a flow cell (area approx. 1 cm^2) and the complete sample holder was mounted onto a goniometer (Huber Diffraktionstechnik GmbH & Co. KG) with sample and detector stepping motors (SLO-SYN® M061-LE02E by Superior Electric).

N-LaSF9 (n_d = 1.85025) glass wafers (25×25×1.5 mm) were purchased from ADVANCED OPTICAL COMPONENTS GmbH and coated with gold using PVD. The actual gold layer thickness was determined using SPR. Subsequently, the wafers were immersed in the adhesion promotor[268] (Chapter 5.2.7) solution (1.2 mg/mL in EtOH) over night, rinsed with abs. EtOH and dried using a compressed nitrogen flow prior to applying a polymer layer.

Kinetic measurements were performed at the fixed angle corresponding to approx. 30 % signal intensity on the left slope of the plasmon minimum. The angular spectra were recorded as reflectivity intensity *versus* angle $I(\theta)$ with θ ranging from 18° to 90°. The obtained spectra were fitted in Winspall software (MPI for polymer research, Mainz) using Fresnel equations.

Spin-coating was carried out using a G3P-8 spin coater by Specialty Coating Systems. The polymer layer on the wafer was photo-crosslinked by UV-irradiation using an Omnicure S1500 UV lamp (250 mW/cm^2; λ = 320–480 nm) for 300 s.

5.1.2.5.1 Parameter calculation for the 2-layer fitting model

For the evaluation of the swollen gels' properties, a 2-layer fitting model was applied.[268,314] Swelling ratio Q and refractive index n_d^{gel} were calculated using equations (71) and (72), where d^{in}, d^{out} and d_0 are the thicknesses of the inner layer, the outer layer, and the dry layer, respectively; n_d^{in} and n_d^{out} are the refractive indexes of the inner and outer layer, respectively.

$$Q = \frac{d^{in} + d^{out}}{d_0} \tag{71}$$

$$n_d^{gel} = n_d^{out} \cdot \frac{d^{out}}{d^{out} + d^{in}} + n_d^{in} \cdot \frac{d^{in}}{d^{out} + d^{in}} \tag{72}$$

Detailed approach for the data evaluation can be found in the corresponding results sections.

5.1.2.5.2 Determination of the LOD

The limit of detection (LOD) was calculated by linear fit of the swelling degree dependence as a function of AN concentration according the equations (73) and (74),[315] where ($Q_i - Q_{r,i}$) is a difference between experimental and fitted value of swelling degree; *n* is the amount of data points; A is a slope of the linear fit.

$$s_{y/x} = \sqrt{\left[\frac{\sum_i \left(Q_i - Q_{r,i}\right)^2}{n-2}\right]} \tag{73}$$

$$LOD = 3\frac{s_{y/x}}{A} \tag{74}$$

5.1.2.6 Microscopy

The microscopic images of the gel layers were taken with a HUND-Wetzlar microscope equipped with an iDS uEye camera, and the images were processed using uEye Cockpit software.

5.1.2.7 Isothermal titration calorimetry

ITC measurements were conducted by K. Hoffmann and L. Wyszynski from a working group of Prof. Dr. Schönhoff (Westfälische Wilhelms-Universität-Münster). For the measurements Nano ITC SV titration calorimeter (TA Instruments) was used with a cell volume of 953 µL and a syringe volume of 250 µL. Data evaluation was conducted using ITCRun v3.6.5 software (TA Instruments), using a single set of equal binding sites model according to equations (75) and (76) (see Chapter 2.4.4.3). In the equations, $\Delta Q(i)$ is the heat absorbed or emitted upon addition of the *i*-th portion of guest solution into the cell with host solution; $Q(i)$ is the integral heat change after *i* portions of the guest solution; $dV(i)$ is the volume of the *i*-th portion, V_0 is the cell volume; *n* is the virtual number of guest molecules per one host molecules, *i.e.*, stoichiometry; ΔH^0 is the standard enthalpy of the complexation reaction; $[H]_0$ and $[G]_0$ are total concentrations of host and guest, respectively, after the *i*-th portion; K_a is the equilibrium constant.

$$\Delta Q(i) = Q(i) + \frac{dV(i)}{V_0} \cdot \left(\frac{Q(i) + Q(i-1)}{2}\right) - Q(i-1) \tag{75}$$

$$Q(i) = \frac{n \cdot [H]_0 \cdot \Delta H^0 \cdot V_0}{2} \cdot \left[1 + \frac{[G]_0}{n \cdot [H]_0} + \frac{1}{n \cdot K_a \cdot [H]_0} - \sqrt{\left(1 + \frac{[G]_0}{n \cdot [H]_0} + \frac{1}{n \cdot K \cdot [H]_0}\right)^2 - \frac{4 \cdot [G]_0}{n \cdot [H]_0}}\right] \tag{76}$$

5.2 Synthetic procedures

5.2.1 Precursor synthesis

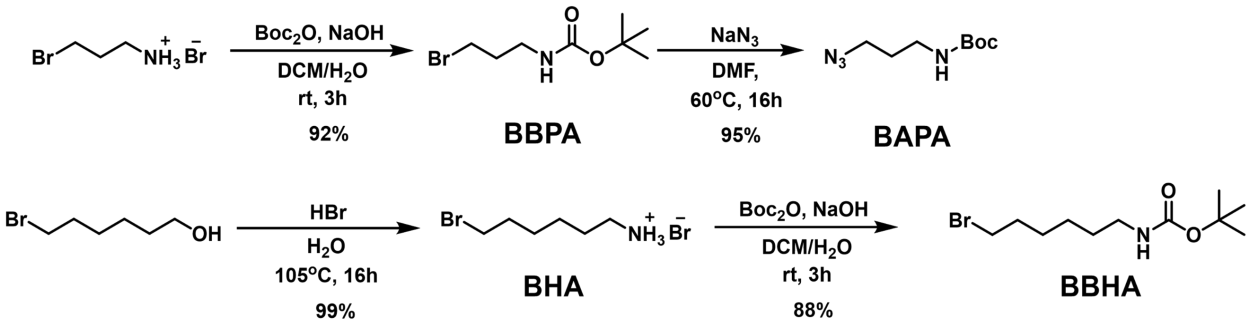

Scheme 11. Synthesis of the precursors BAPA and BBHA.

5.2.1.1 Synthesis of tert-butyl (3-bromopropyl)carbamate (BBPA)

The procedure was adapted from [364].

In a 1000 mL round-bottom flask a solution of 5.6 g (25.7 mmol) Boc_2O in 200 mL DCM was mixed with a solution of 8.5 g (38.8 mmol) 3-bromopropylamine hydrobromide in 100 mL H_2O at vigorous stirring. To the mixture 40 mL 2 M NaOH solution were added dropwise over 15 min. After stirring for 3 h the organic phase was separated and washed with 100 mL 1 M HCl solution and 100 mL brine, then dried over $MgSO_4$ and the solvent was evaporated *in vacuo*. The crude product (yellow oil) was recrystallized from *iso*-hexane. BBPA was obtained as white needle-like crystals (5.65 g; 23.7 mmol; 92 %).

T_{mp} = 37.6 °C (Lit.: 36–38 °C[365]).

^{1}H NMR (700 MHz, $CDCl_3$) δ (ppm) = 4.68 (br s, 1H, N**H**), 3.43 (tr, $^3J_{HH}$ = 6.5 Hz, 2H, Br-C**H**$_2$), 3.26 (m, 2H, NH-C**H**$_2$), 2.04 (quint, $^3J_{HH}$ = 6.3 Hz, 2H, NH-CH$_2$-C**H**$_2$), 1.43 (s, 9H, C**H**$_3$).

^{13}C NMR (176 MHz, $CDCl_3$) δ (ppm) = 156.2 (**C**=O), 79.6 (**C**(CH$_3$)$_3$), 39.2 (NH-**C**H$_2$), 32.9 (NH-CH$_2$-**C**H$_2$), 31.0 (Br-**C**H$_2$), 28.6 (**C**H$_3$).

ESI-MS: cacld for $[M + Na]^+$ *m/z* = 260.0262, found *m/z* = 260.0254.

5.2.1.2 Synthesis of tert-butyl (3-azidopropyl)carbamate (BAPA)

In a 100 mL three-necked flask 0.286 g (4.4 mmol) NaN_3 were dissolved in 15 mL anhydrous DMF und Ar flow. To the solution 1.0 g (4.2 mmol) BAPA in 5 mL DMF were added and the reaction mixture was stirred at 70 °C for 24 h. After the reaction was complete, 20 mL H_2O and 20 mL ethyl acetate were added to the mixture. The phases were separated, and the aqueous phase was extracted with 20 mL EtOAc, then the combined organic phases were washed with H_2O

(3×40 mL), dried over $MgSO_4$, and the solvent was carefully evaporated *in vacuo*. BAPA was obtained as a yellow viscous liquid (0.7503 g; 3.75 mmol; 89 %).

^{1}H NMR (700 MHz, $CDCl_3$) δ (ppm) = 4.66 (br s, 1H, N**H**), 3.35 (tr, $^3J_{HH}$ = 6.7 Hz, 2H, N_3-C**H**$_2$), 3.20 (m, 2H, NH-C**H**$_2$), 1.76 (quint, $^3J_{HH}$ = 6.6 Hz, 2H, NH-CH_2-C**H**$_2$), 1.44 (s, 9H, C**H**$_3$).
^{13}C NMR (176 MHz, $CDCl_3$) δ (ppm) = 156.1 (**C**=O), 79.6 (**C**$(CH_3)_3$), 49.3 (N_3-**C**H_2), 38.2 (NH-**C**H_2), 29.5 (NH-CH_2-**C**H_2), 28.6 (**C**H_3).
ESI-MS: cacld for $[M + Na]^+$ *m/z* = 223.1171, found *m/z* = 223.1152.

5.2.1.3 Synthesis of 6-bromohexan-1-amine hydrobromide (BHA)

The procedure was adapted from [366].
3.05 g (25.6 mmol) 6-aminohexan-1-ol were dissolved in 30 mL 48 % HBr in H_2O. The mixture was heated up to 105 °C and refluxed for 16 h. After the reaction was complete, the solvent was removed *in vacuo* to give BHA as an ocher solid (6.62 g; 25.4 mmol; 99 %).

T_{mp} = 142 °C. (Lit.: 142–143 °C[367]).
^{1}H NMR (700 MHz, D_2O) δ (ppm) = 3.55 (t, $^3J_{HH}$ = 6.7 Hz; 2H, Br-C**H**$_2$), 3.03 (m, 2H, NH_3^+-C**H**$_2$), 1.90 (m, 2H, Br-CH_2-C**H**$_2$), 1.70 (m, 2H, NH_3^+-CH_2-C**H**$_2$), 1.50 (m, 2H, Br-CH_2-CH_2-C**H**$_2$), 1.43 (m, 2H, NH_3^+-CH_2-CH_2-C**H**$_2$).
^{13}C NMR (176 MHz, D_2O) δ (ppm) = 39.5 (NH_3^+-**C**H_2), 35.0 (Br-**C**H_2), 31.8 (Br-CH_2-**C**H_2), 26.8 (Br-CH_2-CH_2-**C**H_2), 26.6 (NH_3^+-CH_2-**C**H_2), 24.7 (NH_3^+-CH_2-CH_2-**C**H_2).
ESI-MS: cacld for $[M + H]^+$ *m/z* = 180.0382, 182.0362, found *m/z* = 180.0400, 182.0382.

5.2.1.4 Synthesis of tert-butyl (6-bromohexyl)carbamate (BBHA)

Solutions of BHA (5.22 g; 20.0 mmol) in 50 mL H_2O and Boc_2O (3.27 g; 15.0 mmol) in 100 mL DCM were combined in a 500 mL round-bottom flask. To the mixture at vigorous stirring (1000 rpm) 20 mL 2 M NaOH in H_2O were added dropwise over 20 min. After reacting for 4 h at RT the organic phase was separated, washed with 100 mL 1 M HCl and 100 mL brine, then dried over $MgSO_4$, and the solvent was evaporated *in vacuo*. BBHA (3.02 g; 10.8 mmol; 72 %) was obtained as slightly yellow oil.

^{1}H NMR (700 MHz, $CDCl_3$) δ (ppm) = 4.51 (br s, 1H, N**H**), 3.39 (t, $^{3}J_{HH}$ = 6.8 Hz; 2H, Br-C**H**$_2$), 3.10 (m, 2H, NH-C**H**$_2$), 1.85 (quint, $^{3}J_{HH}$ = 7.2 Hz; 2H, Br-CH$_2$-C**H**$_2$), 1.48 (m, 2H, NH-CH$_2$-C**H**$_2$), 1.46-1.40 (m, 11H, Br-CH$_2$-CH$_2$-C**H**$_2$ and C**H**$_3$), 1.33 (m, 2H, NH-CH$_2$-CH$_2$-C**H**$_2$).

^{13}C NMR (176 MHz, $CDCl_3$) δ (ppm) = 156.2 (**C**=O), 79.3 (**C**(CH$_3$)$_3$), 40.7 (NH-**C**H$_2$), 34.0 (Br-**C**H$_2$), 32.9 (Br-CH$_2$-**C**H$_2$), 30.1 (NH-CH$_2$-**C**H$_2$), 28.6 (**C**H$_3$), 28.0 (Br-CH$_2$-CH$_2$-**C**H$_2$), 26.1 (NH-CH$_2$-CH$_2$-**C**H$_2$).

ESI-MS: cacld for $[M + Na]^+$ *m/z* = 302.0732, 304.0711, found *m/z* = 302.0732, 304.0710.

5.2.2 Synthesis of the host moiety HT

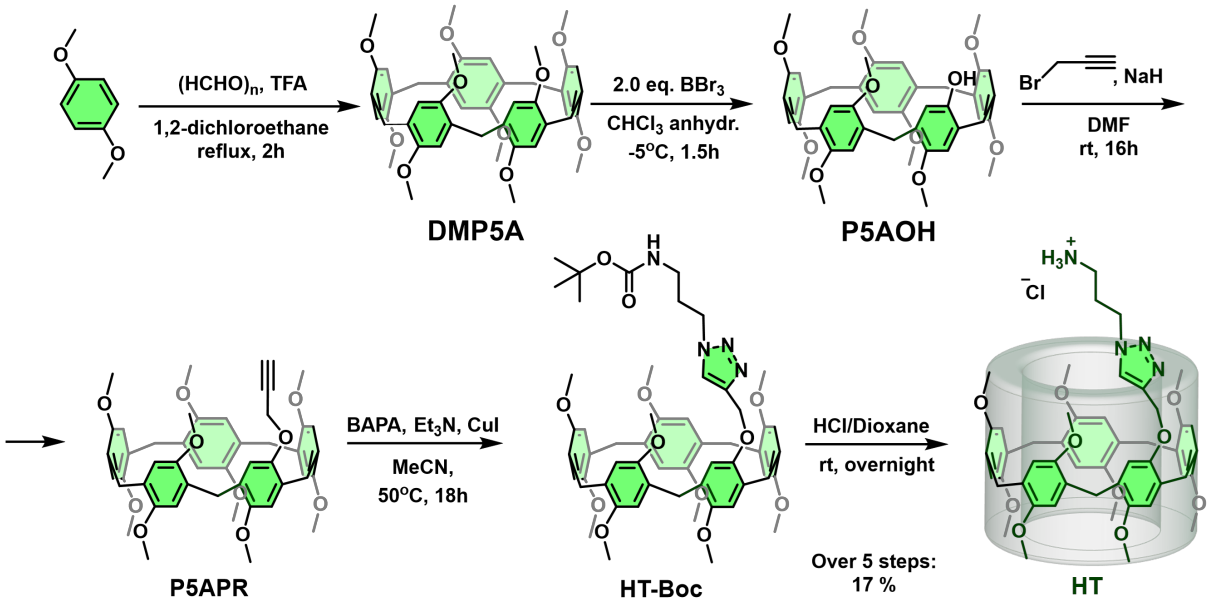

Scheme 12. Synthetic route towards host moiety HT.

5.2.2.1 Synthesis of decamethoxy-pillar[5]arene (DMP5A)

The procedure was adapted from [88].

Into a 500 mL 3-necked round-bottom flask 5.528 g (40 mmol) DMB and 1.20 g (40 mmol) paraformaldehyde were suspended in 180 mL 1,2-DCE followed by the addition of 20 mL TFA. The reaction mixture was refluxed for 2 h. After cooling down the mixture was poured into 800 mL MeOH and the formed precipitate was separated using filter paper. Further, the crude product was resolved in 200 mL DCM and filtered through silica. After solvent evaporation the product was stirred in $CHCl_3$ for 30 min to remove the DCM molecules from the cavity. DMP5A (4.25 g; 5.7 mmol; 71 %) was obtained as a white crystalline solid.

T_{mp} = 248.5–249.5 °C (Lit: 248.8 °C[113]; 248.1–249 °C[368]).

^{1}H NMR (700 MHz, $CDCl_3$) δ (ppm) = 6.83 (s, 10H, C**H**), 3.77 (s, 10H, C**H**$_2$), 3.70 (s, 30H, C**H**$_3$).
^{13}C NMR (176 MHz, $CDCl_3$) δ (ppm) = 150.8 (**C**$_{Ar}$-O), 128.4 (**C**$_{Ar}$-CH_2), 113.9 (**C**$_{Ar}$-H), 55.8 (**C**H_3), 29.6 (**C**H_2).
ESI-MS: cacld for $[M]^+$ *m/z* = 750.3404, found *m/z* = 750.3396.

5.2.2.2 Synthesis of monohydroxy-P5A (P5AOH)[107,108,117]

In a dry 500 mL Schlenk flask under Ar atmosphere 3.2 g (4.26 mmol) DMP5A were dissolved in 200 mL $CHCl_3$ (preliminarily dried by distillation over P_2O_5), and the solution was cooled down to –5 °C on an ice/NaCl bath. After addition of 0.85 mL (8.5 mmol; 2 eq.) BBr_3 the flask was sealed with a septum and the mixture was stirred for 1.5 h. The reaction was quenched by pouring 100 mL H_2O into the mixture at vigorous stirring followed by neutralization by saturated Na_2CO_3 solution. The organic phase was separated, and the solvent was removed *in vacuo*. The crude product was purified by column chromatography (SiO_2; DCM:MeOH 100:0 to 100:1, R_f = 0.11). Since the monohydroxy- and dihydroxy-derivatives have similar retention factors,[117] for the isolation of the product the mixture was precipitated from 10 mL DCM solution into MeOH (40 mL) twice. Monohydroxy-pillar[5]arene (PAOH) was obtained as white to slightly pink solid (0.8623 g; 1.17 mmol; 28 %).

T_{mp} = 179 °C (Lit.: 203 °C[369]).
^{1}H NMR (700 MHz, $CDCl_3$) δ (ppm) = 6.88, 6.74, 6.71, 6.70, 6.66, 6.66 (s, 6H, C**H**); 6.63 (br s, 1H, O**H**); 6.62, 6.61, 6.59 (s, 3H, C**H**); 3.81 (s, 3H, C**H**$_3$); 3.78, 3.78, 3.78, 3.76 (s, 8H, C**H**$_2$); 3.74 (m, 5H, C**H**$_3$ and C**H**$_2$); 3.70, 3.63, 3.61, 3.61, 3.60, 3.57, 3.51 (s, 21H, C**H**$_3$).
^{13}C NMR (176 MHz, $CDCl_3$) δ (ppm) = 152.1, 151.3, 151.2, 151.2, 151.1, 151.1, 151.1, 151.0, 148.8, 147.8 (**C**$_{Ar}$-O); 130.2, 129.5, 128.9, 128.8, 128.5, 128.5, 128.3, 127.9, 127.0, 125.2 (**C**$_{Ar}$-CH_2); 119.1, 114.8, 114.8, 114.7, 114.5, 114.3, 114.3, 114.1, 113.2, 113.1 (**C**$_{Ar}$-H); 56.6, 56.6, 56.3, 56.3, 56.2, 56.1, 56.1, 56.0, 56.0 (**C**H_3); 31.2, 30.3, 30.1, 29.8, 29.1 (**C**H_2).
ESI-MS: cacld for $[M + Na]^+$ *m/z* = 759.3145, found *m/z* = 759.3137.

5.2.2.3 Synthesis of monopropargyloxy-P5A (P5APR)

0.86 g (1.17 mmol) P5AOH were dissolved in 20 mL anhydrous DMF, and the solution was added at a vigorous stirring to a suspension of 95 mg (2.34 mmol; 2 eq.; 60 % in mineral oil) NaH in 2 mL *iso*-hexane in a Schlenk tube under Ar flow. The mixture was diluted with DMF until cherry red color appeared. Then, 0.65 mL (80 % toluene solution; 5.85 mmol; 5 eq.) propargyl bromide

was added and the solution was stirred overnight at room temperature. After the reaction was complete, the mixture was poured into 200 mL DCM and washed with water (4×150 mL) to remove DMF. The organic phase was evaporated *in vacuo* and the crude product was purified by column chromatography (SiO_2; DCM 100%). P5APR was obtained as a white to yellowish solid (0.8759 g; 1.13 mmol; 96 %).

T_{mp} = 156.5–158.5 °C.

^{1}H NMR (700 MHz, $CDCl_3$) δ (ppm) = 6.79, 6.78, 6.78, 6.77, 6.76, 6.75, 6.75, 6.75, 6.74, 6.71 (s, 10H, C_{Ar}**H**); 4.40 (d, $^4J_{HH}$ = 2.36 Hz, 2H, O-C**H**$_2$); 3.79–3.76 (m, 10H, C_{Ar}-C**H**$_2$); 3.71, 3.67, 3.67, 3.66, 3.66, 3.6, 3.65, 3.63, 3.61 (s, 27H, C**H**$_3$); 1.82 (t, $^4J_{HH}$ = 2.02 Hz, 1H, C≡C**H**).

^{13}C NMR (176 MHz, $CDCl_3$) δ (ppm) = 151.5, 151.0, 151.0, 151.0, 151.0, 151.0, 151.0, 151.0, 150.9, 149.1 (**C**$_{Ar}$-O); 129.1, 128.7, 128.7, 128.6, 128.6, 128.5,128.5, 128.4, 128.3, 128.1 (**C**$_{Ar}$-CH_2); 115.8, 114.6, 114.5, 114.4, 114.4, 114.3, 114.2, 114.2, 114.2, 114.1 (**C**$_{Ar}$-H); 78.9 (CH_2-**C**≡CH); 74.8 (C≡**C**H); 56.3 (O-**C**H_2); 56.1, 56.1, 56.1, 56.0, 56.0, 56.0, 56.0, 55.9, 55.9 (**C**H_3); 30.7, 30.0, 29.9, 29.9, 29.2 (C-**C**H_2-C).

ESI-MS: cacld for $[M + H]^+$ *m/z* = 775.3482, found *m/z* = 775.3486.

5.2.2.4 Synthesis of (1-(N-Boc-3-aminopropyl)-1H-1,2,3-triazol-4-yl) methyleneoxy-P5A (HT-Boc)

0.57 g (0.74 mmol) P5APR were suspended in 100 mL MeCN in a 250 mL three-necked flask at 50 °C. 0.2 mL (1.5 mmol, 2 eq.) Et_3N were added to the mixture followed by addition of 95 mg (0.5 mmol; 0.67 eq.) CuI solution in 6 mL MeCN. After stirring for 15 min the mixture turned yellow and 154 mg (0.77 mmol, 1.04 eq.) BAPA were added resulting in disappearance of the color of the solution. The reaction was controlled by TLC (SiO_2 plates, 100 % DCM). After 20 h the reaction was complete, the solvent removed *in vacuo*, the residue was resolved in 80 mL DCM and washed with 80 mL diluted (0.05 M) HCl. An insoluble brown precipitation formed during washing was filtered out, the organic phase of the filtrate was isolated, and DCM was removed *in vacuo*. The crude product was purified by column chromatography (SiO_2; DCM:MeOH 100:0 to 100:1). HT-Boc was obtained as colorless film (0.5448 g; 0.56 mmol; 76 %).

T_{mp} = 159–171 °C.

^{1}H NMR* (700 MHz, MeCN-d_3:$CDCl_3$ 3:1) δ (ppm) = 7.89 (br s, 1H, triazole C**H**); 7.02, 6.92, 6.91, 6.90, 6.89, 6.89, 6.88, 6.87, 6.86, 6.80 (s, 10H, C_{Ar}-**H**); 5.33 (br s, 1H, N**H**); 5.03 (s, 2H, O-

C**H**$_2$-C(-N)=CH); 4.38 (br tr, $^3J_{HH}$ = 6.2 Hz; 2H, N=N-N-C**H**$_2$); 3.76–3.66, 3.56 (m, 37H, O-C**H**$_3$ and C_{Ar}-C**H**$_2$); 3.07 (m, 2H, NH-C**H**$_2$); 2.03 (m, 2H, NH-CH$_2$-C**H**$_2$); 1.41 (s, 9H, C-C**H**$_3$).

^{13}C NMR* (176 MHz, MeCN-d$_3$:CDCl$_3$ 3:1) δ (ppm) = 156.9 (**C**=O); 151.5, 151.0, 151.0, 150.9, 149.7 (**C**$_{Ar}$-O); 145.0 (**C**$_{triaz}$-CH$_2$); 130.0, 129.3, 129.3, 129.2 (**C**$_{Ar}$-CH$_2$); 124.3 (**C**$_{triaz}$-H); 115.5, 114.1, 114.0, 113.9, 113.9, 113.9, 113.9, 113.8, 113.8 (**C**$_{Ar}$-H); 79.3 (**C**(CH$_3$)$_3$); 63.4 (O-**C**H$_2$); 56.3, 56.3, 56.3, 56.2, 56.1, 56.1 (O-**C**H$_3$); 48.4 (triazol-**C**H$_2$); 38.1 (NH-**C**H$_2$); 31.4 (NH-CH$_2$-**C**H$_2$); 29.8, 29.8, 29.7 (C_{Ar}-**C**H$_2$); 28.7 (C(**C**H$_3$)$_3$).

ESI-MS: cacld for [*M* + H]$^+$ *m/z* = 975.4750, found *m/z* = 975.4777. Cacld for [*M* + Na]$^+$ *m/z* = 997.4575, found *m/z* = 997.4599.

*The compound HT-Boc is inclined to formation of inter- or even intramolecular inclusion complexes in CDCl$_3$, where the side chain acts as a guest moiety for the macrocycle. For this reason, CD$_3$CN was used as a co-solvent for the analysis.

5.2.2.5 Synthesis of (1-(3-aminopropyl)-1H-1,2,3-triazol-4-yl) methyleneoxy-P5A hydrochloride (HT)

0.5 g (0.51 mmol) HT-Boc were dissolved in 4 mL 1,4-dioxane followed by addition of 2 mL 4 M HCl in 1,4-dioxane. The mixture was stirred overnight, then evaporated *in vacuo* to give HT as a yellow film-like solid in a quantitative yield.

^{1}H NMR* (700 MHz, MeCN-d$_3$:CDCl$_3$ 3:1) δ (ppm) = 8.04 (s, 1H, C_{triaz}-**H**); 7.90 (br s, 3H, N**H**$_3^+$); 7.03, 6.91, 6.90, 6.89, 6.89, 6.88, 6.88, 6.87, 6.86, 6.81 (s, 10H, C_{Ar}-**H**); 5.03 (s, 2H, O-C**H**$_2$); 4.57 (tr, $^3J_{HH}$ = 6.4 Hz; 2H, triazol-C**H**$_2$); 3.77–3.65, 3.57 (m, 37H, O-C**H**$_3$ and C_{Ar}-C**H**$_2$); 3.03 (m, 2H, NH$_3^+$-C**H**$_2$); 2.39 (quint, $^3J_{HH}$ = 6.1 Hz; 2H, NH$_3^+$-CH$_2$-C**H**$_2$).

^{13}C NMR* (176 MHz, MeCN-d$_3$:CDCl$_3$ 3:1) δ (ppm) = 151.5, 151.0, 151.0, 150.9, 149.6 (**C**$_{Ar}$-O); 145.5 (**C**$_{triaz}$-CH$_2$); 130.0, 129.3, 129.3, 129.3, 129.3, 129.2, 129.1 (**C**$_{Ar}$-CH$_2$); 125.0 (**C**$_{triaz}$-H); 115.5, 114.1, 113.9, 113.9, 113.9, 113.9, 113.8, 113.7 (**C**$_{Ar}$-H); 63.2 (O-**C**H$_2$); 56.4, 56.3, 56.3, 56.3, 56.2, 56.1, 56.0 (**C**H$_3$); 48.0 (triazol-**C**H$_2$); 38.1 (NH$_3^+$-**C**H$_2$); 29.9, 29.8, 29.7, 29.7 (C_{Ar}-**C**H$_2$); 28.5 (NH$_3^+$-CH$_2$-**C**H$_2$).

ESI-MS: cacld for [*M* + H]$^+$ *m/z* = 875.4226, found *m/z* = 875.4221.

*The compound HT is inclined to formation of inter- or even intramolecular inclusion complexes in CDCl$_3$, where the side chain acts as a guest moiety for the macrocycle. For this reason, CD$_3$CN was used as a co-solvent for the analysis.

5.2.3 Synthesis of the water-soluble pillar[5]arene[338]

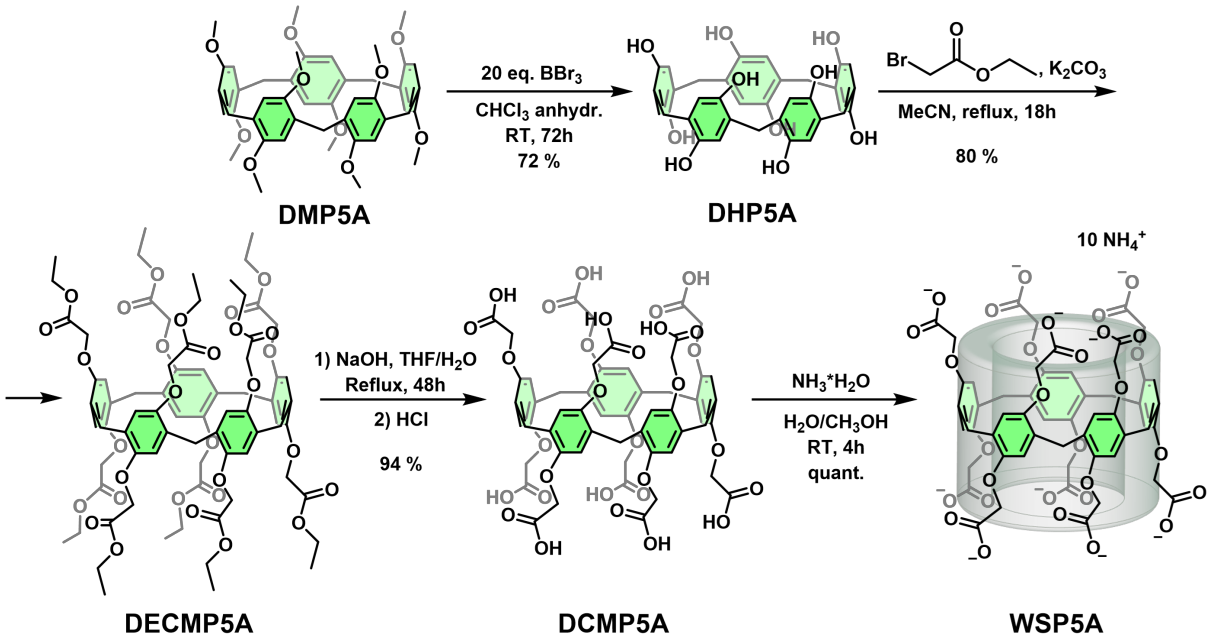

Scheme 13. Synthetic route towards host moiety WSP5A.

5.2.3.1 Case 1: involving isolation of the DHP5A

5.2.3.1.1 Synthesis of decahydroxy-P5A (DHP5A)

2.0 g (2.6 mmol) DMP5A were dissolved in anhydrous $CHCl_3$ (150 mL) in a dry Schlenk flask under Ar. The solution was placed onto an ice bath (0 °C) and 50 mL 1 M BBr_3 in DCM were added. The reaction mixture was stirred at 0 °C for 1 h, then the cooling was removed, and the solution was stirred for 72 h at room temperature. Subsequently, the reaction was quenched by pouring 200 mL water into the flask followed by white precipitate formation. The mixture was filtered through a frit and washed with 60 mL 0.5 M HCl and 60 mL $CHCl_3$. The solid on the frit was resolved in 100 mL MeCN but precipitated from the solution after 10 min. The white crystalline solid was filtered out and dried in vacuo to give the DHP5A (1.14 g; 1.87 mmol; 72 %).

^{1}H NMR (700 MHz, acetone-d_6): 8.01 (s, 10H, O**H**), 6.67 (s, 10H, C**H**), 3.59 (s, 10H, C**H**$_2$).
^{13}C NMR (176 MHz, acetone-d_6): 147.6 (**C**-OH), 128.1 (**C**-CH$_2$), 118.4 (**C**-H), 30.7 (**C**H$_2$).
ESI-MS: cacld for $[M + Na]^+$ *m/z* = 633.1737, found *m/z* = 633.1743.

5.2.3.1.2 Synthesis of deca(ethoxycarbonylmethoxy)-P5A (DECMP5A)

In a three-necked flask 0.15 g (0.25 mmol) DHP5A were dissolved in 15 mL acetone/THF (2:1 v/v) mixture. At stirring 0.96 g (7 mmol) K_2CO_3 and a catalytic quantity of KI were added

followed by 0.76 mL (7 mmol) ethyl bromoacetate. The mixture was heated up to 65 °C and refluxed for 16 h. The formed precipitate was removed by filtration and washed with $CHCl_3$ (10 mL) on the filter. The filtrate was evaporated *in vacuo*, the red residue was resolved in 10 mL $CHCl_3$ and precipitated by dropwise adding MeOH (20 mL) to the solution. The precipitate was filtered out and dried *in vacuo* to obtain DECMP5A as a beige crystalline solid (0.29 g; 0.20 mmol; 80 %).

T_{mp} = 190.9 °C (Lit: 197.2 °C[340], 196.7 °C[126])
^{1}H NMR (700 MHz, $CDCl_3$): 7.04 (s, 10H, C**H**), 4.54 (q, 20H, O-C**H**$_2$-CO), 4.07 (m, 20H, C**H**$_2$-CH_3), 3.85 (s, 10H, C**H**$_2$), 0.96 (t, ^{3}J = 7.14 Hz; 30H, C**H**$_3$).
^{13}C NMR (176 MHz, $CDCl_3$): 169.5 (**C**OO), 149.2 (**C**$_{Ar}$-O), 128.9 (**C**$_{Ar}$-CH_2), 114.7 (**C**H), 65.9 (O-**C**H_2-CO), 61.1 (**C**H_2-CH_3), 29.4 (C_{Ar}-**C**H_2-C_{Ar}), 14.0 (**C**H_3).
ESI-MS: cacld for $[M + Na]^+$ *m/z* = 1493.5415, found *m/z* = 1493.5475.

5.2.3.2 Case 2: Synthesis of DECMP5A; DHP5A is not isolated

2.0 g (2.6 mmol) DMP5A were dissolved in anhydrous $CHCl_3$ (150 mL) in a dry Schlenk flask under Ar. The solution was placed onto an ice bath (0 °C) and 50 mL 1M BBr_3 in DCM were added. The reaction mixture was stirred at 0 °C for 1 h, then the cooling was removed, and the solution was stirred for 72 h at RT. Subsequently, the reaction was quenched by pouring 200 mL water into the flask followed by white precipitate formation. The mixture was filtered through a frit and washed with 150 mL 0.5 M HCl and 100 mL $CHCl_3$ on the frit. The crude DHP5A was resolved in 100 mL MeCN.
To the DHP5A solution in MeCN 9.6 g (70 mmol) K_2CO_3 and a catalytic quantity of KI were added followed by 7.6 mL (70 mmol) ethyl bromoacetate. The solution was heated up to 85 °C and refluxed for 16 h. Then, the formed precipitate was filtered out and washed with 100 mL $CHCl_3$ on the frit. The filtrate was evaporated *in vacuo* and the brown residue was resolved in 100 mL $CHCl_3$ and precipitated by slow adding MeOH (130 mL) to the solution. After filtration and drying *in vacuo* DECMP5A was obtained as light brown solid (2.36 g; 1.6 mmol; 62 % over 2 steps).

5.2.3.3 Synthesis of deca(carboxylmethoxy)-P5A (DCMP5A)

0.5 g (0.34 mmol) DECMP5A were suspended in 60 mL THF followed by the addition of 20 % NaOH solution (15 mL). The mixture was heated up to 65 °C and refluxed for 48. The formed

precipitate was dissolved by adding 20 mL water into the mixture. The aqueous layer was separated and acidified using concentrated HCl until the precipitation occurred. The precipitate was centrifuged, the supernatant decanted, and the procedure was repeated one more time to wash the product. DCMP5A was obtained as light brown solid (0.38 g; 0.32 mmol; 94 %).

T_{mp} = 284.5 °C (Lit: 297.3 °C[126])

^{1}H NMR (700 MHz, DMSO-d_6): 7.02 (s, 10H, C**H**), 4.70-4.32 (dd, 20H, O-C**H**$_2$), 3.72 (br. s, 10H, C_{Ar}-C**H**$_2$).

^{13}C NMR (176 MHz, DMSO-d_6): 170.7 (**C**OOH), 148.6 (**C**$_{Ar}$-O), 127.7 (**C**$_{Ar}$-CH_2), 114.2 (**C**$_{Ar}$H), 65.2 (O-**C**H_2-COO), 28.7 (C_{Ar}-**C**H_2-C_{Ar}).

ESI-MS: cacld for $[M + Na]^+$ *m/z* = 1213.2285, found *m/z* = 1213.2284.

5.2.3.4 Synthesis of decaammonium deca(carboxylatomethoxy)-P5A (WSP5A)

0.35 g (0.29 mmol) DCMP5A were suspended in 20 mL H_2O/MeOH (1:1 v/v) mixture and to the suspension 0.4 mL 25 % $NH_{3\,(aq)}$ were added, which led to the dissolution of the solid. After stirring for 4 h the solution was evaporated, and the residue was dried in vacuo to obtain WSP5A as a brown solid in a quantitative yield.

T_{mp} = 314.0 – 316.0 °C

^{1}H NMR (700 MHz, D_2O): 6.73 (s, 10H, C**H**), 4.28 (s, 20H, O-C**H**$_2$), 3.85 (s, 10H, C-C**H**$_2$).

^{13}C NMR (176 MHz, D_2O): 177.0 (**C**OO), 149.5 (**C**$_{Ar}$-O), 128.9 (**C**$_{Ar}$-CH_2), 115.2 (**C**$_{Ar}$-H), 67.7 (O-**C**H_2), 29.2 (C_{Ar}-**C**H_2-C_{Ar}).

ESI-neg-MS (An^{10-} = $C_{55}H_{40}O_{30}^{10-}$): cacld for $[An^{10-} + 9H^+]^-$ *m/z* = 1189.2314, found *m/z* = 1189.2317; cacld for $[An^{10-} + 8H^+]^{2-}$ *m/z* = 594.1120, found *m/z* = 594.1127; cacld for $[An^{10-} + 7H^+]^{3-}$ *m/z* = 395.7389, found *m/z* = 395.7408; cacld for $[An^{10-} + 6H^+]^{4-}$ *m/z* = 296.5524, found *m/z* = 296.5536.

5.2.4 Synthesis of the guest moieties

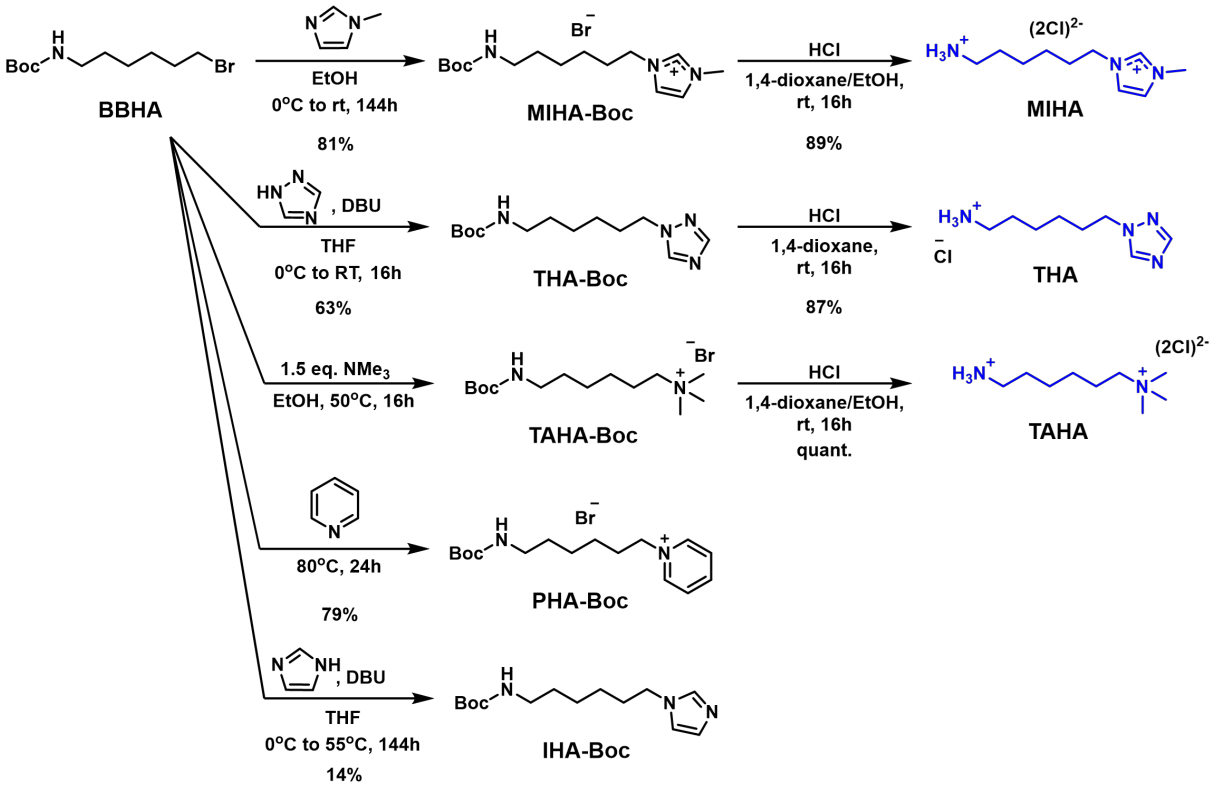

Scheme 14. Synthetic pathways towards guest moieties.

5.2.4.1 Synthesis of 3-(6-((tert-butyloxycarbonyl)amino)hexyl)-1-methyl-1H-imidazol-3-ium bromide (MIHA-Boc)

To the mixture of 0.50 g (1.78 mmol) BBHA in 5 mL EtOH in a pear-shaped flask 0.145 g (1.77 mmol) 1-methyl-1*H*-imidazole were added. The reaction was carried out for 168 h, then the mixture was dissolved in 30 mL H_2O and washed with EtOAc (3×30 mL). Because the crude product still contained starting material, it was resolved in 5 mL EtOH containing 0.20 g (0.71 mmol) BBHA and the mixture was stirred for 72 h. The washing cycles was repeated as described above. The water was evaporated, and the product was dried *in vacuo* at 80 °C for 5 h. MIHA-Boc (0.287 g; 0.80 mmol; 45 %) was obtained as colorless highly viscous liquid.

^{1}H NMR (700 MHz, $CDCl_3$) δ (ppm) = 10.45 (s, 1H, N=C**H**-N), 7.40 (m, 1H, CH_3-N-C**H**=CH), 7.38 (m, 1H, CH_3-N-CH=C**H**), 4.71 (s, 1H, N**H**), 4.33 (t, $^3J_{HH}$ = 7.3 Hz, 2H, imidazolyl-C$\mathbf{H}_2$), 4.11 (s, 3H, N$^-$C$\mathbf{H}_3$), 3.07 (t, $^3J_{HH}$ = 6.3 Hz, 2H, NH-C$\mathbf{H}_2$), 1.92 (m, 2H, imidazolyl-CH_2-C$\mathbf{H}_2$), 1.47 (m, 2H, NH-CH_2-C$\mathbf{H}_2$), 1.41 (s, 9H, C(C$\mathbf{H}_3$)$_3$), 1.36 (m, 4H, imidazolyl-CH_2-CH_2-C$\mathbf{H}_2$ and NH-CH_2-CH_2-C$\mathbf{H}_2$).

^{13}C NMR (176 MHz, $CDCl_3$) δ (ppm) = 156.3 (**C**=O), 138.1 (N=**C**H-N), 123.4 (CH_3-N-**C**H=CH), 122.0 (CH_3-N-CH=**C**H), 79.3 (**C**(CH_3)$_3$), 50.2 (imidazolyl-**C**H_2), 40.3 (NH-**C**H_2), 37.0 (N-**C**H_3), 30.2 (imidazolyl-CH_2-**C**H_2), 29.9 (NH-CH_2-**C**H_2), 28.6 (C(**C**H_3)$_3$), 26.0 (imidazolyl-CH_2-CH_2-**C**H_2), 25.8 (NH-CH_2-CH_2-**C**H_2).
ESI-MS: cacld for $[M]^+$ *m/z* = 282.2176, found *m/z* = 282.2178.

5.2.4.2 Synthesis of 1-(6-ammoniohexyl)-3-methyl-1H-imidazol-3-ium (chloride/bromide) (MIHA)

To the solution of 0.29 g (0.80 mmol) MIHA-Boc in 3 mL H_2O 1 mL HCl (conc.; 12 mmol) were added and the mixture was stirred for 16 h at RT. The solvent was evaporated, and the product was dried *in vacuo* to provide MIHA as a hygroscopic solid in a quantitative yield.

^{1}H NMR (700 MHz, D_2O) δ (ppm) = 8.69 (m, 1H, N=C**H**-N); 7.46 (m, 1H, CH_3-N-C**H**=CH); 7.41 (m, 1H, CH_3-N-CH=C**H**); 4.18 (t, $^3J_{HH}$ = 7.2 Hz, 2H, imidazolyl-C**H**$_2$); 3.87 (s, 3H, N-C**H**$_3$); 2.97 (t, $^3J_{HH}$ = 7.6 Hz, 2H, NH_3^+-C**H**$_2$); 1.87 (tt, $^3J_{HH}$ = 7.5 Hz, 2H, imidazolyl-CH_2-C**H**$_2$); 1.64 (tt, $^3J_{HH}$ = 7.7 Hz, 2H, NH_3^+-CH_2-C**H**$_2$); 1.40 (tt, $^3J_{HH}$ = 7.4 Hz, 2H, NH_3^+-CH_2-CH_2-C**H**$_2$); 1.33 (tt, $^3J_{HH}$ = 7.4 Hz, 2H, triazolyl-CH_2-CH_2-C**H**$_2$).
^{13}C NMR (176 MHz, D_2O) δ (ppm) = 135.8 (N=**C**H-N); 123.5 (CH_3-N-CH=**C**H); 122.1 (CH_3-N-**C**H=CH); 49.3 (imidazolyl-**C**H_2); 39.3 (NH_3^+-**C**H_2); 35.6 (N-**C**H_3); 29.0 (imidazolyl-CH_2-**C**H_2); 26.5 (NH_3^+-CH_2-**C**H_2); 25.0 (NH_3^+-CH_2-CH_2-**C**H_2); 24.9 (imidazolyl-CH_2-CH_2-**C**H_2).
ESI-MS: cacld for $[M]^+$ *m/z* = 182.1652, found *m/z* = 182.1631.

5.2.4.3 Synthesis of tert-butyl (6-(1H-1,2,4-triazol-1-yl)hexyl)carbamate (THA-Boc)

BBHA (3.023 g; 10.8 mmol) was placed in a 250 mL round-bottom flask followed by the addition of 0.623 g (9.0 mmol) 1*H*-1,2,4-triazole in 15 mL THF. The flask was sealed with a septum and cooled down to 0 °C on the ice bath. 1.933 g (12.6 mmol) DBU in 4 mL THF were added dropwise over 15 min. The mixture was stirred for 1 h at cooling, then 16 h at RT. The formed precipitate was filtered out and washed with THF (10 mL) on the frit. The filtrate was evaporated to obtain an orange oil as a crude product. The oil was dissolved in 50 mL EtOAc and washed with 50 mL H_2O, the aqueous phase was extracted with 30 mL EtOAc and the combined organic phases were dried over $MgSO_4$. The product was isolated by column chromatography on silica gel (EtOAc 100 %, the product is in the second fraction, non-UV-active). The evaporation of the solvent gave

THA-Boc as a transparent viscous liquid which crystallized into white solid after several months (1.52 g; 5.7 mmol; 63 %).

T_{mp} = 61 °C.

^{1}H NMR (700 MHz, $CDCl_3$) δ (ppm) = 8.06 (s, 1H, $H5_{triazole}$), 7.93 (s, 1H, $H3_{triazole}$), 4.53 (br s, 1H, N**H**), 4.15 (t, $^3J_{HH}$ = 7.1 Hz; 2H, triazolyl-C**H**$_2$), 3.09 (m, 2H, NH-C**H**$_2$), 1.88 (quint, $^3J_{HH}$ = 7.3 Hz; 2H, triazolyl-CH_2-C**H**$_2$), 1.45 (m, 2H, NH-CH_2-C**H**$_2$), 1.43 (s, 9H, CH_3), 1.37-1.27 (m, 4H, NH-CH_2-CH_2-C**H**$_2$-C**H**$_2$).

^{13}C NMR (176 MHz, $CDCl_3$) δ (ppm) = 156.2 (**C**=O), 152.0 ($C3_{triazole}$), 143.0 ($C5_{triazole}$), 79.3 (**C**$(CH_3)_3$), 49.8 (triazolyl-**C**H_2), 40.5 (NH-**C**H_2), 30.1 (NH-CH_2-**C**H_2), 29.9 (triazolyl-CH_2-**C**H_2), 28.6 (**C**H_3), 26.3, 26.3 (NH-CH_2-CH_2-**C**H_2-**C**H_2).

ESI-MS: cacld for $[M + Na]^+$ *m/z* = 291.1797, found *m/z* = 291.1784.

5.2.4.4 Synthesis of 6-(1H-1,2,4-triazol-1-yl)hexan-1-amine hydrochloride (THA)

To the solution of 0.426 g (1.59 mmol) THA-Boc in 10 mL 1,4-dioxane 3 mL 4 M HCl/dioxane were added. The reaction was monitored by TLC (EtOAc/MeOH 9:1). After the reaction was complete, the solvent was removed *in vacuo* to give THA as white solid (0.297 g; 1.45 mmol; 91 %).

T_{mp} = 153 °C

^{1}H NMR (700 MHz; DMSO-d_6) δ (ppm) = 9.28 (s, 1H, $H5_{triazole}$), 8.47 (s, 1H, $H3_{triazole}$), 8.15 (br s, 3H, NH_3^+), 4.26 (t, $^3J_{HH}$ = 7.0 Hz; 2H, triazolyl-C**H**$_2$), 2.71 (m, 2H, NH_3^+-C**H**$_2$), 1.79 (quint, 2H, triazolyl-CH_2-C**H**$_2$), 1.54 (quint, 2H, NH_3^+-CH_2-C**H**$_2$), 1.33 (quint, 2H, NH_3^+-CH_2-CH_2-C**H**$_2$), 1.22 (quint, 2H, triazolyl-CH_2-CH_2-C**H**$_2$).

^{13}C NMR (176 MHz, DMSO-d_6) δ (ppm) = 147.9 ($C3_{triazole}$), 142.8 ($C5_{triazole}$), 49.44 (triazolyl-**C**H_2), 38.5 (NH_3^+-**C**H_2), 28.5 (triazolyl-CH_2-**C**H_2), 26.6 (NH_3^+-CH_2-**C**H_2), 25.2 (NH_3^+-CH_2-CH_2-**C**H_2), 25.1 (triazolyl-CH_2-CH_2-**C**H_2).

ESI-MS: cacld for $[M + H]^+$ *m/z* = 169.1448, found *m/z* = 169.1446.

5.2.4.5 Synthesis of 6-((tert-butoxycarbonyl)amino)-N,N,N-trimethylhexan-1-aminium bromide (TAHA-Boc)

In a 25 mL flask 1.0 g (3.57 mmol) BBHA was dissolved in 10 mL EtOH, 1.6 mL NMe_3 solution in EtOH (4.2 M, 33 %; 6.7 mmol) were added to the solution. The flask was sealed and placed

onto an oil bath at 50 °C for 20 h. Then, the solvent and the unreacted NMe_3 were evaporated *in vacuo*, followed by careful drying *in vacuo* at 80 °C to remove EtOH completely. TAHA-Boc was obtained as white crystalline solid and was reacted further *in situ*.

^{1}H NMR (700 MHz, DMSO-d_6): 6.78 (t, $^3J_{HH}$ = 5.5 Hz, 1H, N**H**), 3.27 (m, 2H, Me_3N^+-C**H**$_2$), 3.05 (s, 9H, N^+(C**H**$_3$)$_3$), 2.90 (dt, 2H, NH-C**H**$_2$), 1.65 (m, 2H, Me_3N^+-CH_2-C**H**$_2$), 1.43–1.32 (m, 11H, NH-CH_2-C**H**$_2$ and C(**C**H_3)$_3$), 1.32-1.21 (m, 4H, Me_3N^+-CH_2-CH_2-C**H**$_2$ and NH-CH_2-CH_2-C**H**$_2$).
^{13}C NMR (176 MHz, DMSO-d_6): 155.5 (**C**=O), 77.3 (**C**$(CH_3)_3$), 65.2 (Me_3N^+-**C**H_2), 52.1 (N^+(**C**H_3)$_3$), 39.6 (NH-**C**H_2), 29.2 (NH-CH_2-**C**H_2), 28.3 (**C**H_3), 25.7, 25.4 (Me_3N^+-CH_2-CH_2-**C**H_2 and NH-CH_2-CH_2-**C**H_2), 22.0 (Me_3N^+-CH_2-**C**H_2).
ESI-MS: cacld for $[M]^+$ *m/z* = 259.2386, found *m/z* = 259.2363.

5.2.4.6 Synthesis of N^1,N^1,N^1-trimethylhexane-1,6-diaminium (chloride/bromide) (TAHA)

TAHA-Boc was resolved in 2 mL EtOH and to the solution 2 mL 4 M HCl/dioxane were added. The reaction mixture was stirred for one day followed by solvent removal *in vacuo*. After drying *in vacuo* for 5 h at 70 °C TAHA was obtained in a quantitative yield as a highly hygroscopic solid and stored in a desiccator over $CaCl_2$.

^{1}H NMR (700 MHz, DMSO-d_6): 8.12 (br s, 3H, N**H**$_3^+$), 3.33 (m, 2H, Me_3N^+-C**H**$_2$), 3.08 (s, 9H, N^+(C**H**$_3$)$_3$), 2.75 (t, $^3J_{HH}$ = 6.8 Hz, 2H, NH_3^+-C**H**$_2$), 1.67 (m, 2H, Me_3N^+-CH_2-C**H**$_2$), 1.60 (quint, $^3J_{HH}$ = 7.6 Hz, 2H, NH-CH_2-C**H**$_2$), 1.37 (quint, $^3J_{HH}$ = 7.5 Hz, 2H, NH-CH_2-CH_2-C**H**$_2$), 1.28 (m, 2H, Me_3N^+-CH_2-CH_2-C**H**$_2$).
^{13}C NMR (176 MHz, DMSO-d_6): 65.0 (Me_3N^+-**C**H_2), 52.1 (N^+(**C**H_3)$_3$), 38.4 (NH_3^+-**C**H_2), 26.4 (NH-CH_2-**C**H_2), 25.1 (NH-CH_2-CH_2-**C**H_2), 25.0 (Me_3N^+-CH_2-CH_2-**C**H_2), 21.7 (Me_3N^+-CH_2-**C**H_2).
ESI-MS: cacld for $[M]^+$ *m/z* = 159.1861, found *m/z* = 159.1859.

5.2.4.7 Synthesis of 1-(6-((tert-butyloxycarbonyl)amino)hexyl)-pyridin-1-ium bromide (PHA-Boc)

The synthesis was conducted within the scope of D. Helle's Bachelor thesis.[312]
To 0.753 g (2.69 mmol) BBHA in a round-bottom flask 0.4 mL (0.393 g; 4.97 mmol) pyridine were added followed by stirring for 24 h at 80 °C. Subsequently, the mixture was diluted in 15 mL

EtOH and evaporated. The product was dried *in vacuo*. PHA-Boc (0.765 g; 2.13 mmol; 79 %) was obtained as an orange film.

^{1}H NMR (700 MHz, $CDCl_3$) δ (ppm) = 9.55 (m, 2H, C**H**$_{ortho}$); 8.52 (dd, $^{3}J_{HH}$ = 7.8 Hz, 1H, C**H**$_{para}$); 8.13 (dd, $^{3}J_{HH}$ = 6.9 Hz; 2H, C**H**$_{metha}$); 4.99 (t, $^{3}J_{HH}$ = 7.2 Hz, 2H, Py-C**H**$_2$); 4.79 (s, 1H, N**H**); 3.03 (m, 2H, NH-C**H**$_2$); 2.05 (m, 2H, Py-CH_2-C**H**$_2$); 1.44 (m, 2H, NH-CH_2-C**H**$_2$); 1.39 (s, 9H, C(C**H**$_3$)$_3$); 1.35 (m, 4H, Py-CH_2-CH_2-C**H**$_2$ und NH-CH_2-CH_2-C**H**$_2$).
^{13}C NMR (176 MHz, $CDCl_3$) δ (ppm) = 156.3 (**C**=O); 145.4 (**C**H$_{para}$); 145.4 (**C**H$_{ortho}$); 128.6 (**C**H$_{meta}$); 79.2 (**C**(CH$_3$)$_3$); 61.9 (Py-**C**H$_2$); 40.3 (NH-**C**H$_2$); 32.0 (Py-CH_2-**C**H$_2$); 29.8 (NH-CH_2-**C**H$_2$); 28.6 (C(**C**H$_3$)$_3$); 26.1 (NH-CH_2-CH_2-**C**H$_2$); 25.6 (Py-CH_2-CH_2-**C**H$_2$).
ESI-MS: cacld for $[M]^+$ *m/z* = 279.2067, found *m/z* = 279.2082.

5.2.4.8 Synthesis of 1-(6-((tert-butyloxycarbonyl)amino)hexyl)-1H-imidazole (IHA-Boc)

The synthesis was conducted within the scope of D. Helle's Bachelor thesis.[312]
Solution of 1.02 g (3.64 mmol) BBHA in 6 mL THF was combined with a solution of 0.25 g (3.63 mmol) imidazole in 5 mL THF in a round-bottom flask. To the mixture a solution of 0.84 g (5.53 mmol) DBU in 3 mL THF was added dropwise over 15 min at 0 °C. The reaction mixture was stirred for 1 h at cooling and 144 h at 55 °C. A precipitate formed upon addition of 30 mL EtOAc was removed by filtration, and the solvent from the filtrate was removed *in vacuo*. The residue was resolved in EtOAc (40 mL) and washed with water (50 mL). The aqueous phase was extracted once again with 40 mL EtOAc, and the combined organic phases were dried over Na_2SO_4. The solvent was removed by evaporation, and the product was purified by column chromatography (SiO_2; 100 % EtOAc) followed by drying *in vacuo*. IHA-Boc (0.14 g; 0.52 mmol; 14 %) was obtained as a colorless film.

^{1}H NMR (700 MHz, $CDCl_3$) δ (ppm) = 7.49 (s, 1H, N=C**H**-N); 7.06 (s, 1H, CH_2-N-C**H**=CH); 6.90 (s, 1H, CH_2-N-CH=C**H**); 4.51 (s, 1H, N**H**); 3.92 (t, $^{3}J_{HH}$ = 7.1 Hz, 2H, imidazolyl-CH_2); 3.09 (m, 2H, NH-C**H**$_2$); 1.78 (tt, $^{3}J_{HH}$ = 7.2 Hz, 2H, imidazolyl-CH_2-C**H**$_2$); 1.46 (m, 2H, NH-CH_2-C**H**$_2$); 1.43 (m, 9H, C(C**H**$_3$)$_3$); 1.32 (m, 4H, imidazolyl-CH_2-CH_2-C**H**$_2$ and NH-CH_2-CH_2-C**H**$_2$).
^{13}C NMR (176 MHz, $CDCl_3$) δ (ppm) = 156.2 (**C**=O); 137.2 (N=**C**H-N); 129.4 (CH_2-N-**C**H=CH); 119.0 (CH_2-N-CH=**C**H); 79.4 (**C**(CH$_3$)$_3$); 47.2 (imidazolyl-**C**H$_2$); 40.6 (NH-**C**H$_2$); 31.2 (imidazolyl-CH_2-**C**H$_2$); 30.2 (NH-CH_2-**C**H$_2$); 28.6 (C(**C**H$_3$)$_3$); 26.4 (imidazolyl-CH_2-CH_2-C**H**$_2$ and NH-CH_2-CH_2-C**H**$_2$).
ESI-MS: cacld for $[M + H]^+$ *m/z* = 268.2020, found *m/z* = 268.2011.

5.2.5 Synthesis of VDMA[306,307]

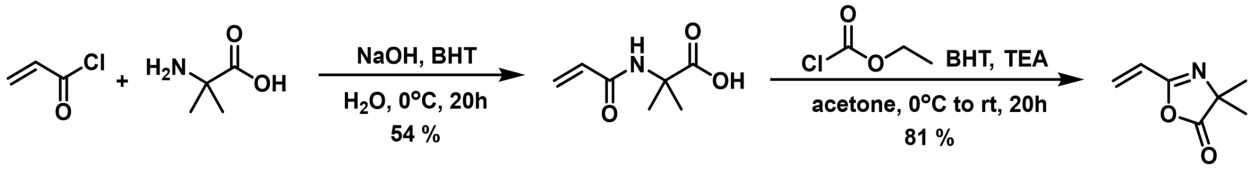

Scheme 15. Synthesis of VDMA.

5.2.5.1 Synthesis of 2-acrylamido-2-methylpropanoic acid

In the solution of 8.85 g (220 mmol) NaOH in 22 mL H_2O 25 mg (0.11 mmol) BHT and subsequently 10.0 g (97 mmol) methyl alanine were dissolved. The solution was cooled down to 0 °C and 9 mL (110 mmol) acryloyl chloride were added dropwise over 30 min. After stirring for 20 h 11.5 mL HCl (conc.) were added, and the mixture was stirred for additional 2 h. The white precipitate was isolated by filtration and washed with 0.1 M HCl on the frit followed by recrystallization from H_2O/EtOH (1:1, v/v). 2-acrylamido-2-methylpropanoic acid was obtained as a white solid (8.20 g; 52.2 mmol; 54 %).

T_{mp} = 192 °C (Lit.: 202 °C[306]; 196–197 °C[370]).
^{1}H NMR (700 MHz; DMSO-d_6) δ (ppm) = 12.17 (br s, 1H, COO**H**); 8.24 (s, 1H, N**H**); 6.25 (dd, $^3J_{HH}$ = 17.1 Hz, $^3J_{HH}$ = 10.3 Hz; 1H, CH_2=C**H**); 6.05 (dd, $^3J_{HH}$ = 17.1 Hz, $^2J_{HH}$ = 2.2 Hz; 1H, C$\mathbf{H}_{cis}$); 5.57 (dd, $^3J_{HH}$ = 10.2 Hz, $^2J_{HH}$ = 2.2 Hz; 1H, C$\mathbf{H}_{trans}$); 1.36 (s, 6H, C$\mathbf{H}_3$).
^{13}C NMR (176 MHz; DMSO-d_6) δ (ppm) = 175.4 (**C**(O)OH); 163.8 (**C**(O)-NH); 131.6 (CH_2=**C**H); 125.3 (**C**H_2=CH); 54.8 (**C**$(CH_3)_2$); 24.9 (**C**H_3).
ESI-MS: cacld for $[M + Na]^+$ *m/z* = 180.0637, found *m/z* = 180.0626.

5.2.5.2 Synthesis of 2-vinyl-4,4-dimethyl azlactone (VDMA)

Under Ar atmosphere 4.0 g (25.5 mmol) 2-acrylamido-2-methylpropanoic acid and 18 mg (0.08 mmol) BHT were suspended in 80 mL acetone. The solid dissolved upon addition of 5.25 mL (38 mmol) triethylamine. The solution was stirred for 20 min and then cooled down to 0 °C followed by adding 2.5 mL (25.5 mmol) ethyl chloroformate dropwise over 20 min. The mixture was stirred for 3 h at 0 °C and then for additional 16 h at RT. Formation of a white precipitate was observed. The precipitate was filtered out and washed with acetone on the frit. The filtrate was evaporated, a white precipitate was formed again. To the residue 50 mL *iso*-hexane was added and the filtration/evaporation cycle was repeated 3 times until no precipitate formation

in the residue occurred. VDMA was obtained as colorless to slightly yellow oil (2.88 g; 20.7 mmol; 81 %).

^{1}H NMR (700 MHz, $CDCl_3$) δ (ppm) = 6.32–6.20 (m, 2H, CH_2=C**H** and C$\mathbf{H}_{cis}$); 5.93 (dd, 1H, C$\mathbf{H}_{trans}$); 1.46 (s, 6H, C$\mathbf{H}_3$).
^{13}C NMR (176 MHz, $CDCl_3$) δ (ppm) = 180.9 (**C**=O); 159.2 (O-**C**=N); 129.2 (**C**H_2); 124.1 (**C**H); 65.9 (**C**$(CH_3)_2$); 24.8 (**C**H_3).
ESI-MS: cacld for $[M + H]^+$ *m/z* = 140.0712, found *m/z* = 140.0706.

5.2.6 Synthesis of the photo-crosslinker DMIEA[213,301]

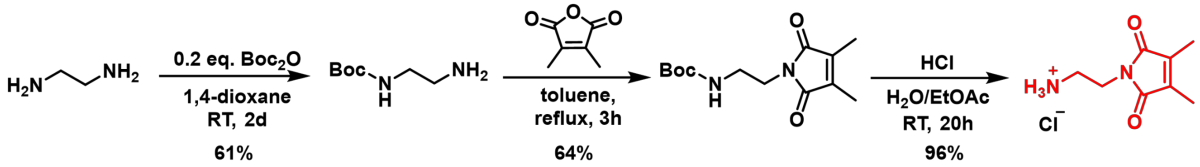

Scheme 16. Synthesis of the crosslinker DMIEA.

5.2.6.1 Synthesis of tert-butyl (2-aminoethyl)carbamate (EDA-Boc)

In a 1000 mL flask with an attached $CaCl_2$ tube 33.3 mL (0.5 mol) ethylene diamine were dissolved in 200 mL 1,4-dioxane and to the mixture a solution of 21.92 g (0.1 mol) di-*tert*-butyl dicarbonate in 200 mL 1,4-dioxane was dropwise added over 3 h. After 48 h the mixture was filtered, and the filtrate was evaporated. To the yellow oily residue 300 mL water were added, which lead to the formation of a white precipitate. After it was removed by filtration, the filtrate was saturated with NaCl, and the formed precipitate was filtered out as well. The yellow solution was extracted with DCM (8×100 mL). The combined organic phases were dried over $MgSO_4$, and the DCM was evaporated to obtain *tert*-butyl (2-aminoethyl)carbamate as a yellow oil (9.73 g; 60.7 mmol; 61 %).

^{1}H NMR (700 MHz, $CDCl_3$) δ (ppm) = 4.94 (br s, 1H, N**H**); 3.17 (br q, 2H, C$\mathbf{H}_2$-NH), 2.79 (t, $^{3}J_{HH}$ = 5.9 Hz; 2H, C$\mathbf{H}_2$-NH_2); 1.43 (s, 6H, C$\mathbf{H}_3$)
^{13}C NMR (176 MHz, $CDCl_3$) δ (ppm) = 156.4 (**C**=O); 79.4 (**C**$(CH_3)_3$); 43.5 (**C**H_2-NH); 42.0 (**C**H_2-NH_2); 28.6 (**C**H_3).
ESI-MS: cacld for $[M + Na]^+$ *m/z* = 161.1402, found *m/z* = 161.1394.

5.2.6.2 Synthesis of tert-butyl (2-(3,4-dimethyl-2,5-dioxo-2,5-dihydro-1H-pyrrol-1-yl)ethyl)carbamate (DMIEA-Boc)

In a 500 mL round-bottom flask equipped with a Dean–Stark apparatus and a reflux 2,3-dimethylmaleic anhydride (7.06 g; 56 mmol) was dissolved in 200 mL toluene. As the mixture was heated up to 130 °C, a solution of EDA-Boc (9.00 g; 56 mmol) in 70 mL toluene was dropwise added within 15 min. After reacting under reflux for 4 h the mixture became orange, the heating was stopped, and the solvent was evaporated. The crude product (orange oil) was dissolved in 30 mL $CHCl_3$ and precipitated into cooled (acetone/N_2 bath) pentane. The solid was collected by filtration and the precipitation was repeated once again. After drying *in vacuo* DMIEA-Boc (9.589 g; 35.74 mmol; 64 %) was obtained as brownish solid.

T_{mp} = 108.5 °C (Lit. 106 °C[301])

^{1}H NMR (700 MHz, $CDCl_3$) δ (ppm) = 4.81 (br s, 1H, N**H**); 3.60 (t, $^3J_{HH}$ = 5.5 Hz; 2H, C**H**$_2$-N); 3.30 (br q, 2H, C**H**$_2$-NH); 1.95 (s, 6H, C(C**H**$_3$)=C(C**H**$_3$)); 1.39 (C(C**H**$_3$)$_3$).

^{13}C NMR (176 MHz, $CDCl_3$) δ (ppm) = 172.4 (N-**C**=O); 156.1 (**C**(=O)-NH); 137.5 (**C**(CH$_3$)=**C**(CH$_3$)); 79.5 (**C**(CH$_3$)$_3$); 40.0 (**C**H$_2$-NH); 38.2 (**C**H$_2$-N); 28.5 (C(**C**H$_3$)$_3$); 8.9 (C(**C**H$_3$)=C(**C**H$_3$)).

ESI-MS: cacld for $[M + Na]^+$ *m/z* = 291.1321, found *m/z* = 291.1311.

5.2.6.3 Synthesis of 1-(2-aminoethyl)-3,4-dimethyl-1H-pyrrole-2,5-dione (DMIEA)

In a 250 mL round-bottom flask 9.0 g DMIEA-Boc were suspended in 100 mL ethyl acetate, and to the mixture 6.5 mL HCl (conc.) were added dropwise over 15 min. After 19 h a brownish precipitate formed was collected by filtration. The filtrate was turbid; therefore, it was filtered once again. Both solid fractions were combined and dried *in vacuo*. DMIEA (6.603 g; 32.26 mmol; 96 %) was obtained as a brownish solid.

T_{mp} = 209–211 °C (decomposition). (Lit. 210 °C[301])

^{1}H NMR (700 MHz, DMSO-d_6) δ (ppm) = 8.20 (br s, 3H, N**H**$_3^+$); 3.65 (t, $^3J_{HH}$ = 6.2 Hz; 2H, C**H**$_2$-N); 2.93 (m, 2H, C**H**$_2$-NH$_3^+$); 1.90 (s, 6H, C**H**$_3$).

^{13}C NMR (176 MHz, DMSO-d_6) δ (ppm) = 171.6 (**C**=O); 136.9 (**C**(CH$_3$)); 37.3 (**C**H$_2$-NH$_3^+$); 35.0 (**C**H$_2$-N); 8.5 (**C**H$_3$).

ESI-MS: cacld for $[M]^+$ *m/z* = 169.0972, found *m/z* = 169.0975.

5.2.7 Synthesis of adhesion promoter[213]

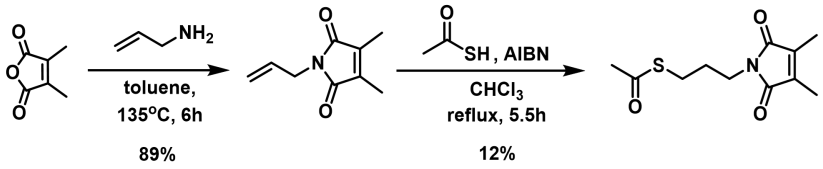

Scheme 17. Synthesis of the adhesion promoter.

5.2.7.1 Synthesis of 1-allyl-3,4-dimethyl-1H-pyrrole-2,5-dione (ADMI)

15 mL (200 mmol) allyl amine were added to the solution of 2,3-dimethylmaleic anhydride (5.00 g; 39.65 mmol) in 50 mL toluene in a 150 mL three-necked flask equipped with a Dean–Stark apparatus and a reflux. The reaction mixture was heated up to 135 °C and stirred for 6 h. Further, the solvent was removed by evaporation and the crude product (yellow oil) was purified by column chromatography (SiO_2; EtOAc:*iso*-hexane 1:2; $R_f = 0.9$). ADMI (5.805 g; 35.14 mmol; 89 %) was obtained as a colorless liquid.

^{1}H NMR (700 MHz, $CDCl_3$) δ (ppm) = 5.79 (ddt, $^3J_{HH}$ = 17.1 Hz, $^3J_{HH}$ = 10.2 Hz, $^3J_{HH}$ = 5.6 Hz; 1H, CH_2=C**H**); 5.16 (ddt, $^2J_{HH}$ = 1.6 Hz, $^3J_{HH}$ = 17.2 Hz, $^4J_{HH}$ = 1.4 Hz; 1H, C**H**$_{cis}$); 5.13 (ddt, $^2J_{HH}$ = 1.3 Hz, $^3J_{HH}$ = 10.3 Hz, $^4J_{HH}$ = 1.3 Hz; 1H, C**H**$_{trans}$); 4.08 (dt, $^2J_{HH}$ = 1.5 Hz, $^3J_{HH}$ = 5.6 Hz; 2H, C**H**$_2$-N); 1.96 (s, 6H, C**H**$_3$).
^{13}C NMR (176 MHz, $CDCl_3$) δ (ppm) = 172.0 (**C**=O); 137.4 (**C**(CH_3)); 132.2 (CH_2=**C**H); 117.5 (**C**H_2=CH); 40.2 (**C**H_2-N); 8.9 (**C**H_3).
ESI-MS: cacld for $[M + H]^+$ *m/z* = 166.0868, found *m/z* = 166.0854; cacld for $[M + Na]^+$ *m/z* = 188.0687, found *m/z* = 188.0676.

5.2.7.2 Synthesis of S-(3-(3,4-dimethyl-2,5-dioxo-2,5-dihydro-1H-pyrrol-1-yl)propyl) ethanethioate (DMIPTA)

In a 100 mL round-bottom flask ADMI (2.50 g; 15.13 mmol), AIBN (0.15 g; 0.91 mmol) and thioacetic acid (1.62 mL; 23.0 mmol) were dissolved in 15 mL $CHCl_3$. The solution was purged with Ar for 30 min followed by stirring at reflux for 5.5 h. Further, the mixture was washed with 25 mL saturated Na_2CO_3 solution and the aqueous phase was extracted with petroleum ether (2×45 mL). The combined organic phases were washed with brine (80 mL) and dried over $MgSO_4$. After evaporation of the solvent *in vacuo* the crude product was purified by column chromatography (SiO_2; EtOAc:*iso*-hexane 1:15; $R_f = 0.1$). DMIPTA (0.43 g; 1.77 mmol; 12 %) was obtained as an orange liquid.

^{1}H NMR (700 MHz, $CDCl_3$) δ (ppm) = 3.53 (t, $^{3}J_{HH}$ = 7.0 Hz; 2H, C**H**$_2$-N); 2.82 (t, $^{3}J_{HH}$ = 7.3 Hz; 2H, C**H**$_2$-S); 2.30 (s, 3H, C**H**$_3$-CO); 1.94 (s, 6H, C(C**H**$_3$)); 1.84 (quint, $^{3}J_{HH}$ = 7.0 Hz; 2H, CH_2-C**H**$_2$-CH_2).

^{13}C NMR (176 MHz, $CDCl_3$) δ (ppm) = 195.7 (**C**(=O)-S); 172.3 (**C**(=O)-N); 137.4 (**C**(CH_3)); 36.9 (**C**H_2-N); 30.8 (**C**H_3-CO); 28.9 (CH_2-**C**H_2-CH_2); 26.5 (**C**H_2-S); 8.9 (C(**C**H_3)).

ESI-MS: cacld for $[M + Na]^+$ *m/z* = 264.0670, found *m/z* = 264.0657.

5.2.8 Synthesis and modification of the co-polymer P10

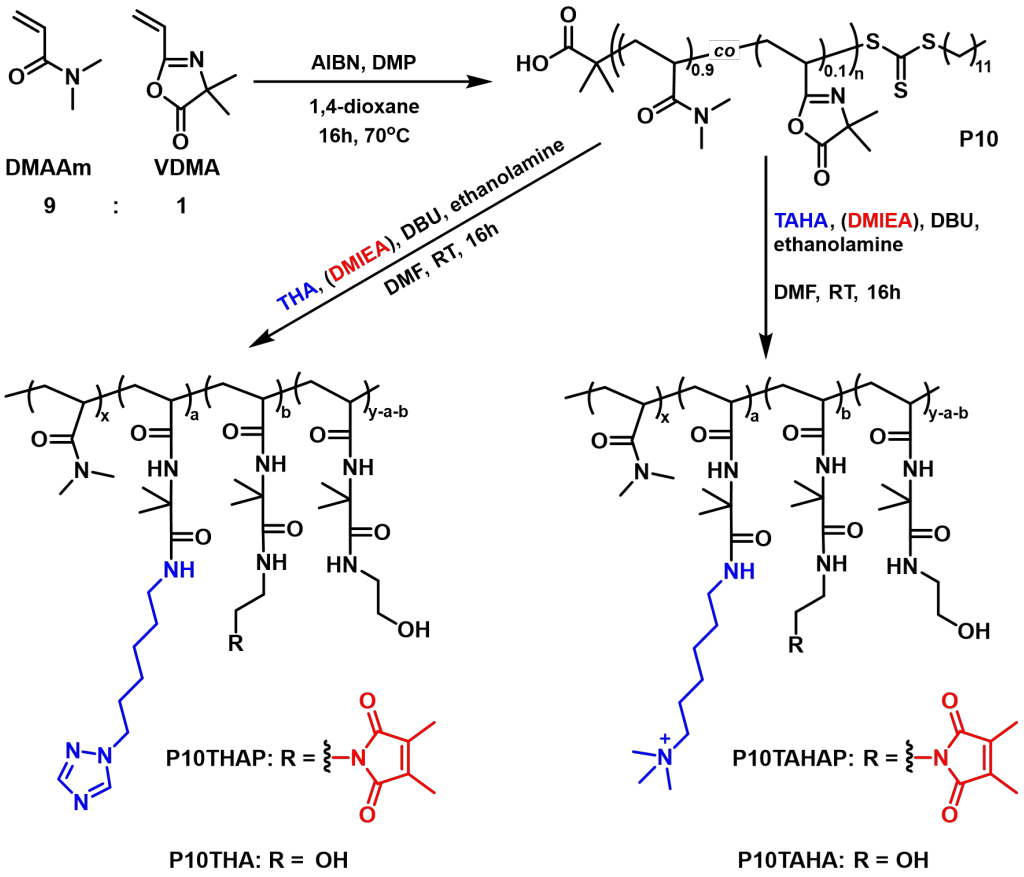

Scheme 18. Synthesis of P10 and modification with guest moieties (and photo-crosslinker). End groups are omitted for simplicity.

5.2.8.1 Synthesis of poly(DMAAm$_{0.9}$-co-VDMA$_{0.1}$) (P10)

In a 25 mL pear-shaped flask 4.0 g (40.4 mmol) DMAAm, 0.628 g (4.5 mmol) VDMA, 20.5 mg (0.06 mmol) DMP and 4.6 mg (0.03 mmol) AIBN were dissolved in 12 mL 1,4-dioxane. The flask was sealed with a septum and the solution was degassed by purging with Ar for 30 min followed by placing into a pre-heated oil bath at 70 °C. After 15 h the reaction was quenched by freezing the mixture in liquid nitrogen and then unsealing the vessel. After the mixture has thawed, it was

diluted with 12 mL THF and dropwise precipitated into cooled (acetone/N_2 bath). The supernatant was decanted, the crude product was resolved in ca. 20 mL THF and dropwise added to Et_2O at RT leading to a formation of a white precipitate which was filtered and dried in vacuo. P10 was obtained as a white solid (4.309 g; 93 %) and stored under inert gas at -25 °C to prevent hydrolysis of VDMA units in the air.

^{1}H NMR (500 MHz; $CDCl_3$) δ (ppm) = 3.42–2.74 (m, 4166H, DMAAm-C**H**$_3$), 2.74–2.11 (m, 775H, backbone-C**H**), 2.09–0.94 (m, 2040H, backbone-C**H**$_2$ and VDMA-C**H**$_3$), 0.87 (t, $^3J_{HH}$ = 6.4 Hz; 3H, $(CH_2)_{11}$-C**H**$_3$).
GPC (HFIP + 0.05 M CF_3COOK, PMMA calibration): M_n = 46500, $Đ$ = 1.82.

5.2.8.2 Synthesis of THA- and DMIEA-modified P10 (P10THAP)

53.0 mg (0.25 mmol) THA were suspended in 3 mL DMF and dissolved upon addition of 70 mg (0.46 mmol) DBU. 50.0 mg DMIEA (0.24 mmol) were dissolved in 2 mL DMF with 50 mg (0.33 mmol) DBU.
To the solution of 508 mg P10 (0.49 mmol VDMA units) in 5 mL DMF the THA solution was added and after stirring for 23 h the DMIEA solution. The reaction was covered from light and stirred at RT for additional 24 h followed by addition of 0.12 mL (1.90 mmol) of ethanolamine and further stirring for 1 h. Afterwards the solution was dropwise added to 120 mL Et_2O at RT, resulting in white precipitation. The suspension was filtered, then the filter cake and the residue in the flask were dissolved in ca. 20 mL acetone, which was removed *in vacuo* and the crude product (a transparent film) was dissolved in 20 mL water and purified by dialysis for 48 h. Freeze-drying of the solution gave product as white solid (0.567 g; 95 %).

^{1}H NMR (500 MHz, D_2O) δ (ppm) = 8.48 (s, 1H, triazole N=C**H**-N-CH_2); 8.08 (s, 1H, triazole N-C**H**=N-N-CH_2); 4.28 (br, 2H, $C_2H_2N_3$-C**H**$_2$); 3.63 (br, 1.8H, DMIEA-C**H**$_2$); 3.28–2.84 (m, 132.5H, N(C**H**$_3$)$_2$ and $C_2H_2N_3$-C_5H_{10}-C**H**$_2$); 2.84–2.35 (m, 23H, backbone C**H**); 1.69 (s, 5H, C(C**H**$_3$)=C(C**H**$_3$)); 1.92–1.12 (m, 71H, backbone C**H**$_2$, C(=O)-NH-C(C**H**$_3$)$_2$ and $C_2H_2N_3$-CH_2-C**H**$_2$-C**H**$_2$-C**H**$_2$-C**H**$_2$).
GPC (HFIP + 0.05 M CF_3COOK, PMMA calibration): M_n = 59800, $Đ$ = 2.04.

5.2.8.3 Synthesis of THA-modified P10 (P10THA)

65.7 mg (0.32 mmol) THA were suspended in 2 mL DMF and dissolved upon addition of 50 mg (0.30 mmol) DBU. The solution was added to 320 mg P10 (0.31 mmol VDMA units) dissolved in 8 mL DMF. The reaction was stirred at RT for 16 h followed by addition of 0.12 mL (1.90 mmol) of ethanolamine and further stirring for 1 h. Afterwards the polymer was dropwise precipitated into 60 mL Et_2O at RT. The suspension was filtered, and the residue as well as the filter cake were dissolved in ca. 10 mL acetone. The solvent was removed *in vacuo* and the crude product (a transparent film) was dissolved in 10 mL water and purified by dialysis for 48 h. Freeze-drying of the solution gave product as white solid (0.340 g; 89 %).

^{1}H NMR (500 MHz, D_2O) δ (ppm) = 8.48 (s, 1H, triazole N=C**H**-N-CH_2); 8.09 (s, 1H, triazole N-C**H**=N-N-CH_2); 4.28 (br, 2H, $C_2H_2N_3$-C**H**$_2$); 3.34–2.84 (m, 82.5H, N(C**H**$_3$)$_2$ and $C_2H_2N_3$-C_5H_{10}-C**H**$_2$); 2.84–2.42 (m, 14H, backbone C**H**); 1.96–1.13 (m, 71H, backbone C**H**$_2$, C(=O)-NH-C(C**H**$_3$)$_2$ and $C_2H_2N_3$-CH_2-C**H**$_2$-C**H**$_2$-C**H**$_2$-C**H**$_2$).
GPC (HFIP + 0.05 M CF_3COOK, PMMA calibration): M_n = 57500, $Đ$ = 1.70.

5.2.8.4 Synthesis of TAHA- and DMIEA-modified P10 (P10TAHAP)

68.0 mg (0.29 mmol) TAHA were suspended in 2 mL DMF and dissolved upon addition of 70 mg (0.46 mmol) DBU. 53.0 mg DMIEA (0.26 mmol) were dissolved in 2 mL DMF with 70 mg (0.46 mmol) DBU.
To the solution of 517 mg P10 (0.50 mmol VDMA units) in 5 mL DMF the TAHA and DMIEA solution was added. The reaction was stirred at RT for 21 h followed by addition of 0.14 mL (2.21 mmol) of ethanolamine and further stirring for 1 h. Afterwards the polymer was precipitated into 90 mL Et_2O at RT. The suspension was filtered, then the filter cake and the residue in the flask were dissolved in ca. 20 mL water, and the crude product was purified by dialysis for 24 h. Freeze-drying of the solution gave product as white solid (0.556 g; 90 %).

^{1}H NMR (500 MHz, D_2O) δ (ppm) = 3.64 (br, 2H, DMIEA-C**H**$_2$); 3.38–3.30 (m, 4.3H, $(CH_3)_3N^+$-C**H**$_2$); 3.30–2.85 (m, 202H, N(C**H**$_3$)$_2$, C**H**$_2$-NH and (C**H**$_3$)$_3$N$^+$); 2.85–2.36 (m, 33H, backbone C**H**); 1.97 (s, 6H, C(C**H**$_3$)=C(C**H**$_3$)); 1.91–1.13 (m, 103H, backbone C**H**$_2$, C(=O)-NH-C(C**H**$_3$)$_2$ and (C**H**$_3$)$_3$N$^+$-CH_2-C**H**$_2$-C**H**$_2$-C**H**$_2$-C**H**$_2$).
GPC (HFIP + 0.05 M CF_3COOK, PMMA calibration): M_n = 66900, $Đ$ = 2.83.

5.2.8.5 Synthesis of TAHA-modified P10 (P10TAHA)

45.0 mg (0.16 mmol) TAHA were suspended in 3 mL DMF and dissolved upon addition of 60 mg (0.39 mmol) DBU. The solution was added to 306 mg P10 (0.30 mmol VDMA units). The reaction was stirred at RT for 18 h followed by addition of 0.10 mL (1.58 mmol) of ethanolamine and further stirring for 1 h. Afterwards the polymer was dropwise precipitated into 50 mL Et_2O at RT. The suspension was filtered, and the residue as well as the filter cake were dissolved in ca. 10 mL H_2O. The crude product was purified by dialysis for 72 h. Freeze-drying of the solution gave product as white solid (0.263 g; 74 %).

^{1}H NMR (500 MHz, D_2O) δ (ppm) = 3.38–3.30 (m, 2H, $(CH_3)_3N^+$-C**H**$_2$); 3.30–2.85 (m, 81.4H, N(C**H**$_3$)$_2$, C**H**$_2$-NH and (C**H**$_3$)$_3N^+$); 2.85–2.42 (m, 13H, backbone C**H**); 1.92–1.20 (m, 42.4H, backbone C**H**$_2$, C(=O)-NH-C(C**H**$_3$)$_2$ and (C**H**$_3$)$_3N^+$-CH$_2$-C**H**$_2$-C**H**$_2$-C**H**$_2$-C**H**$_2$).

GPC (HFIP + 0.05 M CF_3COOK, PMMA calibration): M_n = 61900, $Đ$ = 1.78.

5.2.9 Synthesis and modification of the co-polymer P20

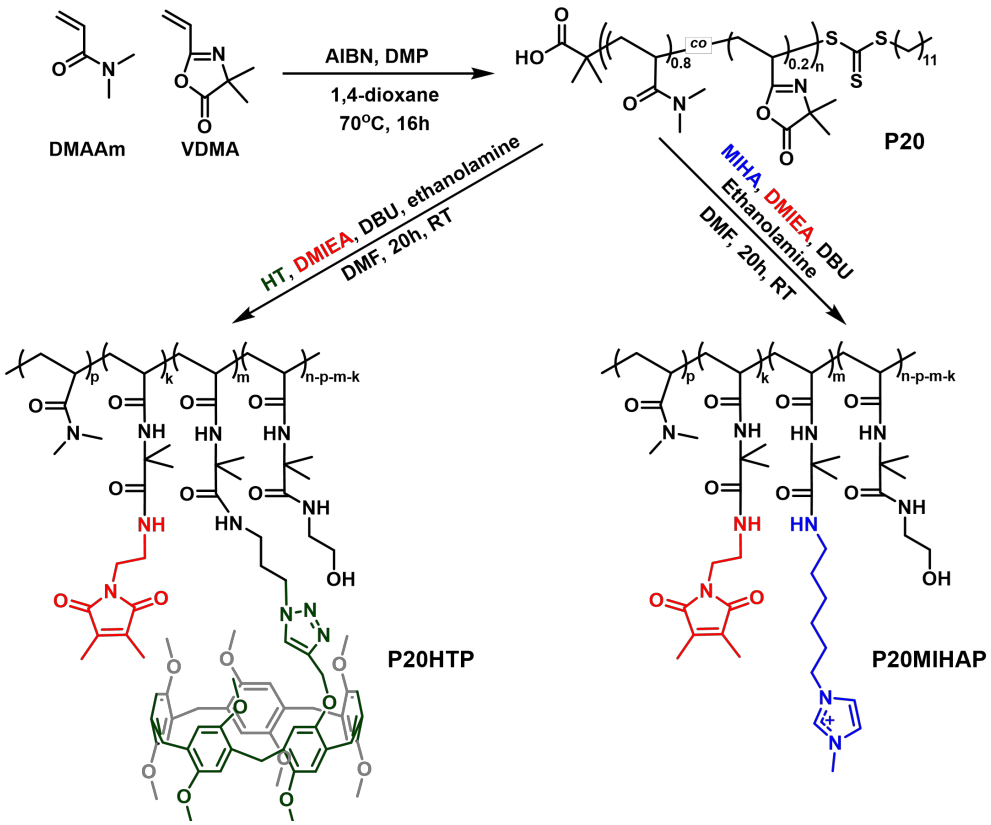

Scheme 19. Synthesis of the co-polymer P20 and its modification with host and guest moieties. End groups are omitted for simplicity.

5.2.9.1 Synthesis of poly(DMAAm$_{0.8}$-co-VDMA$_{0.2}$) (P20)

In a pre-heated Schlenk-tube 0.0115 g (0.032 mmol) DMP, 2.00 g (20.18 mmol) dimethyl acrylamide and 0.698 g (5.02 mmol) VDMA were dissolved in 5 mL 1,4-dioxane and to the solution 0.0026 g (0.016 mmol) AIBN in 1 mL 1,4-dioxane were added. The Schlenk-tube was sealed with a septum, and the mixture was degassed by purging with Ar for 30 min before being placed onto an oil bath at 70 °C. After 16 h the reaction was quenched by freezing the mixture in liquid nitrogen and exposing it to the air. After the solution has thawed, it was diluted with 6 mL THF and precipitated into 150 mL Et_2O (cooled by acetone/N_2 bath). The supernatant was decanted, and the precipitate was resolved in 10 mL THF followed by precipitation in 300 mL Et_2O at RT. The precipitated was isolated by filtration and dried *in vacuo*. P20 was obtained as a white solid (2.262 g; 83 %).

^{1}H NMR (500 MHz, $CDCl_3$) δ (ppm) = 3.62–2.71 (m, 2850H, N(C**H**$_3$)$_2$); 2.71–2.14 (m, 540H, backbone-C**H**); 2.14–0.90 (m, 1720H, backbone-C**H**$_2$ and VDMA-C**H**$_3$); 0.87 (t, $^3J_{HH}$ = 7.0 Hz; 3H, S-C$_{11}$H$_{22}$-C**H**$_3$).
GPC (HFIP + 0.05 M CF_3COOK, PMMA calibration): M_n = 48400, $Đ$ = 2.08.

5.2.9.2 Synthesis of HT- and DMIEA-modified P20 (P20HTP)

To 0.100 g P20 in a pear-shaped flask two solutions were added: a solution of HT (0.132 g; 0.145 mmol) with DBU (0.091 g; 0.598 mmol) in 5 mL DMF and a solution of DMIEA (0.010 g; 0.049 mmol) with DBU (0.030 g; 0.197 mmol) in 2 mL DMF. The reaction mixture was stirred in dark under Ar at RT for 20 h followed by addition of 0.12 mL (1.90 mmol) ethanolamine and subsequent stirring for 1 h. The mixture was precipitated into 100 mL Et_2O at RT and the precipitate isolated by filtration. The crude product was resolved in 20 mL acetone, the solution dialyzed in water for 24 h and freeze-dried to obtain P20HTP (0.180 g; 76 %) as a white solid.

^{1}H NMR (500 MHz, $CDCl_3$) δ (ppm) = 8.00–7.56 (br, 1H, triazole C**H**); 6.89, 6.82–6.62 (br s, 10H, P5A C**H**$_{Ar}$), 5.00 (s, 2H, O-C**H**$_2$-C(-N)=CH); 4.41 (br, 2H, N=N-N-C**H**$_2$); 3.82–3.70 (br s, 10H, P5A C$_{Ar}$-C**H**$_2$); 3.70–3.53, 3.48 (br s, 27H, P5A O-C**H**$_3$); 3.23–2.74 (m, 52H, N(C**H**$_3$)$_2$); 2.74–2.27 (m, 10H, backbone C**H**); 2.27–0.92 (m, 48H, backbone C**H**$_2$, C(=O)-NH-C(C**H**$_3$)$_2$, C(C**H**$_3$)=C(C**H**$_3$), C(=O)-NH-C**H**$_2$-C**H**$_2$).
GPC (HFIP + 0.05 M CF_3COOK, PMMA calibration): M_n = 103200, $Đ$ = 2.21

5.2.9.3 Synthesis of MIHA- and DMIEA-modified P20 (P20MIHAP)

To 0.200 g P20 in a pear-shaped flask two solutions were added: a solution of MIHA (0.078 g; 0.306 mmol) with DBU (0.084 g; 0.552 mmol) in 5 mL DMF and a solution of DMIEA (0.020 g; 0.098 mmol) with DBU (0.041 g; 0.269 mmol) in 1.5 mL DMF. The reaction mixture was stirred at RT for 20 h followed by addition of 0.12 mL (1.90 mmol) ethanolamine and subsequent stirring for 1 h. The mixture was precipitated into 100 mL Et_2O at RT and the precipitate isolated by filtration. The crude product was resolved in 10 mL water, and the solution dialyzed in water for 24 h. The solvent was evaporated *in vacuo* to obtain P20MIHAP (0.243 g; 87 %) as a white solid.

^{1}H NMR (500 MHz, D_2O) δ (ppm) = 7.51 (s, 1H, CH_3-N-CH=C**H**-N); 7.47 (s, 1H, CH_3-N-C**H**=CH-N); 4.22 (t, $^3J_{HH}$ = 6.8 Hz; 2H, CH_3-$C_3H_3N_2^+$-C**H**$_2$); 3.92 (s, 3H, C**H**$_3$-$C_3H_3N_2^+$); 3.30–2.84 (m, 48H, N(C**H**$_3$)$_2$ and $C_3H_3N_2^+$-C_5H_{10}-C**H**$_2$); 2.84–2.35 (m, 8H, backbone C**H**); 1.96 (s, 1H, C(C**H**$_2$)=C(C**H**$_2$)); 1.88 (br, 2H, $C_3H_3N_2^+$-CH_2-C**H**$_2$); 1.85–1.14 (m, 35H, backbone C**H**$_2$, C(=O)-NH-C(C**H**$_3$)$_2$ and $C_3H_3N_2^+$-CH_2-CH_2-C**H**$_2$-C**H**$_2$-C**H**$_2$).

GPC (HFIP + 0.05 M CF_3COOK, PMMA calibration): M_n = 68900, $Đ$ = 2.57.

5.2.9.4 Synthesis of DMIEA-modified P20 (P20PC)

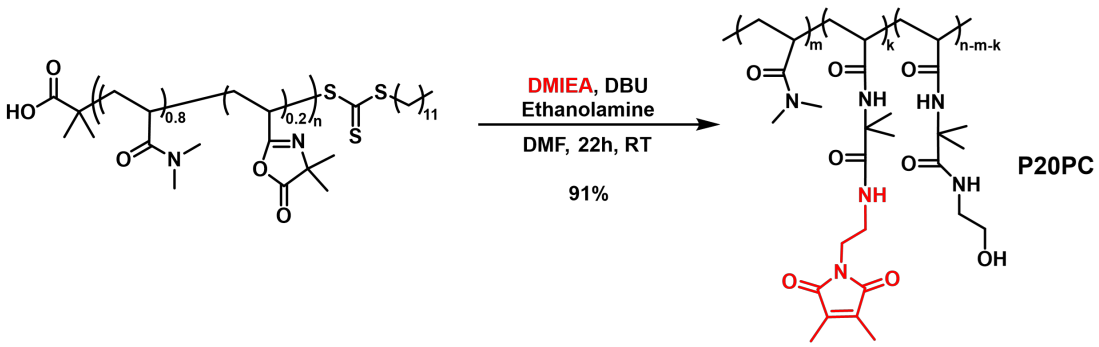

Scheme 20. Synthesis of the photo-crosslinker-modified P20. End groups are omitted for simplicity.

0.300 g P20 dissolved in 5 mL DMF was mixed with a solution of DMIEA (0.108 g; 0.528 mmol) and DBU (0.095 g; 0.624 mmol) in 3 mL DMF in a pear-shaped flask. The reaction mixture was stirred at RT for 22 h followed by addition of 0.12 mL (1.90 mmol) ethanolamine and subsequent stirring for 1 h. The mixture was precipitated into 100 mL Et_2O at RT and the precipitate isolated by filtration. The crude product was resolved in 20 mL water, the solution was dialyzed in water for 72 h, and freeze-dried to obtain P20PC (0.3547 g; 91 %) as a white solid.

^{1}H NMR (500 MHz, D_2O) δ (ppm) = 3.63 (br, 2H, $C_6H_6NO_2$-C**H**$_2$), 3.26–2.83 (m, 35H, N(CH_3)$_2$ and $C_6H_6NO_2$-CH_2-C**H**$_2$); 2.83–2.36 (m, 6H, backbone C**H**); 1.96 (s, 6H, C(C**H**$_3$)=C(C**H**$_3$)); 1.89–0.95 (m, 23H, backbone C**H**$_2$, C(=O)-NH-C(C**H**$_3$)$_2$).

GPC (HFIP + 0.05 M CF_3COOK, PMMA calibration): M_n = 92700, $Đ$ = 4.45.

6 References

[1] L. Voorhaar, R. Hoogenboom, *Chem. Soc. Rev.* **2016**, *45*, 4013.

[2] Y. Gao, M. Wei, X. Li, W. Xu, A. Ahiabu, J. Perdiz, Z. Liu, M. J. Serpe, *Macromol. Res.* **2017**, *25*, 513.

[3] P. Sikdar, M. M. Uddin, T. M. Dip, S. Islam, M. S. Hoque, A. K. Dhar, S. Wu, *Mater. Adv.* **2021**, *2*, 4532.

[4] M. Rodin, J. Li, D. Kuckling, *Chem. Soc. Rev.* **2021**, *50*, 8147.

[5] F. Pinelli, L. Magagnin, F. Rossi, *Mater. Today Chem.* **2020**, *17*, 100317.

[6] J. Homola, *Chem. Rev.* **2008**, *108*, 462.

[7] J. Li, C. Ji, B. Lü, M. Rodin, J. Paradies, M. Yin, D. Kuckling, *ACS Appl. Mater. Interfaces* **2020**, *12*, 36873.

[8] E. A. Appel, J. del Barrio, X. J. Loh, O. A. Scherman, *Chem. Soc. Rev.* **2012**, *41*, 6195.

[9] T. Ogoshi, S. Kanai, S. Fujinami, T. Yamagishi, Y. Nakamoto, *J. Am. Chem. Soc.* **2008**, *130*, 5022.

[10] T. Ogoshi, T. Yamagishi, Y. Nakamoto, *Chem. Rev.* **2016**, *116*, 7937.

[11] X. Shu, S. Chen, J. Li, Z. Chen, L. Weng, X. Jia, C. Li, *Chem. Commun.* **2012**, *48*, 2967.

[12] G. L. Kennedy, *Drug. Chem. Toxicol.* **2004**, *27*, 123.

[13] N. L. Strutt, R. S. Forgan, J. M. Spruell, Y. Y. Botros, J. F. Stoddart, *J. Am. Chem. Soc.* **2011**, *133*, 5668.

[14] Q. Peng, C. Y.-P. Wong, I. W.-Y. Cheuk, J. Y.-C. Teoh, P. K.-F. Chiu, C.-F. Ng, *Int. J. Mol. Sci.* **2021**, *22*.

[15] a) J. M. Lehn, *Pure Appl. Chem.* **1978**, *50*, 871; b) J. M. Lehn, *Science* **1985**, *227*, 849; c) J. M. Lehn, *Science* **1993**, *260*, 1762.

[16] J. W. Steed, J. L. Atwood, *Supramolecular chemistry*, Wiley, Chichester, **2009**.

[17] H.-J. Schneider, *Angew. Chem. Int. Ed.* **2009**, *48*, 3924.

[18] D. B. Varshey, J. R. G. Sander, T. Friščić, L. R. MacGillivray in *Supramolecular chemistry*. *From molecules to nanomaterials* (Eds.: J. W. Steed, P. A. Gale), Wiley, Chichester, **2012**, p. 253.

[19] a) A. Winter, U. S. Schubert, *Chem. Soc. Rev.* **2016**, *45*, 5311; b) H. Li, P. Yang, P. Pageni, C. Tang, *Macromol. Rapid Commun.* **2017**, *38*, 1700109; c) P. Casuso, I. Odriozola, A. Pérez-San Vicente, I. Loinaz, G. Cabañero, H.-J. Grande, D. Dupin, *Biomacromolecules* **2015**, *16*, 3552.

[20] a) N. Holten-Andersen, A. Jaishankar, M. Harrington, D. E. Fullenkamp, G. DiMarco, L. He, G. H. McKinley, P. B. Messersmith, K. Y. C. Lee, *J. Mater. Chem. B* **2014**, *2*, 2467; b) P. Lin, S. Ma, X. Wang, F. Zhou, *Adv. Mater.* **2015**, *27*, 2054; c) A. Andersen, M. Krogsgaard, H. Birkedal, *Biomacromolecules* **2018**, *19*, 1402.

[21] S. Laquerbe, J. Es Sayed, C. Lorthioir, C. Meyer, T. Narita, G. Ducouret, P. Perrin, N. Sanson, *Macromolecules* **2023**, *56*, 7406.

[22] S. K. Yang, S. C. Zimmerman, *Isr. J. Chem.* **2013**, *53*, 511.

[23] a) C. Fonseca Guerra, F. M. Bickelhaupt, J. G. Snijders, E. J. Baerends, *J. Am. Chem. Soc.* **2000**, *122*, 4117; b) H. Szatyłowicz, N. Sadlej-Sosnowska, *J. Chem. Inf. Model.* **2010**, *50*, 2151.

[24] F. H. Beijer, R. P. Sijbesma, H. Kooijman, A. L. Spek, E. W. Meijer, *J. Am. Chem. Soc.* **1998**, *120*, 6761.

[25] S. H. M. Söntjens, R. P. Sijbesma, M. H. P. van Genderen, E. W. Meijer, *J. Am. Chem. Soc.* **2000**, *122*, 7487.

[26] a) B. Zhang, Z. A. Digby, J. A. Flum, E. M. Foster, J. L. Sparks, D. Konkolewicz, *Polym. Chem.* **2015**, *6*, 7368; b) R. Zhang, C. Zhang, Z. Yang, Q. Wu, P. Sun, X. Wang, *Macromolecules* **2020**, *53*, 5937; c) J. Verjans, R. Hoogenboom, *Prog. Polym. Sci.* **2023**, *142*, 101689.

[27] T. Liu, S. Zou, C. Hang, J. Li, X. Di, X. Li, Q. Wu, F. Wang, P. Sun, *Polym. Chem.* **2020**, *11*, 1906.

[28] a) S. Grimme, *Angew. Chem. Int. Ed.* **2008**, *47*, 3430; b) K. Carter-Fenk, J. M. Herbert, *Chem. Sci.* **2020**, *11*, 6758; c) K. Carter-Fenk, J. M. Herbert, *Phys. Chem. Chem. Phys.* **2020**, *22*, 24870.

[29] a) G. B. McGaughey, M. Gagné, A. K. Rappé, *J. Biol. Chem.* **1998**, *273*, 15458; b) K. Carter-Fenk, M. Liu, L. Pujal, M. Loipersberger, M. Tsanai, R. M. Vernon, J. D. Forman-Kay, M. Head-Gordon, F. Heidar-Zadeh, T. Head-Gordon, *J. Am. Chem. Soc.* **2023**, *145*, 24836.

[30] a) G. Némethy, *Angew. Chem. Int. Ed.* **1967**, *6*, 195; b) D. Chandler, *Nature* **2005**, *437*, 640.

[31] F. Biedermann, W. M. Nau, H.-J. Schneider, *Angew. Chem. Int. Ed.* **2014**, *53*, 11158.

[32] a) J. T. Kellis, K. Nyberg, D. Sali, A. R. Fersht, *Nature* **1988**, *333*, 784; b) C. N. Pace, H. Fu, K. L. Fryar, J. Landua, S. R. Trevino, B. A. Shirley, M. M. Hendricks, S. Iimura, K. Gajiwala, J. M. Scholtz, G. R. Grimsley, *J. Mol. Biol.* **2011**, *408*, 514.

[33] T. Potta, C. Chun, S.-C. Song, *Biomacromolecules* **2010**, *11*, 1741.

[34] T. Potta, C. Chun, S.-C. Song, *Biomaterials* **2010**, *31*, 8107.

[35] A. Ustinov, H. Weissman, E. Shirman, I. Pinkas, X. Zuo, B. Rybtchinski, *J. Am. Chem. Soc.* **2011**, *133*, 16201.

[36] a) M. Sayed, H. Pal, *Phys. Chem. Chem. Phys.* **2021**, *23*, 26085; b) X. Ma, Y. Zhao, *Chem. Rev.* **2015**, *115*, 7794.

[37] C. J. Pedersen, *J. Am. Chem. Soc.* **1967**, *89*, 2495.

[38] C. J. Pedersen, *J. Am. Chem. Soc.* **1967**, *89*, 7017.

[39] a) Z. Liu, S. K. M. Nalluri, J. F. Stoddart, *Chem. Soc. Rev.* **2017**, *46*, 2459; b) P. L. Anelli, P. R. Ashton, R. Ballardini, V. Balzani, M. Delgado, M. T. Gandolfi, T. T. Goodnow, A. E. Kaifer, D. Philp, *J. Am. Chem. Soc.* **1992**, *114*, 193; c) R. Jasti, J. Bhattacharjee, J. B. Neaton, C. R. Bertozzi, *J. Am. Chem. Soc.* **2008**, *130*, 17646; d) J. Svec, M. Necas, V. Sindelar, *Angew. Chem. Int. Ed.* **2010**, *49*, 2378; e) D. Zhang, A. Martinez, J.-P. Dutasta, *Chem. Rev.* **2017**, *117*, 4900; f) J. W. Meisel, C. T. Hu, A. D. Hamilton, *Org. Lett.* **2019**, *21*, 7763; g) L. Ustrnul, T. Burankova, M. Öeren, K. Juhhimenko, J. Ilmarinen, K. Siilak, K. A. Mishra, R. Aav, *Front. Chem.* **2021**, *9*, 701028; h) S. Sarkar, P. Ballester, M. Spektor, E. A. Kataev, *Angew. Chem. Int. Ed.* **2023**, *62*, e202214705; i) L. Zhang, Y. Qiu, W.-G. Liu, H. Chen, D. Shen, B. Song, K. Cai, H. Wu, Y. Jiao, Y. Feng, J. S. W. Seale, C. Pezzato, J. Tian, Y. Tan, X.-Y. Chen, Q.-H. Guo, C. L. Stern, D. Philp, R. D. Astumian, W. A. Goddard, J. F. Stoddart, *Nature* **2023**, *613*, 280.

[40] G. Crini, *Chem. Rev.* **2014**, *114*, 10940.

[41] F. Schardinger, *Z. Unters. Nahr- Genussm. Gebrauchsgegenstaende* **1903**, *6*, 865.

[42] G. Yu, K. Jie, F. Huang, *Chem. Rev.* **2015**, *115*, 7240.

[43] a) J. Szejtli, *Chem. Rev.* **1998**, *98*, 1743; b) M. V. Rekharsky, Y. Inoue, *Chem. Rev.* **1998**, *98*, 1875.

[44] G. Szczupaj, J. Wójcik, A. Ejchart, M. Nowakowski, *J. Incl. Phenom. Macrocycl. Chem.* **2024**, *104*, 129.

[45] J. Royes, C. Courtine, C. Lorenzo, N. Lauth-de Viguerie, A.-F. Mingotaud, V. Pimienta, *J. Org. Chem.* **2020**, *85*, 6509.

[46] J.-S. Wu, K. Toda, A. Tanaka, I. Sanemasa, *Bull. Chem. Soc. Jpn.* **1998**, *71*, 1615.

[47] K. Miyamae, M. Nakahata, Y. Takashima, A. Harada, *Angew. Chem. Int. Ed.* **2015**, *54*, 8984.

[48] A. Biwer, G. Antranikian, E. Heinzle, *Appl. Microbiol. Biotechnol.* **2002**, *59*, 609.

[49] a) B. Tian, D. Xiao, T. Hei, R. Ping, S. Hua, J. Liu, *Polym. Int.* **2020**, *69*, 597; b) F. M. Bezerra, M. J. Lis, H. B. Firmino, J. G. Da Dias Silva, R. d. C. S. Curto Valle, J. A. Borges

Valle, F. A. P. Scacchetti, A. L. Tessaro, *Molecules* **2020**, *25*; c) A. Gonzalez Pereira, M. Carpena, P. García Oliveira, J. C. Mejuto, M. A. Prieto, J. Simal Gandara, *Int. J. Mol. Sci.* **2021**, *22*; d) J. Szejtli, *J. Mater. Chem.* **1997**, *7*, 575.

[50] a) W. Xu, X. Li, L. Wang, S. Li, S. Chu, J. Wang, Y. Li, J. Hou, Q. Luo, J. Liu, *Front. Chem.* **2021**, *9*, 635507; b) M. Agnes, E. Pancani, M. Malanga, E. Fenyvesi, I. Manet, *Macromol. Biosci.* **2022**, *22*, e2200090.

[51] a) D. Larsen, S. R. Beeren, *Chem. Sci.* **2019**, *10*, 9981; b) L. Samuelsen, D. Larsen, C. Schönbeck, S. R. Beeren, *Chem. Commun.* **2022**, *58*, 5152.

[52] S. R. Beeren, K. H. Hansen, A. Erichsen, D. Larsen, WO/2024/042228.

[53] G. W. Gokel, W. M. Leevy, M. E. Weber, *Chem. Rev.* **2004**, *104*, 2723.

[54] Y.-S. Jane, J.-S. Shih, *J. Mol. Catal.* **1994**, *89*, 29.

[55] B. L. Williamson, C. S. Creaser, *Int. J. Mass Spectrom.* **1999**, *188*, 53.

[56] N. F. Goldshleger, A. V. Chernyak, A. S. Lobach, I. P. Kalashnikova, V. E. Baulin, A. Y. Tsivadze, *Prot. Met. Phys. Chem. Surf.* **2015**, *51*, 212.

[57] a) P. R. Ashton, P. J. Campbell, P. T. Glink, D. Philp, N. Spencer, J. F. Stoddart, E. J. T. Chrystal, S. Menzer, D. J. Williams, P. A. Tasker, *Angew. Chem. Int. Ed.* **1995**, *34*, 1865; b) P. R. Ashton, E. J. T. Chrystal, P. T. Glink, S. Menzer, C. Schiavo, N. Spencer, J. F. Stoddart, P. A. Tasker, A. J. P. White, D. J. Williams, *Chem. Eur. J.* **1996**, *2*, 709.

[58] a) P. R. Ashton, R. Ballardini, V. Balzani, I. Baxter, A. Credi, M. C. T. Fyfe, M. T. Gandolfi, M. Gómez-López, M.-V. Martínez-Díaz, A. Piersanti, N. Spencer, J. F. Stoddart, M. Venturi, A. J. P. White, D. J. Williams, *J. Am. Chem. Soc.* **1998**, *120*, 11932; b) J. D. Badjic, V. Balzani, A. Credi, S. Silvi, J. F. Stoddart, *Science* **2004**, *303*, 1845.

[59] X. Ji, Y. Yao, J. Li, X. Yan, F. Huang, *J. Am. Chem. Soc.* **2013**, *135*, 74.

[60] A. Zinke, E. Ziegler, *Ber. dtsch. Chem. Ges. A/B* **1944**, *77*, 264.

[61] C. D. Gutsche, *Acc. Chem. Res.* **1983**, *16*, 161.

[62] V. Böhmer, *Angew. Chem. Int. Ed.* **1995**, *34*, 713.

[63] R. Ludwig, *Fresenius J. Anal. Chem.* **2000**, *367*, 103.

[64] P. E. Georghiou in *Calixarenes and beyond* (Ed.: P. Neri), Springer Berlin Heidelberg, New York NY, **2016**, pp. 879–919.

[65] a) J. L. Atwood, G. A. Koutsantonis, C. L. Raston, *Nature* **1994**, *368*, 229; b) T. Suzuki, K. Nakashima, S. Shinkai, *Chem. Lett.* **1994**, *23*, 699.

[66] R. Behrend, E. Meyer, F. Rusche, *Justus Liebigs Ann. Chem.* **1905**, *339*, 1.

[67] W. A. Freeman, W. L. Mock, N. Y. Shih, *J. Am. Chem. Soc.* **1981**, *103*, 7367.

[68] K. Kim, N. Selvapalam, Y. H. Ko, K. M. Park, D. Kim, J. Kim, *Chem. Soc. Rev.* **2007**, *36*, 267.

[69] J. Lagona, P. Mukhopadhyay, S. Chakrabarti, L. Isaacs, *Angew. Chem. Int. Ed.* **2005**, *44*, 4844.

[70] J. Kim, I.-S. Jung, S.-Y. Kim, E. Lee, J.-K. Kang, S. Sakamoto, K. Yamaguchi, K. Kim, *J. Am. Chem. Soc.* **2000**, *122*, 540.

[71] a) H. Isobe, S. Sato, E. Nakamura, *Org. Lett.* **2002**, *4*, 1287; b) S. Y. Jon, N. Selvapalam, D. H. Oh, J.-K. Kang, S.-Y. Kim, Y. J. Jeon, J. W. Lee, K. Kim, *J. Am. Chem. Soc.* **2003**, *125*, 10186.

[72] Y. Miyahara, K. Abe, T. Inazu, *Angew. Chem. Int. Ed.* **2002**, *41*, 3020.

[73] X. X. Zhang, K. E. Krakowiak, G. Xue, J. S. Bradshaw, R. M. Izatt, *Ind. Eng. Chem. Res.* **2000**, *39*, 3516.

[74] a) K. Jansen, H.-J. Buschmann, A. Wego, D. Döpp, C. Mayer, H.-J. Drexler, H.-J. Holdt, E. Schollmeyer, *J. Incl. Phenom. Macrocycl. Chem.* **2001**, *39*, 357; b) A. Wego, K. Jansen, H. Buschmann, E. Schollmeyer, D. Döpp, *J. Incl. Phenom. Macrocycl. Chem.* **2002**, *43*, 201.

[75] S. J. Barrow, S. Kasera, M. J. Rowland, J. del Barrio, O. A. Scherman, *Chem. Rev.* **2015**, *115*, 12320.

[76] L. Cao, M. Śekutor, P. Y. Zavalij, K. Mlinarić-Majerski, R. Glaser, L. Isaacs, *Angew. Chem. Int. Ed.* **2014**, *53*, 988.

[77] J. W. Lee, K. Kim, S. Choi, Y. H. Ko, S. Sakamoto, K. Yamaguchi, K. Kim, *Chem. Commun.* **2002**, 2692.

[78] K. Kim, D. Shetty, K. M. Park in *Macrocyclic and supramolecular chemistry*. *How Izatt-Christensen Award winners shaped the field* (Ed.: R. M. Izatt), Wiley, Chichester West Sussex, **2016**, pp. 127–145.

[79] a) E. A. Appel, F. Biedermann, U. Rauwald, S. T. Jones, J. M. Zayed, O. A. Scherman, *J. Am. Chem. Soc.* **2010**, *132*, 14251; b) Y. Lin, L. Li, G. Li, *Carbohydr. Polym.* **2013**, *92*, 429.

[80] J. Liu, C. S. Y. Tan, O. A. Scherman, *Angew. Chem. Int. Ed.* **2018**, *57*, 8854.

[81] Y. Wang, G. Ping, C. Li, *Chem. Commun.* **2016**, *52*, 9858.

[82] H. Zuilhof, A. C.-H. Sue, J. Escorihuela, *J. Org. Chem.* **2021**, *86*, 14956.

[83] D. Cao, Y. Kou, J. Liang, Z. Chen, L. Wang, H. Meier, *Angew. Chem. Int. Ed.* **2009**, *48*, 9721.

[84] X.-B. Hu, Z. Chen, L. Chen, L. Zhang, J.-L. Hou, Z.-T. Li, *Chem. Commun.* **2012**, *48*, 10999.

[85] a) T. Ogoshi, N. Ueshima, F. Sakakibara, T. Yamagishi, T. Haino, *Org. Lett.* **2014**, *16*, 2896; b) Y. Chen, H. Q. Tao, Y. H. Kou, H. Meier, J. L. Fu, D. R. Cao, *Chin. Chem. Lett.* **2012**, *23*, 509.

[86] S. Santra, I. S. Kovalev, D. S. Kopchuk, G. V. Zyryanov, A. Majee, V. N. Charushin, O. N. Chupakhin, *RSC Adv.* **2015**, *5*, 104284.

[87] M. Holler, N. Allenbach, J. Sonet, J.-F. Nierengarten, *Chem. Commun.* **2012**, *48*, 2576.

[88] T. Boinski, A. Szumna, *Tetrahedron* **2012**, *68*, 9419.

[89] K. Wang, L.-L. Tan, D.-X. Chen, N. Song, G. Xi, S. X.-A. Zhang, C. Li, Y.-W. Yang, *Org. Biomol. Chem.* **2012**, *10*, 9405.

[90] T. Ogoshi, T. Aoki, K. Kitajima, S. Fujinami, T. Yamagishi, Y. Nakamoto, *J. Org. Chem.* **2011**, *76*, 328.

[91] H. Tao, D. Cao, L. Liu, Y. Kou, L. Wang, H. Meier, *Sci. China Chem.* **2012**, *55*, 223.

[92] J. Cao, Y. Shang, B. Qi, X. Sun, L. Zhang, H. Liu, H. Zhang, X. Zhou, *RSC Adv.* **2015**, *5*, 9993.

[93] S. Santra, D. S. Kopchuk, I. S. Kovalev, G. V. Zyryanov, A. Majee, V. N. Charushin, O. N. Chupakhin, *Green Chem.* **2016**, *18*, 423.

[94] M. Da Pian, O. de Lucchi, G. Strukul, F. Fabris, A. Scarso, *RSC Adv.* **2016**, *6*, 48272.

[95] T. Ogoshi, N. Ueshima, T. Akutsu, D. Yamafuji, T. Furuta, F. Sakakibara, T. Yamagishi, *Chem. Commun.* **2014**, *50*, 5774.

[96] M. Da Pian, C. A. Schalley, F. Fabris, A. Scarso, *Org. Chem. Front.* **2019**, *6*, 1044.

[97] N. L. Strutt, H. Zhang, S. T. Schneebeli, J. F. Stoddart, *Acc. Chem. Res.* **2014**, *47*, 2631.

[98] L. Wu, C. Han, X. Jing, Y. Yao, *Chin. Chem. Lett.* **2021**, *32*, 3322.

[99] H. Zhang, Z. Liu, Y. Zhao, *Chem. Soc. Rev.* **2018**, *47*, 5491.

[100] N. L. Strutt, S. T. Schneebeli, J. F. Stoddart, *Supramol. Chem.* **2013**, *25*, 596.

[101] S. Fu, G. An, H. Sun, Q. Luo, C. Hou, J. Xu, Z. Dong, J. Liu, *Chem. Commun.* **2017**, *53*, 9024.

[102] Z. Zhang, Y. Luo, J. Chen, S. Dong, Y. Yu, Z. Ma, F. Huang, *Angew. Chem. Int. Ed.* **2011**, *50*, 1397.

[103] L. Liu, D. Cao, Y. Jin, H. Tao, Y. Kou, H. Meier, *Org. Biomol. Chem.* **2011**, *9*, 7007.

[104] N. Song, D.-X. Chen, Y.-C. Qiu, X.-Y. Yang, B. Xu, W. Tian, Y.-W. Yang, *Chem. Commun.* **2014**, *50*, 8231.

[105] Y. Guan, M. Ni, X. Hu, T. Xiao, S. Xiong, C. Lin, L. Wang, *Chem. Commun.* **2012**, *48*, 8529.

[106] N. Laggoune, F. Delattre, J. Lyskawa, F. Stoffelbach, J. M. Guigner, S. Ruellan, G. Cooke, P. Woisel, *Polym. Chem.* **2015**, *6*, 7389.

[107] T. Ogoshi, K. Demachi, K. Kitajima, T. Yamagishi, *Chem. Commun.* **2011**, *47*, 7164.

[108] Y. Chen, M. He, B. Li, L. Wang, H. Meier, D. Cao, *RSC Adv.* **2013**, *3*, 21405.

[109] W. Xia, X.-Y. Hu, Y. Chen, C. Lin, L. Wang, *Chem. Commun.* **2013**, *49*, 5085.

[110] W. Xia, M. Ni, C. Yao, X. Wang, D. Chen, C. Lin, X.-Y. Hu, L. Wang, *Macromolecules* **2015**, *48*, 4403.

[111] T. Ogoshi, K. Kitajima, S. Fujinami, T. Yamagishi, *Chem. Commun.* **2011**, *47*, 10106.

[112] T. Ogoshi, D. Yamafuji, D. Kotera, T. Aoki, S. Fujinami, T. Yamagishi, *J. Org. Chem.* **2012**, *77*, 11146.

[113] Z. Zhang, B. Xia, C. Han, Y. Yu, F. Huang, *Org. Lett.* **2010**, *12*, 3285.

[114] X.-Y. Hu, P. Zhang, X. Wu, W. Xia, T. Xiao, J. Jiang, C. Lin, L. Wang, *Polym. Chem.* **2012**, *3*, 3060.

[115] J. Chang, Q. Zhao, L. Kang, H. Li, M. Xie, X. Liao, *Macromolecules* **2016**, *49*, 2814.

[116] G. Yu, B. Hua, C. Han, *Org. Lett.* **2014**, *16*, 2486.

[117] J. Han, X. Hou, C. Ke, H. Zhang, N. L. Strutt, C. L. Stern, J. F. Stoddart, *Org. Lett.* **2015**, *17*, 3260.

[118] Y. Kou, H. Tao, D. Cao, Z. Fu, D. Schollmeyer, H. Meier, *Eur. J. Org. Chem.* **2010**, *2010*, 6464.

[119] M. Guo, X. Wang, C. Zhan, P. Demay-Drouhard, W. Li, K. Du, M. A. Olson, H. Zuilhof, A. C.-H. Sue, *J. Am. Chem. Soc.* **2018**, *140*, 74.

[120] P. Demay-Drouhard, K. Du, K. Samanta, X. Wan, W. Yang, R. Srinivasan, A. C.-H. Sue, H. Zuilhof, *Org. Lett.* **2019**, *21*, 3976.

[121] Y. Ma, X. Ji, F. Xiang, X. Chi, C. Han, J. He, Z. Abliz, W. Chen, F. Huang, *Chem. Commun.* **2011**, *47*, 12340.

[122] I. Nierengarten, S. Guerra, M. Holler, J.-F. Nierengarten, R. Deschenaux, *Chem. Commun.* **2012**, *48*, 8072.

[123] H. Deng, X. Shu, X. Hu, J. Li, X. Jia, C. Li, *Tetrahedron Lett.* **2012**, *53*, 4609.

[124] R. Joseph, *ACS Omega* **2020**, *5*, 6215.

[125] I. Nierengarten, S. Guerra, M. Holler, L. Karmazin-Brelot, J. Barberá, R. Deschenaux, J.-F. Nierengarten, *Eur. J. Org. Chem.* **2013**, *2013*, 3675.

[126] T. Ogoshi, M. Hashizume, T. Yamagishi, Y. Nakamoto, *Chem. Commun.* **2010**, *46*, 3708.

[127] T. Ogoshi, R. Shiga, T. Yamagishi, *J. Am. Chem. Soc.* **2012**, *134*, 4577.

[128] a) Z. Li, J. Yang, G. Yu, J. He, Z. Abliz, F. Huang, *Chem. Commun.* **2014**, *50*, 2841; b) X. Chi, M. Xue, *RSC Adv.* **2014**, *4*, 37786.

[129] a) X. Shu, K. Xu, D. Hou, C. Li, *Isr. J. Chem.* **2018**, *58*, 1230; b) S. Sun, X.-Y. Hu, D. Chen, J. Shi, Y. Dong, C. Lin, Y. Pan, L. Wang, *Polym. Chem.* **2013**, *4*, 2224; c) Q. Lin, Y.-Q. Fan, G.-F. Gong, P.-P. Mao, J. Wang, X.-W. Guan, J. Liu, Y.-M. Zhang, H. Yao, T.-B. Wei, *ACS Sustainable Chem. Eng.* **2018**, *6*, 8775; d) Y. Mei, Q.-W. Zhang, Q. Gu, Z. Liu, X. He, Y. Tian, *J. Am. Chem. Soc.* **2022**, *144*, 2351.

[130] a) G. Yu, M. Xue, Z. Zhang, J. Li, C. Han, F. Huang, *J. Am. Chem. Soc.* **2012**, *134*, 13248; b) D. Xia, G. Yu, J. Li, F. Huang, *Chem. Commun.* **2014**, *50*, 3606.

[131] X.-Y. Hu, X. Liu, W. Zhang, S. Qin, C. Yao, Y. Li, D. Cao, L. Peng, L. Wang, *Chem. Mater.* **2016**, *28*, 3778.

[132] W. Chen, Y. Zhang, J. Li, X. Lou, Y. Yu, X. Jia, C. Li, *Chem. Commun.* **2013**, *49*, 7956.

[133] Y. Yao, M. Xue, X. Chi, Y. Ma, J. He, Z. Abliz, F. Huang, *Chem. Commun.* **2012**, *48*, 6505.

[134] Y. Li, J. Wen, J. Li, Z. Wu, W. Li, K. Yang, *ACS Sens.* **2021**, *6*, 3882.

[135] T. Ogoshi, T. Yamagishi, *Eur. J. Org. Chem.* **2013**, *2013*, 2961.

[136] T. Kakuta, T. Yamagishi, T. Ogoshi, *Acc. Chem. Res.* **2018**, *51*, 1656.

[137] T. Ogoshi, K. Demachi, K. Kitajima, T. Yamagishi, *Chem. Commun.* **2011**, *47*, 10290.

[138] K. Han, Y. Zhang, J. Li, Y. Yu, X. Jia, C. Li, *Eur. J. Org. Chem.* **2013**, *2013*, 2057.

[139] Y. Zhou, Z. Li, X. Chi, C. Thompson, Y. Yao, *Chem. Commun.* **2014**, *50*, 10482.

[140] T. Ogoshi, K. Saito, R. Sueto, R. Kojima, Y. Hamada, S. Akine, A. M. P. Moeljadi, H. Hirao, T. Kakuta, T. Yamagishi, *Angew. Chem. Int. Ed.* **2018**, *57*, 1592.

[141] M.-S. Yuan, H. Chen, X. Du, J. Li, J. Wang, X. Jia, C. Li, *Chem. Commun.* **2015**, *51*, 16361.

[142] J. Fan, Y. Chen, D. Cao, Y.-W. Yang, X. Jia, C. Li, *RSC Adv.* **2014**, *4*, 4330.

[143] C. Li, Q. Xu, J. Li, F. Yao, X. Jia, *Org. Biomol. Chem.* **2010**, *8*, 1568.

[144] C. Li, L. Zhao, J. Li, X. Ding, S. Chen, Q. Zhang, Y. Yu, X. Jia, *Chem. Commun.* **2010**, *46*, 9016.

[145] M. Nishio, *Phys. Chem. Chem. Phys.* **2011**, *13*, 13873.

[146] X. Shu, J. Fan, J. Li, X. Wang, W. Chen, X. Jia, C. Li, *Org. Biomol. Chem.* **2012**, *10*, 3393.

[147] X. Lou, H. Chen, X. Jia, C. Li, *Chin. J. Chem.* **2015**, *33*, 335.

[148] X. Shu, W. Chen, D. Hou, Q. Meng, R. Zheng, C. Li, *Chem. Commun.* **2014**, *50*, 4820.

[149] C. Li, S. Chen, J. Li, K. Han, M. Xu, B. Hu, Y. Yu, X. Jia, *Chem. Commun.* **2011**, *47*, 11294.

[150] Y. Liu, F. Zhou, F. Yang, Da Ma, *Org. Biomol. Chem.* **2019**, *17*, 5106.

[151] X. Chi, M. Xue, Y. Yao, F. Huang, *Org. Lett.* **2013**, *15*, 4722.

[152] D. Osella, A. Carretta, C. Nervi, M. Ravera, R. Gobetto, *Organometallics* **2000**, *19*, 2791.

[153] Q. Hao, Y. Chen, Z. Huang, J.-F. Xu, Z. Sun, X. Zhang, *ACS Appl. Mater. Interfaces* **2018**, *10*, 5365.

[154] C. Li, J. Ma, L. Zhao, Y. Zhang, Y. Yu, X. Shu, J. Li, X. Jia, *Chem. Commun.* **2013**, *49*, 1924.

[155] H. Staudinger, *Ber. dtsch. Chem. Ges. A/B* **1920**, *53*, 1073.

[156] W. H. Carothers, *Chem. Rev.* **1931**, *8*, 353.

[157] a) K. Matyjaszewski, J. Xia, *Chem. Rev.* **2001**, *101*, 2921; b) K. Matyjaszewski, *Macromolecules* **2012**, *45*, 4015.

[158] a) J. Chiefari, Y. K. Chong, F. Ercole, J. Krstina, J. Jeffery, T. P. T. Le, R. T. A. Mayadunne, G. F. Meijs, C. L. Moad, G. Moad, E. Rizzardo, S. H. Thang, *Macromolecules* **1998**, *31*, 5559; b) G. Moad, E. Rizzardo, S. H. Thang, *Polymer* **2008**, *49*, 1079.

[159] G. Moad, J. Chiefari, Y. K. Chong, J. Krstina, R. T. A. Mayadunne, A. Postma, E. Rizzardo, S. H. Thang, *Polym. Int.* **2000**, *49*, 993.

[160] T. Früh, U. Schubert, *Nachr. Chem.* **2020**, *68*, 3.

[161] a) A. C. C. de Leon, Í. G. Da Silva, K. D. Pangilinan, Q. Chen, E. B. Caldona, R. C. Advincula, *React. Funct. Polym.* **2021**, *162*, 104878; b) S. Vaz Jr in *Applications of analytical chemistry in industry* (Ed.: S. Vaz), Springer, Cham, **2023**, pp. 127–157.

[162] a) H. L. Fisher, *Ind. Eng. Chem.* **1939**, *31*, 1381; b) M. Akiba, A. S. Hashim, *Prog. Polym. Sci.* **1997**, *22*, 475.

[163] D. Ye, C. Chang, L. Zhang, *Biomacromolecules* **2019**, *20*, 1989.

[164] X. Xu, F. A. Jerca, K. van Hecke, V. V. Jerca, R. Hoogenboom, *Mater. Horiz.* **2020**, *1*, 16071.

[165] R. J. Wojtecki, M. A. Meador, S. J. Rowan, *Nat. Mater.* **2011**, *10*, 14.

[166] a) D. Kuckling, A. Wycisk, *J. Polym. Sci. A Polym. Chem.* **2013**, *51*, 2980; b) M. Wei, Y. Gao, X. Li, M. J. Serpe, *Polym. Chem.* **2017**, *8*, 127.

[167] A. Bordbar-Khiabani, M. Gasik, *Int. J. Mol. Sci.* **2022**, *23*.

[168] S. Wang, P. J. Ong, S. Liu, W. Thitsartarn, Tan, Maureen Janet Beng Hoon, A. Suwardi, Q. Zhu, X. J. Loh, *Chem. Asian J.* **2022**, *17*, e202200608.

[169] X. Xu, F. A. Jerca, V. V. Jerca, R. Hoogenboom, *Macromolecules* **2020**, *53*, 6566.

[170] Y. Song, Y. Liu, T. Qi, G. L. Li, *Angew. Chem. Int. Ed.* **2018**, *57*, 13838.

[171] A. Faghihnejad, K. E. Feldman, J. Yu, M. V. Tirrell, J. N. Israelachvili, C. J. Hawker, E. J. Kramer, H. Zeng, *Adv. Funct. Mater.* **2014**, *24*, 2322.

[172] M. Nakahata, Y. Takashima, H. Yamaguchi, A. Harada, *Nat. Commun.* **2011**, *2*, 511.

[173] W. Xiao, W.-H. Chen, J. Zhang, C. Li, R.-X. Zhuo, X.-Z. Zhang, *J. Phys. Chem. B* **2011**, *115*, 13796.

[174] E. A. Appel, X. J. Loh, S. T. Jones, F. Biedermann, C. A. Dreiss, O. A. Scherman, *J. Am. Chem. Soc.* **2012**, *134*, 11767.

[175] M. Mihajlovic, M. Staropoli, M.-S. Appavou, H. M. Wyss, W. Pyckhout-Hintzen, R. P. Sijbesma, *Macromolecules* **2017**, *50*, 3333.

[176] L. Barbier, P. Pipart, M. Vahdati, C. Lorthioir, Y. Tran, D. Hourdet, *Carbohydr. Polym.* **2024**, *336*, 122126.

[177] a) M. A. Haque, T. Kurokawa, J. P. Gong, *Polymer* **2012**, *53*, 1805; b) X. Xu, V. V. Jerca, R. Hoogenboom, *Mater. Horiz.* **2021**.

[178] C. K. Pandiyarajan, M. Rubinstein, J. Genzer, *Macromolecules* **2016**, *49*, 5076.

[179] X. Zhao, *Soft Matter* **2014**, *10*, 672.

[180] a) S. Yoshida, H. Ejima, N. Yoshie, *Adv. Funct. Mater.* **2017**; b) H. Zhou, X. Jin, B. Yan, X. Li, W. Yang, A. Ma, X. Zhang, P. Li, X. Ding, W. Chen, *Macromol. Mater. Eng.* **2017**, *302*, 1700085.

[181] E. Elacqua, D. S. Lye, M. Weck, *Acc. Chem. Res.* **2014**, *47*, 2405.

[182] S. Tan, J. Cui, Q. Fu, E. Nam, K. Ladewig, J. M. Ren, E. H. H. Wong, F. Caruso, A. Blencowe, G. G. Qiao, *ACS Appl. Mater. Interfaces* **2016**, *8*, 6219.

[183] C. B. Rodell, J. W. MacArthur, S. M. Dorsey, R. J. Wade, L. L. Wang, Y. J. Woo, J. A. Burdick, *Adv. Funct. Mater.* **2015**, *25*, 636.

[184] C. Pan, L. Liu, Q. Chen, Q. Zhang, G. Guo, *ACS Appl. Mater. Interfaces* **2017**, *9*, 38052.

[185] H. Fan, J. Wang, Z. Jin, *Macromolecules* **2018**, *51*, 1696.

[186] J. Guo, C. Yuan, M. Guo, L. Wang, F. Yan, *Chem. Sci.* **2014**, *5*, 3261.

[187] X. L. Gong, Y. Y. Xiao, M. Pan, Y. Kang, B. J. Li, S. Zhang, *ACS Appl. Mater. Interfaces* **2016**.

[188] T. Koga, K. Tomimori, N. Higashi, *Macromol. Rapid Commun.* **2020**, *41*, 1900650.

[189] C. Ma, T. Li, Q. Zhao, X. Yang, J. Wu, Y. Luo, T. Xie, *Adv. Mater.* **2014**, *26*, 5665.

[190] X. Hu, J. Zhou, M. Vatankhah-Varnosfaderani, W. F. Daniel, Q. Li, A. P. Zhushma, A. V. Dobrynin, S. S. Sheiko, *Nat. Commun.* **2016**, *7*, 12919.

[191] J. Li, C. Ji, X. Yu, M. Yin, D. Kuckling, *Macromol. Rapid Commun.* **2019**, *40*, e1900189.

[192] Y. Zhao, M. Li, B. Liu, J. Xiang, Z. Cui, X. Qu, D. Qiu, Y. Tian, Z. Yang, *J. Mater. Chem. B* **2018**, *6*, 1351.

[193] C. Shao, H. Chang, M. Wang, F. Xu, J. Yang, *ACS Appl. Mater. Interfaces* **2017**, *9*, 28305.

[194] R. Du, Z. Xu, C. Zhu, Y. Jiang, H. Yan, H.-C. Wu, O. Vardoulis, Y. Cai, X. Zhu, Z. Bao, Q. Zhang, X. Jia, *Adv. Funct. Mater.* **2020**, *30*, 1907139.

[195] M. Pan, Q.-J. Yuan, X.-L. Gong, S. Zhang, B.-J. Li, *Macromol. Rapid Commun.* **2016**, *37*, 433.

[196] C. Qi, Z. Dong, Y. Huang, J. Xu, C. Lei, *ACS Appl. Mater. Interfaces* **2022**, *14*, 30385.

[197] K. Saha, S. S. Agasti, C. Kim, X. Li, V. M. Rotello, *Chem. Rev.* **2012**, *112*, 2739.

[198] a) R. Pinalli, E. Dalcanale, *Acc. Chem. Res.* **2013**, *46*, 399; b) L. You, D. Zha, E. V. Anslyn, *Chem. Rev.* **2015**, *115*, 7840; c) C. Guo, A. C. Sedgwick, T. Hirao, J. L. Sessler, *Coord. Chem. Rev.* **2021**, *427*.

[199] K. Völlmecke, R. Afroz, S. Bierbach, L. J. Brenker, S. Frücht, A. Glass, R. Giebelhaus, A. Hoppe, K. Kanemaru, M. Lazarek, L. Rabbe, L. Song, A. Velasco Suarez, S. Wu, M. Serpe, D. Kuckling, *Gels* **2022**, *8*.

[200] a) L. Hu, Q. Zhang, X. Li, M. J. Serpe, *Mater. Horiz.* **2019**, *6*, 1774; b) Q. Zhang, Y. Zhang, Y. Wan, W. Carvalho, L. Hu, M. J. Serpe, *Prog. Polym. Sci.* **2021**, *116*, 101386.

[201] a) F. Beckers, J. Rinklebe, *Crit. Rev. Environ. Sci. Technol.* **2017**, *47*, 693; b) H. Needleman, *Annu. Rev. Med.* **2004**, *55*, 209.

[202] N. Dave, M. Y. Chan, P.-J. J. Huang, B. D. Smith, J. Liu, *J. Am. Chem. Soc.* **2010**, *132*, 12668.

[203] Z. E. Jacobi, L. Li, J. Liu, *Analyst* **2012**, *137*, 704.

[204] J. Chu, C. Chen, X. Li, L. Yu, W. Li, M. Cheng, W. Tang, Z. Xiong, *Anal. Chim. Acta* **2021**, *1157*, 338400.

[205] a) V. Mustieles, S. C. D'Cruz, S. Couderq, A. Rodríguez-Carrillo, J.-B. Fini, T. Hofer, I.-L. Steffensen, H. Dirven, R. Barouki, N. Olea, M. F. Fernández, A. David, *Environ. Int.* **2020**, *144*, 105811; b) A. Tarafdar, R. Sirohi, P. A. Balakumaran, R. Reshmy, A. Madhavan, R. Sindhu, P. Binod, Y. Kumar, D. Kumar, S. J. Sim, *J. Hazard. Mater.* **2022**, *423*, 127097.

[206] W. Du, J. Liu, H. Li, C. Deng, J. Luo, Q. Feng, Y. Tan, S. Yang, Z. Wu, F. Xiao, *Anal. Chem.* **2023**, *95*, 4220.

[207] Z. Li, Q. Fan, Y. Yin, *Chem. Rev.* **2022**, *122*, 4976.

[208] J.-Y. Wen, H.-R. Yu, T. Liang, X.-B. Lv, C.-J. Cheng, *New J. Chem.* **2023**, *47*, 10236.

[209] a) R. Mayeux, *NeuroRx* **2004**, *1*, 182; b) R. Liu, X. Wang, K. Aihara, L. Chen, *Med. Res. Rev.* **2014**, *34*, 455.

[210] a) N. J. Serkova, E. J. Gamito, R. H. Jones, C. O'Donnell, J. L. Brown, S. Green, H. Sullivan, T. Hedlund, E. D. Crawford, *Prostate* **2008**, *68*, 620; b) G. F. Giskeødegård, H. Bertilsson, K. M. Selnæs, A. J. Wright, T. F. Bathen, T. Viset, J. Halgunset, A. Angelsen, I. S. Gribbestad, M.-B. Tessem, *PLoS One* **2013**, *8*, e62375.

[211] Q. Shen, C. Fang, L. Hu, M. J. Serpe, *SmartMat* **2024**, *5*.

[212] A. Chilkoti, P. S. Stayton, *J. Am. Chem. Soc.* **1995**, *117*, 10622.

[213] J. Li, X. Yu, A. Herberg, D. Kuckling, *Macromol. Rapid Commun.* **2019**, *40*, e1800674.

[214] I. Sedláková, J. Vávrová, J. Tošner, L. Hanousek, *Tumour Biol.* **2011**, *32*, 311.

[215] a) D.-H. Tuo, T.-H. Shi, S. Ohtani, T. Ogoshi, *Responsive Materials* **2024**, *2*; b) Le Zhou, S. Cao, C. Liu, H. Zhang, Y. Zhao, *Coord. Chem. Rev.* **2023**, *491*, 215260.

[216] a) D. Xia, P. Wang, X. Ji, N. M. Khashab, J. L. Sessler, F. Huang, *Chem. Rev.* **2020**, *120*, 6070; b) Y.-F. Li, Z. Li, Q. Lin, Y.-W. Yang, *Nanoscale* **2020**, *12*, 2180; c) Y. Cheng, X. Lv, B. Liang, X. Wei, P. Wang, D. Xia, *Polym. Chem.* **2023**, *14*, 191.

[217] M. Ni, N. Zhang, W. Xia, X. Wu, C. Yao, X. Liu, X.-Y. Hu, C. Lin, L. Wang, *J. Am. Chem. Soc.* **2016**, *138*, 6643.

[218] S. Wang, Z. Xu, T. Wang, X. Liu, Y. Lin, Y.-Z. Shen, C. Lin, L. Wang, *J. Photochem. Photobiol. A* **2018**, *355*, 60.

[219] Q. Zhang, K.-Q. Li, L.-L. Fan, N. Li, J. Li, H.-M. Guo, *Macromol. Chem. Phys.* **2021**, *222*, 2100018.

[220] V. Kardelis, K. Li, I. Nierengarten, M. Holler, J.-F. Nierengarten, A. Adronov, *Macromolecules* **2017**, *50*, 9144.

[221] J.-F. Chen, P. Chen, *ACS Appl. Polym. Mater.* **2019**, *1*, 2224.

[222] M. Boominathan, J. Kiruthika, M. Arunachalam, *J. Polym. Sci., Part A: Polym. Chem.* **2019**, *57*, 1508.

[223] M. Boominathan, M. Arunachalam, *ACS Appl. Polym. Mater.* **2020**, *2*, 4368.

[224] L. Sheng, H. Liu, Z. Hu, X. Ji, *Chemistry* **2023**, *29*, e202300990.

[225] C. Huang, H. Zhang, Z. Hu, Y. Zhang, X. Ji, *Gels* **2022**, *8*.

[226] Q. Zhang, L.-L. Fan, T.-J. Yue, Z.-G. Hu, N. Li, J. Li, Y.-Q. Jiang, K.-Q. Li, H.-M. Guo, *Macromol. Chem. Phys.* **2022**, 2200253.

[227] P. Thordarson, *Chem. Soc. Rev.* **2011**, *40*, 1305.

[228] P. Thordarson in *Supramolecular chemistry*. *From molecules to nanomaterials* (Eds.: J. W. Steed, P. A. Gale), Wiley, Chichester, **2012**.

[229] K. Hirose, *J. Incl. Phenom. Macrocycl. Chem.* **2001**, *39*, 193.

[230] E. G. Sheetz, D. van Craen, A. H. Flood in *Anion-binding catalysis* (Ed.: O. García Mancheño), Wiley-VCH GmbH, **2022**, pp. 79–109.

[231] E. Bruneau, D. Lavabre, G. Levy, J. C. Micheau, *J. Chem. Educ.* **1992**, *69*, 833.

[232] J. S. Renny, L. L. Tomasevich, E. H. Tallmadge, D. B. Collum, *Angew. Chem. Int. Ed.* **2013**, *52*, 11998.

[233] E. Asmus, *Z. Anal. Chem.* **1961**, *183*, 321.

[234] D. Brynn Hibbert, P. Thordarson, *Chem. Commun.* **2016**, *52*, 12792.

[235] F. Ulatowski, K. Dąbrowa, T. Bałakier, J. Jurczak, *J. Org. Chem.* **2016**, *81*, 1746.

[236] a) J. L. Bennett, G. T. H. Nguyen, W. A. Donald, *Chem. Rev.* **2022**, *122*, 7327; b) E. Largy, A. König, A. Ghosh, D. Ghosh, S. Benabou, F. Rosu, V. Gabelica, *Chem. Rev.* **2022**, *122*, 7720.

[237] a) Y. Cohen, S. Slovak, L. Avram, *Chem. Commun.* **2021**, *57*, 8856; b) S. K. Bharti, R. Roy, *TrAC, Trends Anal. Chem.* **2012**, *35*, 5; c) P. Giraudeau, *Magn. Reson. Chem.* **2017**, *55*, 61.

[238] Atta-ur-Rahman, M. I. Choudhary, Atia-tul-Wahab in *Solving Problems with NMR Spectroscopy*, Elsevier, **2016**, pp. 227–264.

[239] B. Vögeli, *Prog. Nucl. Magn. Reson. Spectrosc.* **2014**, *78*, 1.

[240] J. Feeney, J. Batchelor, J. Albrand, G. Roberts, *J. Magn. Reson.* **1979**, *33*, 519.

[241] L. Fielding, *Tetrahedron* **2000**, *56*, 6151.

[242] D. A. Stauffer, R. E. Barrans, D. A. Dougherty, *J. Org. Chem.* **1990**, *55*, 2762.

[243] J. C. Adrian, C. S. Wilcox, *J. Am. Chem. Soc.* **1991**, *113*, 678.

[244] A. Sedaghat Doost, M. Akbari, C. V. Stevens, A. D. Setiowati, P. van der Meeren, *Trends Food Sci. Technol.* **2019**, *86*, 16.

[245] D. Jeannerat, J. Furrer, *Comb. Chem. High Throughput Screen.* **2012**, *15*, 15.

[246] a) K. F. Morris, C. S. Johnson, *J. Am. Chem. Soc.* **1992**, *114*, 3139; b) C. S. Johnson, *Prog. Nucl. Magn. Reson. Spectrosc.* **1999**, *34*, 203.

[247] a) D. Sinnaeve, *Concepts Magn. Reson. A* **2012**, *40A*, 39; b) P. W. Kuchel, G. Pagès, K. Nagashima, S. Velan, V. Vijayaragavan, V. Nagarajan, K. H. Chuang, *Concepts Magn. Reson. A* **2012**, *40A*, 205; c) L. Avram, Y. Cohen, *Chem. Soc. Rev.* **2015**, *44*, 586.

[248] a) B. M. Tissue in *Foundations of contemporary environmental studies* (Ed.: O. J. Schmitz), Island Press, Washington DC, **2007**, pp. 1–13; b) M. S. H. Akash, K. Rehman in *Essentials of Pharmaceutical Analysis* (Eds.: K. Rehman, M. S. H. Akash), Springer, Singapore, **2020**, pp. 29–56.

[249] a) L. D. Hansen, J. J. Christensen, R. M. Izatt, *Chem. Commun.* **1965**, 36; b) J. J. Christensen, R. M. Izatt, L. D. Hansen, J. A. Partridge, *J. Phys. Chem.* **1966**, *70*, 2003.

[250] a) W. R. Archer, M. D. Schulz, *Soft Matter* **2020**, *16*, 8760; b) M. Bastos, A. Velazquez-Campoy, *Eur. Biophys. J.* **2021**, *50*, 363; c) M. Bastos, O. Abian, C. M. Johnson, F. Ferreira-da-Silva, S. Vega, A. Jimenez-Alesanco, D. Ortega-Alarcon, A. Velazquez-Campoy, *Nat. Rev. Methods Primers* **2023**, *3*.

[251] F. Termühlen, D. Kuckling, M. Schönhoff, *J. Phys. Chem. B* **2017**, *121*, 8611.

[252] T. L. Price, H. W. Gibson, *J. Am. Chem. Soc.* **2018**, *140*, 4455.

[253] V. Upadhyay, A. Lucas, C. Patrick, K. M. G. Mallela, *Methods* **2024**, *225*, 52.

[254] J. E. Ladbury, *Biotechniques* **2004**, *37*, 885.

[255] M. W. Freyer, E. A. Lewis, *Methods Cell Biol.* **2008**, *84*, 79.

[256] E. A. Lewis, K. P. Murphy, *Methods Mol. Biol.* **2005**, *305*, 1.

[257] a) T. Wiseman, S. Williston, J. F. Brandts, L. N. Lin, *Anal. Biochem.* **1989**, *179*, 131; b) W. B. Turnbull, A. H. Daranas, *J. Am. Chem. Soc.* **2003**, *125*, 14859.

[258] J. Broecker, C. Vargas, S. Keller, *Anal. Biochem.* **2011**, *418*, 307.

[259] J. Tellinghuisen, *J. Phys. Chem. B* **2005**, *109*, 20027.

[260] J. Homola, S. S. Yee, G. Gauglitz, *Sens. Actuators B Chem.* **1999**, *54*, 3.

[261] R. W. Wood, *Proc. Phys. Soc. London* **1902**, *18*, 269.

[262] U. Fano, *J. Opt. Soc. Am.* **1941**, *31*, 213.

[263] A. Otto, *Z. Phys. A: Hadrons Nucl.* **1968**, *216*, 398.

[264] E. Kretschmann, H. Raether, *Z. Naturforsch. A* **1968**, *23*, 2135.

[265] J. Homola in *Springer Series on Chemical Sensors and Biosensors*, *Vol. 04* (Eds.: J. Homola, J. Dostálek), Springer, Berlin, New York, **2006**, pp. 3–44.

[266] a) M. J. N. Junk, I. Anac, B. Menges, U. Jonas, *Langmuir* **2010**, *26*, 12253; b) P. W. Beines, I. Klosterkamp, B. Menges, U. Jonas, W. Knoll, *Langmuir* **2007**, *23*, 2231.

[267] D. Kuckling, M. E. Harmon, C. W. Frank, *Macromolecules* **2002**, *35*, 6377.

[268] M. E. Harmon, D. Kuckling, C. W. Frank, *Macromolecules* **2003**, *36*, 162.

[269] D. Kuckling, P. Pareek, *Polymer* **2008**, *49*, 1435.

[270] E. Mauriz, A. Calle, J. J. Manclús, A. Montoya, L. M. Lechuga, *Anal. Bioanal. Chem.* **2007**, *387*, 1449.

[271] N. Soh, T. Watanabe, Y. Asano, T. Imato, *Sens. Mater.* **2003**, *15*, 423.

[272] N. Bellassai, R. D'Agata, V. Jungbluth, G. Spoto, *Front. Chem.* **2019**, *7*, 570.

[273] A. Azzouz, L. Hejji, K.-H. Kim, D. Kukkar, B. Souhail, N. Bhardwaj, R. J. C. Brown, W. Zhang, *Biosens. Bioelectron.* **2022**, *197*, 113767.

[274] A. A. I. Sina, R. Vaidyanathan, S. Dey, L. G. Carrascosa, M. J. A. Shiddiky, M. Trau, *Sci. Rep.* **2016**, *6*, 30460.

[275] a) T. B. A. Akib, S. F. Mou, M. M. Rahman, M. M. Rana, M. R. Islam, I. M. Mehedi, M. A. P. Mahmud, A. Z. Kouzani, *Sensors* **2021**, *21*, 3491; b) S. M. A. Uddin, S. S. Chowdhury, E. Kabir, *Plasmonics* **2021**, *16*, 2025; c) S. Szunerits, H. Saada, Q. Pagneux, R. Boukherroub, *Biosensors* **2022**, *12*, 548; d) Q. Wu, W. Wu, F. Chen, P. Ren, *Analyst* **2022**, *147*, 2809.

[276] Y. Liu, J. Deng, X. Jia, J. Zhou, H. Li, X. Wang, Y. Chen, Z. Qin, Z. Jin, G. Wang, *New J. Chem.* **2024**, *48*, 1502.

[277] R. B. M. Schasfoort in *Handbook of Surface Plasmon Resonance: 2nd Edition* (Eds.: R. B. M. Schasfoort, S. Ricard Blum, J. Eckman, Y. N. Abdiche, R. Karlsson, E. T. Gedig, A. Marquart, P. Schuck, R. Schasfoort, D. Apiyo), Royal Society of Chemistry, **2017**, pp. 1–26.

[278] M. Rodin, D. Helle, D. Kuckling, *Polym. Chem.* **2024**, *15*, 661.

[279] C. Creton, *Macromolecules* **2017**, *50*, 8297.

[280] a) X. Huang, R. Li, Z. Duan, F. Xu, H. Li, *Soft Matter* **2022**, *18*, 3828; b) A. D. O'Donnell, S. Salimi, L. R. Hart, T. S. Babra, B. W. Greenland, W. Hayes, *React. Funct. Polym.* **2022**, *172*, 105209.

[281] a) S. L. Craig, *Angew. Chem. Int. Ed.* **2009**, *48*, 2645; b) M. A. Aboudzadeh, M. E. Muñoz, A. Santamaría, R. Marcilla, D. Mecerreyes, *Macromol. Rapid Commun.* **2012**, *33*, 314; c) Y. Sun, Y.-Y. Ren, Q. Li, R.-W. Shi, Y. Hu, J.-N. Guo, Z. Sun, F. Yan, *Chin. J. Polym. Sci.* **2019**, *37*, 1053.

[282] J. Sautaux, F. Marx, I. Gunkel, C. Weder, S. Schrettl, *Nat. Commun.* **2022**, *13*, 356.

[283] a) M. Ahmadi, A. Jangizehi, S. Seiffert, *Macromolecules* **2022**, *55*, 5514; b) Z. Jing, X. Huang, X. Liu, M. Liao, Y. Li, *Polym. Int.* **2023**, *72*, 39.

[284] a) X. Yang, R. Bai, Z. Zhang, Y. Liu, X. Yan, *J. Polym. Sci.* **2023**, *61*, 1105; b) K. Belal, F. Stoffelbach, D. Hourdet, A. Marcellan, J. Lyskawa, L. de Smet, A. Vebr, J. Potier, G. Cooke, R. Hoogenboom, P. Woisel, *Macromolecules* **2021**, *54*, 1926.

[285] J. Park, Y. Sasaki, Y. Ishii, S. Murayama, K. Ohshiro, K. Nishiura, R. Ikura, H. Yamaguchi, A. Harada, G. Matsuba, H. Washizu, T. Minami, Y. Takashima, *ACS Appl. Mater. Interfaces* **2023**, *15*, 39777.

[286] Y. Guo, Y. Liu, X. Zhao, J. Zhao, Y. Wang, X. Zhang, Z. Guo, X. Yan, *ACS Appl. Mater. Interfaces* **2023**, *15*, 25161.

[287] a) Y. Zhao, Z. Li, Q. Li, L. Yang, H. Liu, R. Yan, L. Xiao, H. Liu, J. Wang, B. Yang, Q. Lin, *Macromol. Rapid Commun.* **2020**, *41*, e2000441; b) P. Chakraborty, H. Oved, D.

Bychenko, Y. Yao, Y. Tang, S. Zilberzwige-Tal, G. Wei, T. Dvir, E. Gazit, *Adv. Mater.* **2021**, *33*, e2008715; c) Y. Liang, Z. Li, Y. Huang, R. Yu, B. Guo, *ACS Nano* **2021**, *15*, 7078; d) Y. Zhao, S. Song, X. Ren, J. Zhang, Q. Lin, Y. Zhao, *Chem. Rev.* **2022**, *122*, 5604.

[288] a) S. J. K. O'Neill, Z. Huang, M. H. Ahmed, A. J. Boys, S. Velasco-Bosom, J. Li, R. M. Owens, J. A. McCune, G. G. Malliaras, O. A. Scherman, *Adv. Mater.* **2023**, *35*, e2207634; b) G. Su, S. Yin, Y. Guo, F. Zhao, Q. Guo, X. Zhang, T. Zhou, G. Yu, *Mater. Horiz.* **2021**, *8*, 1795.

[289] a) C. B. Rodell, R. J. Wade, B. P. Purcell, N. N. Dusaj, J. A. Burdick, *ACS Biomater. Sci. Eng.* **2015**, *1*, 277; b) M. Tao, K. Xu, S. He, H. Li, L. Zhang, X. Luo, W. Zhong, *Chem. Commun.* **2018**, *54*, 4673; c) S. Bernhard, M. W. Tibbitt, *Adv. Drug Deliv. Rev.* **2021**, *171*, 240; d) G. Zhang, J. Li, W. Cai, S. Li, Y. Kong, Z.-Z. Yin, *Microchem. J.* **2023**, *193*, 109160.

[290] a) M. I. Rial-Hermida, D. C. S. Costa, L. Jiang, J. M. M. Rodrigues, K. Ito, J. F. Mano, *Gels* **2023**, *9*; b) R. Ikura, J. Park, M. Osaki, H. Yamaguchi, A. Harada, Y. Takashima, *NPG Asia Mater.* **2022**, *14*.

[291] a) K. Belal, F. Stoffelbach, J. Lyskawa, M. Fumagalli, D. Hourdet, A. Marcellan, L. de Smet, V. R. de La Rosa, G. Cooke, R. Hoogenboom, P. Woisel, *Angew. Chem. Int. Ed.* **2016**, *55*, 13974; b) M. Mauro, *J. Mater. Chem. B* **2019**, *7*, 4234; c) D. Tian, W. Ma, L. Zheng, K. Jiang, H. He, R. Sun, *ACS Appl. Polym. Mater.* **2023**, *5*, 8641.

[292] Z. Huang, X. Chen, S. J. K. O'Neill, G. Wu, D. J. Whitaker, J. Li, J. A. McCune, O. A. Scherman, *Nat. Mater.* **2022**, *21*, 103.

[293] L. Hammer, N. J. van Zee, R. Nicolaÿ, *Polymers* **2021**, *13*.

[294] a) J. Chen, Q. Su, R. Guo, J. Zhang, A. Dong, C. Lin, J. Zhang, *Macromol. Chem. Phys.* **2017**, *218*; b) G. Davidson-Rozenfeld, L. Stricker, J. Simke, M. Fadeev, M. Vázquez-González, B. J. Ravoo, I. Willner, *Polym. Chem.* **2019**, *10*, 4106; c) C. Qian, T.-A. Asoh, H. Uyama, *Macromol. Rapid Commun.* **2020**, *41*, e2000406; d) Y. Liu, L. Wang, H. Lu, Z. Huang, *Chem. Eng. J.* **2022**, *431*, 133338.

[295] a) J. Deng, R. Bai, J. Zhao, G. Liu, Z. Zhang, W. You, W. Yu, X. Yan, *Angew. Chem. Int. Ed.* **2023**, *62*, e202309058; b) N. Liubimtsev, Z. Zagradska-Paromova, D. Appelhans, J. Gaitzsch, B. Voit, *Macromol. Chem. Phys.* **2023**, *224*.

[296] J. Kümper, J. Meyers, R. Sebers, N. Kurig, R. Palkovits, *Green Chem.* **2023**, *25*, 6231.

[297] D. E. Blanco, A. Z. Dookhith, M. A. Modestino, *React. Chem. Eng.* **2019**, *4*, 8.

[298] V. Vaks, V. Anfertev, M. Chernyaeva, E. Domracheva, A. Yablokov, A. Maslennikova, A. Zhelesnyak, A. Baranov, Y. Schevchenko, M. F. Pereira, *Sci. Rep.* **2022**, *12*, 18117.

[299] a) R. A. Woutersen, *Scand. J. Work. Environ. Health* **1998**, *24*, 5; b) D. Coggon, P. Cole, *Scand. J. Work. Environ. Health* **1998**, *24*, 81; c) S. Caito, Y. Yu, M. Aschner, *Neurotoxicology* **2013**, *37*, 93.

[300] a) R. D. Short, W. V. Roloff, L. D. Kier, W. E. Ribelin, *J. Toxicol. Environ. Health* **1990**, *30*, 199; b) B. Shi, L. Shangguan, H. Wang, H. Zhu, H. Xing, P. Liu, Y. Liu, J. Liu, F. Huang, *ACS Materials Lett.* **2019**, *1*, 111.

[301] C. D. Vo, D. Kuckling, H.-J. P. Adler, M. Schönhoff, *Colloid Polym. Sci.* **2002**, *280*, 400.

[302] a) D. Roy, B. S. Sumerlin, *Macromol. Rapid Commun.* **2014**, *35*, 174; b) M. Seuss, W. Schmolke, A. Drechsler, A. Fery, S. Seiffert, *ACS Appl. Mater. Interfaces* **2016**, *8*, 16317; c) W. Schmolke, M. Ahmadi, S. Seiffert, *Phys. Chem. Chem. Phys.* **2019**, *21*, 19623.

[303] a) L. D. Taylor, H. S. Kolesinski, A. C. Mehta, L. Locatell, P. S. Larson, *Makromol. Chem., Rapid Commun.* **1982**, *3*, 779; b) M. W. Jones, S.-J. Richards, D. M. Haddleton, M. I. Gibson, *Polym. Chem.* **2013**, *4*, 717.

[304] a) A. Guyomard, D. Fournier, S. Pascual, L. Fontaine, J.-F. Bardeau, *Eur. Polym. J.* **2004**, *40*, 2343; b) H. T. Ho, M. E. Levere, D. Fournier, V. Montembault, S. Pascual, L. Fontaine, *Aust. J. Chem.* **2012**, *65*, 970; c) C. M. Gardner, C. E. Brown, H. D. H. Stöver, *J. Polym. Sci., Part A: Polym. Chem.* **2012**, *50*, 4674.

[305] a) F. François, C. Nicolas, G. Forcher, L. Fontaine, V. Montembault, *Eur. Polym. J.* **2020**, *141*, 110081; b) L. Jia, S. M. Kilbey, X. Wang, *Langmuir* **2020**, *36*, 10200; c) S. Pascual, T. Blin, P. J. Saikia, M. Thomas, P. Gosselin, L. Fontaine, *J. Polym. Sci., Part A: Polym. Chem.* **2010**, *48*, 5053.

[306] M. E. Levere, H. T. Ho, S. Pascual, L. Fontaine, *Polym. Chem.* **2011**, *2*, 2878.

[307] X. Yu, A. Herberg, D. Kuckling, *Eur. Polym. J.* **2019**, *120*, 109207.

[308] G. Wang, H. Qiang, Y.-Z. Guo, J. Yang, K. Wen, W.-B. Hu, *Org. Biomol. Chem.* **2019**, *17*, 4600.

[309] C. Schönbeck, H. Li, B.-H. Han, B. W. Laursen, *J. Phys. Chem. B* **2015**, *119*, 6711.

[310] L. Alderighi, P. Gans, A. Ienco, D. Peters, A. Sabatini, A. Vacca, *Coord. Chem. Rev.* **1999**, *184*, 311.

[311] F. D'Anna, C. Rizzo, P. Vitale, S. Marullo, F. Ferrante, *New J. Chem.* **2017**, *41*, 12490.

[312] D. Helle, *Bachelorarbeit*, Paderborn University, Paderborn, **2023**.

[313] M. P. Foster, C. A. McElroy, C. D. Amero, *Biochemistry* **2007**, *46*, 331.

[314] M. E. Harmon, D. Kuckling, P. Pareek, C. W. Frank, *Langmuir* **2003**, *19*, 10947.

[315] D. J. Anderson, *Clin. Chem.* **1989**, *35*, 2152.

[316] a) K. Igarashi, K. Kashiwagi, *Int. J. Biochem. Cell Biol.* **2010**, *42*, 39; b) E. Agostinelli, M. P. M. Marques, R. Calheiros, F. P. S. C. Gil, G. Tempera, N. Viceconte, V. Battaglia, S. Grancara, A. Toninello, *Amino acids* **2010**, *38*, 393.

[317] E. Larqué, M. Sabater-Molina, S. Zamora, *Nutrition* **2007**, *23*, 87.

[318] N. A. Sagar, S. Tarafdar, S. Agarwal, A. Tarafdar, S. Sharma, *Med. Sci.* **2021**, *9*.

[319] C. Moinard, L. Cynober, J.-P. de Bandt, *Clin. Nutr.* **2005**, *24*, 184.

[320] a) T. Thomas, T. J. Thomas, *J. Cell. Mol. Med.* **2003**, *7*, 113; b) E. W. Gerner, F. L. Meyskens, *Nat. Rev. Cancer* **2004**, *4*, 781; c) N. Minois, D. Carmona-Gutierrez, F. Madeo, *Aging* **2011**, *3*, 716.

[321] D. H. Russell, *Nat. New Biol.* **1971**, *233*, 144.

[322] Y. Asai, T. Itoi, M. Sugimoto, A. Sofuni, T. Tsuchiya, R. Tanaka, R. Tonozuka, M. Honjo, S. Mukai, M. Fujita, K. Yamamoto, Y. Matsunami, T. Kurosawa, Y. Nagakawa, M. Kaneko, S. Ota, S. Kawachi, M. Shimazu, T. Soga, M. Tomita, M. Sunamura, *Cancers* **2018**, *10*.

[323] a) C. Lo, Y.-L. Hsu, C.-N. Cheng, C.-H. Lin, H.-C. Kuo, C.-S. Huang, C.-H. Kuo, *J. Proteome Res.* **2020**, *19*, 4061; b) A. Lipton, L. M. Sheehan, G. F. Kessler, *Cancer* **1975**, *35*, 464.

[324] J. A. Byun, M. H. Choi, M. H. Moon, G. Kong, B. Chul Chung, *Cancer Lett.* **2009**, *273*, 300.

[325] V. G. Naik, V. Kumar, A. C. Bhasikuttan, K. Kadu, S. R. Ramanan, A. A. Bhosle, M. Banerjee, A. Chatterjee, *ACS Appl. Bio Mater.* **2021**, *4*, 1813.

[326] C. V. Berenguer, F. Pereira, J. S. Câmara, J. A. M. Pereira, *Curr. Oncol.* **2023**, *30*, 2300.

[327] R. L. Siegel, K. D. Miller, N. S. Wagle, A. Jemal, *CA: Cancer J. Clin.* **2023**, *73*, 17.

[328] A. C. Goodwin, S. Jadallah, A. Toubaji, K. Lecksell, J. L. Hicks, J. Kowalski, G. S. Bova, A. M. de Marzo, G. J. Netto, R. A. Casero, *Prostate* **2008**, *68*, 766.

[329] T.-H. Tsoi, C.-F. Chan, W.-L. Chan, K.-F. Chiu, W.-T. Wong, C.-F. Ng, K.-L. Wong, *PLoS One* **2016**, *11*, e0162217.

[330] M. R. Häkkinen, A. Roine, S. Auriola, A. Tuokko, E. Veskimäe, T. A. Keinänen, T. Lehtimäki, N. Oksala, J. Vepsäläinen, *J. Chromatogr. B Analyt. Technol. Biomed. Life Sci.* **2013**, *941*, 81.

[331] Y. Chen, Z. Huang, J.-F. Xu, Z. Sun, X. Zhang, *ACS Appl. Mater. Interfaces* **2016**, *8*, 22780.

[332] C. Zhong, C. Hu, R. Kumar, V. Trouillet, F. Biedermann, M. Hirtz, *ACS Appl. Nano Mater.* **2021**, *4*, 4676.

[333] L. Ling, Z. Zhao, L. Mao, S. Wang, Da Ma, *Chem. Commun.* **2023**, *59*, 14161.

[334] A. Prabodh, L. M. Grimm, P. K. Biswas, V. Mahram, F. Biedermann, *Chem. Eur. J.* **2024**, *30*, e202401071.

[335] Y. Yao, Y. Zhou, J. Dai, S. Yue, M. Xue, *Chem. Commun.* **2014**, *50*, 869.

[336] X. Tan, X. Liu, W. Zeng, Z. Zhang, T. Huang, L. Yu, G. Zhao, *Spectrochim. Acta A Mol. Biomol. Spectrosc.* **2019**, *221*, 117176.

[337] R. Reddy Kothur, B. Anil Patel, P. J. Cragg, *Chem. Commun.* **2017**, *53*, 9078.

[338] C. Li, X. Shu, J. Li, S. Chen, K. Han, M. Xu, B. Hu, Y. Yu, X. Jia, *J. Org. Chem.* **2011**, *76*, 8458.

[339] R. Probst, *Bachelorarbeit*, Paderborn University, Paderborn, **2021**.

[340] R. R. Kothur, J. Hall, B. A. Patel, C. L. Leong, M. G. Boutelle, P. J. Cragg, *Chem. Commun.* **2014**, *50*, 852.

[341] "BindFit v0.5", can be found under http://supramolecular.org.

[342] a) Y. Inoue, T. Hakushi, Y. Liu, L. Tong, B. Shen, D. Jin, *J. Am. Chem. Soc.* **1993**, *115*, 475; b) E. Uria-Canseco, S. Perez-Casas, G. Navarrete-Vázquez, *J. Chem. Thermodyn.* **2019**, *129*, 55.

[343] B. Gómez, V. Francisco, F. Fernández-Nieto, L. Garcia-Rio, M. Martín-Pastor, M. R. Paleo, F. J. Sardina, *Chemistry* **2014**, *20*, 12123.

[344] B. Gómez-González, V. Francisco, R. Montecinos, L. García-Río, *Org. Biomol. Chem.* **2017**, *15*, 911.

[345] L. Samuelsen, R. Holm, A. Lathuile, C. Schönbeck, *J. Pharm. Biomed. Anal.* **2020**, *184*, 113206.

[346] a) J. L. Oscarson, G. Wu, P. W. Faux, R. M. Izatt, J. J. Christensen, *Thermochim. Acta* **1989**, *154*, 119; b) K. Ballerat-Busserolles, M. R. Simond, Y. Coulier, J.-Y. Coxam, *Pure Appl. Chem.* **2014**, *86*, 233.

[347] E. M. Worcester, K. J. Bergsland, D. L. Gillen, F. L. Coe, *Am. J. Physiol. Renal Physiol.* **2018**, *314*, F623-F629.

[348] a) N. E. Good, G. D. Winget, W. Winter, T. N. Connolly, S. Izawa, R. M. Singh, *Biochemistry* **1966**, *5*, 467; b) N. E. Good, S. Izawa, *Methods Enzymol.* **1972**, *24*, 53.

[349] B. Shi, K. Jie, Y. Zhou, J. Zhou, D. Xia, F. Huang, *J. Am. Chem. Soc.* **2016**, *138*, 80.

[350] L. D. Taylor, C. K. Chiklis, T. E. Platt, *J. Polym. Sci. B Polym. Lett.* **1971**, *9*, 187.

[351] Z. Jomeh Farsangi, M. Zhu, X. Song, K. Yang, T. Hoare, *Macromolecules* **2023**, *56*, 4231.

[352] A. E. Smith, X. Xu, C. L. McCormick, *Prog. Polym. Sci.* **2010**, *35*, 45.

[353] D. L. Patton, R. C. Advincula, *Macromolecules* **2006**, *39*, 8674.

[354] C. Y. P. Wilding, S. T. Knox, R. A. Bourne, N. J. Warren, *Macromolecules* **2023**, *56*, 1581.

[355] Y. Terao, S. Sugihara, K. Satoh, M. Kamigaito, *Eur. Polym. J.* **2019**, *120*, 109225.

[356] J. M. Pelet, D. Putnam, *Macromolecules* **2009**, *42*, 1494.

[357] a) A. J. Convertine, N. Ayres, C. W. Scales, A. B. Lowe, C. L. McCormick, *Biomacromolecules* **2004**, *5*, 1177; b) S. Perrier, P. Takolpuckdee, J. Westwood, D. M. Lewis, *Macromolecules* **2004**, *37*, 2709; c) W. Steinhauer, R. Hoogenboom, H. Keul, M. Moeller, *Macromolecules* **2013**, *46*, 1447; d) D. B. Thomas, A. J. Convertine, L. J. Myrick, C. W. Scales, A. E. Smith, A. B. Lowe, Y. A. Vasilieva, N. Ayres, C. L. McCormick, *Macromolecules* **2004**, *37*, 8941.

[358] G. Ercolani, *J. Am. Chem. Soc.* **2003**, *125*, 16097.

[359] Y. Mouhamad, P. Mokarian-Tabari, N. Clarke, R. A. L. Jones, M. Geoghegan, *J. Appl. Phys.* **2014**, *116*.

[360] a) P. Müller-Buschbaum, J. S. Gutmann, M. Wolkenhauer, J. Kraus, M. Stamm, D. Smilgies, W. Petry, *Macromolecules* **2001**, *34*, 1369; b) K. E. Strawhecker, S. K. Kumar, J. F. Douglas, A. Karim, *Macromolecules* **2001**, *34*, 4669; c) N. Chapman, M. Chapman, W. B. Euler, *Polymers* **2021**, *13*.

[361] D. Meyerhofer, *J. Appl. Phys.* **1978**, *49*, 3993.

[362] P. D. Fowler, C. Ruscher, J. D. McGraw, J. A. Forrest, K. Dalnoki-Veress, *Eur. Phys. J. E Soft Matter* **2016**, *39*, 90.

[363] a) A. B. Braunschweig, C. M. Ronconi, J.-Y. Han, F. Aricó, S. J. Cantrill, J. F. Stoddart, S. I. Khan, A. J. P. White, D. J. Williams, *Eur. J. Org. Chem.* **2006**, *2006*, 1857; b) L. Li, G. J. Clarkson, *Org. Lett.* **2007**, *9*, 497.

[364] J. Henig, I. Mamedov, P. Fouskova, É. Tóth, N. K. Logothetis, G. Angelovski, H. A. Mayer, *Inorg. Chem.* **2011**, *50*, 6472.

[365] S. K. V. Vernekar, H. Y. Hallaq, G. Clarkson, A. J. Thompson, L. Silvestri, S. C. R. Lummis, M. Lochner, *J. Med. Chem.* **2010**, *53*, 2324.

[366] K. Kai, H. Fujii, R. Ikenaka, M. Akagawa, H. Hayashi, *Chem. Commun.* **2014**, *50*, 8586.

[367] A. Müller, P. Krauss, *Monatshefte für Chemie* **1932**, *61*, 219.

[368] Y. Ma, Z. Zhang, X. Ji, C. Han, J. He, Z. Abliz, W. Chen, F. Huang, *Eur. J. Org. Chem.* **2011**, *2011*, 5331.

[369] D. N. Shurpik, I. I. Stoikov, *Russ. J. Gen. Chem.* **2016**, *86*, 752.

[370] S. M. Heilmann, K. M. Jensen, L. R. Krepski, D. M. Moren, J. K. Rasmussen, H. K. Smith, *Synth. Commun.* **1987**, *17*, 843.